RELATIONS BETWEEN MICROSTRUCTURE AND CREEP-RUPTURE PROPERTIES OF NICKEL-BASE ALLOYS AS REVEALED BY OVERTEMPERATURE EXPOSURES

BY

John P. Rowe
J. W. Freeman

Final Report

to

NATIONAL AERONAUTICS AND SPACE ADMINISTRATION

Project 02846

September, 1961

CONTENTS

NATIONAL AERONAUTICS AND SPACE ADMINISTRATION

RELATIONS BETWEEN MICROSTRUCTURE AND CREEP-RUPTURE PROPERTIES OF NICKEL-BASE ALLOYS AS REVEALED BY OVERTEMPERATURE EXPOSURES

By John P. Rowe and J. W. Freeman

SUMMARY

An investigation was conducted to determine the effect of repeated brief overheats on the creep-rupture properties of nickel-base alloys and then to correlate the associated structural effects of the overheats with the observed property changes. Overheat temperatures up to 2100°F from base temperatures of 1500° and 1600°F were studied using M252 and Inconel 700 alloys. The overheats were applied every five hours in the absence of stress. Between overheats, the stress causing rupture in approximately 100 hours in a normal rupture test at the base temperature was applied. The number of overheats was varied from a few, up to as many as could be applied before rupture.

The prolongation of rupture life of M252 at 1500°F as a result of overheats to 1900° to 2100°F previously reported was verified for another heat and extended for two heats to rupture tests at 1600°F. The damage from overheats to 1800°F previously reported did not occur in the new heat. The rupture life of Inconel 700 at 1500° or 1600°F was unchanged by overheating to 1800°F and was reduced by overheating to 2000°F or higher.

The increased rupture life of M252 was due to a reduction in the rate of increase in creep rate with testing time as a result of overheating to 1900°F or higher. The reduction in rupture life of Inconel 700 was due to reduced ductility from overheats to 2000°F or higher. Creep resistance was not changed nor was the ductility affected by overheats to 1800°F. A reduction in ductility for M252 had little effect on rupture time.

During exposure in normal tests at 1600°F, the measured size of the $Ni_3(Al,Ti)$ precipitate (γ') in both alloys increased and the amount decreased. Due to the extremely rapid rate of solution and reprecipitation, repeated brief overheats above the γ' solution temperature in both alloys prevented the agglomeration and decrease in amount of γ' . This resulted in increased creep resistance in M252 but caused no change in Inconel 700.

Consideration of the geometry of Weertman's analysis of creep in the presence of a dispersed phase demonstrated that, for the volume fraction of γ' in M252 alloy, changes occurring during exposure at 1600°F in normal tests would be expected to cause a decrease in creep resistance. Thus the maintenance of a fine dispersion by overheating maintained creep resistance. For the larger amount of γ' in Inconel 700 the creep resistance would not be expected to depend strongly on the dispersion. The results confirmed this indication, showing that neither the changes in dispersion during normal tests nor the maintenance of a fine dispersion by overheating affected creep resistance.

Whether the measured decrease in amount of γ' actually occurred or was the result of an etching effect which gave erroneously large particle sizes when the particles were small, could not be determined from the data. The data obtained, however, indicated that the observed particle size and interparticle spacing correlated with the creep rate.

Fracture of both alloys in rupture tests resulted from nucleation of microcracks at the interface between carbides in grain boundaries and the adjacent matrix and their subsequent growth. The M_6C carbides in M252 alloy were not changed by overheating due to their solution temperature being above 2100°F and consequently the ductility was not changed. The $M_{23}C_6$ carbides in Inconel 700 were dissolved and prevented from agglomerating at grain boundaries by overheats to 2000°F or higher because the solution temperature of $M_{23}C_6$ is below 1900°F. The resulting clean grain boundaries in Inconel 700 alloy overheated to these temperatures were subject to rapid crack growth once a crack was nucleated so that ductility and rupture life was reduced. To account for the behavior of the two alloys, it is necessary to accept the fact that while carbides nucleate cracks they also retard crack growth. The full explanation also includes the effect of the strength of the adjacent matrix.

The clarification of the role of the dispersion and amount of γ' gives insight into the causes for the apparent insensitivity of many nickel-base alloys to differences in aging treatments. Of particular significance is the indication that Weertman's treatment of dislocation concepts applies to engineering materials. Also of significance was the indication that the type of carbide in a material is not so important as the response of the carbide to exposure conditions.

The findings of this investigation should have wide general applicability. The limitations which must be considered in specific cases are discussed.

INTRODUCTION

During elevated temperature service, alloys are frequently inadvertently exposed briefly to temperatures above the normal operating temperatures. Such overheats can influence subsequent life at normal conditions by introducing structural changes and, if stress is present, by accelerating creep.

The response to overtemperature exposure of alloys for service in aircraft gas turbines has been the subject of a continuing research program at the University of Michigan sponsored by the National Aeronautics and Space Administration, formerly the National Advisory Committee for Aeronautics. These studies had demonstrated that the structural changes induced by overheating can either increase or decrease subsequent life. The effect depends on both the type of alloy and the overheat conditions. The rupture life at 1500°F of both wrought (ref. 1) and cast (ref. 2) cobalt-base alloys was reduced by the structural changes induced by repeated brief overheats. The loss in life increased with increasing temperature and number of overheats due mainly to reduced creep resistance resulting from acceleration of precipitation and agglomeration reactions.

Extension of the work to the nickel-base precipitation-hardened alloy M252 (ref. 3) demonstrated that the rupture life was increased by the structural changes resulting from repeated brief overheats to temperatures above 1800°F from a base temperature of 1500°F. This phenomenon was confirmed on several heats of the alloy and was shown to result from increased creep resistance.

In these three investigations, the influence of stress during the overheats was evaluated. The results demonstrated that effect of stress could be evaluated using the "addibility-of-life-fractions" rule. Summing the effects of temperature and the percentage of rupture life used up during the overheats, gave close approximations to the experimental rupture times.

The investigation covered by this report was initiated to include studies at a base temperature of 1600°F and to determine if other nickel-base alloys containing Al+Ti would be strengthened by periodic overheating without stress. Another alloy of the same metallurgical type, Inconel 700, was added to the program. Studies were initiated to determine the metallurgical reasons why M252 alloy could be strengthened by overheating above 1800°F and to explain the response of Inconel 700 to overheating.

The overheat exposures were two minutes in duration and were applied every five hours during the course of creep-rupture tests which would normally have fractured in about 100 hours at 1500° and 1600°F. The stress was removed during the overheats and reapplied at the end of each overheat. Variations in the amount of overheating applied were obtained by varying the number of cycles,

always beginning from the start of the test. These conditions were established by discussion of the problem with the NACA Subcommittee on Heat-Resistant Materials.

The investigation was carried out in the Chemical and Metallurgical Engineering Department of the University of Michigan College of Engineering under the sponsorship and with the financial assistance of the National Aeronautics and Space Administration. The work was administered by the University Office of Research Administration.

EXPERIMENTAL PROCEDURES

The general procedure was to determine the effects of repeated, brief overheats on the creep-rupture properties of the alloys investigated and then to relate these effects to the structural changes associated with them.

Material

Two commercial heats of M252 alloy and one commercial heat of Inconel 700 alloy were studied for the major portion of the investigation. Limited studies were also undertaken on three laboratory heats of modified M252 analysis. The chemical analyses of all materials are given in table I.

Commercial Materials. - The two heats of M252 alloy included in the study were available from previous studies. Both were vacuum melted and supplied gratis for the investigation by their manufacturers in the form of centerless ground 7/8-inch diameter bar stock. To improve the uniformity of the material for testing, these bars were rolled to 1/2-inch, round-corner, square bars, using the University of Michigan rolling mill. The rolling was done from 2150°F using nine passes with one reheat. Two heat treatments were used following rolling:

1) Solution treat 1 hour 2150°F, air cool, plus
   Solution treat 4 hours 1950°F, air cool, plus
   Age 15 hours 1400°F, air cool;

2) The same treatment as (1), omitting the 2150°F solution treatment.

Details regarding the use of these treatments follow in the section on results. Overheat testing was conducted with samples from both of the heats of M252 alloy. However, the bulk of the microstructural investigation was conducted with heat 837.

The Inconel 700 alloy used was air-melted by the International Nickel Company and provided through the Curtis-Wright Corporation, Wright Aeronautical Division, in the form of 24-inch lengths of 11/16-inch, round bar stock. At their request, this alloy was not re-rolled prior to testing. It received the following standard heat treatment after cutting into 12-inch lengths:

Solution treat 2 hours 2160°F, air cool;
Age 4 hours 1600°F, air cool.

Laboratory Heats. - The three laboratory heats were melted in the University of Michigan vacuum-induction furnace. One of these heats was nominally M252 alloy. The others were variations of the M252 analysis; one had a 3.0-percent aim aluminum content, and the other contained 4.0-percent molybdenum. The heats were made in an alumina crucible, using virgin melting stock as follows: electrolytic nickel, chromium, cobalt, and manganese; arc-melted molybdenum chips; Ti55A titanium bar stock; 99.99-percent aluminum pig; 99.9-percent silicon powder; and spectrographically pure carbon. Boron was added to all heats as NiB, aiming for 20 ppm.

The resultant 10-pound ingots were 2.5-inches diameter by 7-inches long. They were processed to bar stock with the University of Michigan rolling mill as follows:

1) The ingots were heated for 1/2 hour at the rolling temperature, 2150°F.

2) The ingots were rolled to 7/8-inch round-corner squares, using 22 passes with 21 reheats. These bars were then cooled to room temperature and cut in half.

3) The 7/8-inch bars were reheated to 2150°F, held for 1/2 hour and rolled to 1/2-inch round-corner squares, using 12 passes with two reheats.

This bar stock was then treated using the standard heat treatment with the double solution treatment for M252 alloy as given previously.

Creep-Rupture and Overheat Testing

The creep-rupture and overheat tests were carried out in conventional beam loaded creep-rupture units using specimens with a 0.250-inch diameter and 1-inch gage length. These specimens were machined from the center of the previously described bar stock so that the rolling direction was parallel to the tension axis in all cases. Time-elongation data were taken during the tests with a modified Martens-type extensometer with a sensivity of 0.00001 inch. For all tests, the samples were placed in furnaces which were at

the test temperature and held for four hours before application of the load. Temperature variation along the gage length was limited to ± 3°F.

All overheats were applied using a two-minute exposure to the desired overheat temperature with the load removed from the sample. These cycles were begun five hours following application of the load and were repeated at five hour intervals until the desired number of cycles was accumulated. The test was then allowed to continue at constant load and temperature until fracture.

Interrupted tests (those not permitted to fracture) were shut off after the desired time in test and allowed to cool under load, to provide specimens for study of microstructures at intermediate times during the tests.

Heating Method. - For overheat tests, the conventional units were modified to permit resistance heating of the specimens by passing direct current through the sample. A 400-ampere, direct-current generator was used as a power supply. In order to avoid disturbing the specimen during the test, insulated terminal blocks were fastened to the frame of the unit, level with the top and bottom of the furnace. From these terminals, short leads were fastened to the top and bottom specimen holders before the test was started. Then, for overheating, it was merely necessary to attach the power supply leads to the terminal blocks, completing the circuit to the generator field switch. The top specimen holder was insulated from the frame by means of a transite insert. The whole circuit was grounded either through the beam or through an attached ground wire. A photograph of a unit is shown as figure 1.

Temperature Measurement. - In order to follow the temperature accurately during an overheat, a welding technique (ref. 4) was employed to attach a 22 gage Chromel-Alumel thermocouple to the specimen. An electronic recorder provided a continuous record of the temperature. A schematic sketch of this arrangement is shown as figure 2. Temperature measurement was complicated by two factors. In order to follow the rapidly changing temperatures during an overheat cycle and effect accurate control, the thermocouple wires had to be welded to the sample. This was done with a percussion-type welder. The welded attachment maintained contact between the thermocouple wires and the specimen as reduction in cross section occurred by creep during the tests. In welding the thermocouple wires on the specimen, however, any minute error in positioning either wire caused the direct current from the generator to impress an electromotive force on the thermocouple circuit. This electromotive force varied with the magnitude of the placement error and appeared on the temperature recorder as a temperature effect. To avoid this, two Alumel wires were employed, one deliberately placed on either side of the single Chromel wire. By connecting these two Alumel wires to the extremes of a variable resistance, the variable tap

could be adjusted so that the two electromotive forces obtained cancelled each other, leaving only the thermal electromotive force impressed on the recorder.

Checks were made of the original calibration and the maintenance of calibration of the thermocouples. The system used gave accurate temperature measurements as installed. The overheats did not change the calibration of the thermocouples by more than 1°F, for any of the temperatures used.

Procedure for Overheat Cycles. - After completion of a five-hour period under stress after load application, the following procedure was used in performing an overheat:

1. The temperature was checked and an elongation reading made. At this time, the generator and recorder were attached to the specimen.

2. The load was removed.

3. After a 60 second time lapse, during which the furnace input was cut back and the thermocouple circuit checked, the heating cycle was initiated by applying the maximum generator output of 400 amperes to the specimen. When the desired overheat temperature was attained, the generator output was reduced to a value just sufficient to maintain temperature.

4. At the end of the two minutes at temperature, the power supply was shut off and the specimen allowed to cool. No forced cooling was employed other than that supplied by having allowed the furnace temperature to fall below the base temperature when the input was reduced in step (3).

5. The load was reapplied when the test temperature fell to within 10°F of the base temperature. Although the asymptotic approach of the test temperature to the level of the base temperature introduced some variation in the length of time required to re-establish this level, the samples cooled to 10°F above this level in a reproducible time period. After the load was reapplied, the furnace control was manipulated to bring the test on temperature as soon as possible.

6. When temperature equilibrium was re-established at the base temperature, elongation measurements were taken again and the test continued for five hours until the next cycle. In plotting the time-elongation data, this reading, after reapplication of the load, was assumed to be at the same total deformation as the reading taken just prior to removal of the load at the beginning of the cycle.

This procedure resulted in reproducible temperature patterns from cycle to cycle and between samples or creep-rupture units.

Typical time-temperature patterns for overheats to several of the temperatures used are shown in figure 3.

Experimental Thermal Treatments

During the course of the investigation, various treatments were employed for the purpose of studying the effect of temperature on the structures of the alloys studied. The standard solution and aging treatments used for the original stock have been previously described. Those treatments which were specially designed to study a specific, complex temperature history are described in the results section as the effects associated with them are discussed. The relatively simple treatments used in preparation of material for structural studies are described in the following sections.

Determination of Solution Temperatures. - The samples used in the determination of solution temperatures were thin sections cut from heat-treated bar stock and split longitudinally. These pieces were attached to a wire and placed beside the thermocouple slug in the furnace. Since all treatments of this nature were at least two hours in duration and the samples were small, the time measurement began when the sample was placed in the furnace. At the end of the desired time period, the samples were lifted by the attached wires and rapidly quenched into an iced brine solution containing a well-stirred mixture with excess ice and salt.

Exposure Studies at 1600°F. - Samples for the study of structural changes during exposure at 1600°F were prepared in the same manner as those for the solution treating studies. In addition, a sample with an attached thermocouple was placed in the furnace with the specimens to indicate more exactly the time at which the aging temperature was attained. When the desired time period had elapsed, the samples were removed from the furnace and water quenched.

Hardness

The diamond pyramid hardness (DPH) was measured under a 50-kilogram load. Both diagonals of each of three impressions were measured and the six measurements averaged. A statistical analysis of this technique (ref. 5) had shown that in the range of 300-340 DPH, a hardness difference of 7 DPH was significant. This range of significance increased to 9 DPH in the range from 340-400 DPH.

Metallography

All metallographic samples were mechanically polished on wet silicon carbide papers through 600 grit and then on wet cloths with

Linde A and B powders. Etching followed the procedure developed by Bigelow, Amy and Brockway, (ref. 6), using an etchant composed of 12 parts phosphoric acid (85 percent), 47 parts sulfuric acid (96 percent), and 41 parts nitric acid (70 percent). The etching was done electrolytically at 6 volts and a current density of about 0.8 amperes per square inch. Samples for light microscopy were etched for 5 to 7 seconds, while those for electron microscopy were etched for 1 to 5 seconds, depending on the structure of the particular sample in question.

For electron microscopy, collodion replicas of the metallic surface were used. These were shadowed with palladium to increase the contrast and reveal surface contours. Polystyrene latex spheres were placed on the replicas prior to shadowing to indicate the angle and direction of shadowing and to provide an internal standard for measurement of magnifications. Two sphere sizes were employed, either 2580Å or 3400Å in diameter. The micrographs presented are direct prints from the original negatives; hence, the polystrene spheres appear black and the shadows formed by the palladium appear white.

Counting and Measuring Techniques

During the investigation, specific features of the microstructures were evaluated quantitatively for comparison between samples. These included studies of the γ' phase as well as measurements of grain boundary phenomena. The results of these studies depended strongly on the accuracy and reliability of the techniques employed. The following sections of the report present in detail the methods which were used to provide the measurements of the microstructural features.

Measurements of the γ' Phase. - The measurements of the γ' phase were made from electron micrographs of the samples. The number of particles, volume fraction of γ', particle size, and average interparticle spacing were measured. Although these data were used to evaluate the behavior of the materials at 1600°F, the effect of thermal expansion on the absolute magnitude of the variables was neglected since it was only of the order of 1.5 percent.

The details of the procedures employed are presented in the following sections.

Calculation of number of particles: The number of γ' particles was evaluated in terms of surface density. An area was counted at X11,000 large enough to contain at least 100 particles. The density was then expressed as the number of particles per square inch at X11,000.

Volume fraction estimation by lineal analysis: The technique of lineal analysis provides a convenient method for obtaining information regarding three-dimensional aspects of a solid from a study of a two-dimensional section through its structure. Howard and Cohen (ref. 7) have published a review of the method and its application to metallurgical studies. The measurement of the volume fraction of a sample which is occupied by a uniformly distributed phase proceeds as follows:

1) A random plane section is polished through the sample.

2) A series of straight line traverses is made across this plane with a suitable means for observing the intersection of these lines with the phase boundaries and measuring the length of the line segments which pass over the phase in question.

3) The volume fraction occupied by the phase in question is then equal to the sum of the line segments so measured, divided by the total length of traverse employed.

This method requires only that all measurements be made on the same plane, that the phase distribution be uniform throughout the solid, and that a sufficient number of intersections be measured to give a random sample in the plane.

Lineal analysis has been applied to metallurgical studies through the use of a microscope with a specially designed stage, or by making measurements on photomicrographs of the samples in question. Through the use of enlarged electron micrographs, the method can be extended to the study of extremely small particles of a second phase such as exist in the alloys of the present investigation. Enlargements of electron micrographs at X11,000 provided a total magnification of about X100,000 in the present work.

In order to produce phase contrast prior to replication of the metal surface for electron microscopy, an etch must be employed. The etchant selectively attacks the matrix leaving the γ' particles in relief on the surface. As a result of the essentially spherical shape of the particles throughout the reaction times studied, this etching will introduce an error in the measurements. When the depth of etching becomes large relative to the particle size, the extent of this error becomes significant.

The cause of this error is demonstrated in figure 4, which shows a spherical particle sectioned and polished through its center. After etching, the plane of the surrounding matrix on which measurements must be made is below the plane of polish in the particle. In viewing this particle for measurement, the original plane of polish will appear to represent the circle of contact with the matrix, while the actual contact circle is smaller. Measurements which include this particle will, therefore, give results which are

larger than they should be. The extent of the error will depend on the depth of etching. While the foregoing discussion has considered only the case of a particle sectioned and polished through its center, similar errors will result whenever the etching leaves a particle protruding in such a way that the contact circle with the etched matrix is hidden beneath a larger circle above it.

The objective of the following discussion and calculations is to provide a quantitative measure of these errors which can then be employed to correct for the errors in actual data.

In applying the techniques of lineal analysis to a system in wich particle size is extremely small, certain assumptions are necessary regarding the preparation of the samples and micrographs from which the actual measurements will be taken. These will be discussed briefly.

1) Etching - Several requirements must be met by an acceptable etch. It must selectively attack the matrix around each particle, removing it completely without affecting the size or shape of the precipitate particle. The plane of etching must remain flat so that particles remain attached to the surface until their contact with the surface has been reduced to a point. Implicit in these requirements is the absence of any strain fields or concentration gradients near the particles which might promote uneven etching in these areas. In addition, the etch must reveal particles which are barely exposed during etching. The resolving power of the microscope employed will introduce a limit here as well. A rigorous treatment thus requires infinite resolving power from the microscope.

The degree of approach to these rather severe requirements in the present study is difficult to determine. The etchant employed did leave the γ' particles standing while removing the matrix around them. Variations in etching time did not result in an observable change in the appearance of the particles. Examination of several samples representing a wide range of particle sizes using an interference microscope did not reveal any measurable uneveness of the surface. Whether particles are removed by etching before their contact with the matrix has been reduced to a point, and whether the etch will reveal the tops of barely exposed particles cannot be determined. The limit of resolving power of the microscope will certainly make impossible the detection of the smallest sections. These limitations of the method are those with which the investigator must live. Their nature is such that the errors in absolute values which they engender will be proportionally greater as the size of the particles decreases.

2) Random sample - A primary requirement for any analytical technique is that the sample examined be truly representative of the universe under study. In the present study, the distribution

of γ' throughout the matrix must thus be homogeneous. This homogeneity must hold for the extremely small samples which are studied with electron micrographic methods. A study was made on several samples by repeated replication with intermediate re-polishing and etching. This study demonstrated that the reproducibility of the value of the measured variable was better than 5 percent.

The calculations to follow have been made assuming all of the above idealized conditions. An additional assumption is necessary for these calculations which is not required for the application of the basic technique. In any sample, a distribution of particle sizes will exist. In computing the error in measurement, a single particle size will be assumed. This assumption will have the effect of overestimating the magnitude of the error for larger particles and underestimating the error for smaller particles. These inaccuracies are, therefore, largely self-compensating. The calculations will thus proceed under the assumption of spherical particles of uniform size.

For calculation, let: R = radius of the particles

e = depth of etching (measured from plane of polish)

d = distance from the center of a sphere along the normal to any plane intersecting the sphere.

a = radius of the circle of intersection between the sphere and any plane.

In a polished sample containing a statistically infinite number of randomly dispersed particles, there will be found particles which are sectioned so that all values of d from zero to R are equally likely. Then for an etching depth, $\bar{e}$, the particles fall into four groups (fig. 5) on the basis of the location of the polish plane relative to their centers:

(1) Case A - All planes whose d values fall between the distances e and R above the sphere center after polishing. After etching, the true contact area for these particles will still be seen and measurements from them will not contain any error.

(2) Case B - All planes whose d values were less than the distance e above the center of the sphere after polishing. The etching for these particles will take the etch plane below the center of the sphere so that a great circle will be observed in every case in this group, rather than the smaller, true contact area.

(3) Case C - All planes between the center of the sphere and the distance R-e below the center after polishing. These particles will have a smaller contact area after etching than their original area in the polished plane, although the area in the polished plane will continue to appear.

(4) Case D - All planes farther than a distance R-e below the center of the sphere. These particles will be removed by etching. The random dispersion of the system will result in the exposure of the top of another particle for each one removed. The distribution of contact areas in this group of newly exposed particles will thus be identical to that in the original group before etching and no error will enter from this group.

In order to correct for the error made on measurement of an actual micrograph, it will be necessary to compute the average value for the radii of the circles of intersection in each of the four groups above, before and after etching. These average values can then be used with the known relative frequencies of occurrence to compute a correction factor.

The calculation of the average radius in each of the above intervals of interest can be made using the following general approach, applied, in this instance, to the limiting case for the average value of the radius of the circles sectioned by polishing, before any etching. For every sphere sectioned a given distance above its center, there will be a sphere sectioned at the same distance below its center. Thus, only those sectioned on one side of their centers need be considered. The remaining group will have an identical average. Using the previously defined variables, the calculation is as follows (fig. 6).

The values of d can range from 0 to R for this case. Dividing this interval into j sub-intervals, the following definitions are made:

n_i = number of planes in i^{th} sub-interval

a_i = average radius of the circle intersection in the i^{th} sub-interval

d_i = average value of d in the i^{th} sub-interval

If N = total number of planes observed,

$$n_i = \frac{N}{j} = \Delta n \text{ and } \sum_{i=1}^{j} n_i = N$$

The average value for $\underline{a}$ in the entire group is then given by:

$$\bar{a} = \frac{1}{N} \sum_{i=1}^{j} n_i a_i$$

But $a_i = \sqrt{R^2 - d_i^2}$

and $d_i = i \frac{R}{j} = \frac{n}{N} R$

Then $\bar{a} = \lim_{j \to \infty} \left[\frac{1}{N} \sum_{i=1}^{j} \sqrt{R^2 - \frac{n^2 R^2}{N^2}} \; \Delta n \right]$

and $\bar{a} = \frac{R}{N} \int_0^N \sqrt{1 - \frac{n^2}{N^2}} \; dn$

Integrating and substituting limits, we then have:

$$\bar{a} = \frac{R\pi}{4}$$

Using this mathematical method, the average value for $\underline{a}$ can be computed in each of the groups of interest. These will be outlined in their order of increasing complexity using the general formula:

$$\bar{a} = \frac{1}{N} \int_0^N \sqrt{R^2 - d_i^2} \; dn$$

I - Those planes in interval $\underline{B}$ on figure 5. For these planes, $\underline{d}$ values range from $\underline{0}$ to $\underline{e}$. Thus

$$d_i = \frac{i}{j} e = \frac{n}{N} e$$

Then $$\bar{a} = \frac{1}{N} \int_0^N \sqrt{R^2 - \frac{e^2 n^2}{N^2}} \; dn$$

Integrating and substituting limits, we have:

$$\bar{a} = \frac{1}{2}\left(\sqrt{R^2 - e^2} + \frac{R^2}{e}\sin^{-1}\frac{e}{R}\right)$$

For unit value of R, this becomes:

$$\bar{a}_1 = \frac{1}{2}\left(\sqrt{1 - e^2} + \frac{1}{e}\sin^{-1}e\right) \qquad [\,\Phi_1\,]$$

II - Those planes in interval C on figure 5. The value for d in this group ranges from 0 to R-e. Thus

$$d_i = \frac{n}{N}(R-e) \quad \text{and}$$

$$\bar{a}_2 = \frac{1}{N}\int_0^N \sqrt{R^2 - \frac{n^2}{N^2}(R-e)^2}\; dn$$

Then $$\bar{a}_2 = \frac{1}{2}\left[\sqrt{2Re-e^2} + \frac{R^2}{R-e}\sin^{-1}\left(\frac{R-e}{R}\right)\right]$$

For unit value of R:

$$\bar{a}_2 = \frac{1}{2}\left[\sqrt{2e-e^2} + \frac{1}{1-e}\sin^{-1}(1-e)\right] \qquad [\,\Phi_2\,]$$

III - Next, consider those planes which were in group C of figure 5 before etching. After etching, the values for d will all be increased by an amount e.

For this case $\bar{a}_3 = \frac{1}{N} \int_0^N \sqrt{R^2 - \left[\frac{n}{N} (R-e) + e \right]^2} \, dn$

After integrating this case:

$$\bar{a}_3 = \frac{1}{2(R-e)} R^2 \left[\frac{\pi}{2} - \sin^{-1} \left(\frac{e}{R} \right) \right] - e\sqrt{R^2 - e^2}$$

For R = 1, $\bar{a}_3 = \frac{1}{2(1-e)} \left(\frac{\pi}{2} - \sin^{-1} e - e\sqrt{1-e^2} \right)$ $[\Phi_3]$

IV - Finally, consider those planes in group D of figure 5. These planes have d values ranging from R-e to R. For this group, $d_i = (R-e) + \frac{ne}{N}$, and

$$\bar{a}_4 = \frac{1}{N} \int_0^N \sqrt{R^2 - \left(\frac{ne}{N} + R-e \right)^2} \, dn$$

$$\bar{a}_4 = \frac{\pi R^2}{4e} - \frac{(R-e)}{2e} \sqrt{2Re - e^2} - \frac{R^2}{2e} \sin^{-1} \left(\frac{R-e}{R} \right)$$

For unit R:

$$\bar{a}_4 = \frac{1}{2e} \left[\frac{\pi}{2} - (1-e) \sqrt{2e-e^2} - \sin^{-1} (1-e) \right] \qquad [\Phi_4]$$

These equations cover the case where the etching depth does not exceed the particle radius ($e \leqslant R$). When the depth of etching exceeds the length of the radius, the error remains constant at the value obtained for $e = R$. That is, for $e > R$, one half of the particles will be viewed correctly, while the other half will be measured on great circles rather than the correct contact area.

To apply a correction to a single number which is the algebraic sum of several other numbers, each one of which has a distinct and separate error, the following correction factor is defined:

$$\text{correction factor} = \frac{\text{true value}}{\text{measured value}}$$

If three values, a_1, a_2, a_3 appear at frequency f_1, f_2, f_3, and if their true values are t_1, t_2, t_3,

$$\text{correction factor} = \frac{f_1t_1 + f_2t_2 + f_3t_3}{f_1a_1 + f_2a_2 + f_3t_3}$$

This reasoning can apply for any number of variables. Using the groups of figure 5, the following summary indicates the values for computation of a correction factor to apply to the measured data:

Case	Measured $\bar{a}$	True $\bar{a}$	Fraction of Total Observations
A	Φ_2	Φ_2	$\frac{R-e}{2R}$
B	R	Φ_1	$\frac{e}{2R}$
C	Φ_2	Φ_3	$\frac{R-e}{2R}$
D	Φ_4	Φ_4	$\frac{e}{2R}$

Up to this point, all calculations have been based on the radii of the circles in the polished and etched planes. In lineal analysis, however, measurements are made based on the chords intercepted by a random line through the above described array of circles. The error in each of the above groups will, therefore, be found by comparing the sum of all possible chord lengths in the measured and in the true circles. This sum, when integrated to include all chords, will represent the area of the circle in question, which is proportional tp the square of its radius. In evaluating the correction factor, each of the $\bar{a}$ terms must, therefore, be squared whenever it appears.

The correction factor can then be written for R = 1:

$$\text{Correction factor} = \frac{\frac{(1-e)}{2}\left|\Phi_2\right|^2 + \frac{e}{2}\left|\Phi_1\right|^2 + \frac{(1-e)}{2}\left|\Phi_3\right|^2 + \frac{e}{2}\left|\Phi_4\right|^2}{(1-e)\left|\Phi_2\right|^2 + \frac{e}{2} + \frac{e}{2}\left|\Phi_4\right|^2}$$

Having set $\underline{R} = 1$ above, is equivalent to evaluating the ratio of $\frac{\underline{e}}{R}$ for each case. That is, $\underline{e}$ in the above equation must be based on unit value for the radius of the spheres. The evaluation of the correction factor is thus plotted on figure 7 as a function of $\frac{\underline{e}}{R}$. The values range from 1.0 when no etching has been applied, to a value of 0.764 when the etching depth equals or exceeds the particle radius. This value results from the value for $\underline{a}$ of $\frac{R}{4}$ as previously evaluated for $\underline{e}$ $\underline{R}$. In this case, the correction factor becomes (for $\underline{R} = 1$):

$$\frac{\frac{1}{2}\left(\frac{\pi}{4}\right)^2 + \frac{1}{2}\left(\frac{\pi}{4}\right)^2}{\frac{1}{2}(1)^2 + \frac{1}{2}\left(\frac{\pi}{4}\right)^2} = 0.764$$

To apply the correction factor to a measured value, the ratio of the etching depth to the particle radius must be estimated. This was done by measuring the angle of shadowing and employing this to measure the average etching depth for each sample. The average particle radius was then estimated by measuring the largest particles on the plate. From these measurements, the correction could be read from figure 7 and applied to the measured value for the amount of γ'. These corrected values are the ones tabulated in table IV.

Calculation of average particle size: Using the data giving the volume fraction of precipitate in each structure, together with counts of the surface density of γ' particles (number per unit area on a given plane), the average particle diameter can be computed. For this calculation, let:

h = diameter of average particle

n = surface density of γ' particles, measured as the number of particles per square inch at X11,000

f = the corrected volume fraction of precipitate in the sample = area fraction on any plane

A_p = area of the circle of intersection of the sectioning plane with the average particle

D_p = diameter of a circle of area A_p

Then:
$$\frac{f}{n} = A_p = \frac{\pi D_p^2}{4}$$

$$D_p^2 = \frac{4A_p}{\pi}$$

$$D_p = \sqrt{\frac{4A_p}{\pi}}$$

During the foregoing calculation of the correction factor for volume fraction measurements, the diameter of the average circle in the plane of sectioning after correction was shown to equal $\frac{\pi}{4}$ times the diameter of the spheres from which the sections were cut.

$$\text{Therefore, } h = \frac{4}{\pi} D_p = \frac{4}{\pi} \sqrt{\frac{4A_p}{\pi}}$$

$$\text{But } A_p = \frac{f}{n}$$

$$\text{Thus } h = \frac{4}{\pi} \sqrt{\frac{4}{\pi}} \sqrt{\frac{f}{n}} = 1.436 \sqrt{\frac{f}{n}}$$

These values for h are in terms of inches on the micrographs at X11,000 from which n was measured. To convert to angstrom units in the actual sample, these numbers must be multiplied by 2.31×10^4.

Then to convert directly from the measured variables:

$$h = 33{,}200 \sqrt{\frac{f}{n}} \text{ Å}$$

Calculation of inter-particle spacing: Having established the amount of precipitate and the average particle size in the preceding sections, there is clearly a unique value for the average distance between particles. That is, there is a relationship between the volume fraction of precipitate, average particle size, and average distance between particles such that, for a given value of volume fraction, fixing either of the two remaining variables automatically fixes the value of the other. Thus, the values for inter-particle spacing, λ, can be computed from the values for volume fraction, f, and particle size, h, derived in the previous sections.

The basis for the calculation was provided by assuming that the dispersion of γ' spheres would approximate the face-centered cubic arrangement, which is the most efficient way to pack spheres in a volume. Using this arrangement, about 74 percent of the total volume of the solid can be filled by the spheres. This limiting value is attained when the spheres touch across the diagonal of one of the faces of a unit cell of the face-centered array.

In computing the average distance between particles, the average of the two distances of closest approach was taken. The calculation was made using the following variables as defined by figure 8 which represents one face of a face-centered cubic unit cell:

S = distance between particle centers along the edge of the face

h = diameter of spheres

λ_s = distance between the edges of particles along the face edge

λ_d = distance between the edges of particles along the face diagonal

f = volume fraction of unit cell filled by spheres.

λ_a = average distance between particles based on a weighted average of λ_s and λ_d.

The following relations among these variables can be written on purely geometrical considerations:

$$\lambda_s = S - h$$

$$\lambda_d = \frac{\sqrt{2}S}{2} - h$$

$$f = \frac{4 \times \text{volume of one sphere}}{\text{volume of unit cell}} = \frac{4\pi h^3}{6S^3}$$

From the expression for f,

$$S = \sqrt[3]{\frac{2\pi}{3f}}\, h$$

In a face-centered array, each sphere will be surrounded by twelve nearest neighbors which are a distance λ_d away, and six neighbors which are a distance λ_s away. The average value of the distance between spheres on this basis then becomes:

$$\lambda_a = \frac{12\lambda_d + 6\lambda_s}{18} = \frac{2\lambda_d + \lambda_s}{3}$$

Substituting the values of λ_d and λ_s defined above, the value for λ_a reduces to:

$$\lambda_a = \frac{1 + \sqrt{2}}{3} S - h$$

Then by substituting the relation for S above:

$$\lambda_a = \left[\left(\frac{1 + \sqrt{2}}{3} \right) \left(\sqrt[3]{\frac{2\pi}{3f}} \right) - 1 \right] h$$

This equation thus defines the relation between the average inter-particle spacing and the particle size as a function of the volume fraction occupied by the spheres. This relationship (as shown in figure 41a) was then used to compute λ_a from the previously determined values of f and h. As shown in figure 41a, the limiting value for this relation occurs at a value of f, of about 74 percent which is reached when λ_d reaches zero. The value of λ_s is at its minimum at this point. Hence, the value of λ_a remains finite and the curve of λ_a/h versus f reaches its limit at a value for λ_a/h greater than zero.

The results of the calculations for λ_a based on the above relation are included in table IV. Throughout the text and in this table, this value will be referred to simply as λ, and is defined as average inter-particle spacing.

Studies of Grain Boundary Phenomena. - Measurements of grain boundary phenomena were made at X1000 with the light microscope, using an oil immersion lens. These included the number of microcracks and the number of "depleted grain boundaries." An area of 0.002 square inches was surveyed in four strips 0.0025 by 0.2 inches. These strips were parallel to the specimen axis and at the center of the reduced section in samples from interrupted tests. Measurements on completed test samples were taken on the section adjacent to the fracture. A "depleted grain boundary" was counted when a clear white strip of matrix, free of γ' particles, was clearly seen along a grain boundary. Microcracks, greater than 1 micron in length, were counted; these were easily distinguished from other features of the structure due to their complete blackness. Each distinct microcrack was counted.

X-Ray Diffraction

Identification of carbides was made by extraction of the particles in a solution of methanol and bromine. A sigma phase in laboratory heat 1172 was extracted with hot aqua-regia. The extracts were washed, dried and placed in a glass capillary. A standard powder camera was then used to obtain patterns from the extracts using filtered Cu radiation with a 10 hour exposure. Analysis of these patterns by comparison with standard patterns then completed the phase identification.

PHENOMENOLOGICAL EFFECTS OF OVERHEATING

A previous report (ref. 3) had presented the results of overheating M252 alloy from a base temperature of 1500°F. For the present investigation, this was extended to include a base temperature of 1600°F. Another alloy of a similar metallurgical type, Inconel 700, was added to the program and the effects of overheating from both 1500° and 1600°F determined. The effects of overheating were determined by the changes in rupture time under the stress normally causing rupture in 100 hours.

The overheat temperature for M252 alloy covered the range of 1650° to 2000°F for the base temperature of 1500°F, and the range of 1800° to 2100°F using the base temperature of 1600°F. Inconel 700 alloy was studied with overheat temperatures ranging from 1800° to 2200°F. The number of applied overheats varied from as few as three, to as many as could be applied at five-hour intervals during the life of the test specimen. The load was removed during the overheat exposures to avoid the influence of accelerated creep due to the presence of stress.

The test data (tables II and III) are summarized in the following sections. The data from normal, constant-temperature tests are presented to define the base properties of the materials. The changes in rupture time, rupture elongation, and creep resistance which resulted from overheating, are then defined by comparison with the base properties. These data thus indicate the property changes which were caused by the structural changes induced by overheating.

M252 Alloy

The rupture time data from the normal, constant-temperature, creep-rupture tests on the two heats of M252 alloy (fig. 9) indicated that the strength level of these two heats was typical for the alloy. On the basis of limited testing, the following stresses were selected for the base testing conditions to cause rupture in about 100 hours. Further testing defined the actual rupture time ranges indicated by the dashed curves of figure 9 and included in the following tabulation. These ranges then formed the criterion by which significant changes in rupture time from overheating were determined.

Heat	Temperature (°F)	Stress (psi)	Rupture Time (hours)
837	1600	18,000	72-97
HT-28	1600	20,000	(109-112)*
837	1500	33,000	68-86
HT-28	1500	34,000	65-105

*Based on two tests

The bars on which the data were taken for heat HT-28 at a base temperature of 1500°F (ref. 3) were heat treated as follows:

(a) Heated 4 hours at 1950°F and air cooled;

(b) Heated 15 hours at 1400°F and air cooled.

The above treatment was standard for M252 alloy at the time when these data were taken.

The tests on heat HT-28 at 1600°F and on heat 837 at both base temperatures were from material with the following treatment, which became accepted since the data of reference 3 were taken:

(a) Heated 1 hour at 2150°F, air cooled;

(b) Heated 4 hours at 1950°F, air cooled;

(c) Heated 15 hours at 1400°F, air cooled.

The elongation and reduction of area (table II) were high and within the expected degree of reproducibility. Creep curves for the normal rupture tests at the stresses used in the overheat tests

(figures 10a, 11, 12 and 13) showed that in all cases the creep rate increased from the start of the test, and that a large portion of the elongation was accumulated during the final few hours of testing. The creep curves exhibited normal agreement between tests and were highly reproducible for heat 837 at 1600°F.

Typical microstructures are shown (fig. 14) for both heats in the heat treated condition and after rupture testing at 1600°F.

The effects of the repeated overheating on the creep-rupture properties of M252 alloy can be summarized as follows:

(1) A sufficient number of overheats to 1900° and 2000°F from the base temperature of 1500°F, and overheats to 2000° and 2100°F from a base temperature of 1600°F, resulted in significantly increased rupture time (fig. 15) for both heats. From 5 to 10 cycles of overheating, applied from the start of the tests, were necessary to increase the rupture time to the point where it was definitely beyond the range for the normal tests. Overheats to 1800°F from either 1500° or 1600°F did not significantly affect the rupture time of heat 837. When heat HT-28 was overheated to 1800°F from 1600°F, the rupture time was reduced slightly. Overheats on heat HT-28 to 1650° or 1800°F from 1500°F resulted in times slightly below the range for normal tests.

(2) Elongation and reduction of area were reduced by overheating (fig. 16 and table II). Overheating to 1650° or 1800°F was generally more damaging to ductility than overheating to the higher temperatures. In addition, tests at the base temperature of 1500°F suffered greater ductility losses for a given overheat condition than those at 1600°F. Several overheats again were necessary before the loss was sufficient to bring the elongation values below the range of normal tests.

(3) Overheating to 1900°, 2000°, or 2100°F reduced the rate of increase in creep rate (figs. 10-13) below that of normal tests. Overheats to 1650° or 1800°F accelerated creep for heat HT-28 (figs. 12 and 13), while overheats to 1800°F had little effect on heat 837 (figs. 10b and 10c). When the overheats were discontinued before rupture occured, the creep rate showed no sudden change. It gradually increased to the relatively high creep rate characteristic of the alloy during the final hours of testing prior to fracture.

For M252 alloy, overheats altered rupture time by changing creep resistance. Overheats to 1800°F slightly reduced rupture time for the heat in which it reduced creep resistance slightly. In all cases, overheats to 1900°F or higher increased rupture time by increasing creep resistance. The reduction in elongation as a result of overheats had no significant effect on rupture time because the specimens simply fractured with less elongation during the last few hours of the tests when the creep rate was extremely fast.

Inconel 700 Alloy

The results of the normal creep-rupture tests for the Inconel 700 material (table III) are plotted as figure 17. It was originally estimated on the basis of limited data that the following stresses would cause rupture in about 100 hours:

1600°F -------- 29,000 psi

1500°F -------- 43,000 psi

These stresses were those selected for the overheat tests. Subsequent testing at these stresses disclosed a wide scatter in rupture times (fig. 17). Analysis of the data of table III and of the creep curves from tests at 1600°F (fig. 18a) showed that specimens from an individual bar of stock exhibited similar properties. The scatter was due to variations in the properties between bars of stock supplied.

It was noted that those specimens with the longest rupture time also had the highest elongation. Thus, there was a correlation between rupture time and elongation (fig. 19).

The creep curves at 1600°F (fig. 18a) showed that the Inconel 700 exhibited a brief period of decreasing creep rate followed by a period of essentially constant creep rate. The time period at which the creep rate increased varied to a considerable extent between bars. Those which required the longest time for an increase in the creep rate also had the highest elongation. During the period of decreasing and constant creep rate, there was no significant difference between specimens from the different bars. The essential difference causing the variation in rupture time was the time at which creep rate increased and the amount of subsequent elongation before fracture. The behavior in normal creep-rupture tests at 1500°F was similar to that at 1600°F. (fig. 20).

Typical microstructures (fig. 21) are shown for material as heat treated and after rupture testing at 1600°F. No significant differences were observed to account for the variations in creep-rupture properties. There were some differences in grain size which did not correlate with the properties. The only exception was the abnormally high elongation of samples from bar 50 associated with a smaller than average grain size.

Because the creep-rupture characteristics were only reproducible between specimens from the same bar, it was necessary to evaluate the effects of overheating in terms of the normal properties of each bar. This was not recognized until a good deal of testing had been completed. Consequently, there are many results from overheat tests in table III where the normal properties are not available for the bar from which the specimens were taken. This type of data was

available for most of the specimens overheated from 1600°F. At 1500°F, however, normal test data were not available for all of the bars which provided specimens for overheat testing. Normal rupture tests (table III) had been conducted at both 1500° and 1600°F for three other bars. In addition there were test results at 1600°F available for the bars from which the specimens were taken for overheat tests at 1500°F. The rupture times for the three bars tested at both 1500° and 1600°F were plotted as a function of test temperature. The values for the tests at 1600°F for bars used for overheat tests at 1500°F were then plotted at 1600°F and extrapolated to 1500°F parallel to the three known curves. This resulted in estimated values of normal rupture time at 1500°F for each bar used for overheat tests at 1500°F and an estimate of the range in times between bars at 1500°F. These estimated values appear in table III on figure 22.

The influence of overheating on Inconel 700 alloy from 1600°F was as follows:

(1) The rupture times at 1600°F were generally unchanged from that of the normal test by overheats to 1800°F (fig. 22). Overheats to 2000°, 2100°, or 2200°F caused a reduction in nearly every case. The rupture time of each overheated specimen is compared to that from a normal test on a specimen from the same bar as that used for the overheat test. Apparently from 3 to 5 overheats had to be applied before the reduction in rupture time was large enough to be significant. The extent of reduction in rupture time appeared to be about the same for all three of the higher overheat temperatures. The higher temperature overheats also possibly reduced rupture life at 1500°F more than at 1600°F.

(2) The elongation at fracture (fig. 23 and table III) was reduced by overheats to 2000°F and higher, but was unaffected by overheats to 1800°F. The elongation values from the tests overheated from 1600°F are plotted on figure 19 against the time for rupture, together with the data from the normal rupture tests. These extend the correlation to shorter rupture time and lower elongation and demonstrate that elongation also correlated with rupture time for overheated tests. There were not sufficient normal tests at 1500°F on specimens from the same bars as those used for overheat tests. Such data as were available indicated that overheating affected ductility at 1500°F the same as it did at 1600°F.

(3) Creep resistance (fig. 18) was unaffected by overheats to temperatures over the entire range of temperatures used in the investigation. When the overheat temperatures were 2000°F and higher, the creep curves show that rapid creep to fracture started at shorter time periods and fracture occurred with reduced elongation during this period. The larger the number of overheats, the shorter the time at which deviation followed by rapid failure occurred. These characteristics are most evident in figures 18b through 18i, which compare

creep curves for specimens from individual bars. The data for tests overheated from 1500°F were not as conclusive due to the lack of comparative normal creep data for specimens from a given bar. The available data (fig. 20) indicated that the effects of overheating on creep were similar to those for 1600°F.

In the case of Inconel 700, overheating to 1800°F did not change creep resistance or ductility. Consequently, it did not change rupture time. When the overheat temperatures were 2000°F or higher, rupture time was reduced because the ductility was reduced. There was no effect on creep resistance up to the point where fracture occurred.

METALLURGICAL CAUSES OF OVERHEAT PHENOMENA

The influence of overheating on rupture life must have been due to the effects of overheating on the microstructural features controlling creep resistance and elongation. The data outlined in the previous section further showed that the response of M252 to overheating depended primarily on the effect on creep resistance, while it depended on the influence on ductility for Inconel 700, although they were both nickel-base alloys primarily strenghtened by γ' precipitates. The microstructures of the two alloys were, therefore, studied to provide an explanation of the influence of overheating on creep-rupture properties and to determine why the two responded differently.

The γ' precipitate was studied in its relation to creep resistance. The processes leading to fracture, particularly the structural changes at the grain boundaries were related to the ductility.

To keep the work within practical limits, these studies were limited to samples from tests at the normal base temperature of 1600°F, and in the case of M252 alloy, largely to heat 837. These limitations were justified since overheating had the same qualitative effect on creep-rupture properties at base temperatures of 1500° or 1600°F, and in the case of the M252, for both heats.

Limited data were obtained concerning the influence of chemical composition on various aspects of the structural features.

Microstructural Features and Creep Resistance

The creep resistance of nickel-base alloys alloyed with Al+Ti depends primarily on the precipitation of γ'. The state of the γ' was, therefore, studied for both the M252 and Inconel 700 alloys.

Changes in γ' During Exposure at 1600°F. - The γ' in the matrix of both alloys was in the form of small spheroidal particles (figs. 24 and 25), the number, size, and spacing of which depended on the times of exposure at 1600°F. Using samples given the standard heat treatment for the alloys, the state of the γ' was measured as a function of exposure time at 1600°F for time periods up to 200 hours. Measurements were made from electron micrographs of the samples using the techniques described in the Procedures Section. These measurements (table IV) show that after any given time of exposure to 1600°F, Inconel 700 contained a larger amount of γ' than did the M252 as would be expected from its higher Al+Ti content. These data show the following effects of increasing time of exposure to 1600°F on the γ' in either of the alloys:

(1) The size of the γ' particles increased (fig. 26);

(2) The number of particles decreased (fig. 27);

(3) The spacing between particles increased (fig. 28);

(4) The measured volume of γ' decreased (fig. 29).

For M252 alloy, the γ' particles could not be resolved after the standard heat treatment (solution treat plus age 16 hours at 1400°F). About one hour at 1600°F was required for the particles to grow to a measurable size. For Inconel 700 alloy the standard heat treatment included aging at 1600°F so that the γ' particles could be measured in this condition. During the first few hours of exposure to 1600°F, the γ' particle size in M252 grew rapidly to that in Inconel 700 and both alloys had similar size particles for most of the exposure periods.

All of the observed changes would be expected for the precipitation and growth of particles of a compound, except for the apparent decrease in volume. This is unusual for a precipitation process since the volume of precipitate would normally be expected to increase if it changed at all.

In order to establish that the measured changes in γ' were representative of the structural changes which occurred during rupture testing at 1600°F, a group of samples from both interrupted and completed rupture tests were examined. The presence of stress did not affect the general response of the γ' precipitation reaction (table IV and figs. 28-29). For Inconel 700 alloy, there were no significant differences in the γ' between the rupture test samples and those exposed without stress for the same time period. The measurements on samples from the rupture tests on M252 alloy, although showing the same trends in response, indicated the presence of slightly greater amounts of γ' than the samples heated without stress for the same time period. A sample exposed without stress for 50 hours in a rupture unit indicated (table IV) that this arose from the slower cooling rate from the test temperature in the rupture units than was

used for the small water-quenched samples. This effect in M252 alloy and the lack of a similar effect in Inconel 700 alloy will be discussed in detail later.

For both alloys, all of the changes in structure observed to occur with increasing time of exposure at 1600°F would usually be expected to lead to a decrease in creep resistance with time during tests at 1600°F. For M252 alloy, such was the case: the creep rate increased from the start of the tests (fig. 10). Tests on Inconel 700, however, (fig. 18a) exhibited a definite period of decreasing creep rate followed by a period of nearly constant creep rate so that the normal relation between a precipitate and creep resistance did not hold for this alloy. Following the period of constant-rate creep, the creep rate of Inconel 700 samples increased quite rapidly leading to fracture.

Considerable variation was noted between specimens from different bars in the time at which acceleration of creep occurred. Data from samples of bar 15 and bar 20 (table IV) showed, however, that there was no difference between these bars in the rate at which the state of the γ' changed with increasing time of exposure at 1600°F, although a test from bar 20 showed accelerated creep much earlier than one from bar 15. Thus, there was necessarily a difference in the state of the γ' in these two bars at the time that accelerated creep began, so that the γ' could not have controlled the time at which the acceleration of creep took place.

Thus, although the same type of changes in the γ' were noted in both alloys during exposure at 1600°F, they did not appear to be equally related to the creep characteristics in normal creep-rupture tests.

Effect of Overheating on the γ' Precipitate. - Examination of the structures of samples from both alloys which had either been interrupted immediately following an overheat, or fractured soon after an overheat (figs. 30, 31, and 32), demonstrated that, for both alloys, overheats to 2000° or 2100°F resulted in a fine dispersion of small particles. The dispersion and apparent amount of γ' was about the same as that obtained during the first 2 to 10 hours of constant temperature exposure to 1600°F. Thus, since no net structural changes resulted throughout the period of application of the overheats, these data indicated that each overheat to these temperatures was effective in arresting the agglomeration and apparent decrease in amount of γ' which had taken place during the preceding 5 hours at 1600°F.

When samples were allowed to continue at 1600°F after a limited number of overheats to 2000° or 2100°F, the size and spacing of the γ' particles increased. At the same time, the number of particles and the apparent volume fraction of γ' decreased.

Overheats to 1800°F yielded a structure with a mixed particle size for both alloys. As a result, the average size and spacing of the precipitates could not be calculated. The apparent volume fraction of γ', as measured from such samples, however, was not significantly different from that in normal tests after the same amount of time at 1600°F (table IV). Since the creep resistance was not measurably changed by overheats to 1800°F, the effective particle size and dispersion were apparently similar on the average to those in the normal tests.

Relation Between γ' Solution Temperature and Effects of Overheating. - Published data (ref. 8) suggested that the temperatures of overheating which maintained the fine dispersion and large apparent amounts of precipitate were above the equilibrium solution temperature for the γ'. They further suggested that the solution temperature for γ' was near 1800°F in M252 and above 1800°F in Inconel 700. To confirm these indications, the solution temperature under near-equilibrium conditions was determined for both M252 and Inconel 700. In addition, the solution temperatures were established for heat HT-28 of M252 and for three experimental alloys produced for the present investigation. Small samples were heated for four hours to a series of temperatures spanning the expected solution temperature and quenched in iced-brine. In this way, based on both the disappearance of the original γ' particles and a drop in hardness, the solution temperature was determined to within 25°F. Data from M252 (heat 837) and Inconel 700 alloys are included (figs. 33, 34, and 35) to demonstrate these effects. Both the micrographs and the hardness values taken from samples heated above the solution temperature for the γ' indicate that the severe quench used on the small samples suppressed the γ' reaction fairly completely. The large particles remaining in the structures of both alloys are carbides.

Based on these results, the indicated solution temperature ranges are plotted on figure 36 as a function of total Al+Ti content in each alloy. The overheat temperatures maintaining fine γ' in both alloys were above the temperature for complete solution of γ'. Overheats to 1800°F were just above the solution temperature for M252, while they were well below for Inconel 700.

For comparison with the present data, the curve reported by Betteridge and Franklin (ref. 8) for solution of γ' in 80 Ni-20 Cr and 60 Ni-20 Cr-20 Co alloys containing a 2:1 ratio of Ti : Al is shown. Also plotted on this figure are the results of the solution temperature determinations on the other experimental materials from the present investigation. Good agreement was obtained between the data reported by Betteridge and Franklin and those from the present study.

The foregoing studies considered the γ' reaction under conditions which approached equilibrium. By comparison, the two-minute exposures to the overheat temperatures were of relatively short duration.

Yet since the overheats to the higher temperatures kept the γ' precipitate fine, the particles must have gone into solution and reprecipitated during cooling to the base testing temperature. The rates of solution and reprecipitation of the γ', therefore, necessarily had to be rapid. This was confirmed by iced-brine quenching a small sample of M252 from heat treated bar stock after each step in the following treatment:

1) Held four hours at 1600°F to provide a resolvable precipitate size and dispersion;

2) Heated from 1600° to 2000°F and held for two minutes;

3) Cooled to 1600°F and held for five minutes;

4) Held an additional five minutes at 1600°F for a total of 10 minutes.

Heating and cooling rates closely reproduced the conditions in an overheat test. The microstructures of these specimens (fig. 37) show that complete solution of the γ' took place during step (2) and the reprecipitation occurred during step (3). The additional five minutes holding in step (4) did not result in a detectable change in structure.

Additional information concerning the amount of time required for precipitation of the γ' following an overheat was provided by a distinct thermal arrest (fig. 38) in the cooling curves from overheats to temperatures above the γ' solution temperature. These thermal arrests occurred about 100-150°F below the equilibrium solution temperature for the γ' in each alloy. Since no other phase changes were observed, the thermal arrests must have resulted from the $\gamma - \gamma'$ reaction. This further confirmed that reprecipitation of γ' took place during cooling to 1600°F.

Comparison of the cooling curve from an overheat (fig. 38) with the amount of super-cooling below the equilibrium solution temperature indicated by the thermal arrests to be required to initiate reprecipitation, shows that the reaction actually began about 1 to 1-1/2 minutes after the temperature entered the two phase $\gamma + \gamma'$ region and was essentially complete in about one minute. Both M252 and Inconel 700 alloys had thermal arrests during cooling from 2000° or 2100°F, the overheat temperatures which caused complete solution during the overheats. On the other hand, the samples which were overheated to 1800°F did not exhibit thermal arrests on cooling. The structure of both alloys after overheating to 1800°F gave evidence that partial solution of the γ' had taken place during the overheats but that a large proportion of the γ' particles remained undissolved. For Inconel 700 alloy, this effect related basically to the fact that the equilibrium solution temperature was considerably above 1800°F so that the potential for complete solution did not exist. For M252

alloy, the solution temperature was just below 1800°F. For this alloy, the two minutes at 1800°F were insufficient for complete solution during an overheat.

These data demonstrated that the rate of solution and reprecipitation of γ' was amazingly rapid at 2000° or 2100°F. However, since the maintenance of the fine dispersion and high apparent volume of γ' in the structure required relatively complete solution of the γ' the two-minute cycles employed were not effective when the overheat temperature was only slightly above the equilibrium solution temperature. By inference from these data, the effect of overheats to temperatures well below the γ' solution temperature (e.g. overheats to 1650° from 1500°F) would be to accelerate the agglomeration and apparent decrease in amount of precipitate during normal testing.

Relation Between Structure and Creep Resistance. - Based on the theoretical consideration of dislocation movement during secondary creep, Weertman (ref. 9) developed equations relating creep rate to the microstructure of alloys containing a dispersed second phase. A summary of his theory and its application to the data of the present investigation follows.

Basis of Weertman's theory: When stress is large enough to activate the Frank-Read sources in the alloy, but not sufficiently large to generate and move enough dislocations to cause pile-up at the dispersed particles, the creep rate will be governed by the rate of climb of the dislocations over the dispersed phase and can be written:

$$K_1 = \frac{\pi D b^3 \sigma}{4\sqrt{2}\, kTh^2} \qquad \text{where,} \qquad \text{(a)}$$

K = creep rate

D = coefficient of self-diffusion

b = length of Burger's vector for dislocations

σ = stress

k = Boltzman's constant

T = absolute temperature

h = particle size

μ = shear modulus

λ = distance between particles

The limit imposed on this equation (no pile-up of dislocations) should be met so long as $\sigma < \frac{\mu b}{2\lambda}$. When the only variation is the dispersed

phase for a given test temperature, equation (a) can be written

$$K_1 = C_1 \frac{\sigma}{h^2}, \qquad (b)$$

When $\sigma > \frac{\mu b}{2}$, the stress is high enough to cause pile-up to occur and force dislocations past the particles by pinching off loops around them. The rate controlling aspect then becomes the speed with which the loops are annihilated by climb to dislocations of opposite sign. Weertman showed that in this stress range the creep rate can be expressed as follows:

$$K_2 = \frac{\pi D \sigma^4 \lambda^2}{8\sqrt{2}\, kT\mu^3 h}$$

For a given alloy and test temperature with only the dispersed phase changing, this reduces to

$$K_2 = C_2 \frac{\sigma^4 \lambda^2}{h} \qquad (d)$$

The values for K_2 are valid up to the point where $\sigma^2 = 2\mu kT/\lambda b^2$. At this point, the velocity of climb assumes a new form and the creep rate equation must be changed. The following considerations of the structures demonstrate, however, that the conditions under which K_3 is valid were never approached for the tests carried out on M252 and Inconel 700.

The stress and test temperature were constant for each alloy in this investigation. The limiting factors, in terms of the changing structure, can then be written as follows:

K_1 holds when $\lambda < \mu b/2\sigma$

K_2 holds for $\lambda > \mu b/2\sigma$ up to $\lambda = \frac{2\mu kT}{\sigma^2 b^2}$

The values for these limiting quantities were estimated for both alloys. In making these estimates, the value for μ was calculated from the values of E at 1600°F of about 19 x 10^6 usually measured for these alloys, and assuming the theoretical value for Poisson's ratio of 0.25 for isotropic materials. This gave $\mu = 7.6 \times 10^6$. The value for b, the Burger's vector, was based on the assumption that b would equal the slip distance in the unit cell of the matrix. For FCC systems, this is [110] (111), which equals $\frac{\sqrt{2}}{2}(a_o)$. For $a_o = 3.58$ Å, b then equals 2.5Å. Under these assumptions, the theoretical limits on λ for which the equation K_1 and K_2 were valid were as follows:

Alloy	$\mu b/2\sigma$	$2\mu kT/\sigma^2 b^2$
M252	528Å	17,150Å
Inconel 700	328Å	6,610Å

For both alloys, comparison of the experimentally determined values of λ (table IV) with those calculated from Weertman's theory and tabulated above showed that the actual values for λ were near the lower end of the range in which Weertman's derivation indicated K_2 to be valid. The upper limit of λ for which K_2 should hold, as predicted by Weertman's theory, was clearly beyond the largest values for λ obtained experimentally.

Since the actual values of λ were in the range where Weertman's theory predicts behavior according to his K_2 relationship, and the alloys did not exhibit the behavior required by K_1, the data indicated that the testing was conducted in the range of structure for which K_2 was valid.

When the alloys were overheated to 2000° or 2100°F, the values of λ remained near the levels ordinarily obtained after about 2 to 10 hours of exposure during a normal creep rupture test. The behavior for both alloys thus would be expected to follow:

$$K_2 = C_2 \frac{\sigma 4 \lambda^2}{h}$$

Since the stress was nearly constant during the tests, at least up to the point where tertiary creep began to occur, the changes in creep rate should be linearly proportional to the changes in the structure reflected by the ratio, λ^2/h.

Application to experimental data: The instantaneous creep rates were plotted against λ^2/h for both alloys (figs. 30 and 40). Although K_2 is defined for secondary creep, the test data were plotted from the beginning of the tests for comparison with the theory, since it was not clear from the creep data exactly how to define secondary creep.

For M252 alloy, the creep rate values were measured from an average creep curve drawn from the creep durves of figure 10a. Under the test conditions used, secondary creep for a stable structure should begin at about 10 hours and extend to about 40 hours. The data showed (fig. 39) that the creep rate changed in a nearly linear fashion with changes in λ^2/h from the 10th to the 40th hours. This suggests, therefore, that the increase in creep rate during this period was due to the increase in particle spacing, λ , and size, h. During the first 10 hours, the creep rate was higher than that suggested by the nearly-linear trend of the succeeding data points, as would be expected from a tendency for normal primary creep to be superimposed on the changing effect of structure. Similarly, beyond 40 hours, the

deviation from the suggested linearity could be due to the effect of third-stage creep being superimposed on the effect of the changing structure. The strain in the material had exceeded 3 percent at this time and the increase in stress which resulted should begin to cause an acceleration of creep rate in a constant load test. In addition, internal microcracking as well as surface cracking could be contributing to the tertiary creep.

The structure parameter, λ^2/h, increased considerably during the course of normal creep-rupture tests. When M252 alloy was overheated to 2000° or 2100°F, however, the resultant structural changes restored the value of the parameter to the same level as it was at the beginning of the tests. The creep rate, after an overheat cycle, was also at the level shown at the beginning of testing, as would be predicted by the lower parameter level. In tests which were repeatedly overheated, this creep rate prevailed until the creep strain reached about 3 percent. At this time, as previously discussed, tertiary creep began to be superimposed on the creep rate due to structure alone. Thus, even though the influence of the instability of the γ' between overheats was uncertain, the data indicated good agreement between the structural parameter and creep rate. This agreement indicated that the improved creep resistance from overheating to 2000° or 2100°F was the result of retention of a smaller particle spacing, λ, and size, h, in M252.

For Inconel 700 alloy, the values of creep rate plotted on figure 40 were taken from the curves of figure 18a. During the period of decreasing creep rate and the first hours of constant rate creep, the samples all exhibited similar behavior so that the creep rates for the first 25 hours of the tests could be measured from an average curve representative of all data. As previously discussed, however, a considerable difference existed between the original pieces of bar stock in the time at which the creep rate began to increase. Therefore, in measuring the creep rates during this period from figure 18a, measurements were made from an average curve representing samples which exhibited an early increase in creep rate, as well as from a curve representing samples with the longest durations constant-rate creep. Both sets of measurements are included on figure 40.

The relation of creep rate to the structural parameter, λ^2/h, was quite different from that of M252. The actual values of the parameter were much smaller for Inconel 700 than for M252 alloy after the same times at 1600°F. In addition, the parameter values remained nearly constant during the duration of the tests, only changing from about 115 to 300Å even though the agglomeration which occurred during the tests caused a considerable increase in γ' particle size, h. At the same time, the creep rate decreased for the first 2 to 3 hours of the tests and then remained essentially constant out to about 25 hours.

Thus, in Inconel 700 alloy, the changes in structure which did occur during normal testing had only a small effect on the parameter,

λ^2/h. Since creep rate appeared to depend on the structural variables represented by the parameter, the existence of a time period during which the creep rate did not change significantly was not surprising. Thus, even though the normal structural changes were prevented by overheating to 2000°F or higher, no significant effect on creep rate could result.

The increase in creep rate which occurred beyond 25 hours probably resulted from the factors which ultimately caused fracture rather than from the changing structure of the intragranular γ', as represented by λ^2/h.

Discussion of structural parameter: The reason for the difference in sensitivity of the structural parameter, λ^2/h, of Inconel 700 and M252 to agglomeration of the γ' precipitate during exposure at 1600°F can be deduced from consideration of the geometry of the distribution of the precipitate particles. For a given volume fraction of randomly-dispersed uniform-sized spherical particles, the ratio λ/h is constant, regardless of the number of particles and their size. As the volume fraction of precipitate being considered is changed, the required ratio λ/h also changes. The dependence of λ/h on f (f = volume fraction) is such that as f increases, the value of λ/h decreases (fig. 41a), reaching the theoretical limit for f=0.74 when the spheres touch one another. This relationship can be easily extended to Weertman's creep dependence factor of λ^2/h. Using the data of figure 41a, values for λ^2/h were calculated as a function of h for two levels of f, 0.25 and 0.40. These levels were taken as being approximately representative of M252 and Inconel 700 during secondary creep, respectively. The results of these calculations (fig. 41b) demonstrate that when the amount of precipitate in a system is relatively low (as in M252), the value of λ^2/h is sensitive to changes in h and varies with h over a wide range of values. When f is larger (as in Inconel 700), λ^2/h has much lower values and does not change so much with changes in h.

Weertman's postulation that creep rate should be related directly to the parameter, λ^2/h, therefore seems to explain the observed effects of overheating in fairly fundamental terms. The difference in behavior between M252 and Inconel 700 stemmed from the geometric consequences of the difference in the amount of γ' in their structures. That is to say, overheating could only improve the creep resistance of a material in which changes in the state of the γ' would cause changes in the parameter λ^2/h. M252 was sensitive to changes in the state of the γ' while Inconel 700 because of its higher amount of γ', was not.

In the foregoing discussion, no attempt was made to calculate creep rates quantitatively from Weertman's equation. However, the prediction of creep rate in Equation (c) was shown to reduce to:

$$K_2 = C_2 \sigma^4 \lambda^2/h$$

for constant temperature. Thus further reduced to

$$K_2 = (C_2 \sigma^4)\ \lambda^2/h$$

for constant stress so that the creep rate became a function of λ^2/h alone. From this viewpoint, figure 41b indicated that for the particle sizes existing in M252 alloy during secondary creep, it should have had much lower creep resistance than Inconel 700.

In conducting the tests, a stress of 18,000 psi was used for M252 and 29,000 psi for Inconel 700. Weertman's theory states that the difference in stress would be properly taken into account by the equation:

$$K_2 = C_2 \sigma^4 \lambda^2/h$$

A plot of creep rate versus $\sigma^4\lambda^2/h$ (fig. 42), however, showed that the creep rate of M252 was considerably higher than it was for Inconel 700 for a given value of $\sigma^4\lambda^2/h$. Thus, introducing stress into the equation did not correlate the creep rates of the two alloys to the single curve which would be expected.

The reasons for the lack of a quantitative agreement of creep rate between the two alloys through use of Weertman's equation were not established. Some rough checks of the relationship between stress and creep rate indicated that σ^4 is at least nearly correct. In attempting to correlate the data from the two alloys, the assumption was made that the matrix characteristics of the two alloys were approximately the same and, therefore, the value of the constant C_2 would be the same. C_2 contains two terms which, however, could be quite different for the two alloys. D was defined by Weertman as the coefficient of self diffusion for the metal being considered. In the derivation, however, this was a simplification to represent vacancy diffusion. The compositional differences between the two alloys are such that there could easily be a considerable difference in vacancy diffusion. The constant also includes the shear modulus, μ. If there was a marked difference in the way μ falls off with temperature, it also could be quite different between the two alloys.

In addition to the possibility that differences in the constant between the two alloys could account for the lack of quantitative agreement when creep rates were compared between the two alloys, one other factor should be considered. The calculations based on Weertman's parameter were actually only effective in comparing changes in creep resistance for a given material. The level of strength for any material will depend on many other variables as well as on the state of the γ'. Such effects can also influence the results for a given alloy. For example, the creep resistance of M252 was higher after overheats to 2100°F than after overheats to 2000°F. Since there was no significant difference in the γ' dispersion for these two temperatures of overheating, some other factor than γ' was influencing creep resistance for this alloy.

In view of the complexity of the situation, further work would be required to determine the specific cause for the lack of quantitative agreement between the two alloys. Since the difference in response to overheating between the two alloys was accountable on the basis of the geometrical aspects of the γ' distribution, the lack of quantitative agreement probably involves the factors in the constant C_2 in Weertman's equation.

Apparent Variations in Amount of γ'

The apparent decrease in amount of γ' within the grains during exposure to 1600°F was seemingly anomalous, being foreign to the usual concepts of precipitation processes. In addition, the volume fraction which was occupied by the γ' within the grains early during exposure to 1600°F seemed very high.

Comparison With Published Phase Diagrams. - As a reference against which the volume fraction data could be compared, the published phase relationships for alloys of the same general type as those being studied were reviewed. Betteridge and Franklin (ref. 8) determined the solution temperature for the γ' phase in alloys containing various amounts of Al and Ti in an 80 Ni-20 Cr or 60 Ni-20 Co-20 Cr matrix with the Ti:Al ratio equal to 2:1. These data were previously compared with the solution temperature for the γ' for alloys of the present investigation, and fair agreement was found. Taylor (ref. 10) reported a more comprehensive study of the phase relations in the Ni-Cr-Ti-Al system under conditions approaching equilibrium at 1382°F (750°C) and 1832°F (1000°C). His data permit an estimation of the effect of variations in the Ti:Al ratio and, in addition, permit inclusion of the effect of the solubility of Cr in the γ' phase. Rogen and Grant (ref. 11) published results of chemical analyses of extracted γ' precipitates showing the presence of 4 to 5-percent Cr.

The available data from the present investigation were used to estimate the phase boundaries for M252 and Inconel 700 alloys. These estimates were based on the experimental solution temperatures for the γ' and the amounts of γ' at 1600°F suggested by the volume fraction data of figure 29. The solution temperature data fixed one point on the boundary between the γ and $\gamma+\gamma'$ fields. A second point at 1600°F was located so that the amount of precipitate calculated by the lever arm rule would agree with that estimated from figure 29 by extrapolation of the curves to the minimum values suggested by the data (15 to 16-percent for M252 and 26-percent for Inconel 700). This point was also chosen so that the γ' would contain approximately the amount of Cr reported by Rogen and Grant. These estimated diagrams (figs. 43 and 44) were then compared with the data of Betteridge and Franklin and of Taylor. The following points can be noted from these comparisons:

(1) For M252 (fig. 42), the boundary between the γ' and $\gamma + \gamma'$

fields was less steep than that reported by either of the former studies, and fell at lower values of Al+Ti for any given temperature.

(2) To make this boundary parallel to those of the other two investigations would have required that the $\gamma+\gamma'-\gamma'$ phase boundary be located at about 10-percent Cr, or that the equilibrium amount of γ' be much lower than is suggested by figure 29. Hence, the $\gamma'-\gamma+\gamma'$ boundary was placed at 5-percent Cr to maintain agreement with the data of Rogen and Grant, and the $\gamma+\gamma'-\gamma$ boundary was located as shown.

(3) For Inconel 700 alloy, the estimated phase diagram (fig. 44) showed better agreement with the published diagrams than was obtained for M252. The $\gamma+\gamma'-\gamma$ boundary was between those of the two previous studies and parallel to them. The $\gamma'-\gamma+\gamma'$ boundary was located at 4-percent Cr, which was in rather close agreement with Taylor's work.

These volume percentages of γ' are, however, much lower than the measured values at the start of testing. In fact, the apparent volume of γ' initially present in both alloys was considerably larger than was possible for the Al+Ti in the alloys, if the γ' is considered to be stoichiometric Ni_3Al containing Ti and Cr as suggested by the approximated diagrams. The maximum possible amount of γ' for this condition, assuming the solubility for Cr indicated by figures 43 and 44, calculates to be:

	M252 (heat 837)	Inconel 700
Titanium (atomic percent)	3.34	2.35
Aluminum (atomic percent)	2.10	6.48
Al+Ti (atomic percent)	5.44	8.83
Cr in γ' (atomic percent)	(5/20)(5.44)= 1.36	(4/21)(8.83)= 1.68
Al+Ti+Cr (atomic percent)	6.80	10.51
Maximum γ' (volume %)	4 x 6.8 =27.2	4 x 10.5 = 42.

Even though these maximum possible volume percentages are larger than those suggested by the phase diagrams, the apparent volume fraction of γ' initially measured was still larger. Furthermore, the progressive decrease in amount of precipitate during exposure would require explanation even if there were sufficient Al+Ti in the alloy to permit formation of the large amounts of γ'.

Possible Explanations of Apparent Volume Changes. - There are basically two avenues of approach to the question of decreasing apparent amounts of precipitate during exposure at 1600°F. Either a true volume fraction change occurred, or the measurements of volume fraction were in error in such a way that the apparent amount of precipitate became smaller as the particle size increased. Since the scope of the present study did not include sufficiently detailed information to permit an unequivocal choice between these possibilities, both of them will be discussed and related to the pertinent results of the present investigation.

Errors in particle measurement: The similarity of crystallographic structure between γ and γ' suggested the possibility of an error in location of the interface between the two phases. It also suggested the possibility of coherency with a compositional and strain gradient at the interface. These effects could result in the etching indicating particles larger than the true γ' size. If this were so, the error in volume percentage would be largest when the particles were smallest and most numerous. As the particle size increases, this error would decrease and the values approach more nearly the true volume fraction. Rough calculations suggested that all the measured volume decrease could be accounted for on this basis. However, the etching developed a sharp interface between matrix and γ' with no indication that gradients were influencing the defined particle sizes.

An error of this nature would not alter the way in which creep resistance changes were qualitatively accounted for by the changing particle sizes. Only the magnitude of the numbers would be changed. Calculations were carried out assuming that the measured change in volume fraction was an etching effect. This, however, did not make the agreement in quantitative prediction of creep rate any better than was found in the previous section.

The minimum volume fractions suggested after 200 hours exposure by figure 29 were in fair agreement with those predicted from the phase diagrams as previously discussed. This, however, did not aid in establishing whether there was a true volume decrease or an etching effect.

Actual decrease in amount of γ': An equally satisfactory mechanism to explain the abnormally high initial apparent volume of γ' and its decrease with time of exposure could be predicted on the initial formation of non-stoichiometric γ'. This approach was used by Underwood et al (ref. 12) to explain a larger than expected amount of precipitate in Cu-Al alloys. Bigelow (ref. 13) has suggested mechanical entrapment of matrix atoms in γ' to account for an abnormally large volume of γ' in Al+Ti bearing nickel-base alloys.

The reaction by which γ' forms in M252 and Inconel 700 has been shown to be very rapid. It is, in fact, difficult to suppress the reaction on cooling from the solution temperature. Certainly, it was not suppressed under the cooling conditions used for solution treating the creep-rupture and overheat test specimens. Thus, the conditions for entrapment existed.

Bigelow's mechanism would not only provide for entrapment but would imply the precipitation from solution of an initially larger amount of Al+Ti than would exist at equilibrium. Due to the violence of the reaction, all or nearly all the Al+Ti would initially participate in precipitation. Then, during subsequent exposure to 1600°F, the composition would tend to return to equilibrium. At first, there

would be solution of the smaller particles formed during cooling from solution treatment. When the equilibrium Al+Ti in the matrix was restored by this process, some particles would begin to grow at the expense of others. This would allow the entrapped matrix atoms to return to the matrix from those particles which disappeared. Eventually, the point would be reached at which entrapped matrix atoms would have to diffuse to the surface of the particle in which they were contained in order to return to solution.

Comparison of the rate at which the apparent volume of γ' decreased, with the rate at which the number of particles decreased, suggested that if this type of mechanism was occurring, most of the separation of foreign atoms from the γ' occurred by solution of the whole particles during agglomeration.

An actual decrease in the amount of γ' present in the matrix of the material could be explained by an alternative to Bigelow's mechanism, if the γ' itself dissolved matrix atoms at the high temperatures which were then rejected at lower temperatures due to decreased solubility. Guard and Westbrook (ref. 14) have summarized the alloying behavior of γ'. Their study demonstrated the following:

1) Ti and Cr will substitute for Al in γ'. This factor was taken into account in calculating the amount of γ' possible in the alloys.

2) Co will substitute for Ni in γ'. This would not increase the amount of γ' which can form.

3) Mo is nearly completely insoluble in γ'.

4) The solubility of those elements which do dissolve in γ' increases with decreasing temperature.

These results demonstrate that the changes in the amount of γ' present in the alloys cannot be accounted for on the basis of solid solution of matrix elements in the γ'. Thus, Bigelow's mechanism appears to present the most plausible explanation for a true volume decrease of γ'.

In formulation of the preceding discussion, consideration was given to the progressive accumulation of massive γ' in the grain boundaries, a phenomenon described in the following section on ductility. The actual amount of γ' involved in this process proved to be virtually impossible to measure in a quantitative way. An approximation was made of the amounts of γ' in the grain boundaries of both alloys after 200 hours of exposure to 1600°F. These approximations showed that the fraction of the total structure which was represented by the γ' in the grain boundaries after this time period was of the order of 2 percent. Thus, although it must be conceded that migration of γ' to the grain boundaries did contribute to the decrease in amount within the grains as exposure time increased, this was only part of the total change measured.

Overheating during rupture tests to temperatures above the solution temperature for γ' maintained the apparent particle size and volume of γ' close to that for both alloys after exposure to 1600°F for from 2 to 10 hours. The precipitation of γ' after an overheat, however, had to take place at temperatures above 1600°F. Using the concept of the entrapment mechanism to explain these effects, the amount of precipitate would have been very high, for the first precipitation of γ' from the solution-treated condition. Then, during cooling to 1600°F, the smaller particles re-dissolved while others grew. Conditions were such that the relatively brief time above 1600°F was sufficient to cause changes similar to those resulting from solution treating and reheating to 1600°F for 2 to 10 hours.

Comparison of the two suggested explanations: In summary of the preceding discussions, the concession must be made that the data from the present investigation do not clearly fit either of the two suggested mechanisms to the definite exclusion of the other.

Additional information was available from data from a series of small samples of M252 which were heated directly to 1600°F after solution treatment without the prior age at 1400°F. The size, number, and spacing of the γ' particles as well as the apparent volume fraction of γ' in the structure were compared (figs. 26 through 29) with similar data from samples given the 1400°F age prior to exposure at 1600°F. The material given the prior age at 1400°F exhibited a larger apparent volume of precipitate in the form of more particles of essentially the same size as those in the material exposed without prior aging. This difference in amount of precipitate remained over the range of exposure times at 1600°F while both materials evidenced a decrease in the apparent amount of γ'.

In addition, there are data on figure 29 for the structure of material from stress-rupture test specimens which showed that slow cooling from 1600°F resulted in additional precipitation during the cooling. This additional precipitate took the form of larger particles and yielded the same number of particles as similar material which was cooled rapidly from the exposures at 1600°F.

The existence of a larger number of particles in the material which was pre-aged at 1400°F seems relatively straight forward in any case. For a normal precipitation phenomenon, the lower solubility of Al and Ti in the matrix at 1400°F would have resulted in a greater potential for initial precipitation than at 1600°F and permitted more particles to grow. Alternatively, under the proposed entrapment mechanism, the nucleii would have already been present, having formed during cooling from solution treatment. Then, on reheating, a greater number of nucleii were above the critical size for survival at 1400°F than at 1600°F. Thus, more particles would be expected to have formed initially in any case.

If the apparent decrease in volume fraction was actually the result of an etching effect of some sort, then the actual amount of γ' could be assumed to be constant during exposure to 1600°F. Furthermore, the amount of γ' in the material which was pre-aged at 1400°F would be expected to decrease rapidly to the equilibrium amount at 1600°F as agglomeration of the particles permitted re-saturation of the matrix at 1600°F. On this basis, the two curves on figure 29 should have merged by the time 50 hours had elapsed. That is, although there were more particles in the material pre-aged at 1400°F, they would not be expected to grow to the same size as those exposed directly to 1600°F after solution treatment since the amount of γ' should be the same in both of them by this time. Since the data do not show that the amounts became equal at the longer time periods, this approach would require that the etching effect be greater in the material which was pre-aged at 1400°F so that the apparent amount of precipitate remained above that in the samples in which the 1400°F age was omitted. At the same time, the persistence of a different etching effect between the two materials out to 50 hours at 1600°F seems rather unlikely.

The concept of the proposed entrapment mechanism as previously discussed would also predict behavior of the type observed. Within this framework, the observed differences would be real, resulting from the greater number of particles able to survive the first few hours of exposure to 1600°F.

In either case, when samples were slow cooled from 1600°F after 50 hours or more exposure, the decreasing solubility of the matrix for the Al+Ti then caused additional precipitation of γ' on the already existing, fairly large particles. This resulted in an increase in the amount of precipitate present. The ease with which the additional γ' precipitated during slow cooling suggests that the "foreign" atoms in the precipitate would return to the matrix in much less time at 1600°F than is suggested by the data. Therefore, the idea of mechanical entrapment is not entirely satisfactory.

Thus, neither the assumption of an error in particle measurement nor of a true volume decrease is completely compatible with the data. There is obviously the possibility that both factors entered into the observed measurements to some degree.

Microstructural Features and Ductility

The elongation of Inconel 700 alloy at fracture was rather low and the creep rates were comparatively low throughout normal tests. Consequently, the rupture life was highly dependent on elongation. The reduction in elongation from overheats to temperatures of 2000°F and higher, therefore, resulted in significantly reduced life even though creep resistance was unaffected.

For the high-ductility M252 alloy, a large fraction of the elongation in normal rupture tests was accumulated during the last few hours of testing when the creep rate was very rapid. Overheating reduced the amount of elongation which could occur during this period. Since rupture life would have been extended only a few hours if this loss had not occurred, the reduction in ductility of M252 alloy from overheating did not significantly reduce rupture life.

When overheats reduced ductility, the amount of reduction increased with the number of overheats applied. Thus, when a limited number of overheats was applied and the specimen then continued to rupture at constant temperatures, the reduction in ductility was less than when the overheating was continued until rupture occurred.

The structures of both alloys were examined for the metallurgical factors responsible for the observed ductility in the rupture and overheat tests.

Inconel 700 Alloy. - The structure of Inconel 700 alloy after the standard heat treatment consisted of fine intragranular γ' particles (fig. 25), carbide particles (later shown to be $M_{23}C_6$), both within the grains and in the grain boundaries (figs. 21 and 25), and the usual random dispersion of larger angular Ti(C, N) particles (fig. 21). During exposure at 1600°F, with or without stress, the size and number of the grain-boundary $M_{23}C_6$ carbides increased (fig. 25). At the same time, the amount of intragranular $M_{23}C_6$ decreased. When stress was absent, there was an accumulation of massive γ' along all the grain boundaries which enveloped the grain-boundary carbides (fig. 25).

The presence of stress during exposure to 1600°F (fig. 45) caused the disappearance of the fine γ' particles from strips of matrix adjacent to grain boundaries transverse to the applied stress. (This will hereafter be referred to as "γ' depletion"). It also reduced the accumulation of the massive γ' in many of the grain boundaries transverse to the applied stress. Microcracks formed in the transverse grain boundaries between carbides and the depleted matrix. Comparison of the structure of a sample from a rupture test interrupted after 30 hours, with the structure of a sample from a completed rupture test (table V) demonstrated that this γ' depletion and microcracking had begun after 30 hours of testing and increased progressively out to rupture. Fracture occurred intergranularly by the growth and eventual linkage of a series of microcracks across the sample. This process of structural alteration by γ' depletion and microcracking leading to fracture has previously been reported

by Decker (ref. 15) and Weaver (ref. 16) in alloys containing predominantly $M_{23}C_6$ carbides.

The only carbides identified by X-ray diffraction analysis of residues extracted from a rupture test specimen (tables VI and VII) were $M_{23}C_6$ and Ti(C, N). The Ti(C, N) particles were easily identified in the microstructure by their appearance. They were only occasionally in the grain boundaries, and remained unchanged in size or dispersion throughout testing. Thus, these analyses indicate that the carbides which formed in the boundaries during testing were $M_{23}C_6$.

When samples were overheated to 2000°F or higher, the structural changes associated with rupture in the normal creep-rupture tests were drastically altered. Microcracking was virtually prevented up to the point of fracture. A sample interrupted after six overheats to 2000°F (table V) contained practically no microcracks. This was also true for those samples which ruptured soon after the application of the last overheat. In all cases, however, fracture was intergranular as it was in the normal creep-rupture tests.

Associated with the prevention of microcracking by overheats to 2000°F and higher was the virtual elimination of nearly all carbides from the grain boundaries, and the absence of γ' depletion adjacent to the transverse grain boundaries (fig. 46). In addition, the blocky γ' was eliminated from all the grain boundaries. Almost no precipitate remained in the grain boundaries.

Intergranular cracks originating at the surface were observed in all specimens. Since there was no significant change in the number or size of the intergranular surface cracks present in all specimens, these cracks were apparently not a factor in the ductility effects observed.

Specimens were overheated to 2000° or 2100°F for a limited number of times and then allowed to continue to fracture at constant temperature. Examination of these specimens after fracture (fig. 47) showed that the structural changes observed in the grain boundaries of samples from normal tests had begun to take place after overheating was discontinued. Carbide precipitation in the grain boundaries, γ' depletion, and microcracking were all observed. Massive γ' also appeared in all of the grain boundaries except some of those which were transverse to the applied stress. As the time between the last applied overheat and rupture increased, these

structure characteristics continued to change much the same as they would have in a normal creep-rupture test which had been in progress for the time since the last overheat.

X-ray diffraction analysis of extracted residues from a sample which received 6 overheats to 2100°F and then continued an additional 49 hours to rupture (table VII) indicated that the predominant carbide type was still $M_{23}C_6$ as it was after normal testing, although a detectable amount of M_6C had formed.

None of the conditions of overheating to 1800°F noticeably affected the grain boundary structural alterations observed in constant temperature tests. As a consequence, overheats to this temperature had no significant effect on the elongation.

M252 Alloy. - In M252 alloy, X-ray diffraction analysis of extracted residues from normal creep-rupture tests (tables VI and VII) indicated that M_6C was the only carbide type present, as appears to be characteristic of alloys with high molybdenum (ref. 17). The microstructure, after the standard heat treatment, showed a dispersion of fine intragranular γ' (fig. 24) and a dispersion of M_6C throughout the structure (figs. 14 and 24), both in the grain boundaries and within the grains. During exposure with or without stress to 1600°F, the carbide distribution was unaffected and remained discontinuous in the grain boundaries [fig. 48(a) and (b)]. Considerable massive γ' appeared in the grain boundaries (fig. 24), around and between the carbides. When a stress was present, the matrix adjacent to many of the transverse grain boundaries showed γ' depletion and the massive γ' was absent from these boundaries. Microcracks were observed (fig. 30) in these areas between the carbides and the depleted matrix. Measurements of the number of microcracks (table VIII) demonstrated that after 50 hours in a normal creep-rupture test, there was a detectable number of cracks and that after rupture, this number was considerably greater. Furthermore, the number of cracks at rupture in M252 alloy was greater than that in Inconel 700 alloy.

Overheats to 2000° or 2100°F from a base temperature of 1600°F had no effect on the size or distribution (fig. 48) of the carbides in M252 alloy. There was, however, a considerable decrease in the amount of γ' depletion adjacent to the transverse grain boundaries as well as in the amount of γ' agglomeration which occurred at the grain boundaries. Analysis of residues from a specimen overheated to 2000°F (table VII) showed no change with overheating in type of carbide. The number of microcracks at

fracture was not changed. Examination of a sample which had been overheated to 2000° F from a base temperature of 1500° F indicated, by comparison with a normal creep-rupture test at 1500° F, that more microcracks had formed in the overheated sample than in the normal test specimen. The elongation under these conditions was reduced more than it was in the tests at 1600 °F (table II and fig. 16).

Examination of samples after overheats from 1600° to 1800° F, the temperature which reduced elongation the most, showed that there were more areas of γ' depletion and more microcracks (table VIII) in this condition than in the normal test samples.

Samples from tests overheated to 2000° F a limited number of times and continued to fracture indicated that γ' depletion took place after overheating was stopped, and blocky γ' formed in the longitudinal grain boundaries, much the same as in normal tests. No change in number of microcracks from that in a normal test could be detected.

The samples which were overheated a limited number of times to 1800° F did not provide a clear picture of the response of the structure after overheating was stopped. There were fewer microcracks and less γ' depletion than was observed when overheats were continued to rupture. The microcracking and γ' depletion appeared to be greater, however, in every case than in a normal rupture test.

Interpretation of Data. - Microcracks originated at carbides when they were present in the grain boundaries in both alloys. Since the nucleation and growth of microcracks caused fracture, carbides were a major factor in the effects of overheating on ductility. This was most strikingly shown by the absence of microcracking when the carbides were practically eliminated from the grain boundaries of Inconel 700 alloy by overheating to 2000° or 2100° F. This was nearly as striking for overheating M252 alloy to 2000° or 2100 °F since neither the amount of microcracking nor the carbides in the grain boundaries were affected, although the alteration of the γ' was very striking.

The outstanding feature of the relation of carbides to microcracking was the evidence that there was little difference in the effectiveness of M_6C and $M_{23}C_6$ carbides. It seems probable, therefore, that the hard unyielding nature of carbides of either type can lead to stress concentrations causing microcracking. Whether or not they do is dependent on the characteristics of the remainder of the structure, as will be discussed. If this is correct, the high ductility associated with alloys with predominantly M_6C carbides is not due to a better bond between M_6C and the matrix.

Rather, it must either reflect associated differences in other structural features which tend to reduce the susceptibility to crack nucleation and growth; or, reflect inherent differences in the form and distribution of the two carbides.

In this connection, it is important to note that the M_6C carbides in M252 were not altered by overheating. Overheating to 2000° and 2100°F not only prevented the formation of the $M_{23}C_6$ carbides in the grain boundaries of Inconel 700 but also dissolved those which had formed during heat treatment. Beattie (ref. 18) has reported that the solution temperature for $M_{23}C_6$ is below 2000°F, while it is considerably higher for M_6C. This explains the influence of overheating on the $M_{23}C_6$ carbides in Inconel 700 and the lack of influence on the M_6C carbides in M252. Probably, their state and distribution in M252 were largely governed by history of the material prior to the final treatment at 1950°F. In Inconel 700, they were dissolved during solution treatment and then reprecipitated during subsequent exposure to lower temperatures.

Grain boundary carbides did not accumulate in Inconel 700 samples which were overheated to 2000°F or higher unless overheating was discontinued. Although some M_6C carbides formed under these conditions, they did not alter the subsequent ductility of the samples.

The data suggest that stress concentrations develop around carbide particles when stress is applied. The structure acts to relieve these concentrations by localized creep in the adjacent matrix. Continued overall creep, however, renews the stress concentration. Finally, when the available ductility in the matrix adjacent to the carbide particle has been exhausted through localized creep, a microcrack forms. The nucleation of microcracks at the carbide particles is, therefore, governed by the creep characteristics of the alloy.

The growth of microcracks, once they have formed, should also be governed by the creep characteristics of the material, although the influence of excess phases in the grain boundaries will also be important. Creep characteristics will govern both the efficiency of the stress relief provided by the initial formation of the cracks, and the stress level applied to the cracks after they have nucleated.

Weaver (ref. 16) has noted that the ease of crack propagation increases as the excess phases in the grain boundaries decrease from continuous films to discontinuous particles to clean grain boundaries.

In summary of these generalities, the following factors can be listed as contributing to the nucleation and growth of microcracks, and the eventual complete fracture of a specimen.

1) Cracks nucleated as the result of stress concentrations which occur at carbides in the grain boundaries transverse to the applied stress. The type of carbide, per se, is not important. The form and quantity of the carbide exerts the most important influence.

2) Creep in the matrix adjacent to the carbide particles acted to relieve the stress concentration. Since depletion of γ' from these areas generally occurred, they were weaker than the bulk of the matrix and could deform readily under the applied stress concentrations to provide relief. At the same time, the depletion would tend to result in concentration of overall creep strain in these weakened areas.

3) Overall creep in the sample served to continually renew the concentration of stress around a carbide particle, and at a crack after it had nucleated.

A consideration of the specific way in which these factors related to the behavior of each alloy follows.

M252 alloy: The carbides in M252 were stable during normal testing. The creep resistance of this alloy was relatively lower than that of Inconel 700. Microcracking in M252 was, therefore, mainly governed by creep strain as it served to produce stress concentrations around the grain boundary carbides and cause nucleation and growth of microcracks.

The accumulation of massive γ' in the grain boundaries of M252 during normal tests did not occur in many of the transverse grain boundaries. Thus, the cracks grew along these boundaries in accordance with the discontinuous nature of the existing carbides.

When M252 was overheated to 1800° F, the main structural change introduced was an increase in the amount of depletion of γ' from the transverse grain boundaries. This resulted in an increased number of microcracks. Thus, in this case, the increased amount of creep occurring at the grain boundaries more than offset the increased tendency for stress relief by localized creep around the carbides. The net result was a decrease in the total elongation

required to link the microcracks and cause fracture. As previously discussed, this did not significantly change the rupture time since the overall creep resistance of the material was not affected, and the creep characteristics were such that a large fraction of the total deformation took place during the last few hours of the tests.

When specimens were overheated from 1600° to 2000° or 2100°F, the most significant effect was the increased overall creep resistance. Accompanying this effect was a decrease in the amount of γ' depletion. The increase in creep resistance served to decrease the rate at which stress concentrations could build up in the grain boundaries, while the decreased depletion made more difficult the relief of stress concentrations by localized creep. The net result was no change in the amount of microcracking which took place. The slight reduction in elongation which was caused by overheating to 2000° or 2100°F was apparently the result of an increased rate of crack growth.

When the base test temperature was 1500°F for M252, the applied stress was higher and there was a greater relative increase in the creep resistance of the matrix from overheating. The net effect in this case was an increase in the amount of microcracking with a consequent decrease in ductility as a result of the linkage of microcracks at lower total creep strain.

Inconel 700 alloy: Inconel 700 differed from M252 in several factors which govern crack nucleation and growth. The overall creep resistance of Inconel 700 was comparatively much higher. Thus, the applied stress was much higher to obtain rupture in about the same time as M252. Carbides had to grow in the grain boundaries during the tests. As a consequence, there was a period early in the tests when the stress concentrating effect of carbides was rather small.

As the carbide particles increased in size, the stress concentrations increased. The high creep resistance of the matrix forced a relatively large fraction of the total strain into the grain boundary areas. Eventually, a crack was nucleated, and grew under the continuing application of stress. As a result of the higher creep resistance of Inconel 700 causing a larger fraction of the total strain to go to the grain boundaries, the microcracks grew and linked together to cause fracture at lower total creep strain than was required by M252. The need for the carbide particles to form in the grain boundaries during creep was probably an important factor limiting the number of microcracks, as well as increasing the tendency for crack growth.

None of the structural factors of normal tests were changed by overheats to 1800°F. Consequently, the ductility was not altered. Since the creep resistance was not changed either, rupture time remained unaffected.

When the overheat temperature was 2000° or 2100°F, carbides were practically eliminated from the grain boundaries. This removed the main source of stress concentration for microcracking. The concurrent prevention of the accumulation of massive γ' in the boundaries left a relatively clean grain boundary with little resistance to crack propagation. When a microcrack finally did form, it grew rapidly to cause fracture. Thus, failure occurred during the 5 hours under stress between overheats, even though no microcracks were intially present at the start of the five-hour period.

The factors controlling the nucleation of a crack after overheating to 2000° or 2100°F are less clear. The test results show that it was delayed in relation to a normal test. Apparently, the absence of stress-raising carbides required more overall creep deformation before some other factor nucleated a crack. The concentration of creep strain in the grain boundaries, with little opportunity for the relief of the resulting stress concentration, particularly at triple points, may have caused a crack to form. Fracture also could have been caused by a surface crack. In any event, a crack, which was necessary to nucleate fracture, occurred and grew rapidly before the overall strain attained the same amount as was possible with the inhibitants to crack growth in a normal test.

Since the effects of overheating on the grain boundaries were the same with overheats to either 2000° or 2100°F, and creep resistance was unaffected in either case, the decrease in ductility was the same for both overheat temperatures.

Discussion for both alloys: The reason why overheating to 1800°F increased γ' depletion in M252 alloy and had no effect on γ' depletion in Inconel 700 is not clear. One possibility suggested by the available information is related to the solution temperature for γ', which is very close to 1800°F for M252 and considerably higher for Inconel 700. This may have accelerated depletion in some unknown way. The larger amount of creep deformation experienced by M252 before fracture could also have been involved. A further difference existed between the alloys in the response of this factor to overheating. When the overheat temperature was 2000°F or higher, γ' depletion was prevented in Inconel 700 alloy, while it was only reduced in M252.

The cause of γ' depletion and the prevention of the accumulation of massive γ' at transverse grain boundaries is not understood. These phenomena occurred in both alloys. It would seem that they must have been caused by alteration of the phase relationships by stress and strain effects at the grain boundaries. As previously discussed, γ' was unstable and it would be relatively easy for such a factor to operate.

The foregoing discussion regarding the influence of overheating on the ductility process has not specifically considered the effect of a limited number of overheats (i.e., tests in which considerable time elapsed after application of an overheat before fracture occurred). The data showed that samples from such tests exhibited an effect intermediate to that of a normal rupture test and a test to which overheats had been repeatedly applied until fracture. In all cases, this was accounted for by the return of the structural changes, after overheating was stopped, to the process of a normal creep-rupture test. This acted to offset a portion of the effect of the overheats which had been applied and reduced the extent of the decrease in elongation.

The nucleation and growth of microcracks leading to rupture has been shown to be closely related to, and probably governed by, the ability of the two alloys to relieve stress concentrations at the grain-boundary carbides by local creep in the adjacent matrix. The definite possibility that stress relief was accelerated by the increased temperature during the overheats has not been mentioned. The experimental evidence, as presented in the foregoing analysis, indicates that this factor was not important in the control of response to overheating. The Inconel 700 data at first suggested that the lack of microcracking in samples overheated to 2000°F and higher was, at least partly, due to accelerated stress relief. Overheating to the same temperatures, however, did not alter the number of microcracks in M252 alloy. Further study then showed that alteration of the grain-boundary precipitates was responsible for the effects in Inconel 700 alloy. It appears, therefore, that the role of accelerated stress relief during the overheats was either small or masked under the conditions of the experiments.

Previous mention was made of the difference in grain size between the M252 and Inconel 700 alloys after standard heat treatment, as well as the variable grain size between the individual bars of Inconel 700 alloy. Larger grain size has generally been associated, in published data, with lower ductility in creep-rupture tests. For this reason, recognition must be made of the fact that the larger grains of Inconel 700 alloy may have affected the response of the fracture mechanism to overheating, in comparison to the finer grained M252 alloy, in some way which was not evident in the data. On the other hand, the fracture mechanism suggested by the data indicates that the factors which control ductility do not depend directly on grain size. Apparently, in most cases, the variation in grain size in a material occurs under conditions in which the structural features actually responsible for ductility effects are also changed. Thus, although a grain size change is observed, it is not, *per se*, responsible for the change in available ductility.

The factors governing ductility are complex and interrelated in ways which make a generalized prediction of ductility difficult.

Apparently, nucleation of cracks becomes more difficult when grain boundaries are free of excess phases or when the excess phases have complete continuity in the boundaries. In the former case, growth would be comparatively easy. In the latter, growth would be quite difficult. Thus, since a completely continuous carbide network is virtually impossible, and intermediate discontinuous network should be most favorable. Apparently, the very rapid growth when there is less excess phase in the boundary more than offsets the fact that there are fewer sites for nucleation. As the amount of excess phase increases, the number of nucleation sites increases reducing the amount of crack growth required before they link together to cause fracture. At some intermediate amount of excess phase, there will be a point where the nucleation and growth characteristics balance to give optimum resistance to failure by cracking.

In addition, both nucleation and growth of microcracks appear to be closely related to creep resistance. Many of these related effects, however, tend to offset one another making prediction of the net effect virtually impossible. For example, a highly creep resistant matrix would tend to restrict the amount of overall deformation which occurs, thereby reducing the build-up of stress concentrations in the grain boundaries. At the same time, however, the matrix adjacent to the grain boundary carbide particles would be less able to relieve the stress concentrations by localized creep. Conversely, when the creep resistance is low, the creep strain required to nucleate a crack can be obtained with comparative ease, but the tendency for cracks to grow will be smaller due to the more complete relief of stress concentrations when a crack forms. The way in which these variables inter-play will be a function of the combined effect of test temperature, stress, and creep rate being considered.

Role of Additional Composition Variables

The response of M252 and Inconel 700 to overheating has been considered up to this point in terms of effects dependent on the amount of Al+Ti present, and the influence of Mo content on the carbide reactions. Originally, the response to overheating of M252 alloy with 10-percent Mo as compared to that of the 4-percent Mo in Inconel 700 suggested that molybdenum content itself could be a controlling factor. Accordingly, a program was started to study the role of molybdenum but not pursued extensively when the interpretation previously discussed became evident and when experimental difficulties were encountered.

The major alloying elements which were varied are summarized in the following comparison with M252 and Inconel 700:

Material	Alloy Content (weight percent)				
	Co	Mo	Ti	Al	Al+Ti
M252 (heat 837)	9.70	10.00	2.71	0.96	3.67
Heat 1171	10.27	10.11	2.54	1.27	3.81
Inconel 700	28.69	3.08	2.02	3.13	5.15
Heat 1172	10.28	10.13	2.65	2.99	5.64
Heat 1173	10.22	4.13	2.57	0.82	3.39
Waspaloy	13.29	2.89	2.30	1.50	3.80

The complete analyses are given in table I. Heat 1171 was included to be a control laboratory heat of M252.

The results from the study of these materials is detailed in the following sections.

Sluggish γ' Precipitation. - Heat 1173 was prepared with the intention of studying the role of molybdenum by reducing its level to 4 percent in a material which was otherwise similar to M252 alloy. As the data (table IX and figs. 49 and 50) show, however, the behavior of the material was so inconsistent with expected characteristics that it could not be relied upon to show the role of molybdenum.

The normal creep-rupture strength at 1600°F of heat 1173 (table IX) was about the same as heat 837 of M252 but lower than heat HT-28. The elongation at fracture (21 to 25 percent) was intermediate to Inconel 700 and M252. The creep behavior in normal tests (fig. 49) was also intermediate to that of M252 and Inconel 700.

Ten overheats to 1800° or 2000°F had the following effects (table IX) on the creep-rupture properties of heat 1173 at 1600°F:

(1) Overheats to both 1800° and 2000°F reduced rupture time (fig. 50). The reduction was less for overheats to 2000°F than for overheats to 1800°F.

(2) Elongation (fig. 50) was unaffected by overheats to 1800°F and increased by overheats to 2000°F.

(3) Creep resistance was affected the same by overheating to either 1800° or 2000°F (fig. 49). Immediately following each overheat exposure, the creep rate was very high. It then decreased with time up to the subsequent overheat.

The reduction in rupture life was due to the greatly accelerated creep rate between overheats. This led to the accumulation of more creep-strain at a given time than in constant temperature tests, with a consequent reduction in rupture time.

The acceleration of creep rate was caused by an extremely low rate of reprecipitation of γ' after overheating. Overheats to 1800°F, as well as 2000°F, dissolved the γ'. The solution temperature for γ' in this heat was sufficiently below 1800°F (fig. 36) so that the γ' was dissolved during the 2 minutes at 1800°F during an overheat. When a sample was cooled back to 1600°F and the load reapplied, γ' had not reprecipitated. Consequently, the creep resistance was very low. As γ' slowly reprecipitated, the creep resistance returned, and the creep rate decreased.

The sluggishness of γ' reprecipitation was evident in several ways. No halts in the cooling curves after overheating were observed as they were for heats 837 and HT-28. Small samples were heated to 2000°F and cooled back to 1600°F at the same rates as those during overheat exposures. These were quenched after varying times at 1600°F. After 5 minutes at 1600°F, there was very little γ' evident in the microstructure (fig. 51). Even after 40 minutes, the amount of γ' was small and in the form of relatively large particles. It seems quite evident that at 1600°F the γ' reprecipitated very slowly with a much less favorable dispersion than it did in M252 alloy as previously described.

The relatively low Mo content of heat 1173 was suspected to be related to the slow rate of reprecipitation at the low solution temperature. The availability of Waspaloy stock with still lower Mo (2.89 percent) and only slightly higher Al+Ti (3.80 percent) afforded an opportunity to check this. Small samples were heated to 2000°F for 2 minutes, cooled to 1600°F and held 5 minutes. There were large amounts of γ' in the Waspaloy structure similar to M252 control samples from heat 837 (fig. 51). This indicated that the low Mo of heat 1173 alone was not responsible for the sluggish reprecipitation of γ' after overheating.

The analysis for aluminum and titanium in heat 1173 was checked and agreed with the initial analyses. In addition, the measured solution temperature for γ' (fig. 36) seemed to agree with the analyzed Al+Ti content.

The behavior of this heat presents a paradox. It does not seem reasonable that the slightly low Al+Ti (3.39 percent) in comparison to the amount in heat 837 of M252 (3.67 percent) or in the Waspaloy (3.80 percent), could be responsible for the sluggishness of reprecipitation. Boron additions presumably reduce the rate of γ' precipitation. The analyzed boron content of heat 1173 was similar

to HT-28 of M252. Since the γ' precipitated rapidly in HT-28, it appears that boron was not responsible.

Heat 1173 was also unusual in that the γ' redissolved during an overheat to 1800°F. The γ' in heat 837, whose solution temperature was somewhat higher than that of heat 1173 but still well below 1800°F, did not dissolve appreciably.

The temperature for reprecipitation of γ' during cooling from an overheat for the materials with 10-percent Mo (fig. 36) suggests that reprecipitation should have occurred in heat 1173 at about 1600°F. The temperature of reprecipitation for Inconel 700, however, was considerably lower in relation to its solution temperature than it was for the materials with 10-percent Mo. It is possible that Mo raises the temperature of reprecipitation. If this should be the case, the temperature for reprecipitation of γ' for heat 1173 at the cooling rates obtained from the overheat exposures could have been suppressed well below 1600°F. It is further possible that it could have been suppressed even more than is suggested by fig. 36 if the effect should happen to intensify as the Al+Ti is reduced. This does not, however, explain why the γ' in Waspaloy reprecipitated. Either there is an unusual sensitivity to the exact amounts of Al and Ti in the alloys, or some unidentified factor was involved in heat 1173.

A residue extracted from a constant temperature rupture test at 1600°F discontinued after 50 hours contained both $M_{23}C_6$ and M_6C. This would be expected for the "intermediate" Mo content of 4 percent. There is nothing, however, in this to suggest why the rate of reprecipitation of γ' after overheating was so slow.

The sample overheated to 2000°F for 10 times and then continued to rupture had fewer microcracks than a constant temperature test. It is presumed that this was due to solution of $M_{23}C_6$ carbides from the grain boundaries during the overheats to 2000°F. However, this type of study was not pursued further when it was recognized that the results apparently were not clarifying the role of Mo. It is only interesting to note that in this alloy, nucleation of microcracking and crack growth apparently were governed by creep strain. So far as these processes were concerned, they were probably governed by carbides in the grain boundaries and the accumulation of creep strain. Whether the strain accumulated at the rate of normal tests or at the greatly accelerated rates after overheating made no difference. The only unexpected factor was the absence of increased elongation as a result of the reduced creep resistance from overheating, since this might be expected to allow easier relief of stress concentrations around the carbide particles, thus delaying the formation of microcracks.

High Mo With High Ti+Al. - Heat 1172 was made to provide Al+Ti in the range of that in Inconel 700 alloy in the presence of 10-percent Mo. The Ti content was kept at the 2.5 percent of M252 and the Al raised to 3 percent. The rupture strength (table IX) was low by comparison to other alloys with similar Ti+Al content. The 100-hour rupture strength at 1600°F was 8,000 to 10,000 psi lower than that of Inconel 700 alloy. The ductility was slightly higher.

Ten overheats to 1800° or 2000°F caused the following changes in rupture properties at 1600°F (table IX):

(1) Rupture time (fig. 52) was slightly reduced by overheats to 1800°F and significantly increased when the overheat temperature was 2000°F. Ten overheats more than doubled life and indicated that continued overheating to rupture would have prolonged rupture time to that typical of Inconel 700.

(2) Elongation (fig. 52) was increased by overheats to 1800°F and unchanged by overheats to 2000°F.

(3) The creep resistance (fig. 53) was reduced by overheats to 1800°F and markedly increased by those to 2000°F.

Apparently, the rupture time was reduced at 1800°F due to the reduction in creep resistance, even though elongation was increased. The marked increase in creep resistance from overheats to 2000°F was responsible for the increased rupture time, since elongation was not changed.

The microstructure of this alloy after creep-rupture testing at 1600°F (fig. 54) contained a needle-like acicular phase. This phase was extracted with hot aqua regia and identified by X-ray diffraction as sigma phase (table X). Qualitative spectrographic analysis of the residue indicated a predominance of Cr, substantial Mo, and some Ni, a composition consistent with sigma phase. Ti and Al were not detected.

The sigma phase was not present in identifiable amounts in the alloy following the original heat treatment (fig. 54). Overheating to 2000°F prevented its appearance although it did form in a specimen which was overheated a limited number of times and then allowed to continue to rupture at 1600°F.

The combination of 10-percent Mo with 5.6-percent Al+Ti in heat 1172 was sufficient to shift the phase diagram to the point where sigma phase could form during testing at 1600°F. Overheating to 1800°F accelerated the reaction. The results indicate that 2000°F was above the solution temperature for the sigma phase, since over-

heats to this temperature prevented its accumulation by periodically redissolving it.

The appearance of sigma phase in alloys is known to reduce creep resistance and rupture strength. It also causes an increase in elongation in rupture tests at elevated temperatures. The unexpectedly low normal rupture and creep strength level in heat 1172 was, therefore, apparently due to the formation of sigma phase during testing.

Measurements of the amount of γ' in the matrix areas between the sigma needles yielded the volume fraction which would be expected for an alloy with 5 to 6-percent Al+Ti. The presence of the sigma phase throughout the structure, however, reduced the overall volume fraction of γ' to a much lower value. Since the sigma contained no Al or Ti, the reduction in the overall amount of γ' present could have been due to a change in the matrix composition associated with the formation of the sigma phase. The appearance of a very heavy layer of γ' in the grain boundaries of heat 1172, by comparison with Inconel 700 alloy, however, suggested that the formation of the sigma phase also forced γ' to the boundaries. In any case, the lower overall amount of γ' in the structure probably contributed to the lower creep resistance in the presence of the sigma phase.

The data indicated that, when the formation of sigma phase was suppressed by overheating to 2000°F, the strength level was consistent with that to be expected at the 5 to 6-percent Al+Ti level. At this level, precipitation of γ' occurred during cooling from the overheats. The data were not sufficiently detailed to determine whether the high molybdenum in heat 1172, by comparison to that in Inconel 700 alloy, caused an increase in the rate of the γ' reaction. When the data for heat 1172 were complicated by the formation of the sigma phase, further studies of this heat seemed of questionable value.

Laboratory Melted M252 Alloy. - When laboratory heats 1172 and 1173 were made to study the effects of Mo content, a control heat, 1171, of M252 alloy was also melted. Its rupture strength at 1600°F (table IX) was on the high side for M252 alloy, while the ductility was somewhat low. Overheating had the following effects (table IX):

(1) Overheating to 1800°F did not significantly alter rupture time (fig. 55), elongation (fig. 55), or creep resistance (fig. 56).

(2) Overheats to 2000°F increased rupture time and elongation (fig. 55) and also increased creep resistance (fig. 56).

The amount of testing, as well as the structural studies, was extremely limited. The limited results were sufficient, however,

to indicate that the laboratory heat of M252 did respond to overheating generally the same as the larger heats with only minor differences. Examination of the structure of a sample which had been overheated to 2000°F (fig. 57) showed a large apparent amount of γ' in the form of small particles as was the case for the large heats. The increased creep resistance from overheating to this temperature was, therefore, due to the retention of a high-strength dispersion of γ'.

The higher rupture strength and lower elongation, in comparison to heat 837, were partially investigated. The Al+Ti in heat 1171 was 3.81 percent. This is sufficiently higher than the 3.67 percent Al+Ti in heat 837 to account for most of the increased creep resistance, although the higher boron content of heat 1171 would also favor high creep resistance. Constant temperature tests at 1600°F resulted in more microcracking than was observed for heat 837. X-ray diffraction of a residue from a specimen exposed under stress at 1600°F for 50 hours showed a significant amount of $M_{23}C_6$ as well as the expected M_6C. It is assumed, in view of previous discussions, that the $M_{23}C_6$ probably precipitated in the grain boundaries during testing and nucleated more cracks than occurred in the larger heats with only M_6C carbides. The elongation was, therefore, reduced. The exclusion of $M_{23}C_6$ from the grain boundaries by overheating to 2000°F would account for the increased elongation. Elongation changes, however, had a small effect on rupture time due to the high total elongation at fracture. It is assumed that $M_{23}C_6$ formed in heat 1171 because a high constant temperature of working (2150°F) dissolved some of the M_6C. This reprecipitated at lower temperatures as $M_{23}C_6$.

There was no evidence in the data to indicate that the γ' reaction in the laboratory heat was any slower than in the larger heats during cooling from overheats to 2000°F. The cooling curves from overheats to 1800°F exhibited no halts indicating that the γ' was not dissolved, as was the case for the larger heats. The apparently anomolous response of the ductility of heat 1171 after overheats to 1800°F was not studied. Either the one test was not typical or some other factor was involved.

Role of Molybdenum. - The original intent of the laboratory heats was to clarify the role of molybdenum. Early in the investigation, it appeared that high Mo might be the key to increased rupture time

from higher temperature overheats. By the time the results from the laboratory heats became available, the progress of the structural studies on M252 and Inconel 700 was pointing to what seem to be adequate explanations. For this reason, no further attempts were made to study the role of Mo.

So far as this investigation is concerned, it appears as if the main effect of high molybdenum, such as the 10 percent in M252 alloy, is to promote the formation of relatively stable M_6C carbides in preference to $M_{23}C_6$ carbides. The resultant effect on properties has been covered in detail previously. There may be additional effects which have not been clearly revealed by the present investigation. The data indicated, for example, that Mo level may influence the kinetics of γ' precipitation. The primary role of Mo, as indicated by the present studies, appears to be its effect on carbides.

Generality of Results

The results of this investigation point to structural concepts for the types of alloys studied which, in themselves, are more important than the original limited objective of defining and explaining the varied effects of overheating on creep-rupture properties.

The indication that the relation between γ' dispersion and creep resistance can be approached with the fundamental concepts developed by Weertman offers a great deal of encouragement to the possibility of utilizing basic concepts in engineering alloys. Moreover, for the first time, an adequate interpretation is presented of apparently unexplainable responses to heat treatment. For instance, in earlier studies of Udimet 500 alloy (ref. 5), aging was found to have little effect on the rupture life at 1600°F. It now seems clear that this was due to the insensitivity of creep resistance to γ' dispersion to be expected for the volume fraction of γ' in that alloy. Alloys with lower amounts of Al+Ti, however, had been found to be quite sensitive to aging, as the analysis in this report would predict, for the smaller volume fraction of γ' and the consequent sensitivity to γ' dispersion. The fact must be kept in mind, however, that while the sensitivity to γ' dispersion increases for lower levels of Al+Ti, the attainable strength levels and maximum service temperatures also decrease.

The results also show that the major effects of the complicated solution and aging treatments which have been developed in engineering practice for the higher Al+Ti alloys are related primarily to control of ductility. Apparently, these treatments operate mainly through

effects on carbides and their influence on crack initiation and growth.

The data supporting the geometrical aspects of the γ' dispersion are rather limited. They seem adequate, however, to establish the qualitative effects with considerable confidence. It is recognized, however, that as stress and temperature are changed, the significance of the geometry of the γ' dispersion can also change, as predicted by Weertman, in accordance with the way dislocations move under the varying conditions.

The fact must also be kept in mind that the treatment of dispersion has assumed spherical γ' particles. For higher levels of Al+Ti, the γ' particles are known to become blocky. While the general concepts developed in the present study may apply, care should be exercised in their use under these conditions. Also of importance is the fact that in complex materials, other factors than the γ' dispersion operate to establish the overall strength level. The changes in strength resulting from changes in dispersion of the precipitate will be superimposed on the inherent strength level of the material.

In so far as the effects of overheating are concerned, the qualitative effects, as established for γ' and ductility, are believed to be applicable for a wide range of alloys and conditions of exposure. The problem is reduced to determining the details as they apply to each specific alloy and exposure condition. In this respect, attention is directed to the fact that the results in this investigation were limited to overheats without stress from 1600°F for two alloys. Only one schedule of overheating was used and the tests were limited to one stress at 1600°F for each alloy. Qualitatively, the results explain tests at 1500°F and for other stresses, as reported in reference 3. There seems to be every reason to expect that they apply to other alloys of the same type with suitable modification for the details of composition and test conditions.

Previous work (ref. 3) demonstrated that, to a first approximation, the influence of stress during an overheat can be estimated by the addibility-of-life-fractions rule combined with data on the effects of thermally-induced structural changes on the properties at the base temperature. The two effects are very nearly additive in most cases.

In general, application of the results of these studies to prediction of the behavior of an alloy under service conditions must be done carefully. The general principles developed should add to the insight available into many problems. In frequent cases, however, other effects such as thermal shock may be far more important in limiting materials which have suffered overtemperature during actual service.

CONCLUSIONS

The extension of creep-rupture life of M252 alloy at 1500°F through thermally-induced structural changes from repeated brief overheats to 1900°F or higher was confirmed and extended to testing at 1600°F. Overheats to lower temperatures either did not change or slightly reduced rupture life.

Extension of creep-rupture life by overheating to sufficiently high temperatures is not necessarily typical of all Al+Ti bearing nickel-base alloys. The rupture life of Inconel 700 was not extended but was reduced by overheating above 1800°F. Overheats to 1800°F did not affect life.

The rupture life of M252 was improved when overheating prevented the deterioration of creep resistance characteristic of normal creep rupture tests. Improvement in life was caused by the solution and reprecipitation of γ' preventing the agglomeration and decrease in amount of γ' which occurs under constant temperature conditions. This was possible due to the very high reaction rates for solution and precipitation of γ' in these alloys.

In Inconel 700 alloy, the prevention of agglomeration and decrease in amount of γ' did not affect creep resistance. Rupture life was reduced in this alloy as a result of a reduction in ductility for overheats above 1800°F.

The influence of the dispersion of γ' decreases as the amount of γ' present is increased. For the volume of γ' present in M252 alloy, creep resistance depended on the dispersion of the γ', while it was nearly independent of the dispersion for the volume of γ' present in Inconel 700.

The role of γ' dispersion was clarified by using Weertman's equations based on dislocation theory for creep in a metal containing a dispersed phase.

The demonstration of the role of γ' dispersion in creep resistance should have wide applicability in the explanation of many features of the physical metallurgy of such alloys.

The measured amount of γ' in both alloys decreased during exposure at 1600°F. In addition, the amounts measured when the particles were small were larger than would be expected at equilibrium. Whether these effects resulted from a spurious etching effect when the particles were small, or from non-stoichiometric precipitation of the γ' could not be determined with certainty.

Fracture in the rupture tests occurred by nucleation of microcracks at carbides in the grain boundaries and their subsequent growth. In M252 alloy, overheating did not significantly change the carbides, due to the high solution temperature of the M_6C carbides characteristic of this alloy. In Inconel 700, overheats to 2000°F or higher dissolved the characteristic $M_{23}C_6$ carbides due to their relatively low solution temperature and prevented them from forming in the grain boundaries. The resultant clean grain boundaries were subject to very rapid crack growth once a microcrack formed thus reducing ductility and decreasing rupture life.

The results indicate that the type of carbide present in the grain boundaries was not important. The size, shape, and distribution of the particles controlled their effect on microcracking.

The interrelations between creep resistance and microcracking are applied in the report to the fracture of both alloys.

Apparently, the primary effect of molybdenum in M252 is to make M_6C the characteristic carbide. The occurrence of sigma phase as a result of high molybdenum in the presence of increasing amounts of Al+Ti causes low strength.

University of Michigan,
Ann Arbor, Mich., September, 1961

REFERENCES

1. Rowe, John P., Freeman, J. W.: "Effect of Overheating on Creep-Rupture Properties of S-816 Alloy at 1500°F." NACA TN 4081, December 1957.

2. Rowe, John P., Freeman, J. W.: "Effect of Overheating on Creep-Rupture Properties of HS-31 Alloy at 1500°F." NACA TN 4083, December 1957.

3. Rowe, John P., Freeman, J. W.: "Effect of Overheating on Creep-Rupture Properties of M252 Alloy." NACA TN 4224, March 1958.

4. Miller, B. A., Winward, J. M., Smith, W. K.: "High-Heating -Rate Strength of Three Heat-Resistant Metals." NAVORD Rep. 2017, NOTS 670, Naval Ord. Lab., March 16, 1953.

5. Decker, R. F., Rowe, John P., Bigelow, W. C., Freeman, J. W.: "Influence of Heat Treatment on Microstructure and High-Temperature Properties of a Nickel-Base Precipitation-Hardening Alloy." NACA TN 4329, July 1958.

6. Bigelow, W. C., Amy, J. A., Brockway, L. O.: "Electron Microscopic Identification of the γ' Phase of Nickel-Base Alloys." Proc. ASTM, Vol. 56, 1956, p. 945.

7. Howard, R. T., Cohen, M.: "Quantitative Metallography by Lineal Analysis and Point Counting." Metals Technology TP 2215, August 1947.

8. Betteridge, W., Franklin, A. W.: "Progress in Nickel-Chromium Base Alloys for Service at High Temperatures." Revue de Metallurgie, Vol. 53, 1956, p. 271. (French).

9. Weertman, J.: "Theory of Creep of Dispersion Hardened Alloys." NRL Report 5123, April 15, 1958.

10. Taylor, A.: "Constitution of Nickel-Rich Quaternary Alloys of the Ni - Cr - Ti - Al System." Journal of Metals, Vol. 8, 1956, p. 1356.

11. Rogen, N. E., Grant, N. J.: "The Growth of $Ni_3(Al,Ti)$ Precipitates in a Ni - Cr - Ti - Al Alloy." Trans. ASME, Vol. 218, Feb. 1960, p. 180.

12. Underwood, E. E., Marsh, L. L., and Manning, G. K.: "Creep of Aluminum-Copper Alloys During Age Hardening." NACA TN 4036, February 1958.

13. Bigelow, W. C., Amy, J. A.: "Electron Metallographic Studies of Nickel-Base Heat-Resistant Alloys." WADC 58-406, August 1958.

14. Guard, R. W., Westbrook, J. H.: "Alloying Behavior of Ni_3Al (γ' Phase)." Trans. AIME, Vol. 215, 1959, p. 807.

15. Decker, R. F., Freeman, J. W.: "Mechanism of Beneficial Effects of Boron and Zirconium on Creep-Rupture Properties of a Complex Heat-Resistant Alloy." NACA TN 4286, August 1958.

16. Weaver, C. W.: "Intergranular Cavitation, Structure, and Creep of a Nimonic 80A-Type Alloy." Journal of the Institute of Metals, Vol. 88, 1960, p. 296.

17. Beattie, H. J., Ver Snyder, F. L.: "The Influence of Molybdenum on the Phase Relationships of a High Temperature Alloy." Trans. ASM, Vol. 49, 1957, p. 883.

18. Beattie, H. J.: "Aging Reactions in Rene 41." General Electric Company Report DF59SL314, May 15, 1959.

TABLE I

CHEMICAL COMPOSITION OF EXPERIMENTAL MATERIALS

Material	Composition (Weight Percent)										
	C	Mn	Si	Cr	Ni	Co	Mo	Ti	Al	Fe	B
M252 (Heat 837)[1]	0.16	0.82	0.60	18.70	54.15	9.70	10.00	2.71	0.92	2.20	0.0007
M252 (Heat HT-28)[2]	0.12	0.10	0.35	19.22	54.38	9.73	10.18	2.40	1.12	2.40	0.0014
Inconel 700[3]	0.12	0.07	0.24	15.70	46.30	28.69	3.08	2.02	3.13	0.65	0.0074
M252 (Heat 1171)[4]	0.11	0.36	0.45	20.01	54.88	10.27	10.11	2.54	1.27	(5)	0.0022
Heat 1172[4]	0.15	0.31	0.49	19.94	53.06	10.28	10.13	2.65	2.99	(5)	0.0029
Heat 1173[4]	0.16	0.31	0.47	20.05	61.27	10.22	4.13	2.57	0.82	(5)	0.0017

1. Vacuum melted and supplied by the General Electric Company as 7/8-inch diameter bar stock.
2. Vacuum melted and supplied by the Haynes Stellite Company as 7/8-inch diameter bar stock.
3. Heat Y7952, melted by the International Nickel Company, and supplied through the Curtis-Wright Corporation, Wright Aeronautical Division as 11/16-inch diameter bar stock.
4. Heats vacuum melted at the University of Michigan.
5. Not reported.

TABLE II

RESULTS OF TESTS ON M252 ALLOY

Heat Number	Base Conditions		Overheat Conditions		Rupture Data		
	Temperature (°F)	Stress (psi)	Temperature (°F)	Number of Cycles	Time (hr)	Elongation (% in 1 inch)	Reduction of Area (%)
837	1500[1]	15,000	-	-	644.8	47	58
		20,000	-	-	251.7	36	54
		25,000	-	-	153.8	39	47
		30,000	-	-	49.9	36	49
		30,000	-	-	61.6	38	48
		30,000	-	-	62.7	47	58
		34,000	-	-	38.2	40	50
837	1500[2]	34,000	-	-	60.1	28	43
		33,000	-	-	75.9	38	39
		33,000	-	-	81.7	38	45
		32,000	-	-	94.0	37	42
		22,000	-	-	427.0	34	46
		33,000	1800	17	86.7	19	45
		33,000	1800	10	77.0	27	42
		33,000	2000	24	114.3	12	16
		33,000	2000	10	98.5	36	42
		33,000	2100	20	125.9	26	37
837	1600[2]	27,000	-	-	11.0	38	45
		18,000	-	-	71.9	34	50
		18,000	-	-	75.4	47	51
		18,000	-	-	82.5	48	53
		18,000	-	-	88.3	52	54
		18,000	-	-	91.5	46	57
		18,000	-	-	97.0	45	54
		18,000	-	-	50.0 (Interrupted test)		
		18,000	1800	12	73.8	25	55
		18,000	1800	10	50.0 (Interrupted test)[3]		
		18,000	1800	6	73.4	38	39
		18,000	1800	3	76.7	48	53
		18,000	2000	27	137.7	40	33
		18,000	2000	10	98.6	43	47
		18,000	2000	10	50.0 (Interrupted test)[3]		
		18,000	2000	5	88.2	46	47
		18,000	2100	20	138.6	41	39
		18,000	2100	10	100.4	35	38
		18.000	2100	10	50.2 (Interrupted test)		
		18.000	2100	5	92.7	49	50
HT-28	1500[4]	21,000	-	-	736.0	61	62
		24,000	-	-	573.9	39	61
		24,000	-	-	450.4	46	55
		26,500	-	-	356.0	36	59
		26,500	-	-	317.8	40	56
		30,000	-	-	207.7	43	58
		34,000	-	-	105.2	45	54
		34,000	-	-	81.6	49	58
		34,000	-	-	79.2	41	55
		35,000	-	-	70.9	26	41
		34,000	1650	18	84.9	37	49
		34,000	1650	11	54.8	34	42
		34,000	1650	7	50.6	28	44
		34,000	1800	10	52.7	22	27
		34,000	1800	9	48.1	25	37
		34,000	1800	5	68.2	38	52
		34,000	1900	30	181.6	23	45
		34,000	1900	15	137.3	35	53
		34,000	2000	30	211.3	16	50
		34,000	2000	15	170.9	25	46
HT-28	1600[2]	20,000	-	-	112.4	56	64
		20,000	-	-	109.4	78	64
		20,000	1800	10	89.4	28	62
		20,000	2000	10	134.7	56	51

(1) Data from ref. (1). Material rolled from 1950°F, solution treated 4 hours at 1950°F, and aged at 1400°F for 15 hours.

(2) Material rolled from 2150°F, solution treated 1 hour 2150°F plus 4 hrs 1950°F, and aged at 1400°F for 15 hours.

(3) Interrupted test conditions at which two tests were exposed.

(4) Data from ref. (1). Material was rolled from 2150°F, solution treated 4 hours at 1950°F, and aged at 1400°F for 15 hours.

TABLE III

RESULTS OF TESTS ON INCONEL 700 ALLOY

Bar	Sample	Base Conditions		Overheat Conditions		Rupture Data		
		Temperature (°F)	Stress (psi)	Temperature (°F)	Number of Cycles	Time (hr)	Elongation (% in 1 inch)	Reduction of Area (%)
11	D	1500	34,000	-	-	803.5	11	12
12	A	1500	40,000	-	-	208	7	10
16	D	1500	43,000	-	-	122.6	6	9
17	C	1500	45,000	-	-	44.5	4	2
19	-	1500	43,000	-	-	92 Estimated(1)		
19	C	1500	43,000	2000	4	18.6	3	5
20	-	1500	43,000	-	-	80 Estimated(1)		
20	D	1500	43,000	1800	13	71.8	4	4
20	C	1500	43,000	1800	10	70.7	6	5
20	B	1500	43,000	2000	7	34.5	1	2
21	B	1500	43,000	2100	4	18.5	2	2
23	B	1500	43,000	-	-	129.5	7	12
24	D	1500	43,000	-	-	65.4	6	7
25	-	1500	43,000	-	-	102 Estimated(1)		
25	B	1500	43,000	1800	10	104.8	4	7
11	A	1600	20,000	-	-	633.0	18	21
12	B	1600	28,000	-	-	103.6	16	22
13	B	1600	29,000	2000	6	54.7	10	10
14	A	1600	29,000	-	-	89.2	17	22
14	B	1600	29,000	1800	14	69.5	10	15
14	D	1600	29,000	2000	6	30.0 (Interrupted test)		
15	C	1600	29,000	-	-	90.0	18	20
15	D	1600	29,000	-	-	30.0 (Interrupted test)		
15	B	1600	29,000	2000	12	55.7	4	8
16	A	1600	29,000	-	-	83.8	14	Data not available
16	B	1600	29,000	2100	11	53.1	4	5
18	A	1600	25,000	-	-	229.1	13	17
19	A	1600	29,000	-	-	76.6	13	20
19	B	1600	29,000	-	-	63.1	8	13
20	A	1600	2,,000	-	-	62.7	10	14
22	C	1600	16,500	-	-	977.3	8	10
22	D	1600	29,000	2000	3	34.5	4	5
23	C	1600	29,000	-	-	65.4	13	21
23	D	1600	29,000	2100	6	79.4	8	14
23	A	1600	29,000	2100	3	71.8	13	16
24	C	1600	29,000	-	-	53.8	8	14
24	B	1600	29,000	2000	6	33.7	4	4
24	A	1600	29,000	2000	3	35.2	3	5
25	A	1600	29,000	-	-	73.6	12	20
25	C	1600	29,000	1800	7	78.9	14	15
25	D	1600	29,000	2100	3	62.5	9	15
50	A	1600	29,000	-	-	50.2	12	14
50	C	1600	29,000	-	-	49.0	13	13
50	D	1600	29,000	-	-	47.9	12	15
50	B	1600	29,000	-	-	45.7	12	15
50	F	1600	29,000	1800	8	44.9	9	11
50	G	1600	29,000	2100	5	25.4	3	6
50	H	1600	29,000	2200	4	32.5	4	6
51	C	1600	29,000	-	-	86.8	13	15
51	B	1600	29,000	-	-	83.1	15	19
51	A	1600	29,000	-	-	72.9	19	18
51	D	1600	29,000	-	-	65.6	15	18

(1) Values estimated from data at 1600°F. Range in time at 1500°F and 43,000 psi estimated to be 60 - 140 hours.

TABLE IV

SUMMARY OF γ' PRECIPITATION FACTORS

For M252 and Inconel 700 Alloys

Alloy	Condition of Testing	Time at 1600°F (hr)	Volume Fraction γ' (%)	γ' Particles, Number per in^2 at X11,000	Inter-particle Distance, λ (Å)	γ' Particle Size, h (Å)	Structural Parameter λ^2/h
M252 (heat 837)	Material with Standard Heat Treatment, exposed without stress at 1600°F	1	43.5	1430	202	578	71
		4	31.0	596	385	756	196
		8	30.0	406	477	900	253
		16	27.0	292	585	1010	339
		24	25.0	169	808	1280	510
		50	24.0	94	1095	1685	710
		102	23.0	78	1220	1805	825
		212	19.5	54	1540	2000	1185
	Material after Standard Solution Treatment without 1400°F age, exposed without stress at 1600°F	4	26.5	470	463	786	273
		8	23.0	221	722	1070	488
		15	21.0	183	820	1125	598
		24	21.0	150	905	1240	660
		48	18.5	89	1210	1515	966
	Stress Rupture Test[1]	54I[2]	28.5	96	995	1810	547
	Stress Rupture Test	104	24.5	73	1220	1920	775
	Sample exposed without stress under same conditions as rupture test	54	28.0	103	990	1760	557
	10 overheats to 1800°F	54I	29.0	95	1015	1785	575
	10 overheats to 2000°F	54I	39.5	440	397	992	159
	10 overheats to 2000°F	54I	35.0	688	350	770	159
	10 overheats to 2100°F	54I	37.5	880	288	685	121
Inconel 700	Material with Standard Heat Treatment, exposed without stress at 1600°F	0	48.5	700	262	872	78
		4	45.5	430	356	1080	117
		11	43.5	400	383	1095	134
		22	40.5	330	448	1165	172
		48	35.5	225	595	1320	268
		95	33.0	149	755	1570	364
		212	30.5	108	920	1770	479
	Stress Rupture Test	34I	39.0	263	512	1280	205
	Stress Rupture Test	67	35.5	160	707	1570	319
	Stress Rupture Test	94	33.5	117	842	1775	400
	6 overheats to 2000°F	34I	46.0	646	288	885	94
	12 overheats to 2000°F[3]	60	39.5	616	336	840	132

(1) Samples for stress rupture tests all received the standard heat treatments prior to testing. Time at 1600°F includes 4 hour preheat in rupture unit.

(2) "I" indicates test interrupted at indicated time.

(3) Sample ruptured 5 minutes after application of last overheat.

TABLE V

SUMMARY OF FRACTURE VARIABLES

INCONEL 700 ALLOY

Bar	Sample	Overheat Conditions		Rupture Time	Time after Last OH	No. of Cracks per 0.002 in^2
		Temperature (°F)	Number of Cycles			
15	D	None		30I[1]	30	4
50	D	None		48	48	87
20	A	None		63	63	24
23	C	None		65	65	17
25	A	None		74	74	16
15	C	None		90	90	32
14	B	1800	14	70	<1	28
22	D	2000	3	34	19	6
24	A	2000	3	35	20	4
14	D	2000	6	30I	0	<1[2]
13	B	2000	6	55	25	8
24	B	2000	6	34	4	2
15	B	2000	11	56	1	<1[2]
23	A	2100	3	72	57	22
25	D	2100	3	63	48	29
50	G	2100	5	25	<1	<1[2]
23	D	2100	6	79	49	19
16	B	2100	11	53	<1	<1[2]

(1) "I" indicates test interrupted at indicated time.

(2) Samples in which few, if any cracks could be found other than the fracture itself.

TABLE VI

X-RAY DIFFRACTION DATA FROM RUPTURE SAMPLES OF M252 AND INCONEL 700 ALLOYS

(Analyses from residues extracted from rupture samples with bromine)

Alloy	Measured Values		Identification of Measured Lines in Pattern*					
	d (hkl)	Intensity	M_6C a_o=11.00Å	M_6C' a_o=10.85Å	hkl	$M_{23}C_6$ a_o=10.65Å	Ti(C, N)	Cr_2O_3
M252	3.30	vw	X	X	311			
	3.17	vw	X		}222			
	3.12	vw		X				
	2.74	mw	X		}400			
	2.70	mw		X				
	2.52	m	X		}331			
	2.48	m		X				
	2.24	ms	X		}422			
	2.21	ms		X				
	2.12	vs	X		}511 or 333			
	2.08	vs		X				
	1.94	m	X		}440			
	1.915	m		X				
	1.83	mw	X		}600			
	1.81	mw		X				
	1.655	w	X		}533			
	1.635	vvw		X				
	1.54	mw	X		}444			
	1.52	mw		X				
	1.43	mw	X		}731 or 553			
	1.405	mw		X				
	1.345	mw	X		}733			
	1.326	mw		X				
	1.297	s	X		}660			
	1.279	s		X				
Inconel 700	3.64	vvw						X
	2.65	vw						X
	2.49	s					X	
	2.45	w					(X)	
	2.39	mw				X		
	2.23	vvw						X
	2.16	s				X	X	
	2.12	mw					X	
	2.05	m				X		
	1.88	w				X		
	1.80	mw				X		
	1.77	vvw				X		
	1.69	vw				X		
	1.665	vvw						X
	1.61	vw				X		
	1.525	ms					X	
	1.50	mw					X	

* Check (X) shows that measured line corresponds to data from the literature for the indicated phase.

TABLE VII

SUMMARY OF X-RAY DIFFRACTION RESULTS FROM BROMINE-EXTRACTED RESIDUES

Alloy	Overheat Conditions[1]		Test Duration (hours)	Phases Identified				
	Temperature (°F)	Number		$M_{23}C_6$ a_o=10.65A	M_6C a_o=11.0A	M_6C' a_o=10.85A	Ti(C, N)	Cr_2O_3
M252	--- None ---		50		X	X		
	--- None ---		97		X	X		
	2000	10	50		X	(X)[2]		
Inconel 700	--- None ---		65	X			X	X
	--- None ---		90	X			X	X
	2100	6	79	X	(X)[3]		X	X

(1) All tests conducted with base temperature of 1600°F. Overheats for two minutes every five hours.
(2) Only stronger M_6C' lines appeared in this pattern.
(3) A few lines appeared from the M_6C pattern.

TABLE VIII

SUMMARY OF FRACTURE VARIABLES

M252 ALLOY

Overheat Conditions		Rupture Time	No. of Cracks per 0.002 in^2	No. of Depl G. B.[1] per 0.002 in^2
Temperature (°F)	Number of Cycles			
None		50I[2]	6	160
None		97.0	61	--
1800	10	50I	16	350
1800	12	73.8	93	--
2000	10	50I	5	20
2000	27	137.7	64	--

(1) Grain boundary depletion could not be measured quantitatively in fractured specimens.

(2) "I" indicates test interrupted at indicated time.

TABLE IX

TEST RESULTS FROM LABORATORY HEATS

Heat	Base Conditions		Overheat Conditions		Rupture Data		
	Temp (°F)	Stress (psi)	Temp (°F)	Number of Cycles	Time (hr)	Elongation (% in 1 inch)	Reduction of Area (%)
1173	1600	16,000	---	---	160.8	25	29
		16,000	---	---	141.0	23	29
		16,000	---	---	121.7	21	30
		16,000	---	---	50.0	(Interrupted Test)	
		16,000	1800	10	61.4	22	44
		16,000	2000	5	160.5	29	26
		16,000	2000	10	88.7	41	46
		16,000	2000	10	50.0	(Interrupted Test)	
1171	1600	20,000	---	---	124.6	39	50
		20,000	---	---	107.7	33	47
		20,000	---	---	50.0	(Interrupted Test)	
		20,000	1800	10	130.4	38	49
		20,000	2000	10	142.6	52	38
		20,000	2000	10	50.0	(Interrupted Test)	
1172	1600	20,000	---	---	70.5	20	27
		20,000	---	---	53.0	22	35
		20,000	---	---	50.0	(Interrupted Test)	
		20,000	1800	10	51.9	28	33
		20,000	2000	10	94.3	26	29
		20,000	2000	10	128.1	15	23
		20,000	2000	10	50.0	(Interrupted Test)	

TABLE X

X-RAY IDENTIFICATION OF SIGMA PHASE IN HEAT 1172

(Analysis of residue extracted with hot aqua regia from rupture sample)

Measured Values		Identification of Measured Lines*			
d (hkl)	Intensity	Sigma	Cr_2O_3	Al_2O_3	TiC
2.47	vvw	X	X		
2.39	w	X			
2.29	mw	X			
2.15	ms	X	X		X
2.09	m	X			
2.06	m	X		X	
2.04	m	X			
1.995	ms	X			
1.955	ms	X			
1.91	ms	X			
1.855	vvw	X			
1.815	vvvw		X		
1.79	mw	X			

* Check (X) shows that measured line corresponds to data from the literature for the indicated phase.

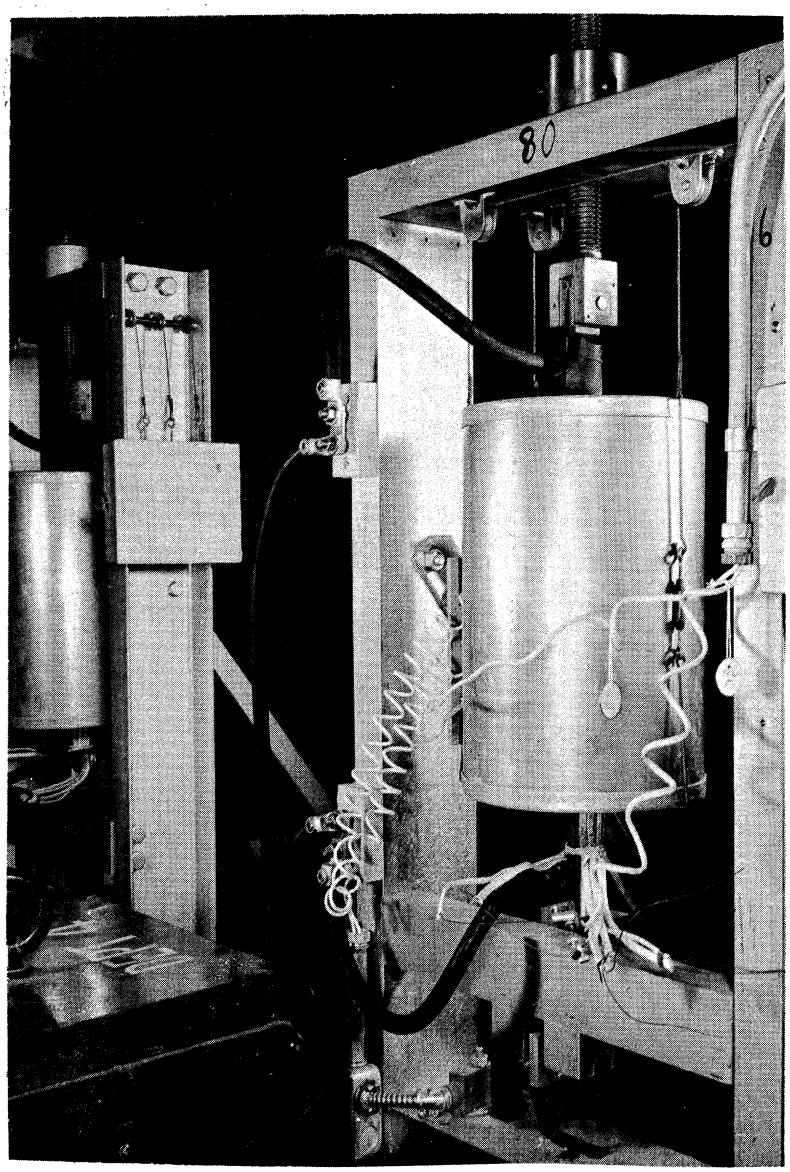

Figure 1. - Photograph showing creep-rupture unit modified for use in overheating by resistance heating.

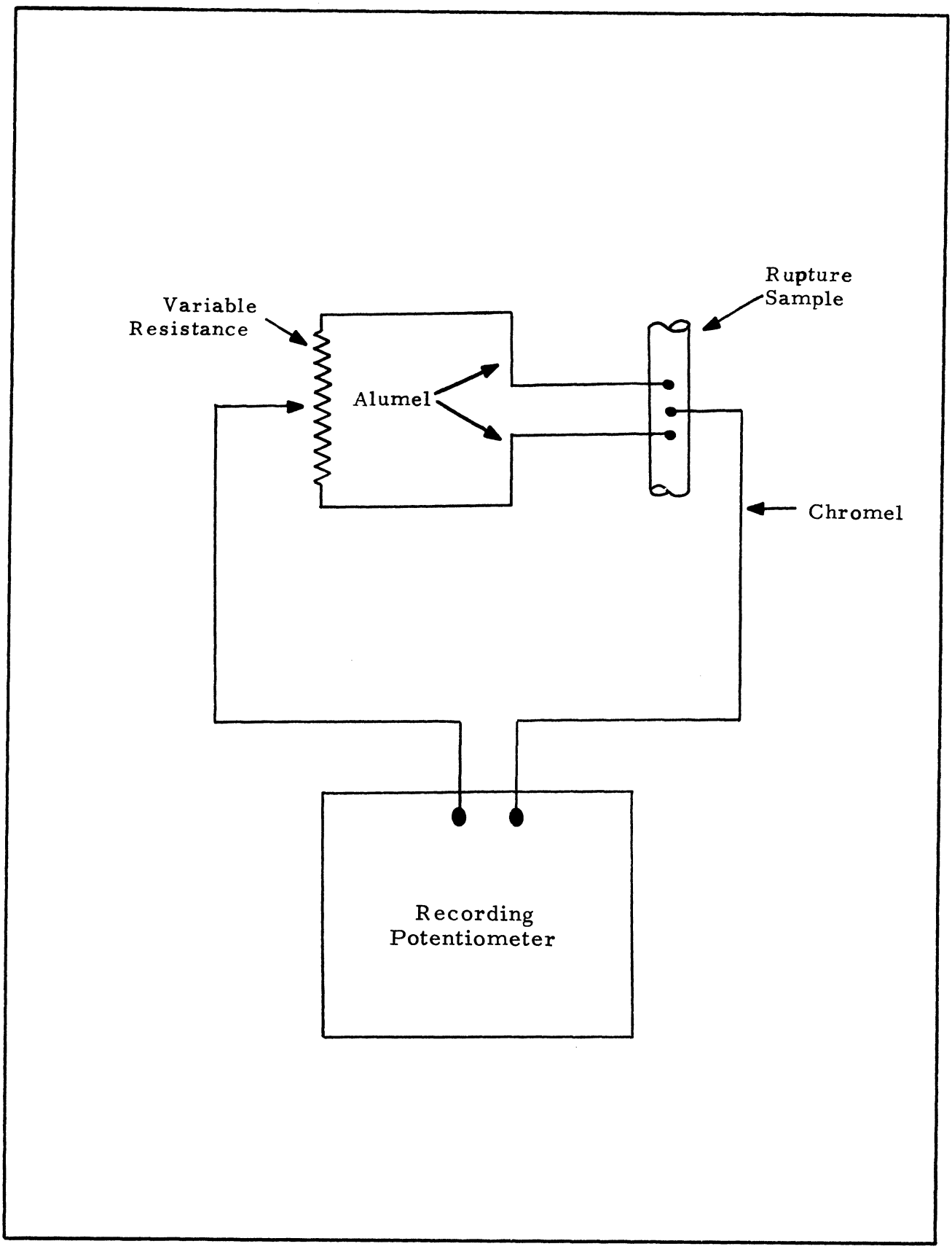

Figure 2. - Schematic wiring diagram of the system used for measurement of temperature during overheats to avoid extraneous emf from heating current.

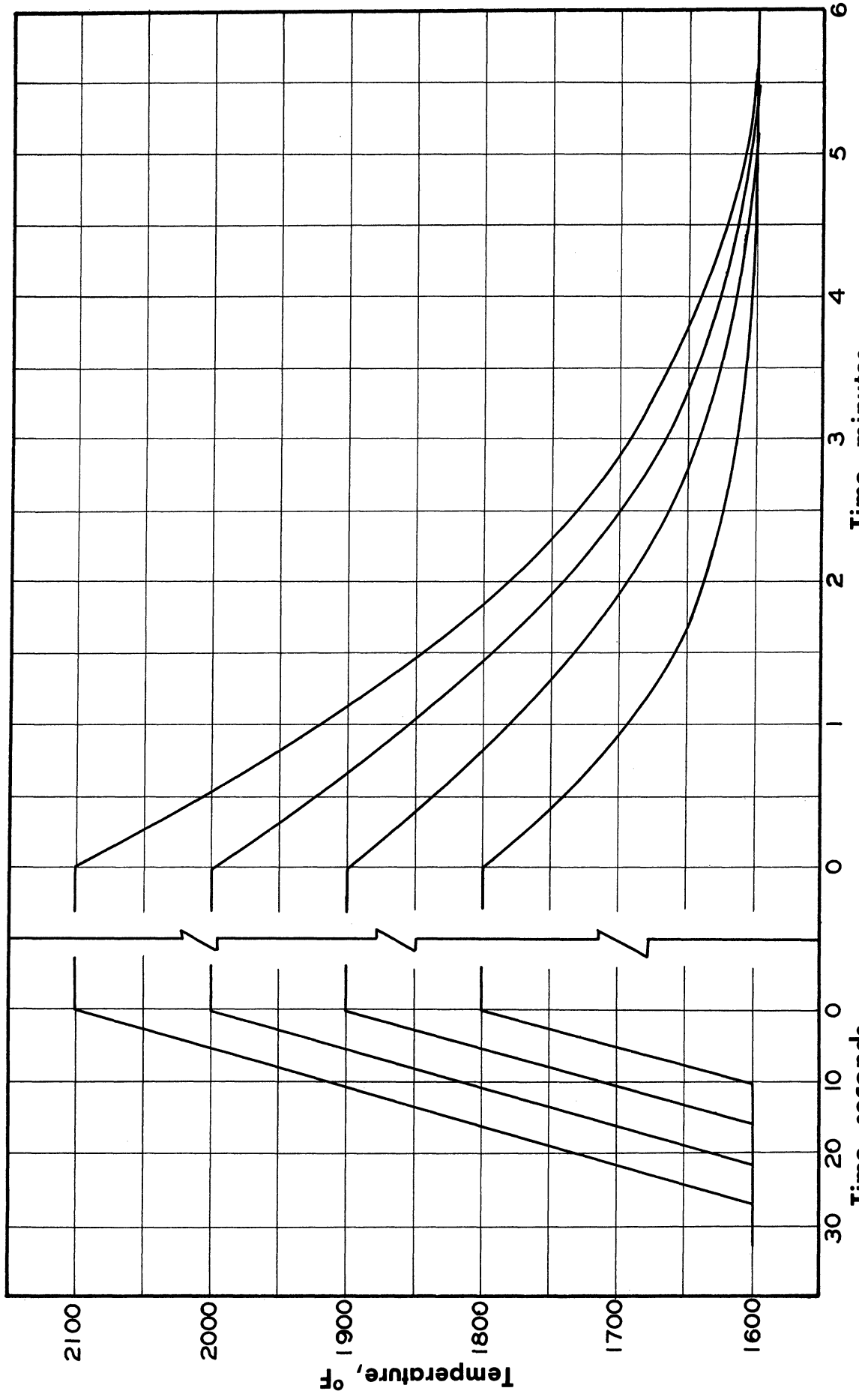

Figure 3. - Typical time-temperature curves for several of the overheat temperatures employed.

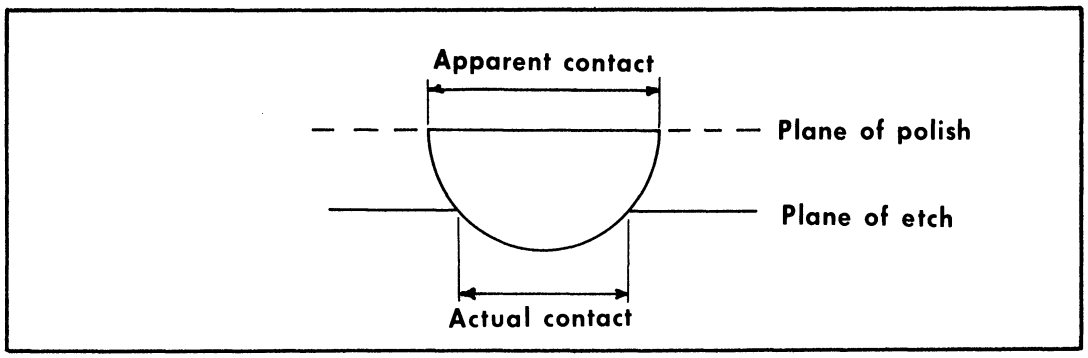

Figure 4. - Schematic representation of the cause of error in measurements of the contact area between a spherical particle and the surrounding matrix after etching the matrix below the plane of polish.

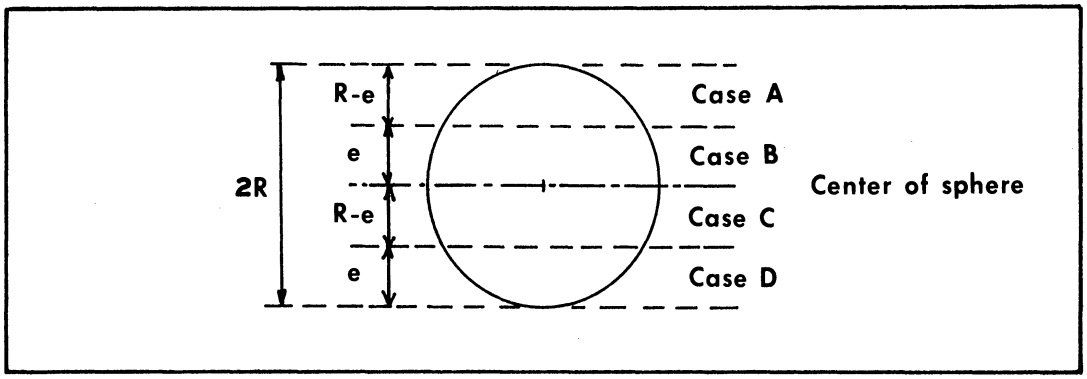

Figure 5. - Representation of four cases into which spherical particles were grouped for calculation of the error in measurements using lineal analysis. (e = depth of etching)

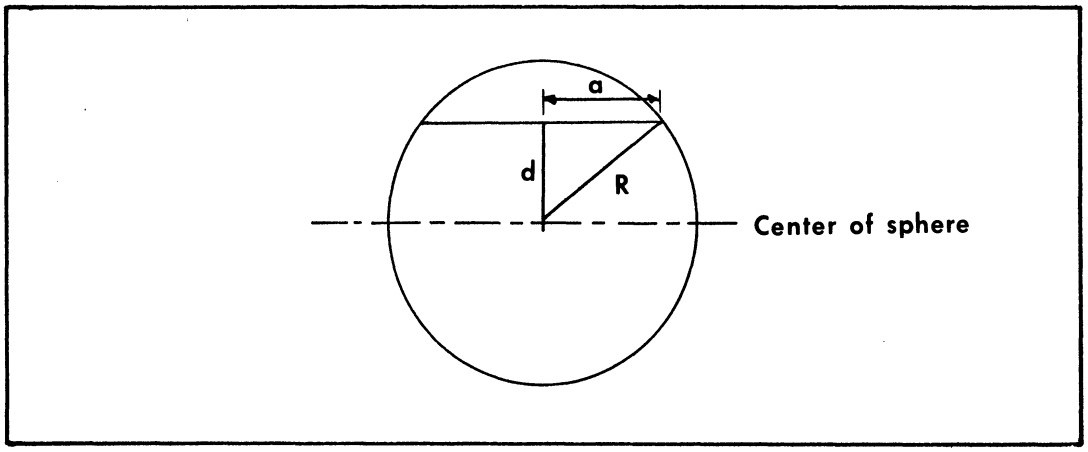

Figure 6. - Diagram illustrating the variables employed in computing the mean radius of the circle cut by sections polished in a random array of spheres.

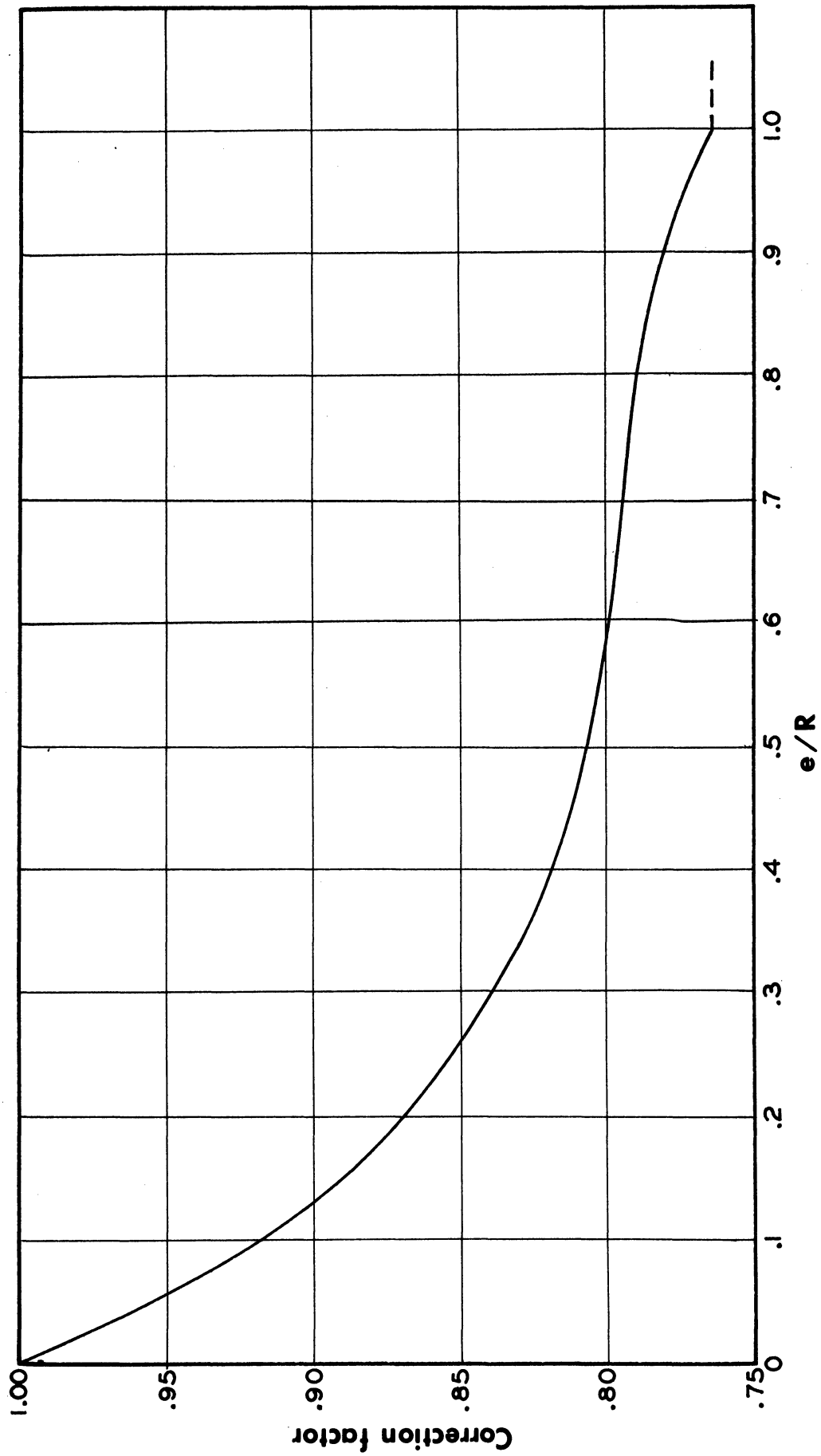

Figure 7. - Correction factor for errors resulting from etching a depth e below the plane of polish as a function of the ratio e/R (R = particle radius).

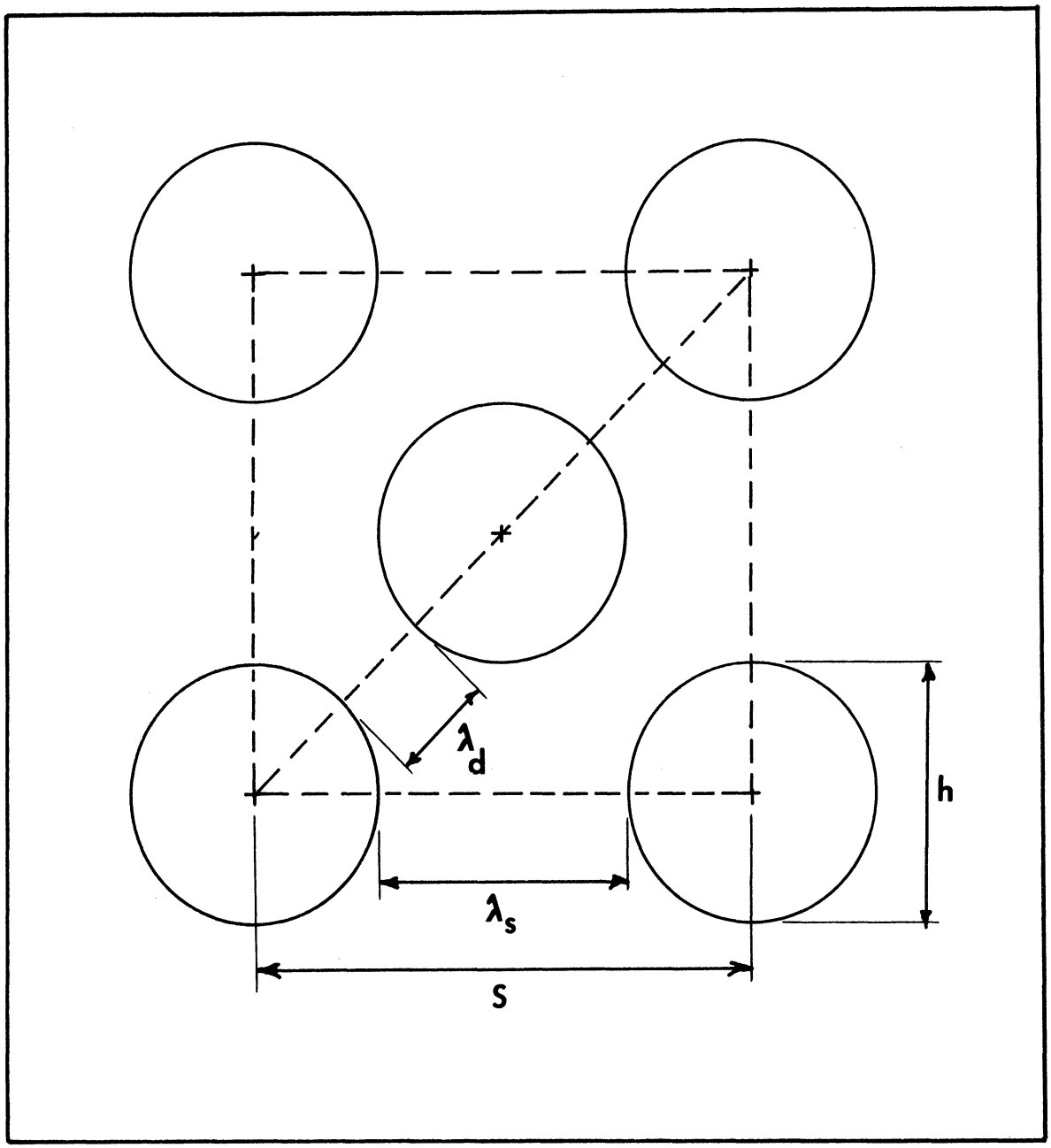

Figure 8. - Representation of one face of a face-centered cubic cell, defining the variables used in the calculation of inter-particle spacing.

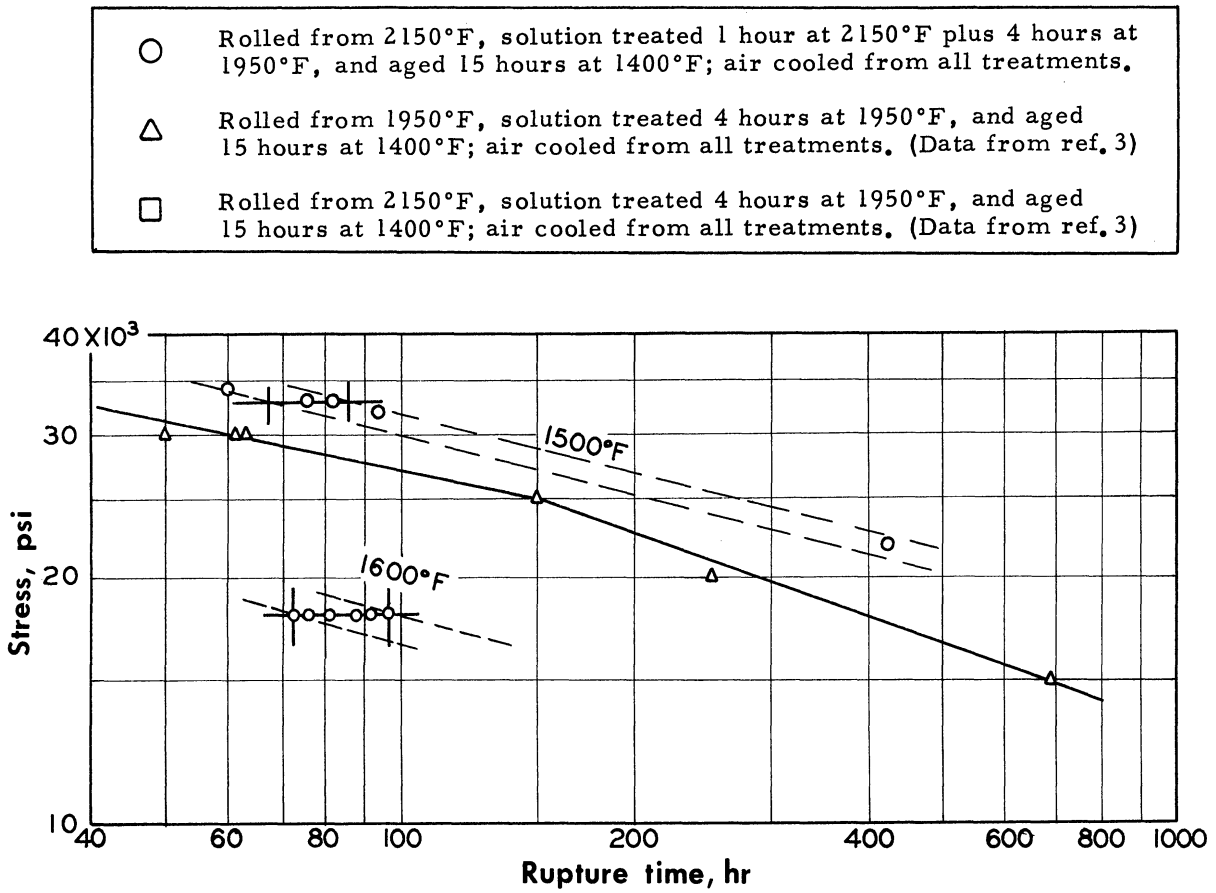

(a) Heat 837.

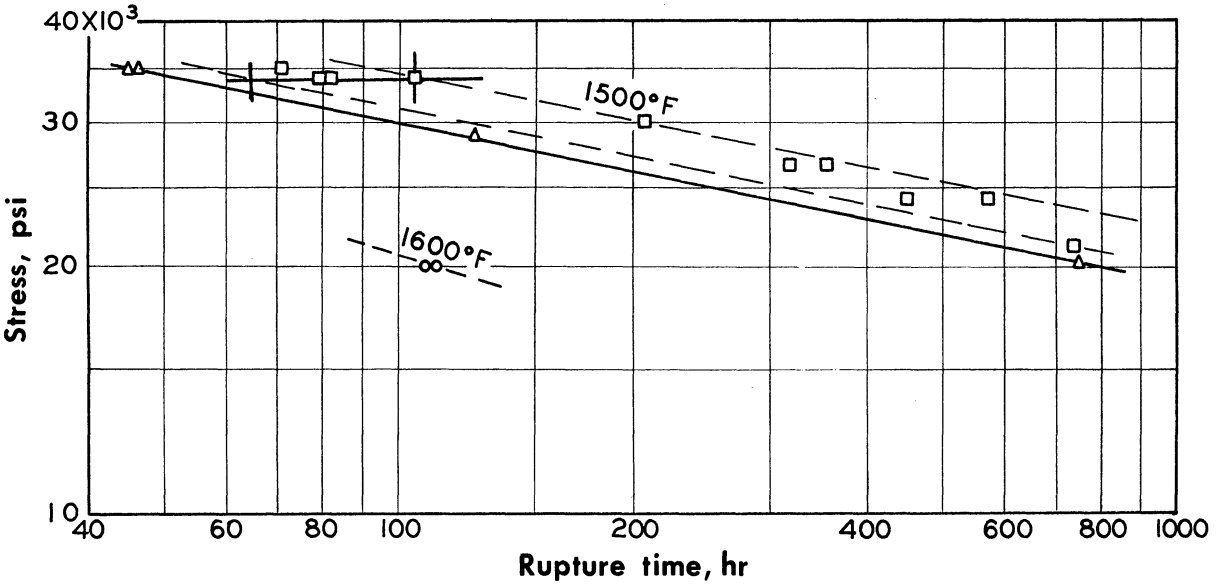

(b) Heat HT-28.

Figure 9. - Curves of stress against rupture time at 1500° and 1600°F from normal rupture tests on the two heats of M252 alloy used in the investigation, showing at the stresses used for overheat tests, the ranges in rupture time predicted by the available data.

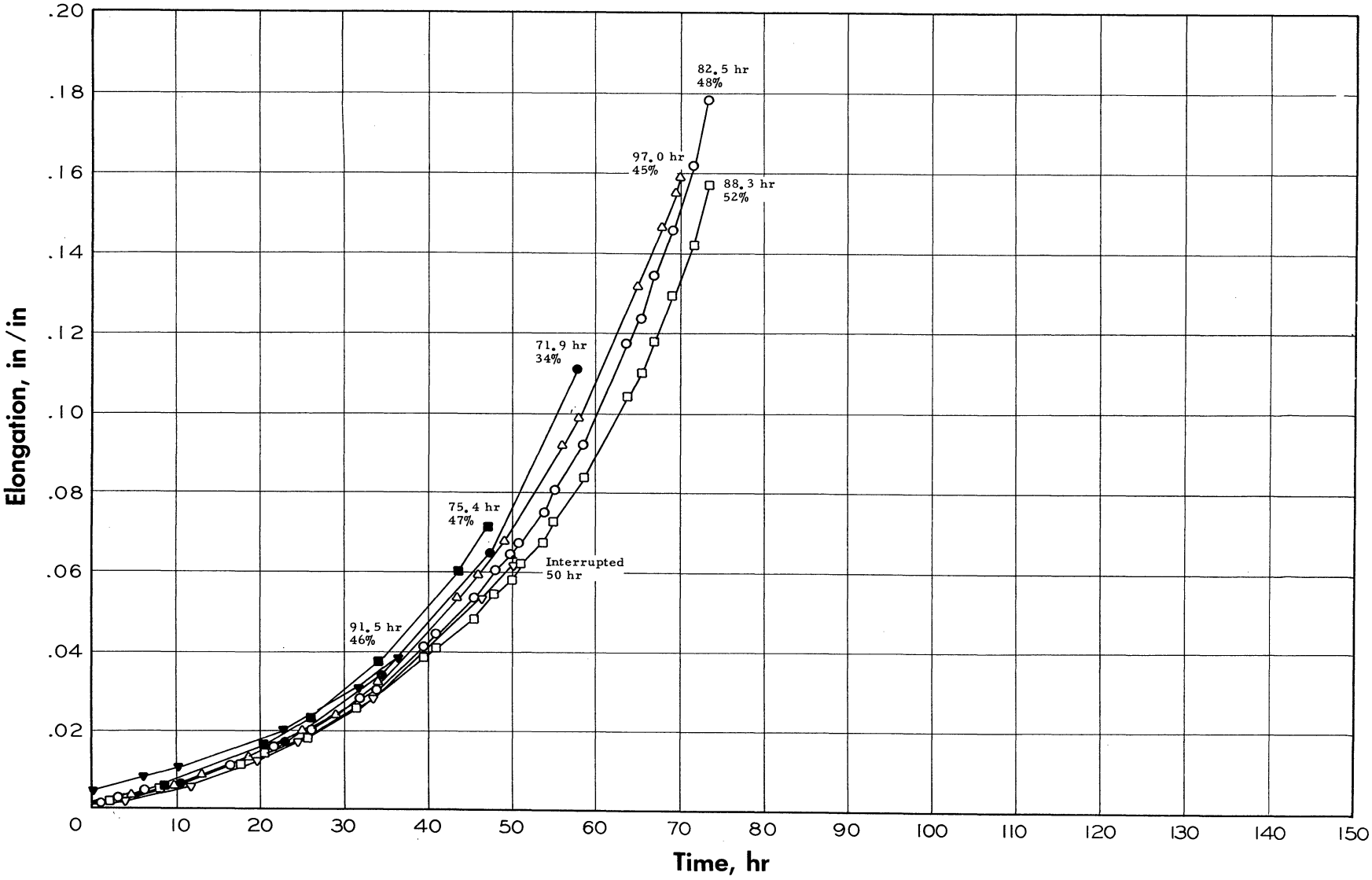

(a) Normal creep rupture tests.

Figure 10. - Comparative creep curves at 1600°F and 18,000 psi for heat 837 of M252 alloy for the indicated test conditions. Solid points indicate period of application of overheats. Number of overheats, time for rupture and elongation at rupture indicated for each curve.

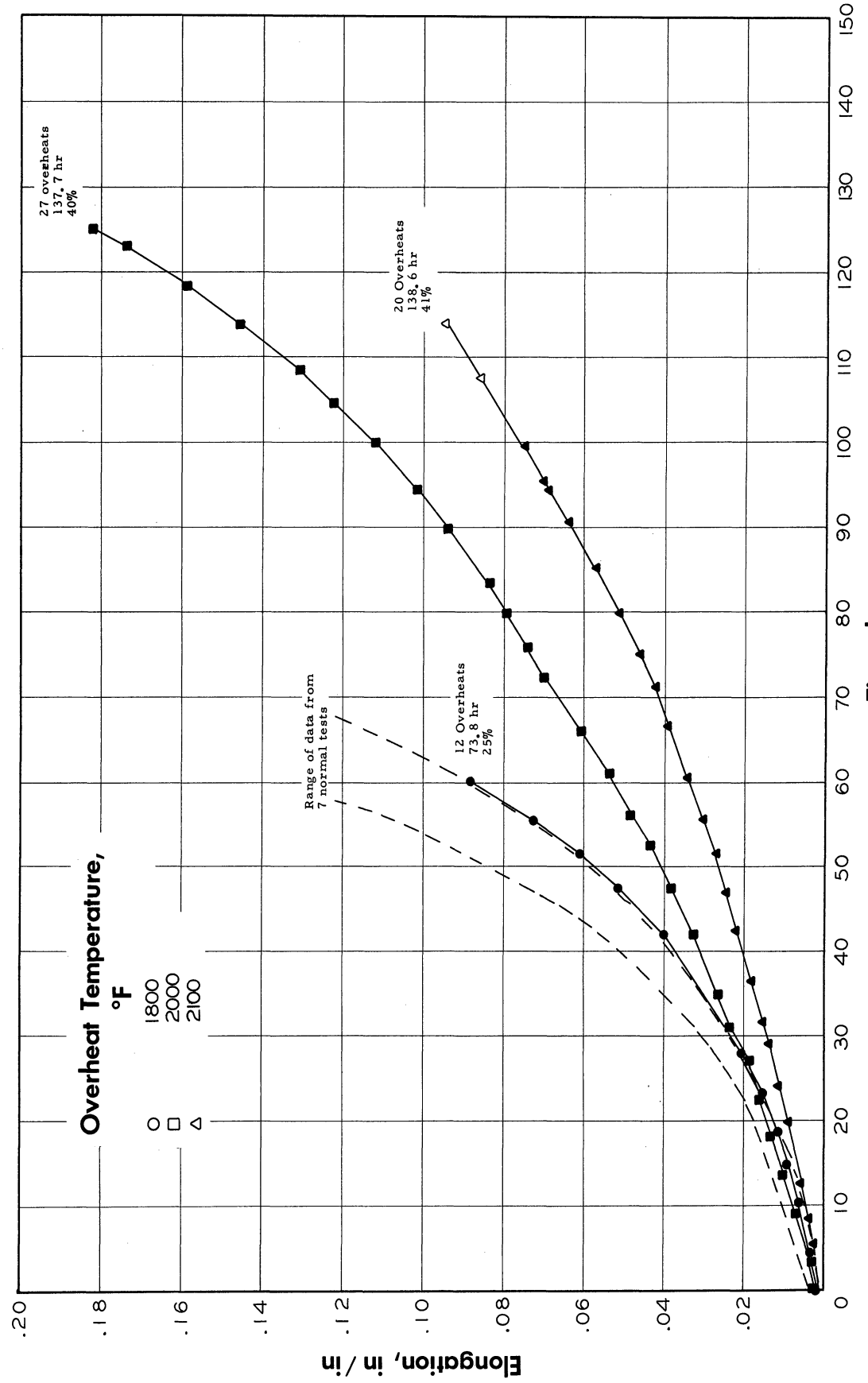

(b) Tests receiving the greatest number of overheats to each temperature.

Figure 10. - Continued. Comparative creep curves at 1600°F and 18,000 psi for heat 837 of M252 alloy for the indicated test conditions. Solid points indicate period of application of overheats. Number of overheats, time for rupture and elongation at rupture indicated for each curve.

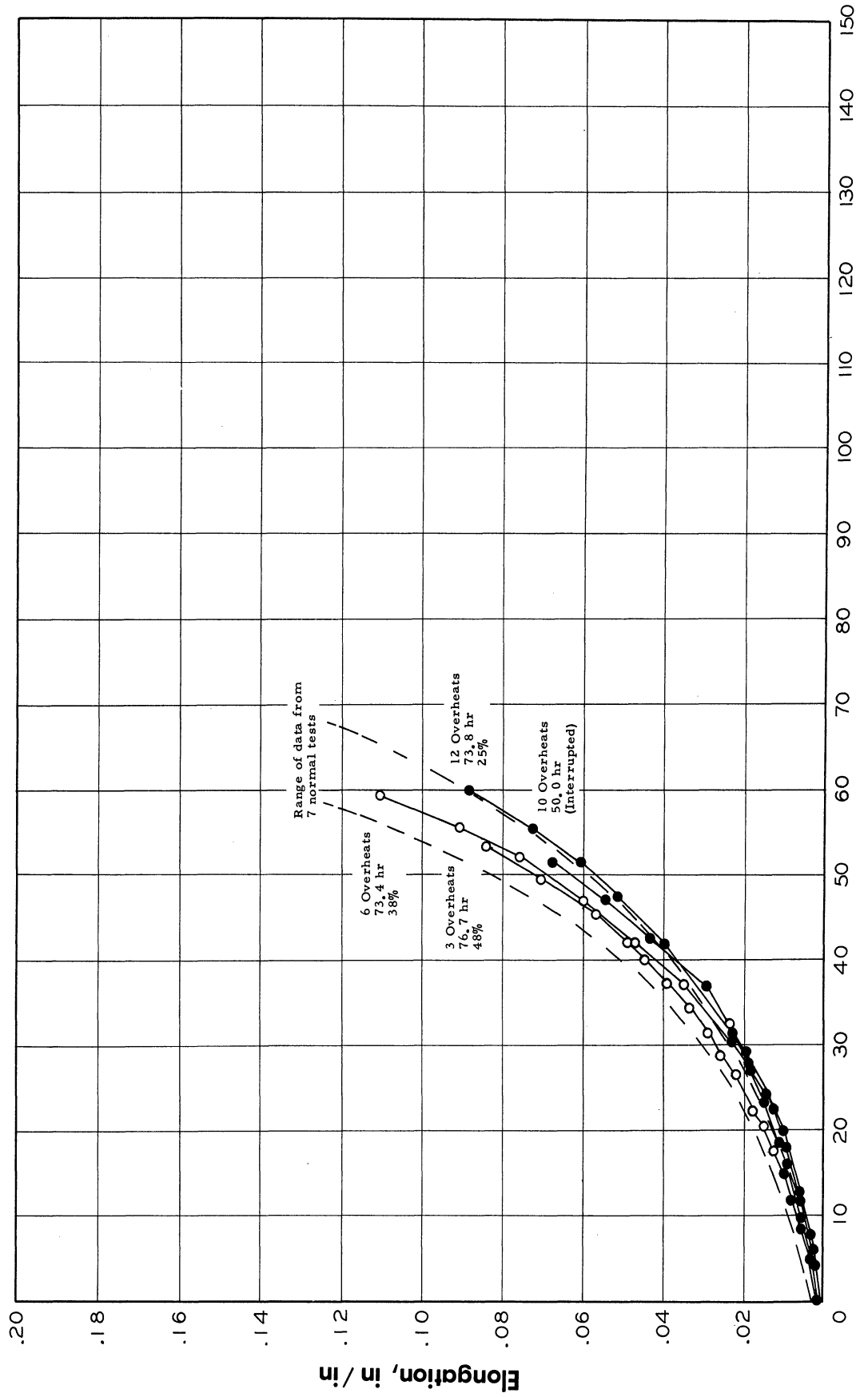

(c) Tests overheated to 1800°F.

Figure 10 - Continued. Comparative creep curves at 1600°F and 18,000 psi for heat 837 of M252 alloy for the indicated test conditions. Solid points indicate period of application of overheats. Number of overheats, time for rupture and elongation at rupture indicated for each curve.

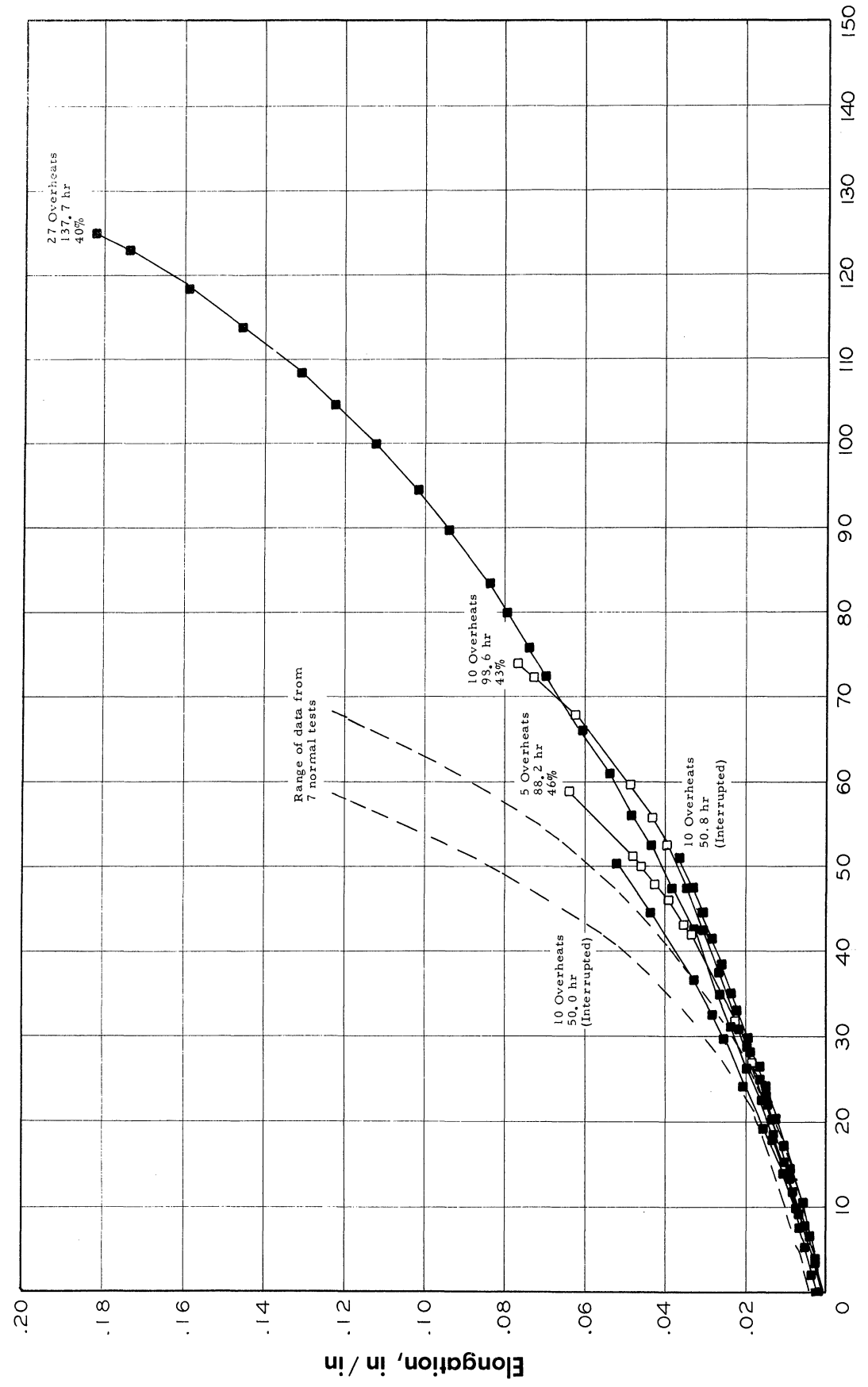

(d) Tests overheated to 2000°F.

Figure 10. - Continued. Comparative creep curves at 1600°F and 18,000 psi for heat 837 of M252 alloy for the indicated test conditions. Solid points indicate period of application of overheats. Number of overheats, time for rupture and elongation at rupture indicated for each curve.

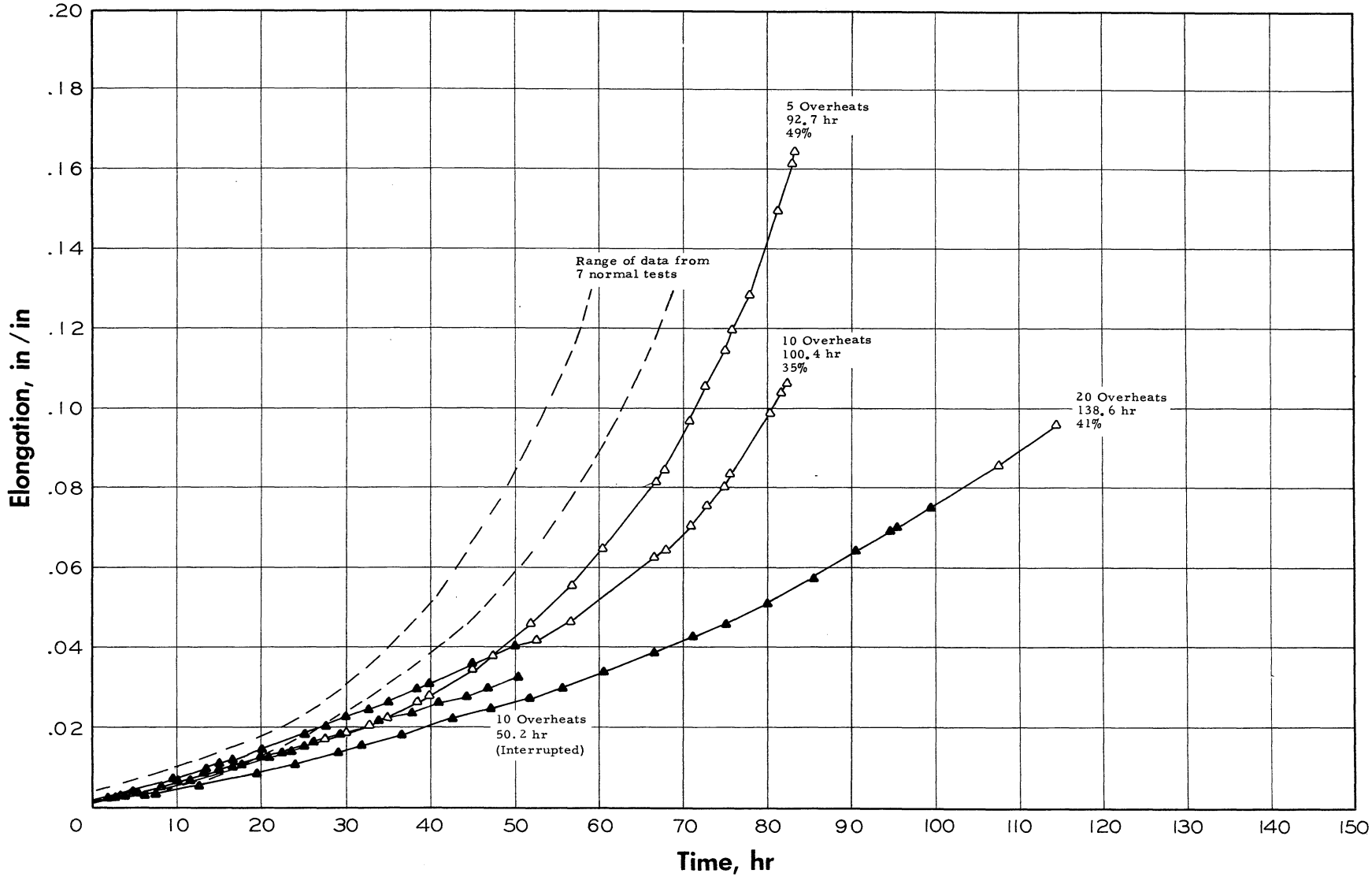

(e) Tests overheated to 2100°F.

Figure 10. - Concluded. Comparative creep curves at 1600°F and 18,000 psi for heat 837 of M252 alloy for the indicated test conditions. Solid points indicate period of application of overheats. Number of overheats, time for rupture and elongation at rupture indicated for each curve.

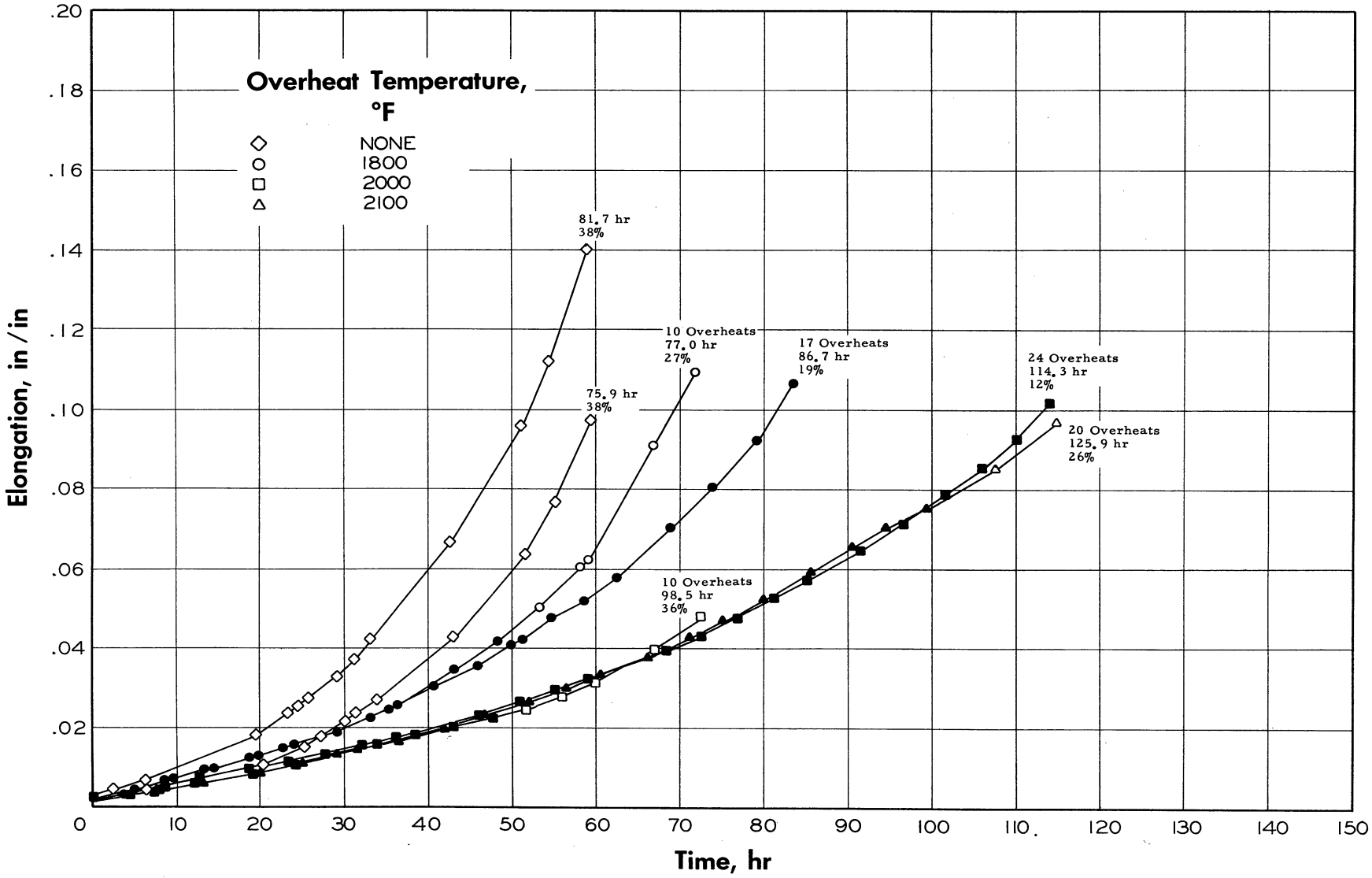

Figure 11. - Comparative creep curves at 1500°F and 33,000 psi for heat 837 of M252 alloy for the indicated test conditions. Solid points indicate period of application of overheats. Number of overheats, time for rupture and elongation at rupture indicated for each curve.

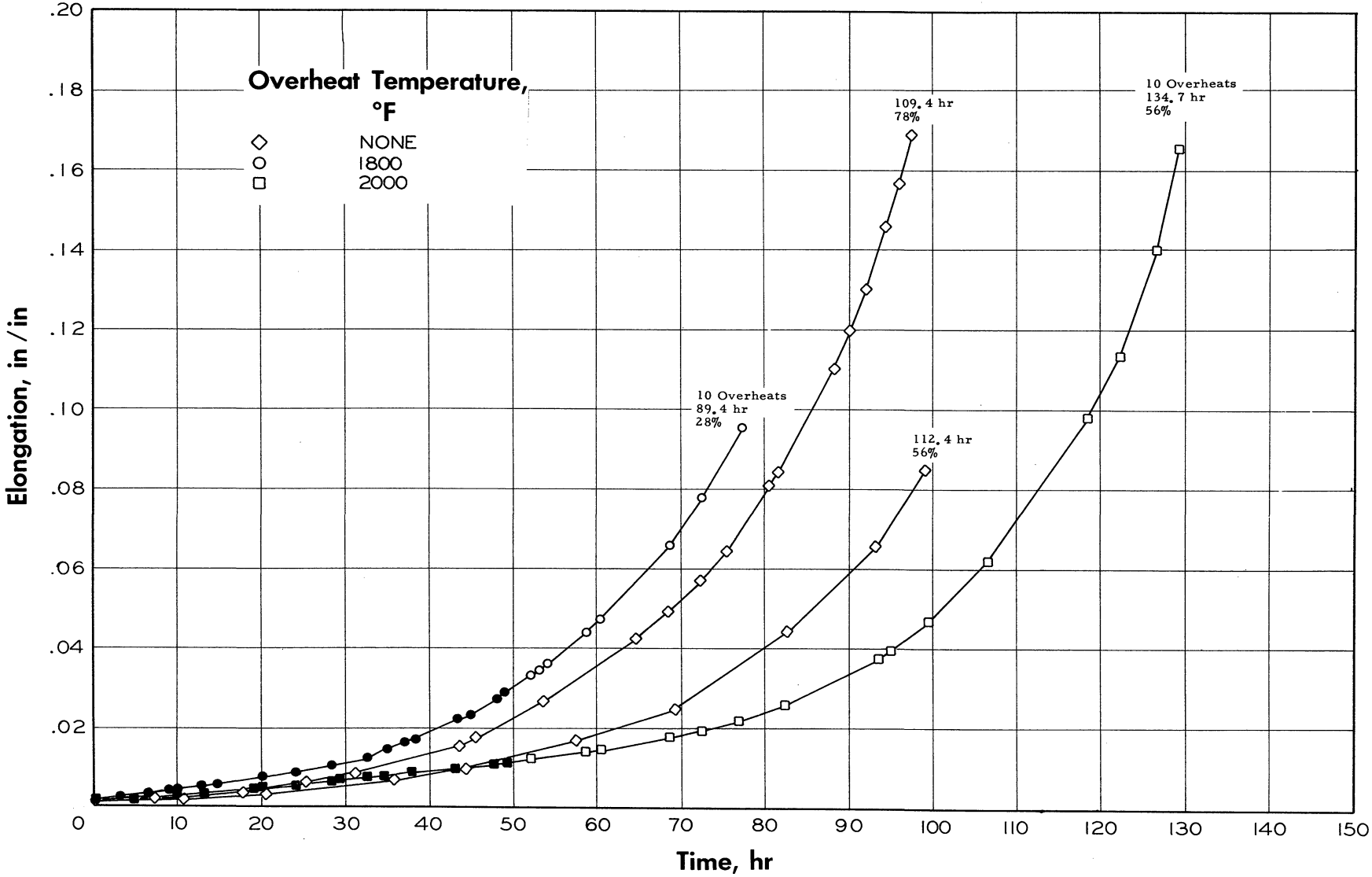

Figure 12. - Comparative creep curves at 1600°F and 20,000 psi for heat HT-28 of M252 alloy for the indicated test conditions. Solid points indicate period of application of overheats. Number of overheats, time for rupture and elongation at rupture indicated for each curve.

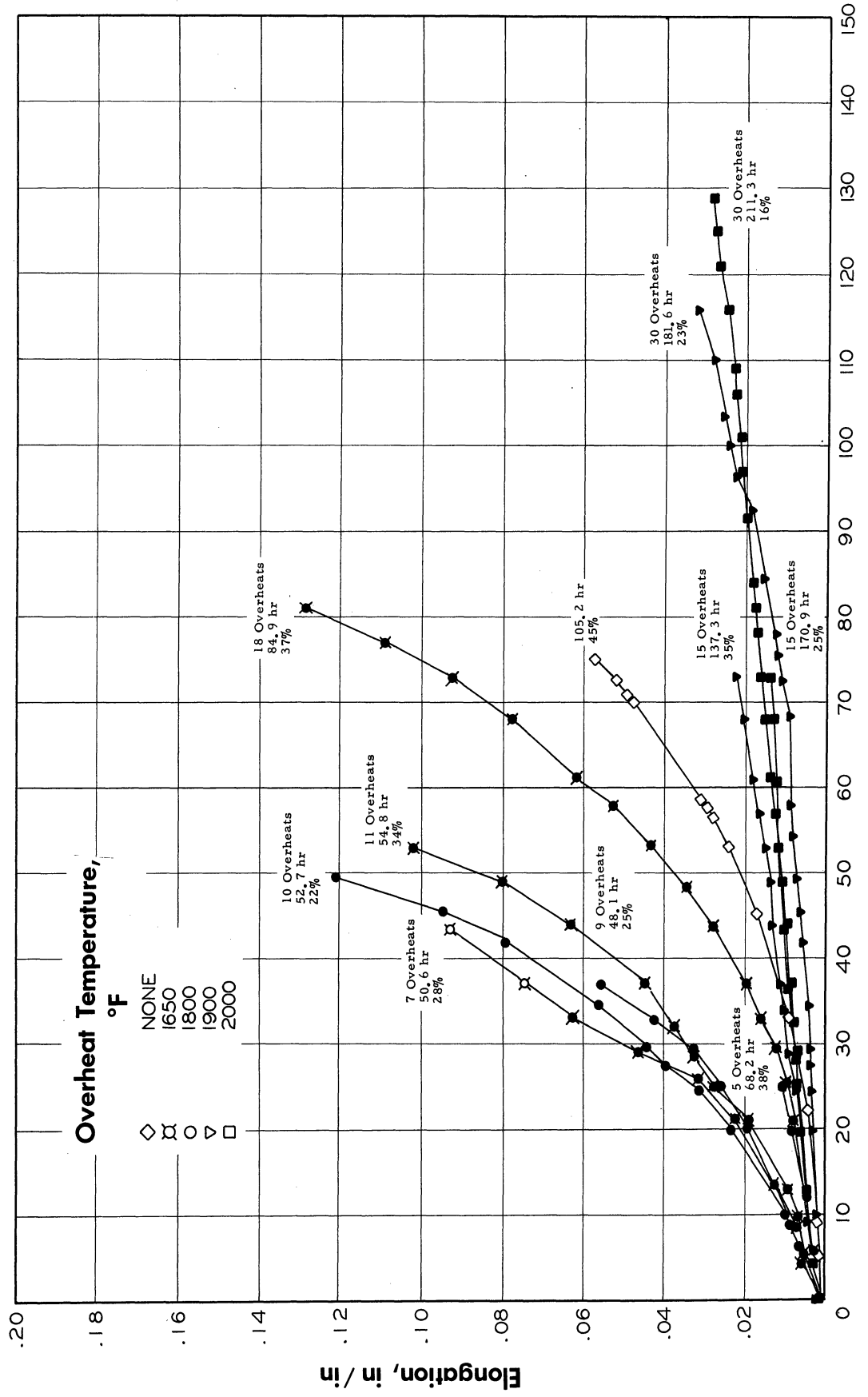

Figure 13. - Comparative creep curves at 1500°F and 34,000 psi for heat HT-28 of M252 alloy for the indicated test conditions. Solid points indicate period of application of overheats. Number of overheats, time for rupture and elongation at rupture indicated for each curve.

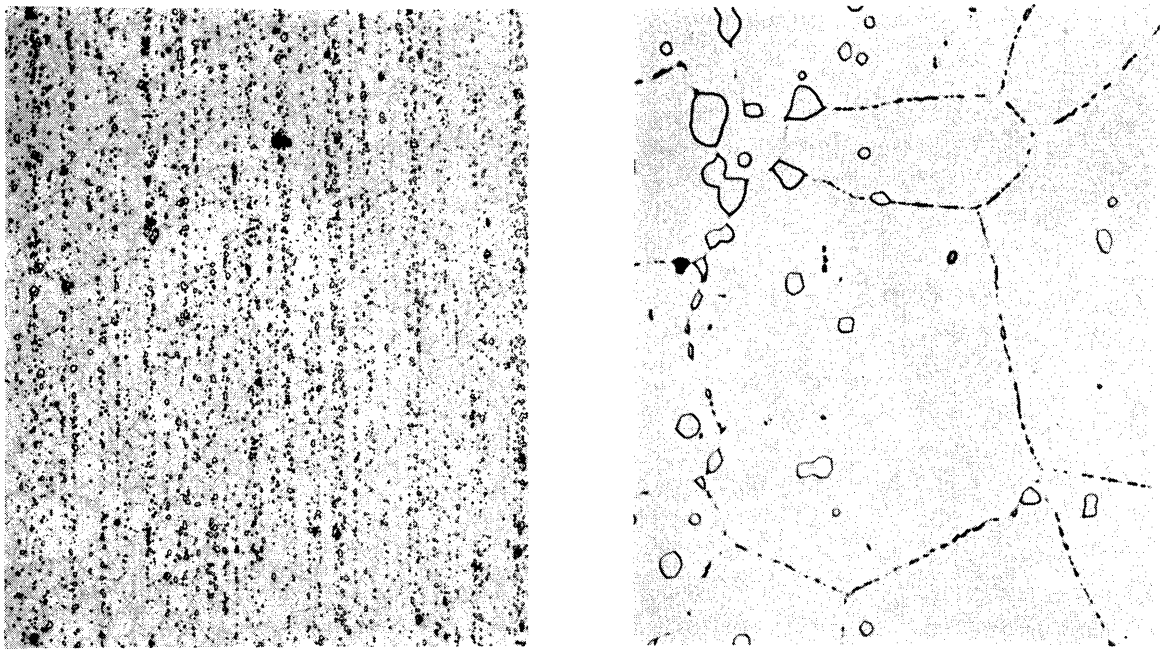

X100 X1000

(a) Heat 837, as heat-treated.

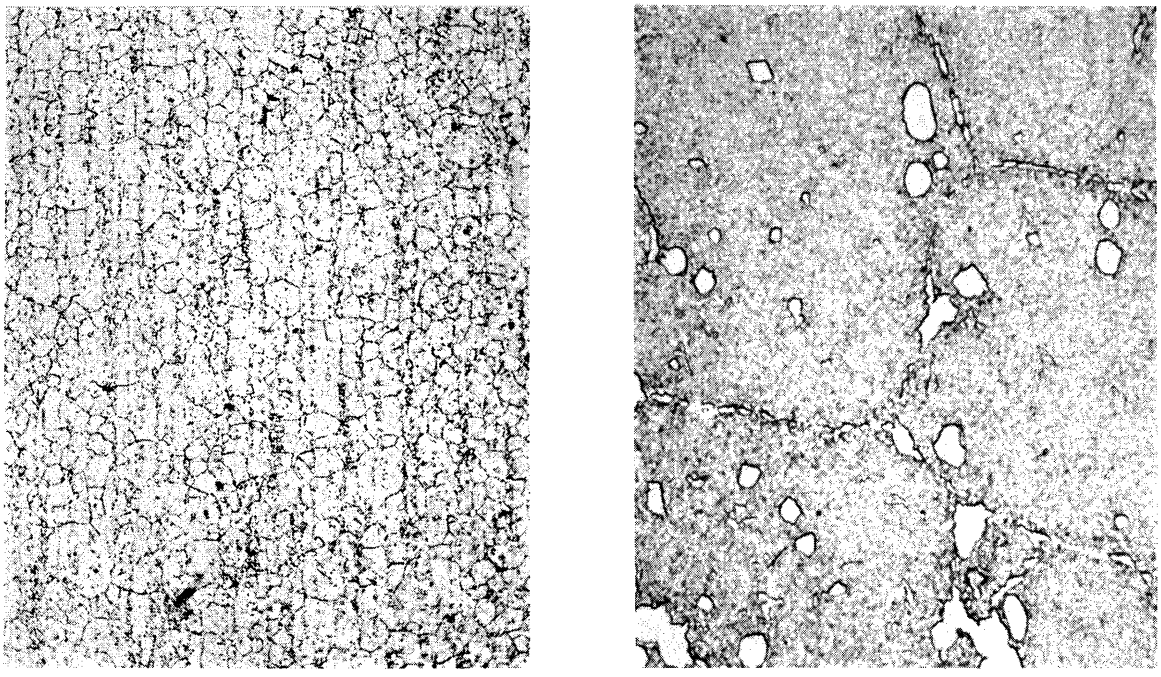

X100 X1000

(b) Heat 837 after rupture testing at 1600°F and 18,000 psi. Interrupted at 50.0 hours.

Figure 14. - Microstructures of M252 heats after heat treatment and after rupture testing at 1600°F.

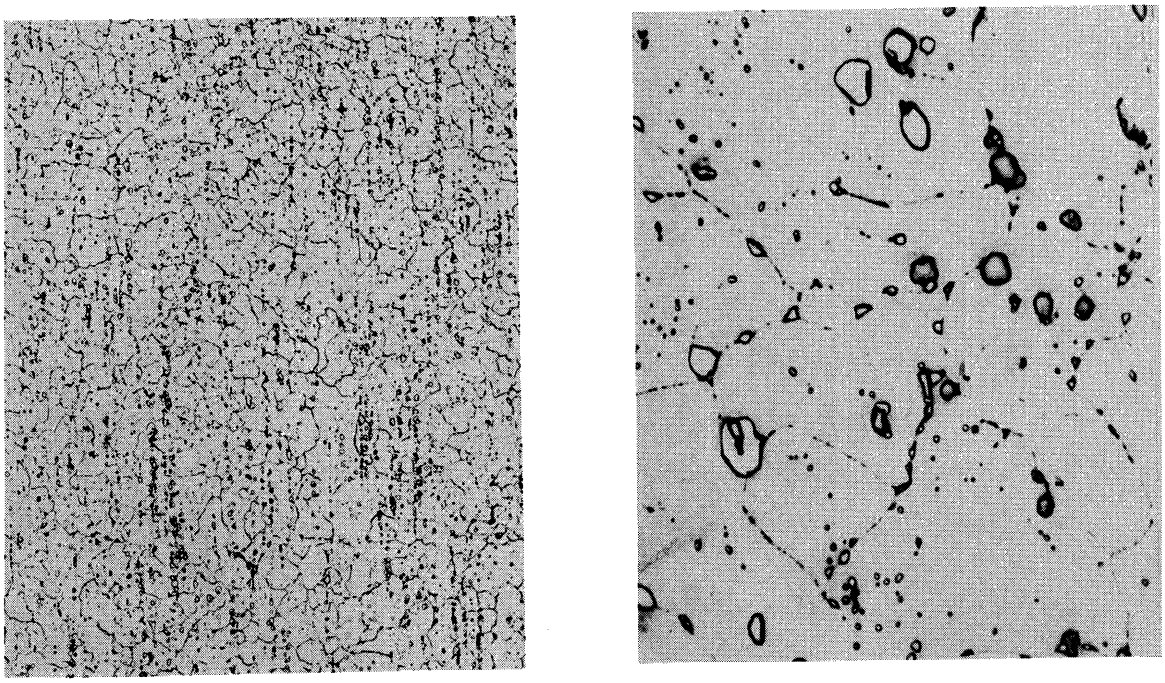

X100 X1000

(c) Heat HT-28, as heat-treated.

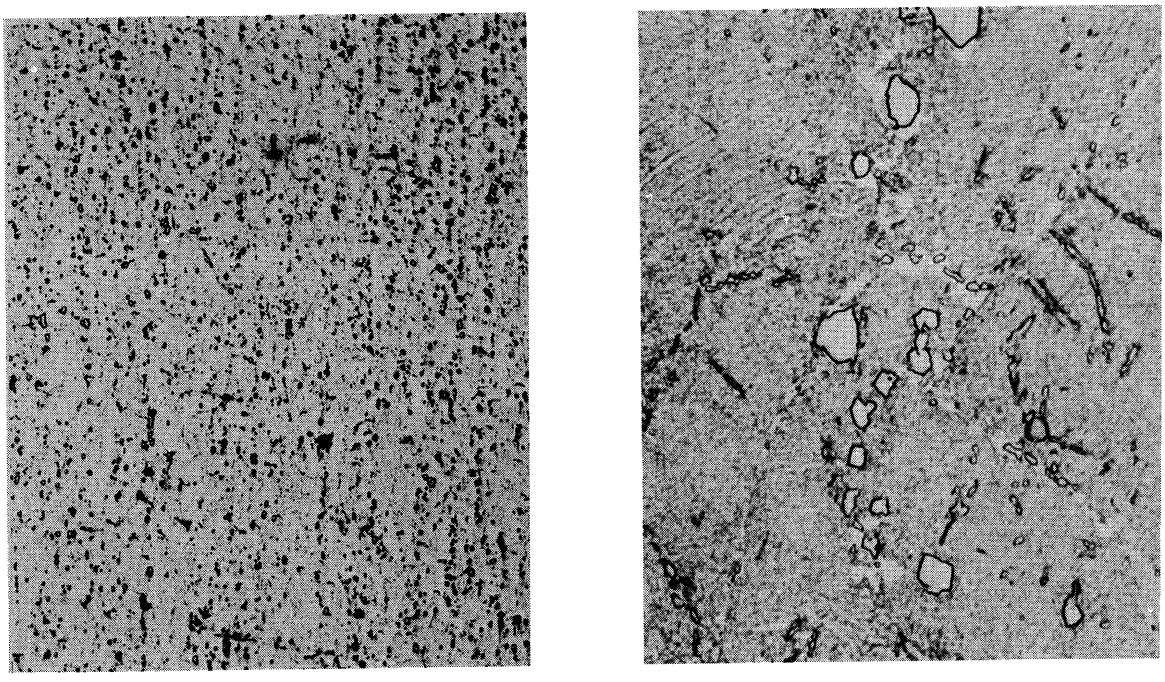

X100 X1000

(d) Heat HT-28 after rupture testing at 1600°F and 20,000 psi. Rupture time, 109.4 hours.

Figure 14. - Concluded. Microstructures of M252 heats after heat treatment and after rupture testing at 1600°F.

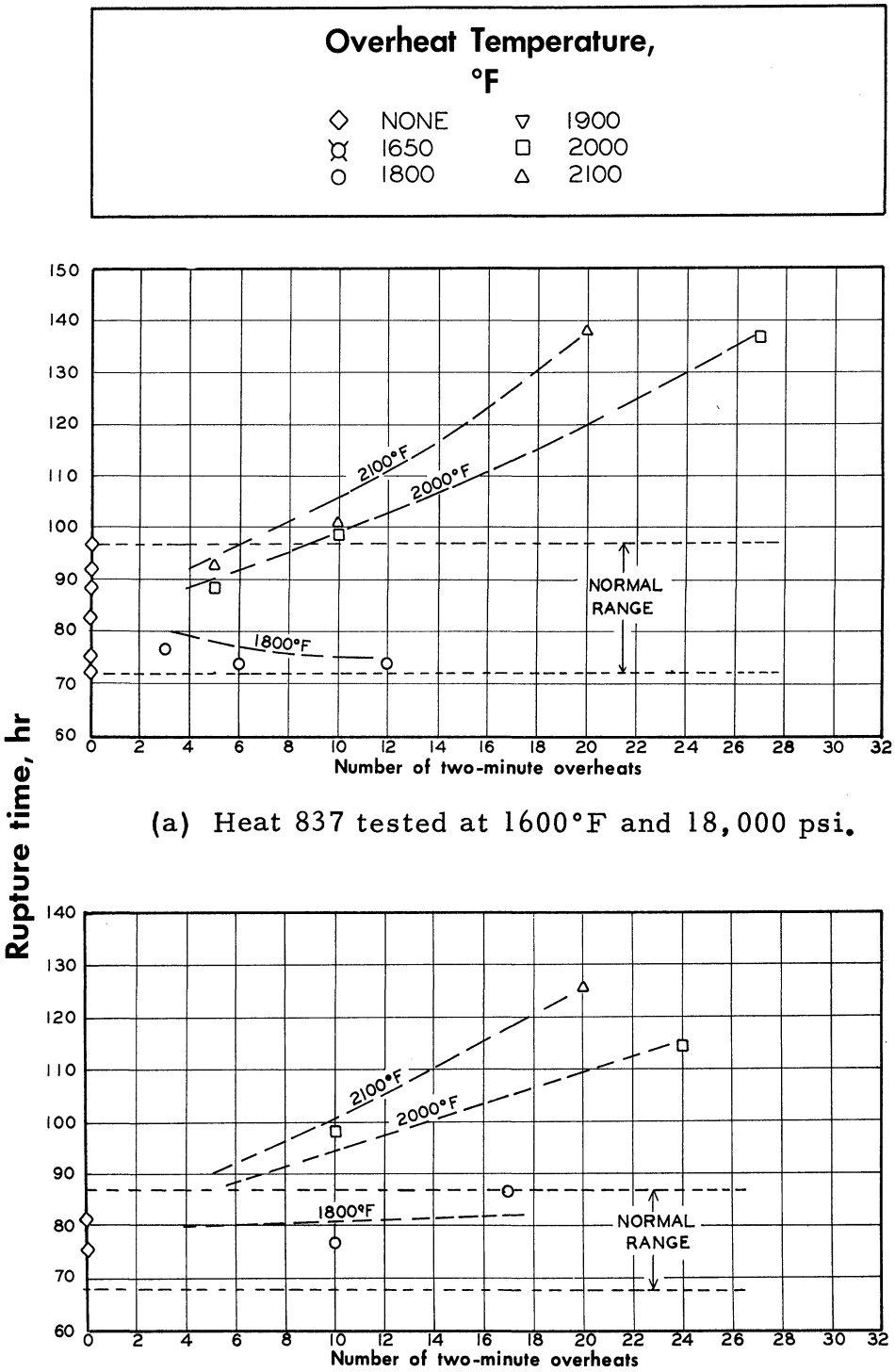

(a) Heat 837 tested at 1600°F and 18,000 psi.

(b) Heat 837 tested at 1500°F and 33,000 psi.

Figure 15. - Effect of number of overheats on the rupture time of M252 alloy for the overheat temperatures and base conditions indicated. Overheats were of two minutes duration applied every five hours from the beginning of the test.

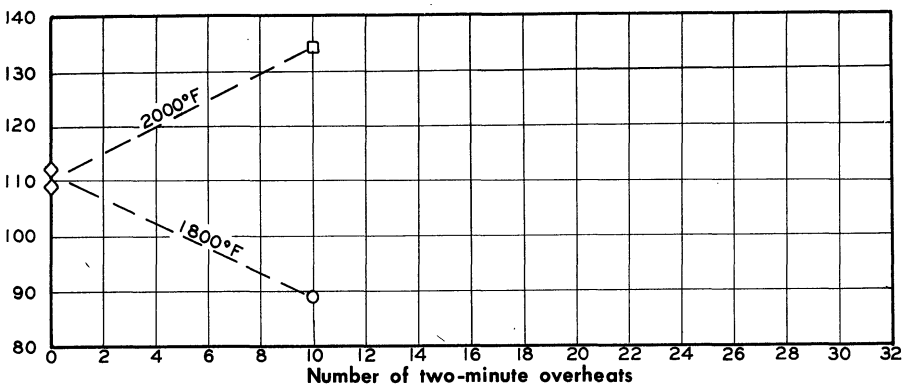

(c) Heat HT-28 tested at 1600°F and 20,000 psi.

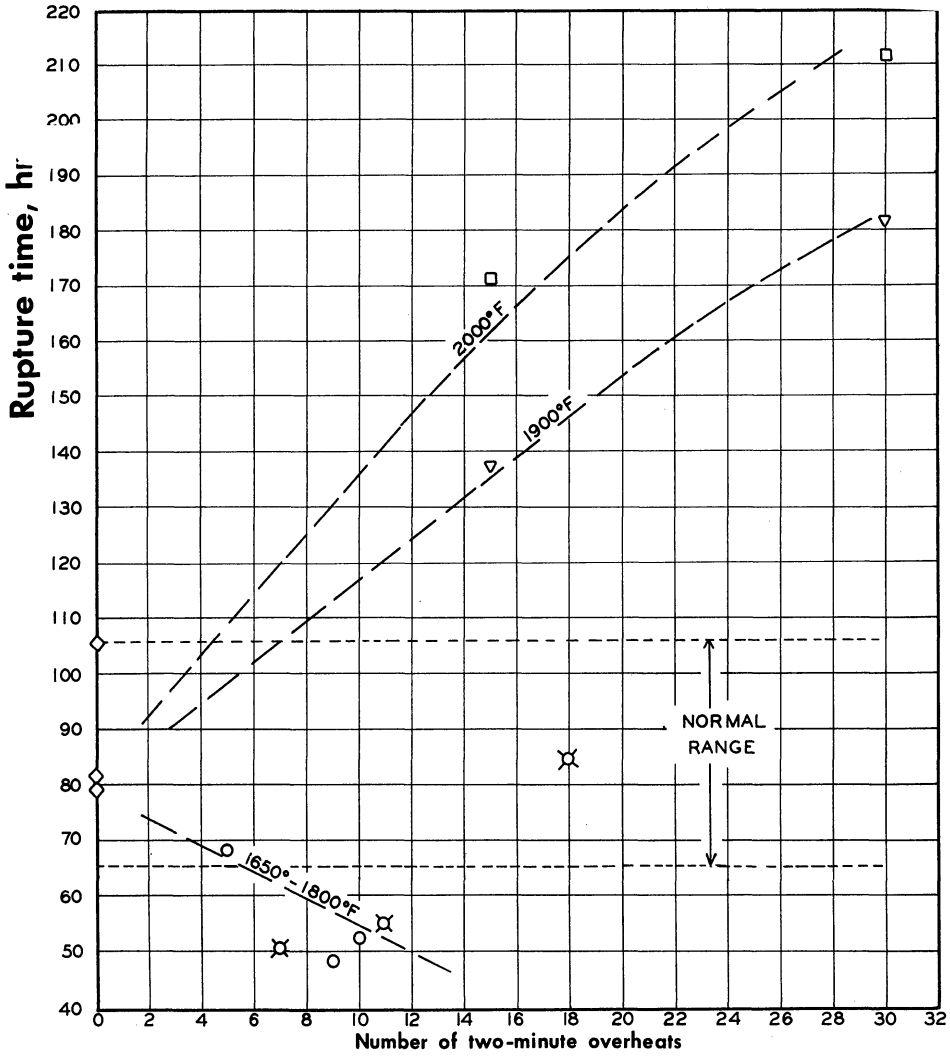

(d) Heat HT-28 tested at 1500°F and 34,000 psi. (Data from ref. 1).

Figure 15. - Concluded. Effect of number of overheats on the rupture time of M252 alloy for the overheat temperatures and base conditions indicated. Overheats were of two minutes duration applied every five hours from the beginning of the test.

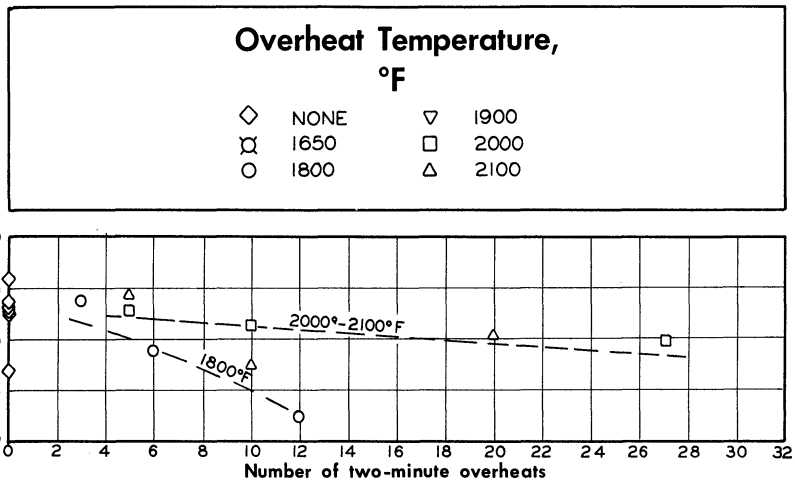

(a) Heat 837 tested at 1600°F and 18,000 psi.

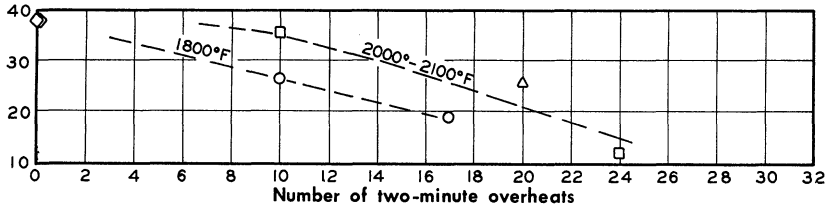

(b) Heat 837 tested at 1500°F and 33,000 psi.

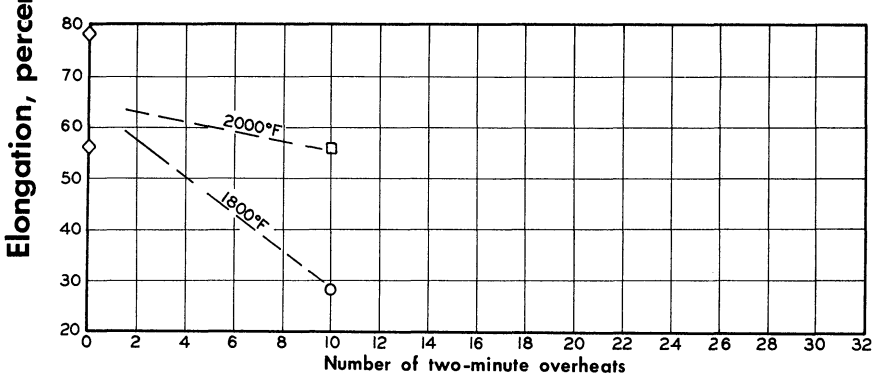

(c) Heat HT-28 tested at 1600°F and 20,000 psi.

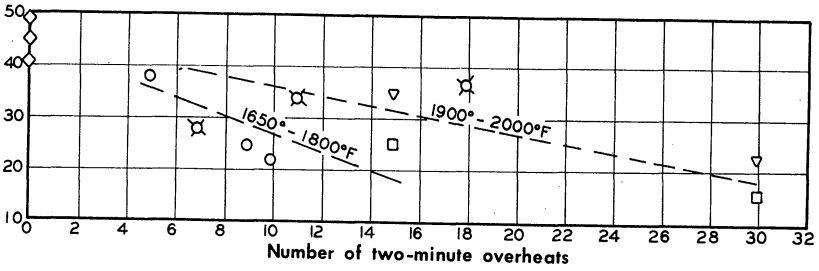

(d) Heat HT-28 tested at 1500°F and 34,000 psi. (Data from ref. 1.

Figure 16. - Effect of number of overheats on the elongation at fracture of M252 alloy for the overheat temperatures and base conditions indicated. Overheats were of two minutes duration applied every five hours from the beginning of the test.

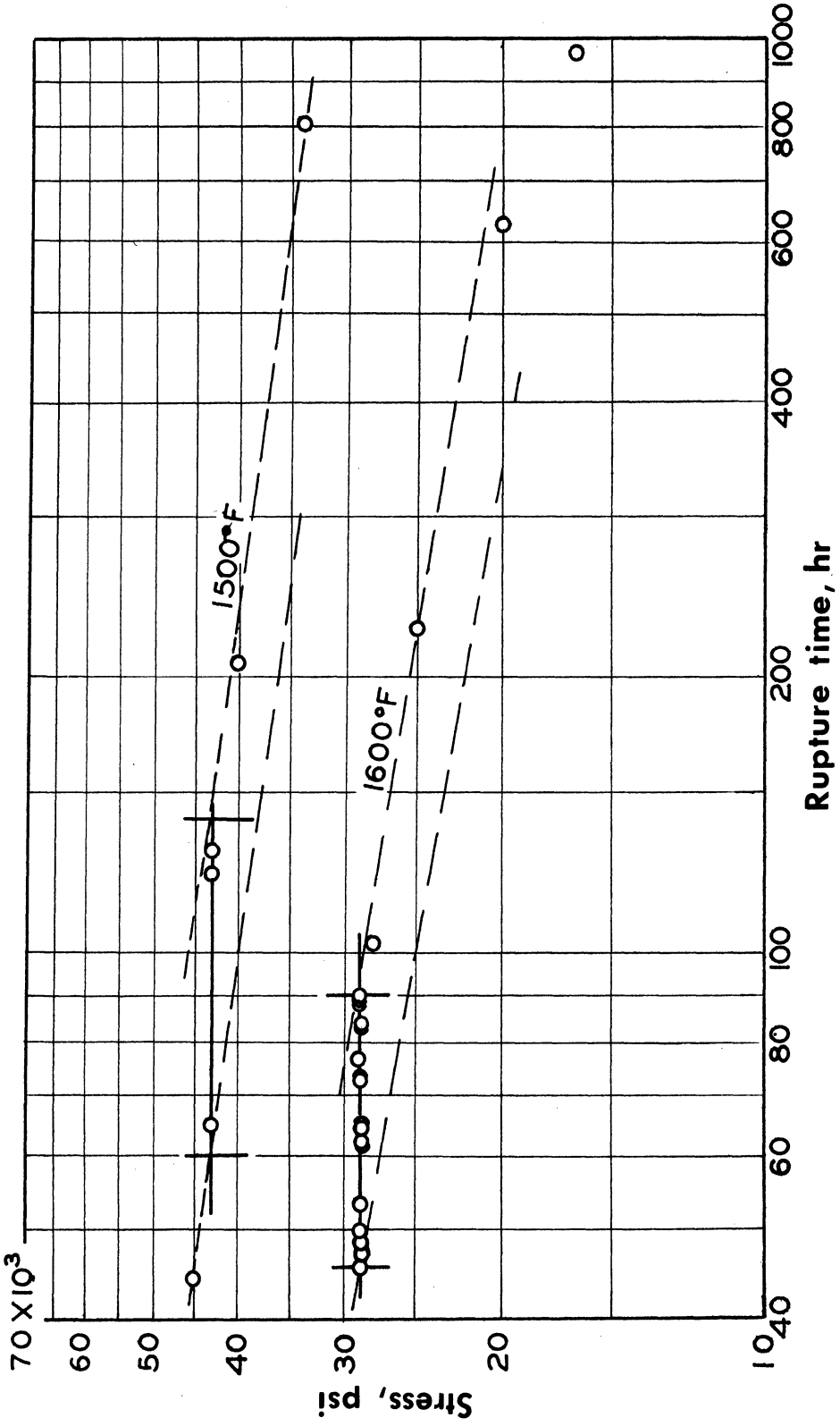

Figure 17. - Curves of stress against rupture time at 1500° and 1600°F from normal rupture tests on the heat of Inconel 700 alloy used in the investigation, showing at the stresses used for the overheat tests, the ranges in rupture times predicted by the available data. (See text for explanation of range at 1500°F.)

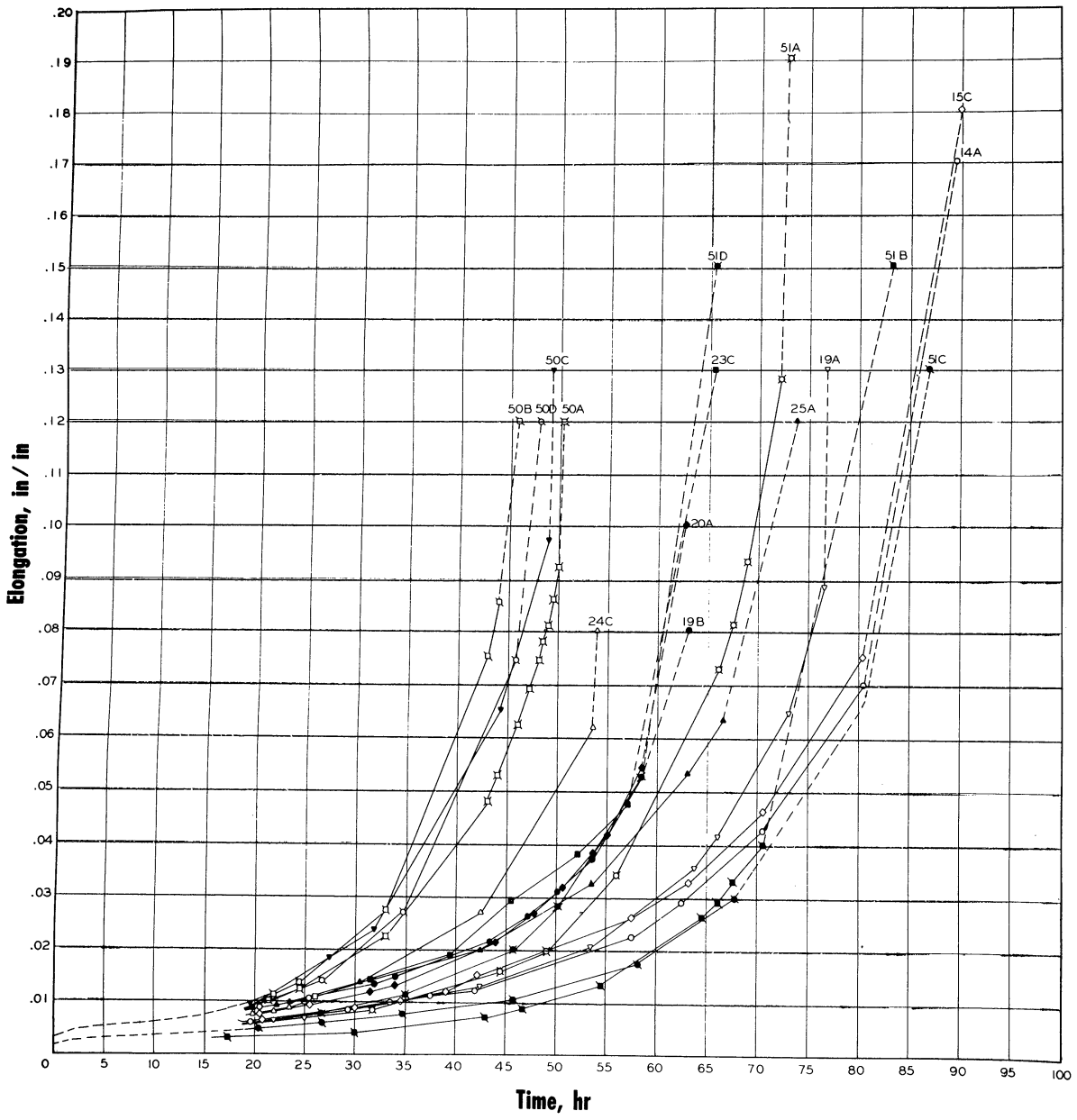

(a) Normal creep rupture tests showing complete curves terminating at final rupture time and elongation. (Data omitted for first 20 hours for clarity.)

Figure 18. - Comparative creep curves at 1600°F and 29,000 psi for Inconel 700 alloy for the indicated test conditions. Solid points indicate period of application of overheats. Sample number, number of overheats, rupture time, and elongation at fracture indicated for each curve.

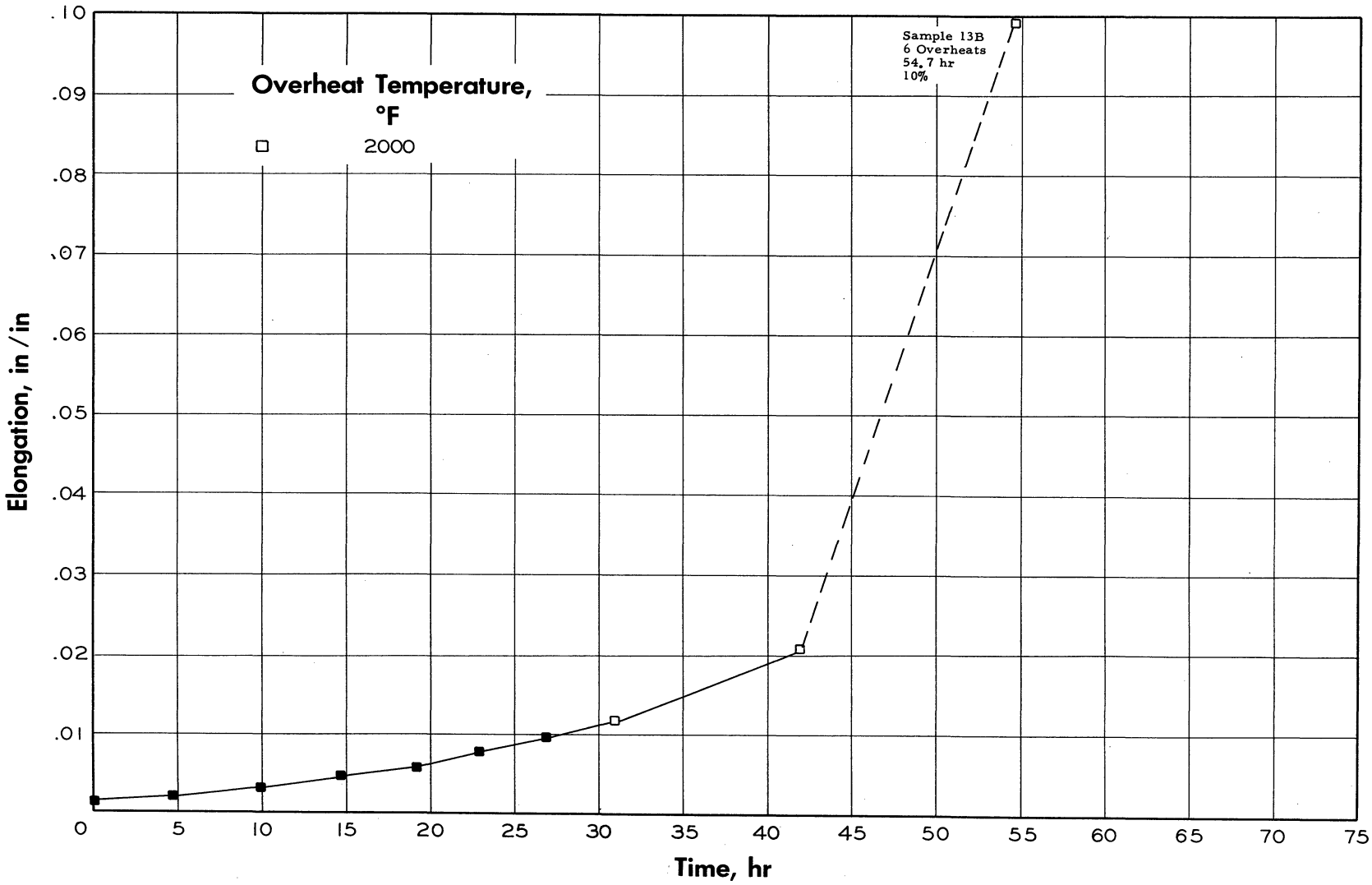

(b) Tests from bar 13.

Figure 18. - Continued. Comparative creep curves at 1600°F and 29,000 psi for Inconel 700 alloy for the indicated test conditions. Solid points indicate period of application of overheats. Sample number, number of overheats, rupture time, and elongation at fracture indicated for each curve.

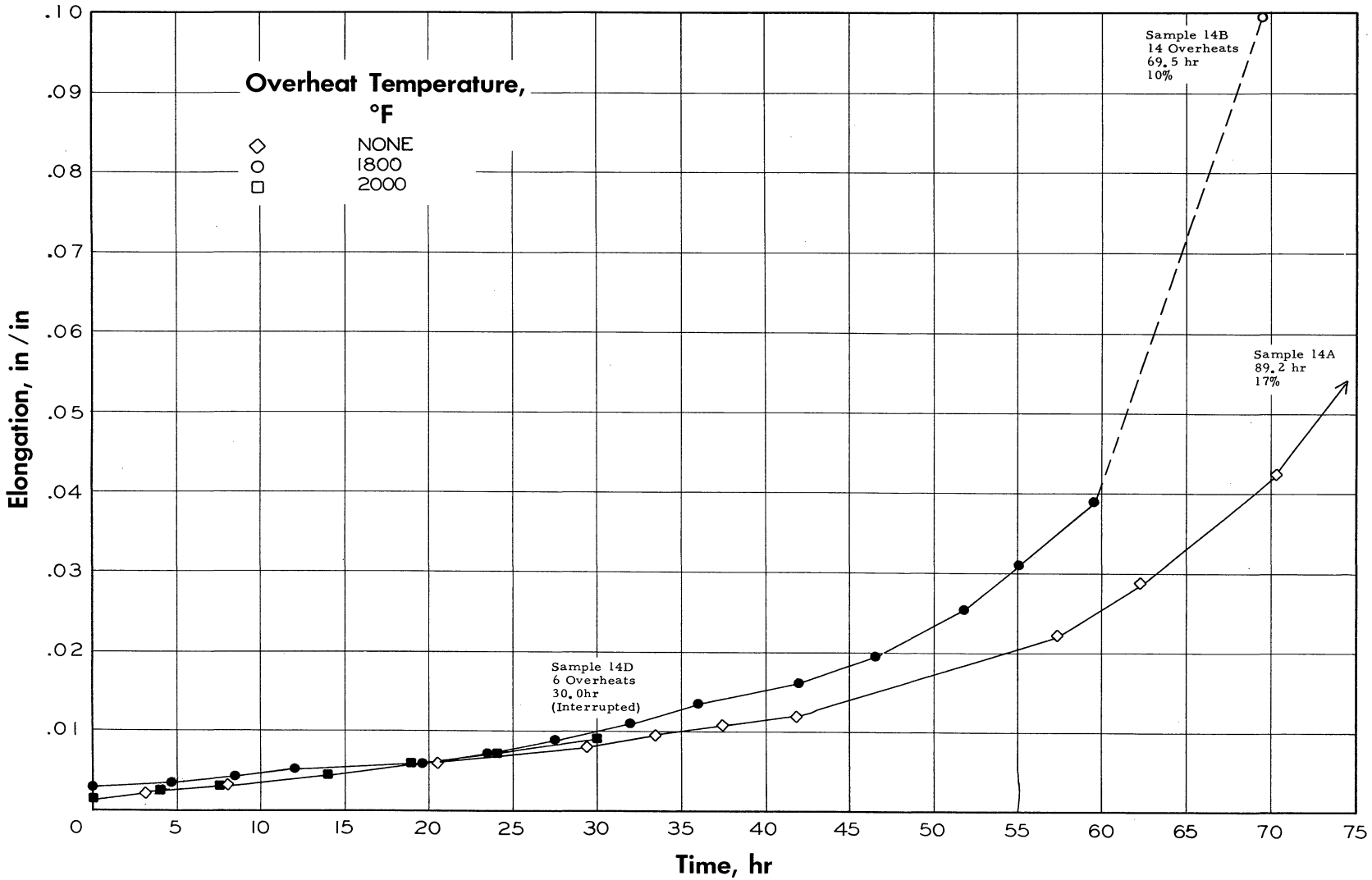

(c) Tests from bar 14.

Figure 18. - Continued. Comparative creep curves at 1600°F and 29,000 psi for Inconel 700 alloy for the indicated test conditions. Solid points indicate period of application of overheats. Sample number, number of overheats, rupture time, and elongation at fracture indicated for each curve.

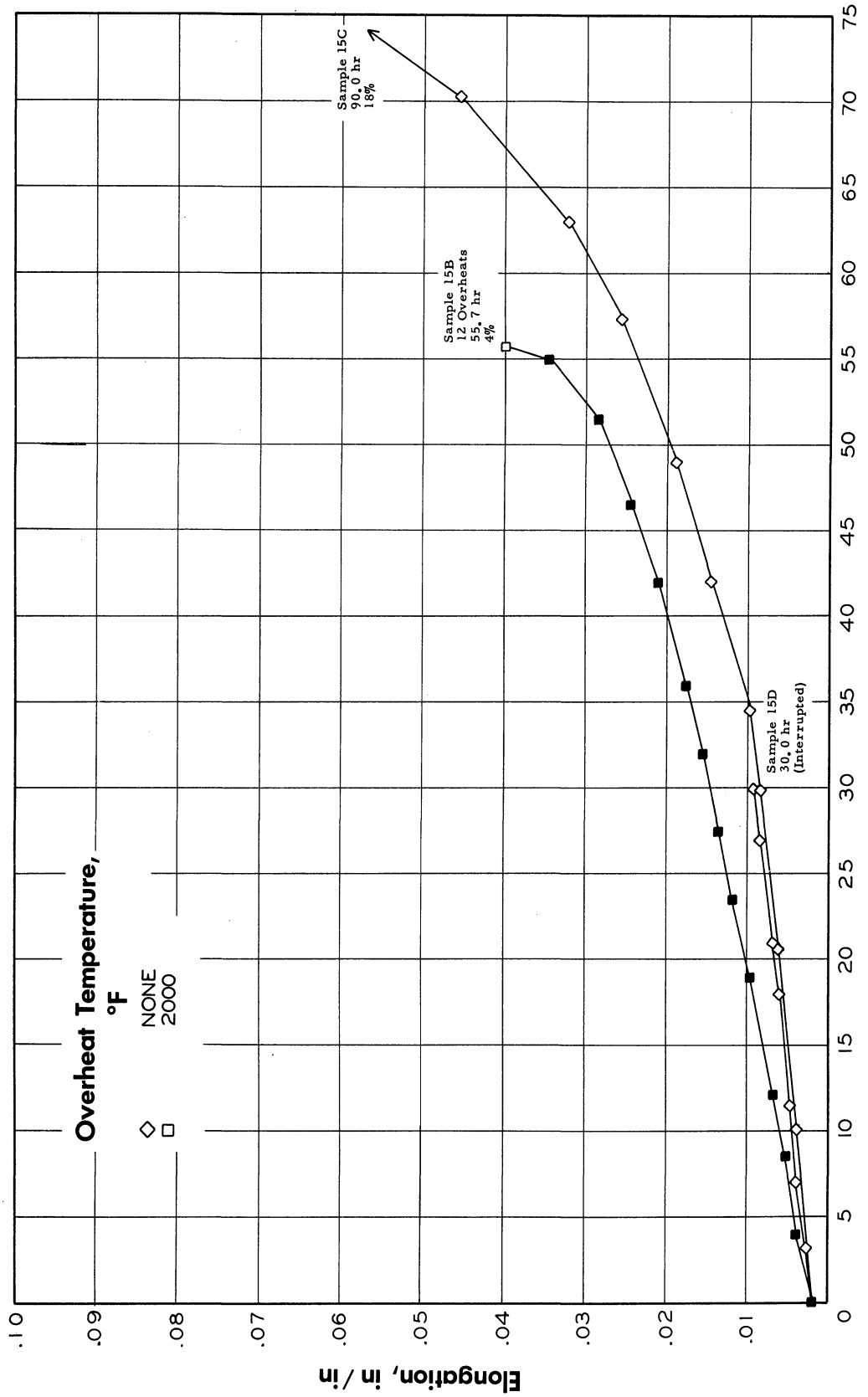

(d) Tests from bar 15.

Figure 18. - Continued. Comparative creep curves at 1600°F and 29,000 psi for Inconel 700 alloy for the indicated test conditions. Solid points indicate period of application of overheats. Sample number, number of overheats, rupture time, and elongation at fracture indicated for each curve.

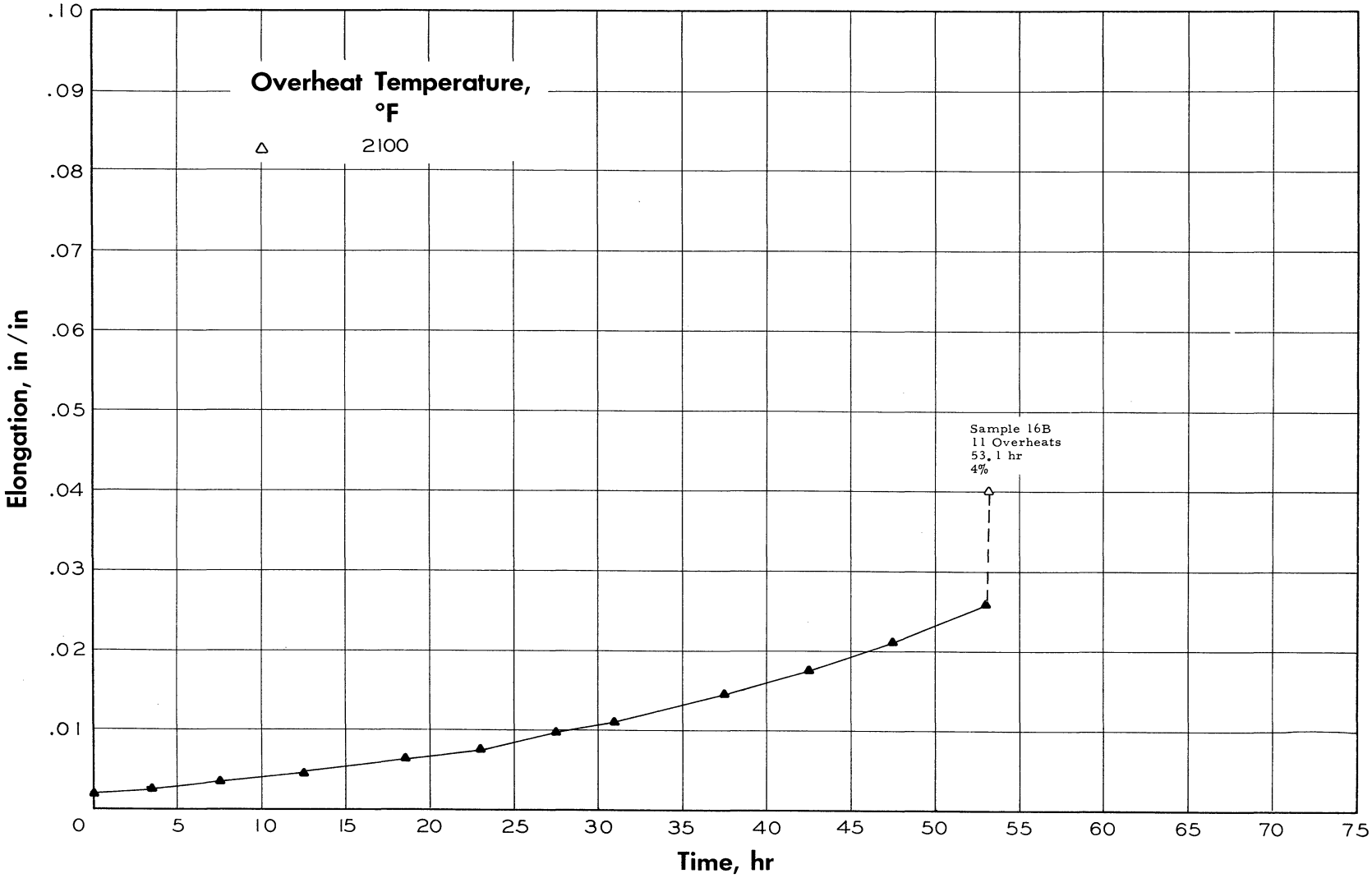

(e) Tests from bar 16.

Figure 18. - Continued. Comparative creep curves at 1600°F and 29,000 psi for Inconel 700 alloy for the indicated test conditions. Solid points indicate period of application of overheats. Sample number, number of overheats, rupture time, and elongation at fracture indicated for each curve.

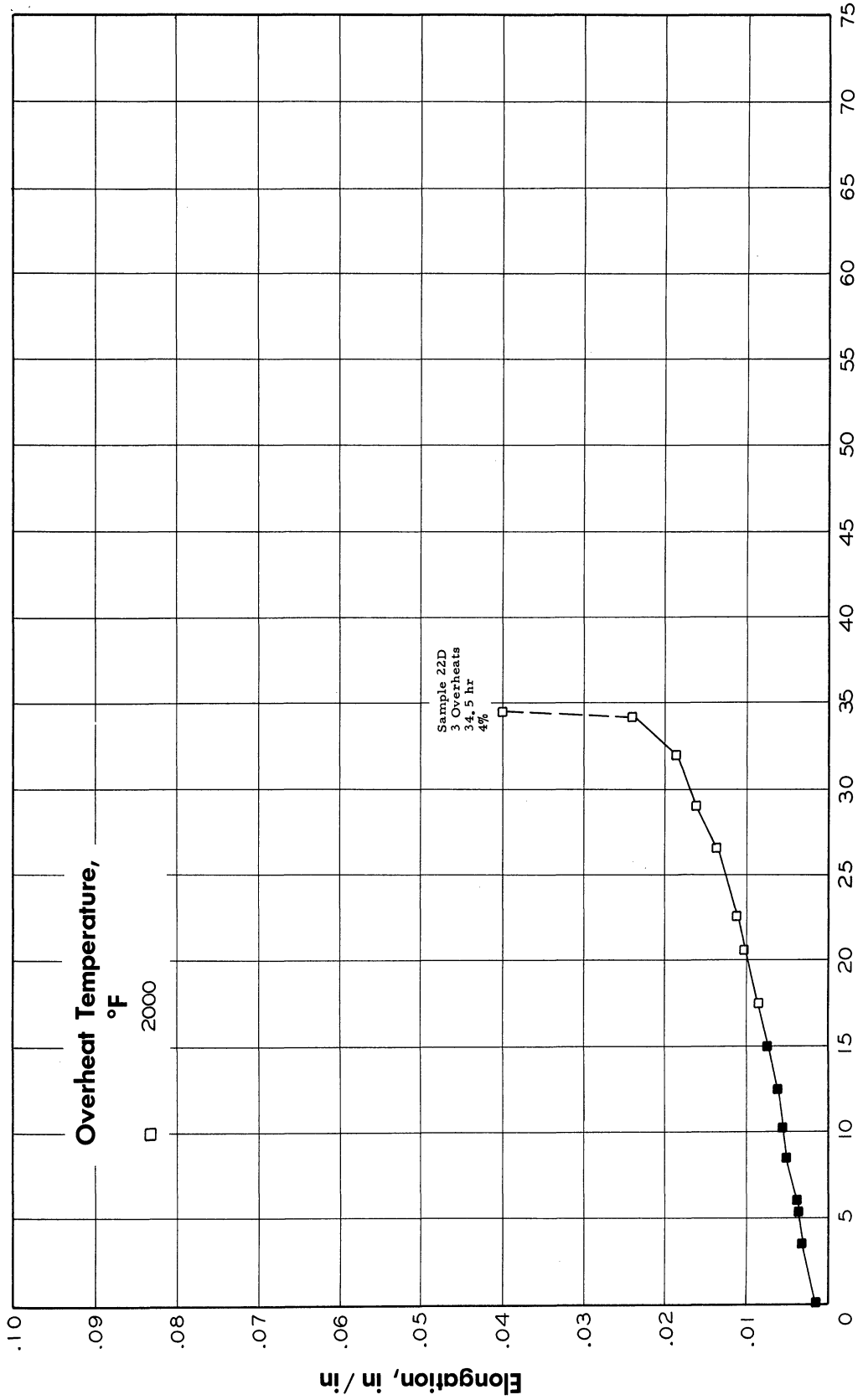

(f) Tests from bar 22.

Figure 18. - Continued. Comparative creep curves at 1600°F and 29,000 psi for Inconel 700 alloy for the indicated test conditions. Solid points indicate period of application of overheats. Sample number, number of overheats, rupture time, and elongation at fracture indicated for each curve.

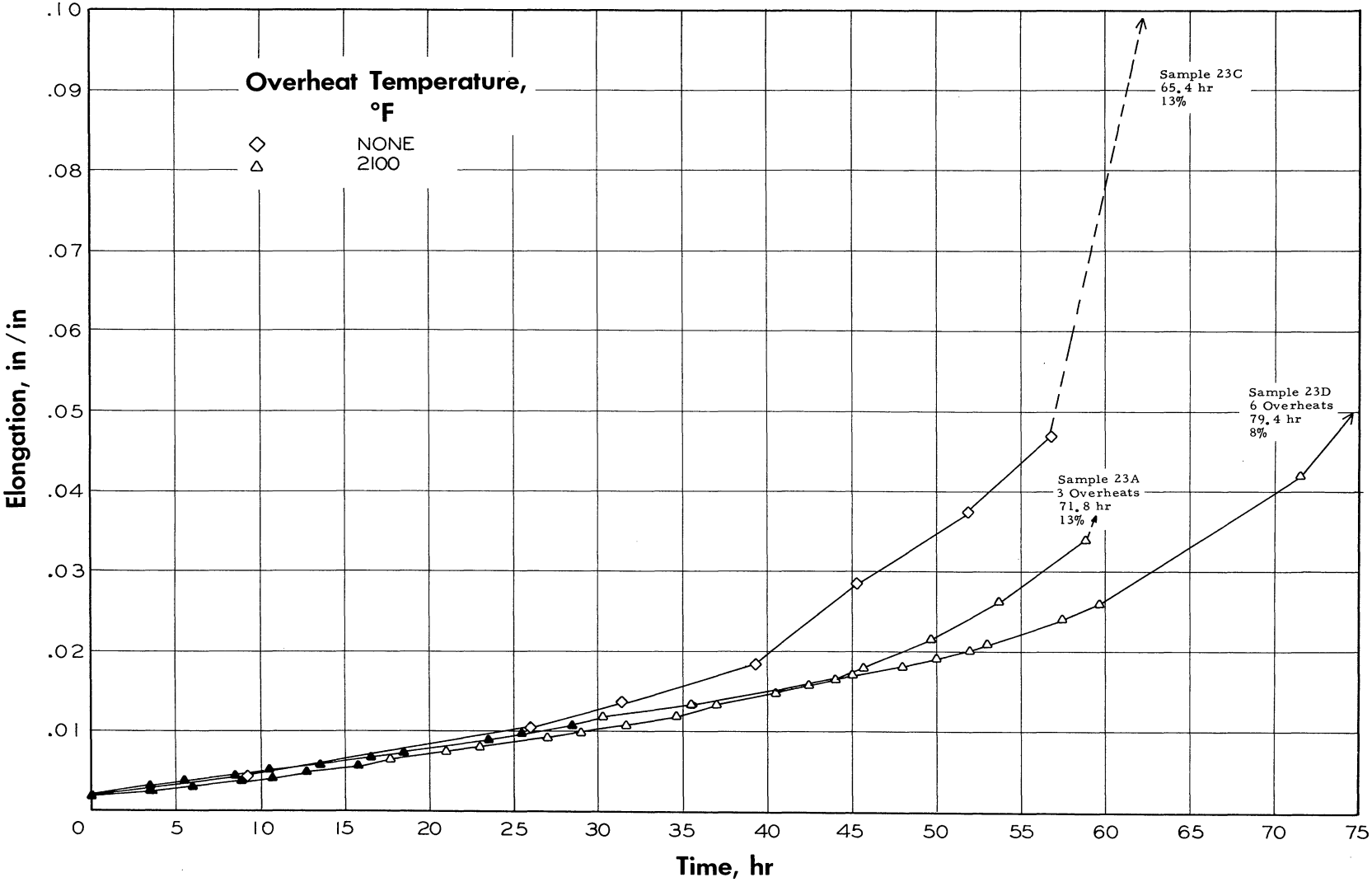

(g) Tests from bar 23.

Figure 18. - Continued. Comparative creep curves at 1600°F and 29,000 psi for Inconel 700 alloy for the indicated test conditions. Solid points indicate period of application of overheats. Sample number, number of overheats, rupture time, and elongation at fracture indicated for each curve.

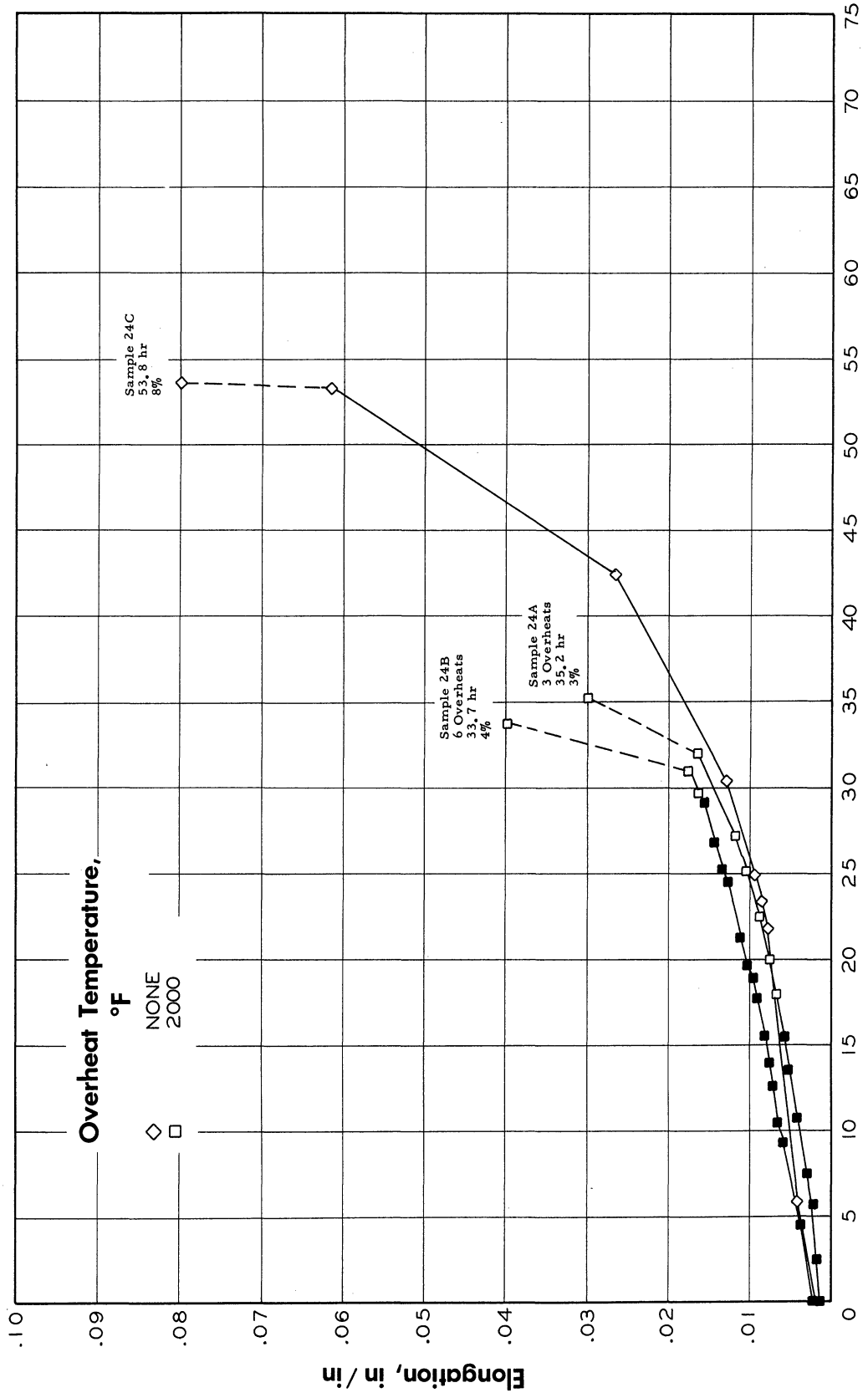

(h) Tests from bar 24.

Figure 18. - Continued. Comparative creep curves at 1600°F and 29,000 psi for Inconel 700 alloy for the indicated test conditions. Solid points indicate period of application of overheats. Sample number, number of overheats, rupture time, and elongation at fracture indicated for each curve.

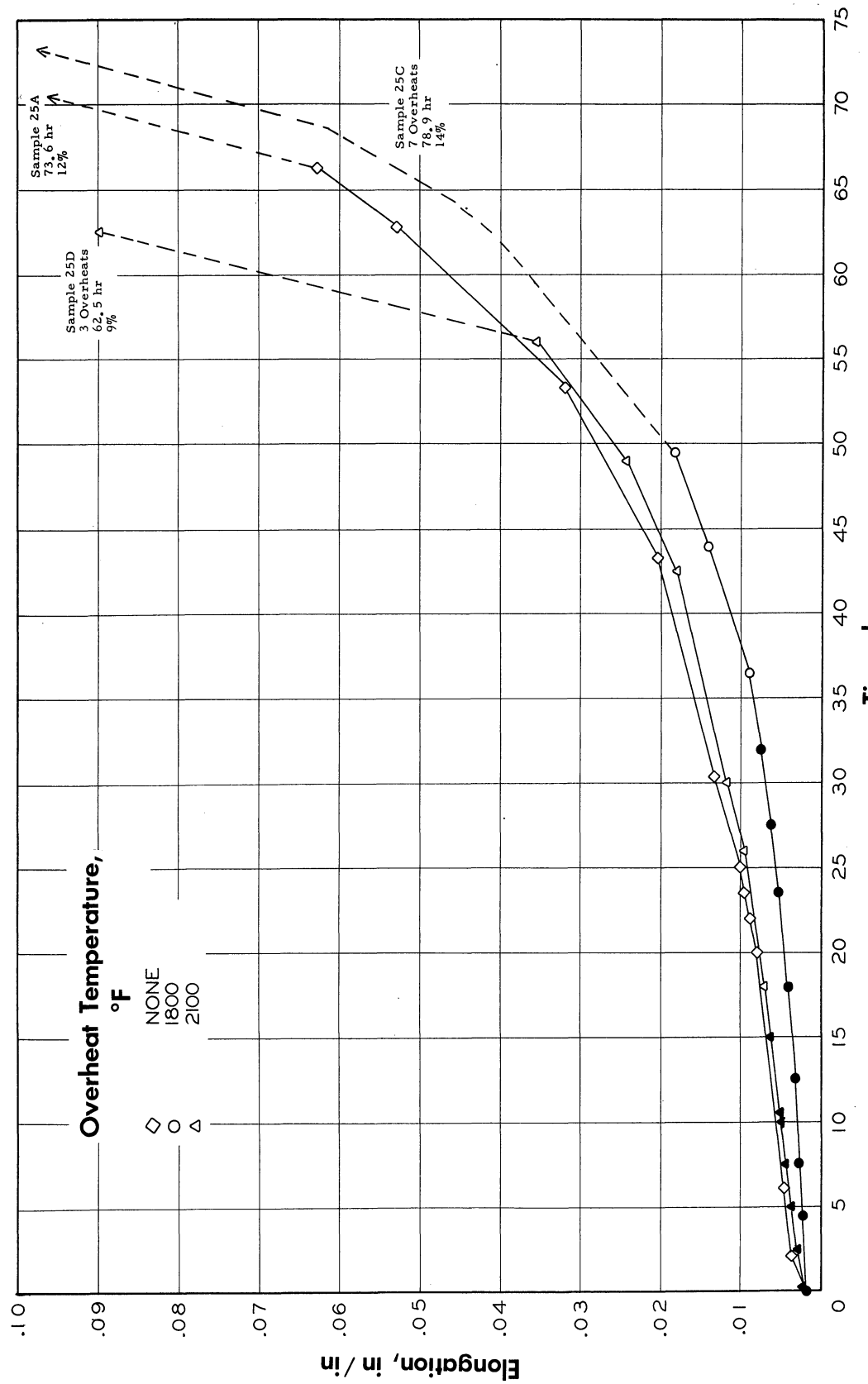

(i) Tests from bar 25.

Figure 18. - Continued. Comparative creep curves at 1600°F and 29,000 psi for Inconel 700 alloy for the indicated test conditions. Solid points indicate period of application of overheats. Sample number, number of overheats, rupture time, and elongation at fracture indicated for each curve.

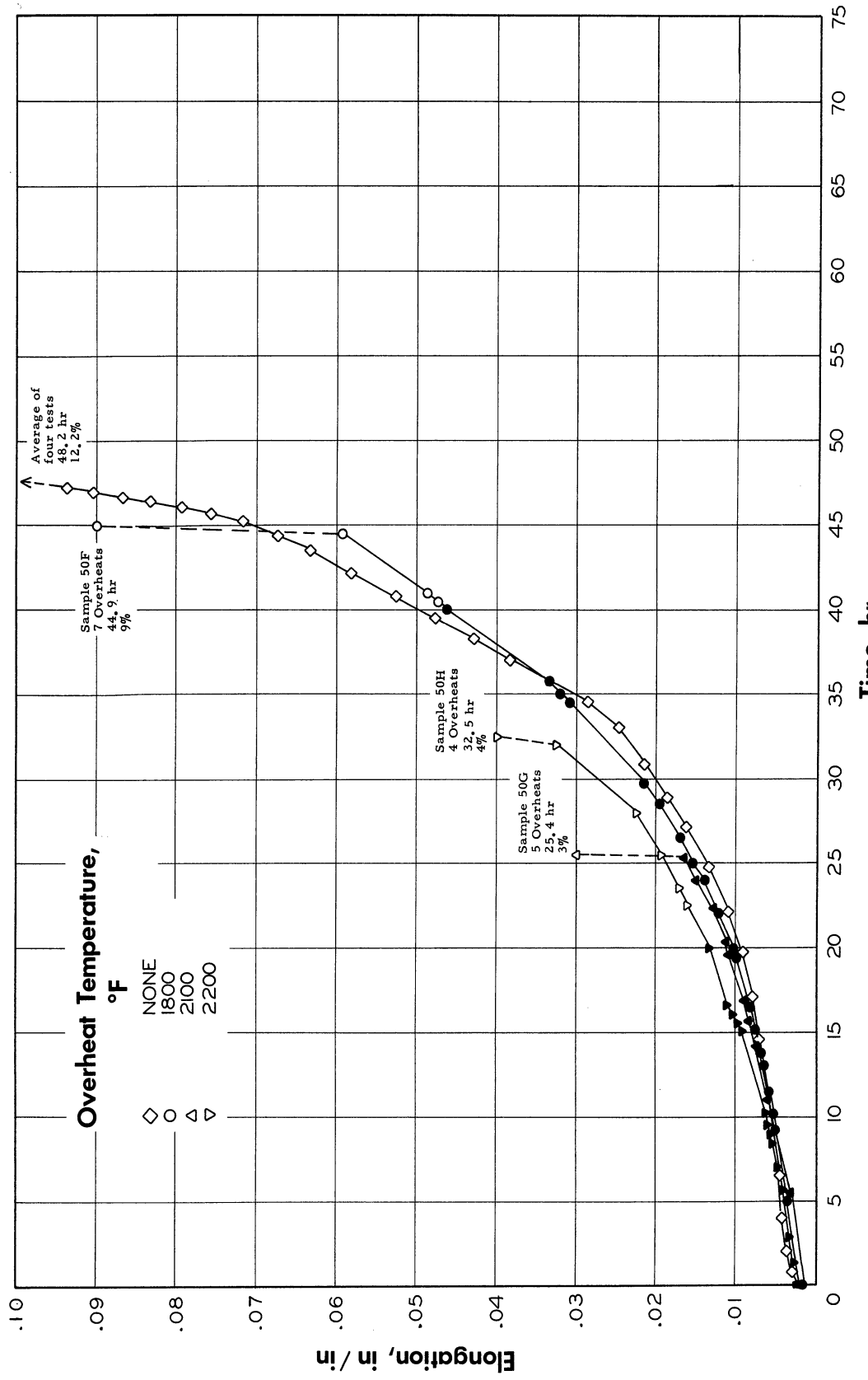

(j) Tests from bar 50.

Figure 18. - Concluded. Comparative creep curves at 1600°F and 29,000 psi for Inconel 700 alloy for the indicated test conditions. Solid points indicate period of application of overheats. Sample number, number of overheats, rupture time, and elongation at fracture indicated for each curve.

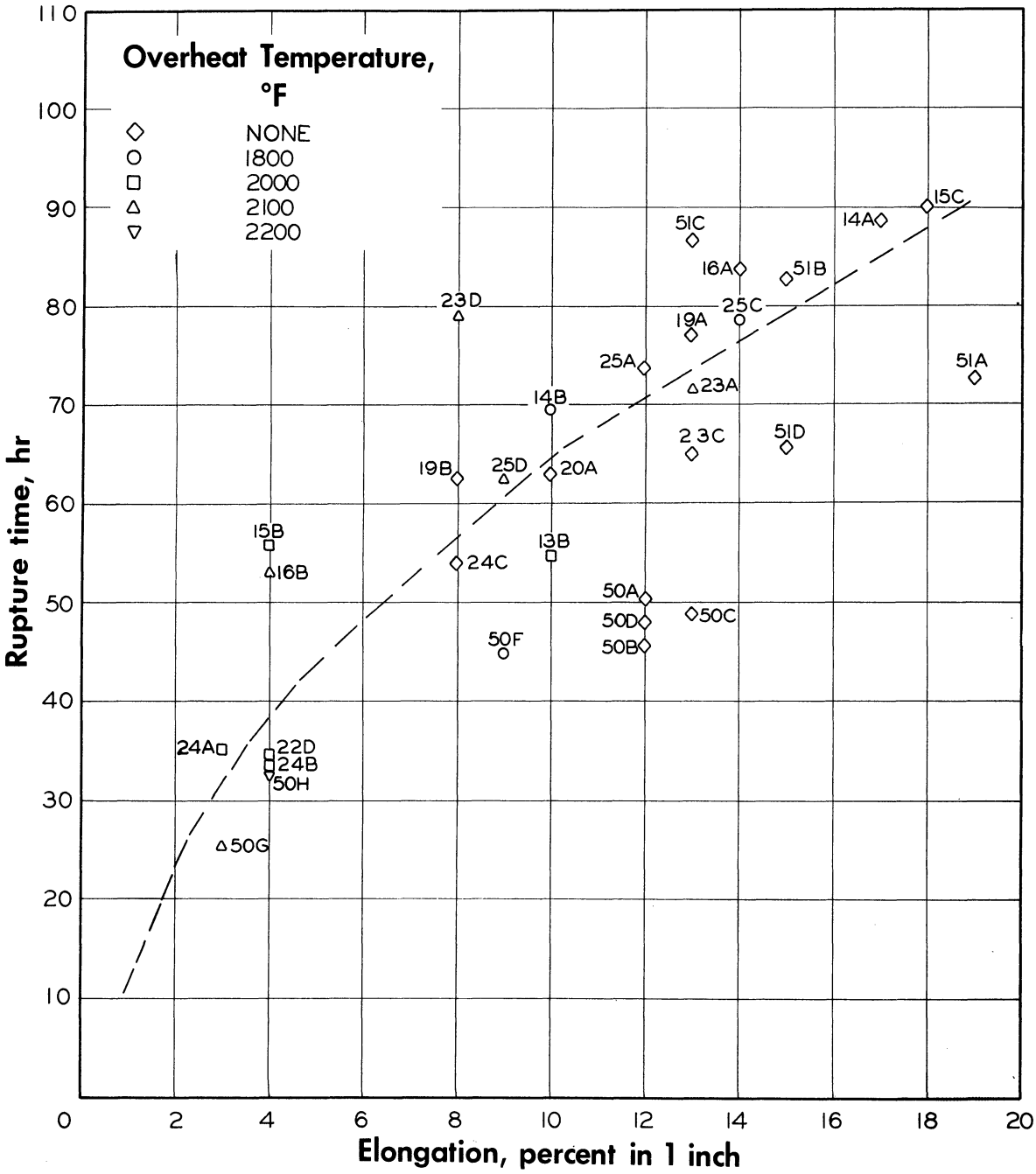

Figure 19. - Rupture time against elongation at fracture for tests on Inconel 700 alloy at 1600°F and 29,000 psi under the indicated test conditions. Specimen numbers indicated for each point.

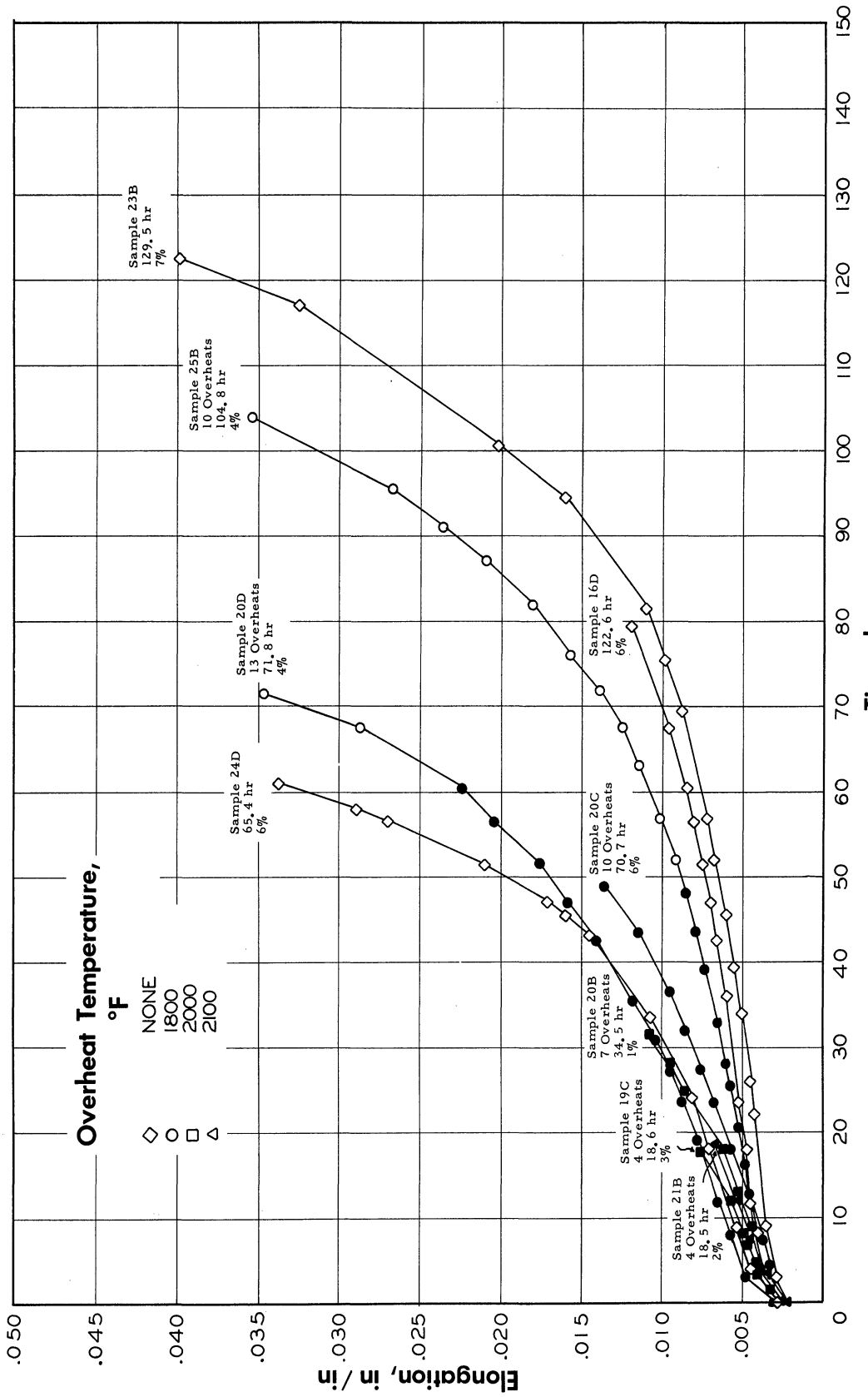

Figure 20. - Comparative creep curves at 1500°F and 43,000 psi for Inconel 700 alloy for the indicated test conditions. Solid points indicate period of application of overheats. Sample number, number of overheats, rupture time, and elongation at fracture indicated for each curve.

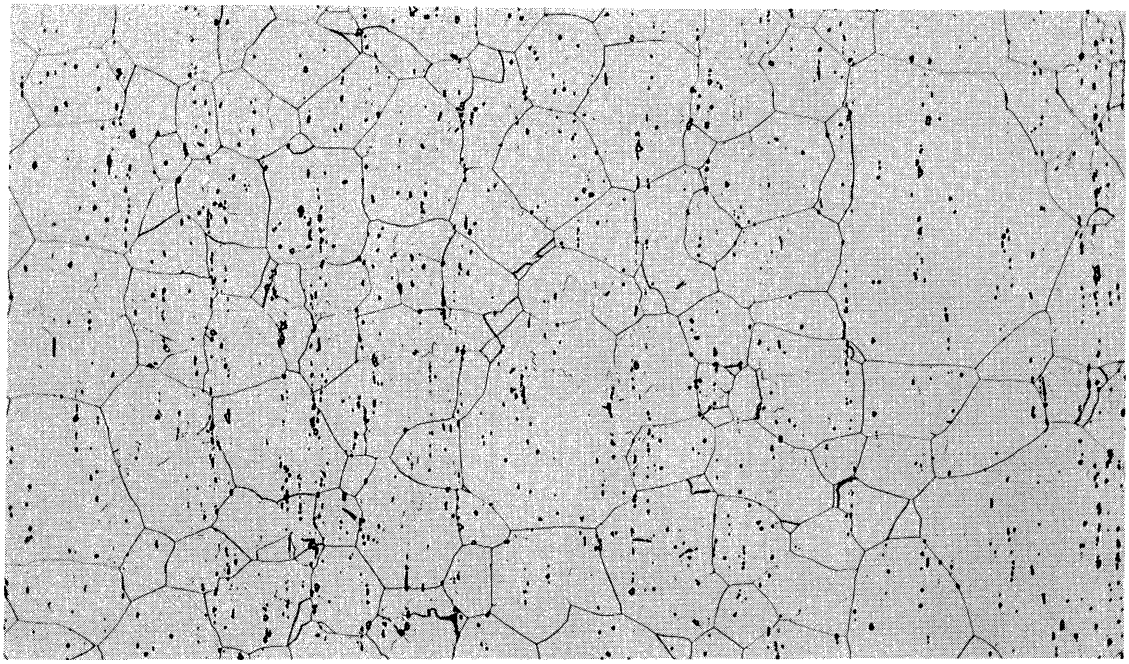

X100

(a) Bar 14, as heat-treated. Rupture time 88-90 hours at 1600°F, 29,000 psi.

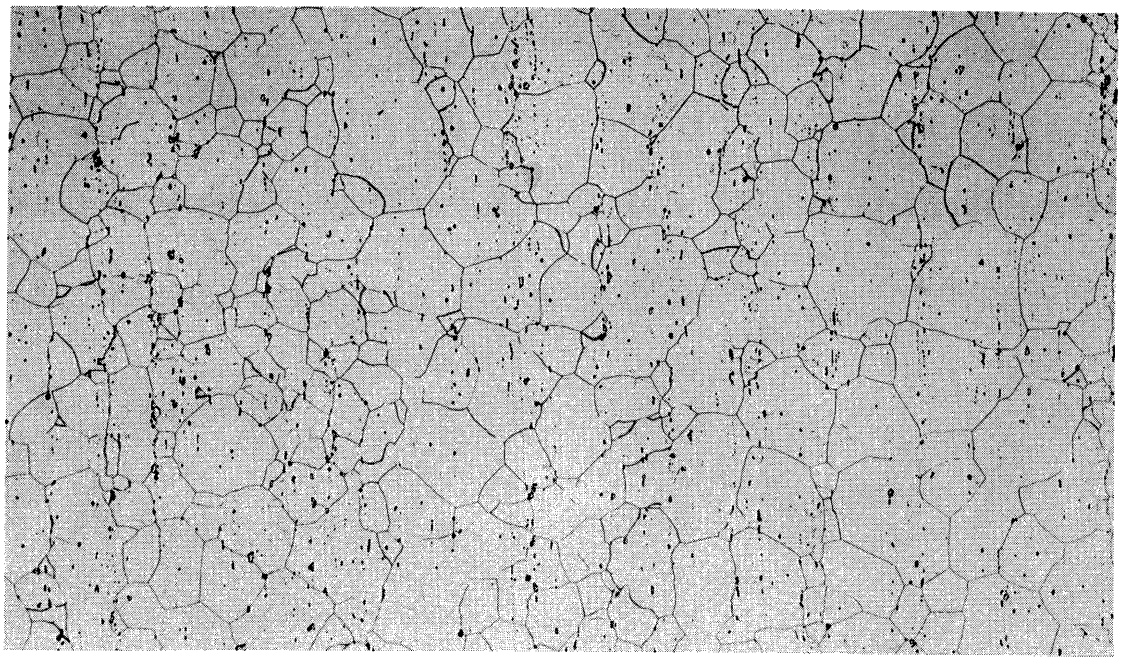

X100

(b) Bar 50, as heat-treated. Rupture time 45-50 hours at 1600°F, 29,000 psi.

Figure 21. - Microstructures of Inconel 700 alloy after heat treatment and after rupture testing at 1600°F.

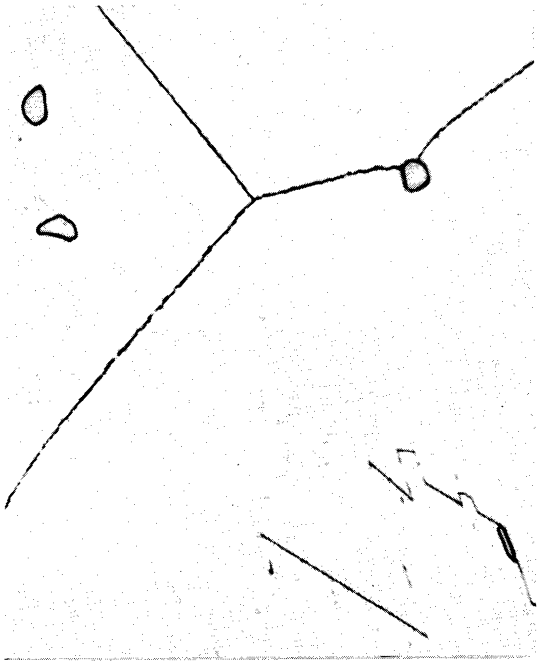

X1000

(c) Typical grain boundary appearance, as heat-treated.

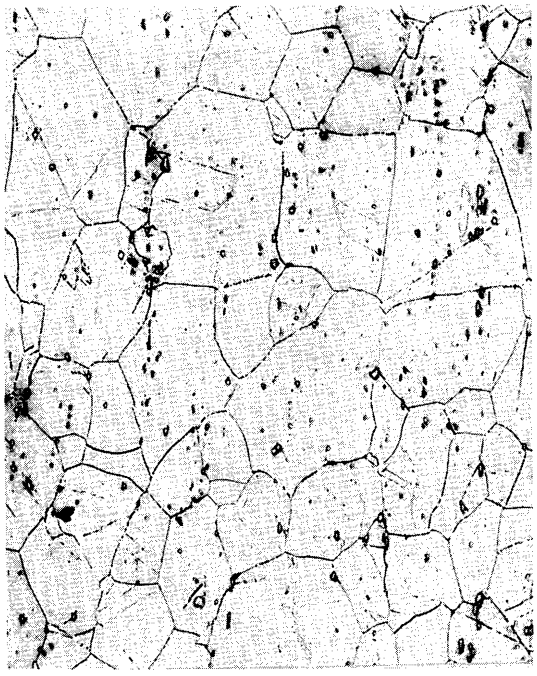

X100

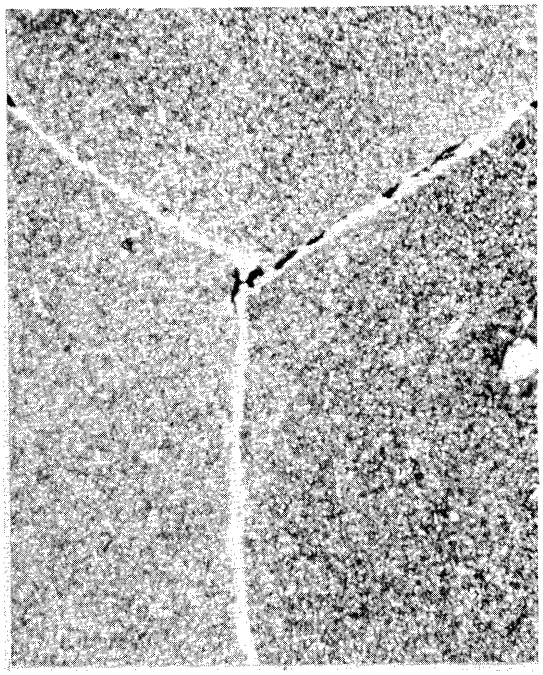

X1000

(d) Bar 15 after rupture testing at 1600°F and 29,000 psi. Rupture time 90.0 hours.

Figure 21. - Concluded. Microstructures of Inconel 700 alloy after heat treatment and after rupture testing at 1600°F.

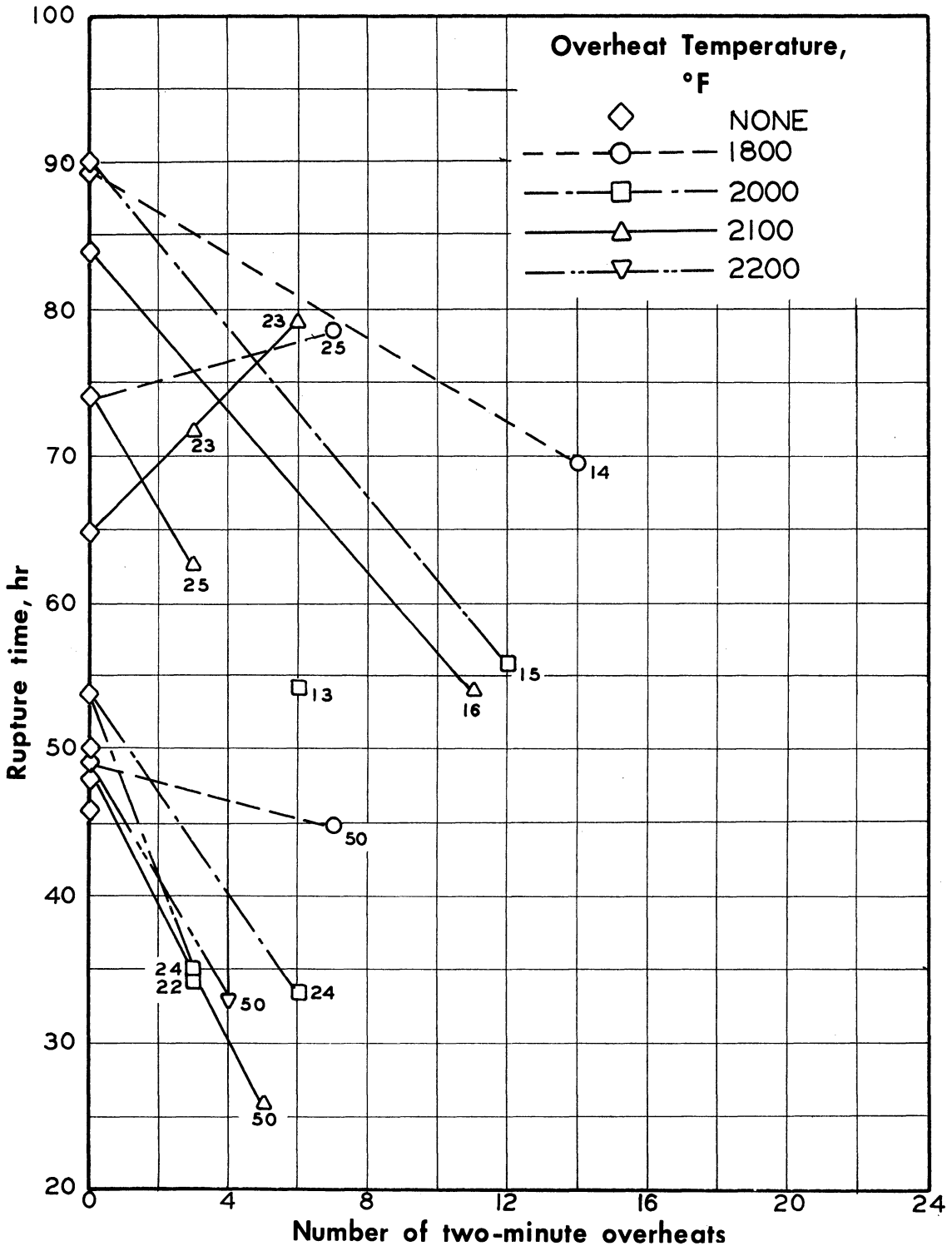

(a) Tests at 1600°F and 29,000 psi.

Figure 22. - Effect of number of overheats on the rupture time of Inconel 700 alloy for the overheat temperatures and base conditions indicated. Overheats were of two minutes duration applied every five hours from the beginning of the test. Bar number indicated for each overheat test. Overheat results compared to normal test from same bar wherever possible.

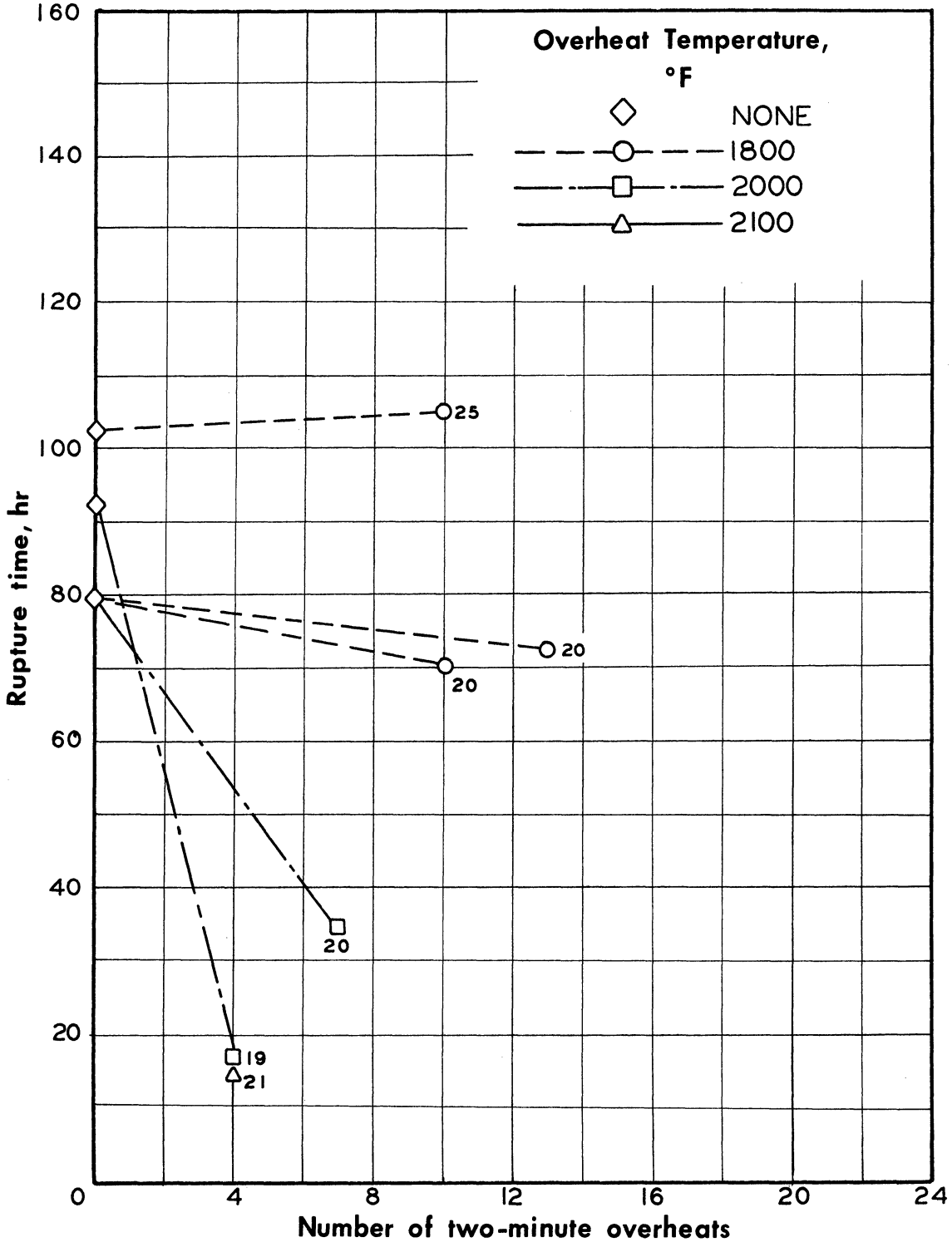

(b) Tests at 1500°F and 43,000 psi. (Values for normal tests estimated.)

Figure 22. - Concluded. Effect of number of overheats on the rupture time of Inconel 700 alloy for the overheat temperatures and base conditions indicated. Overheats were of two minutes duration applied every five hours from the beginning of the test. Bar number indicated for each overheat test. Overheat results compared to normal test from same bar wherever possible.

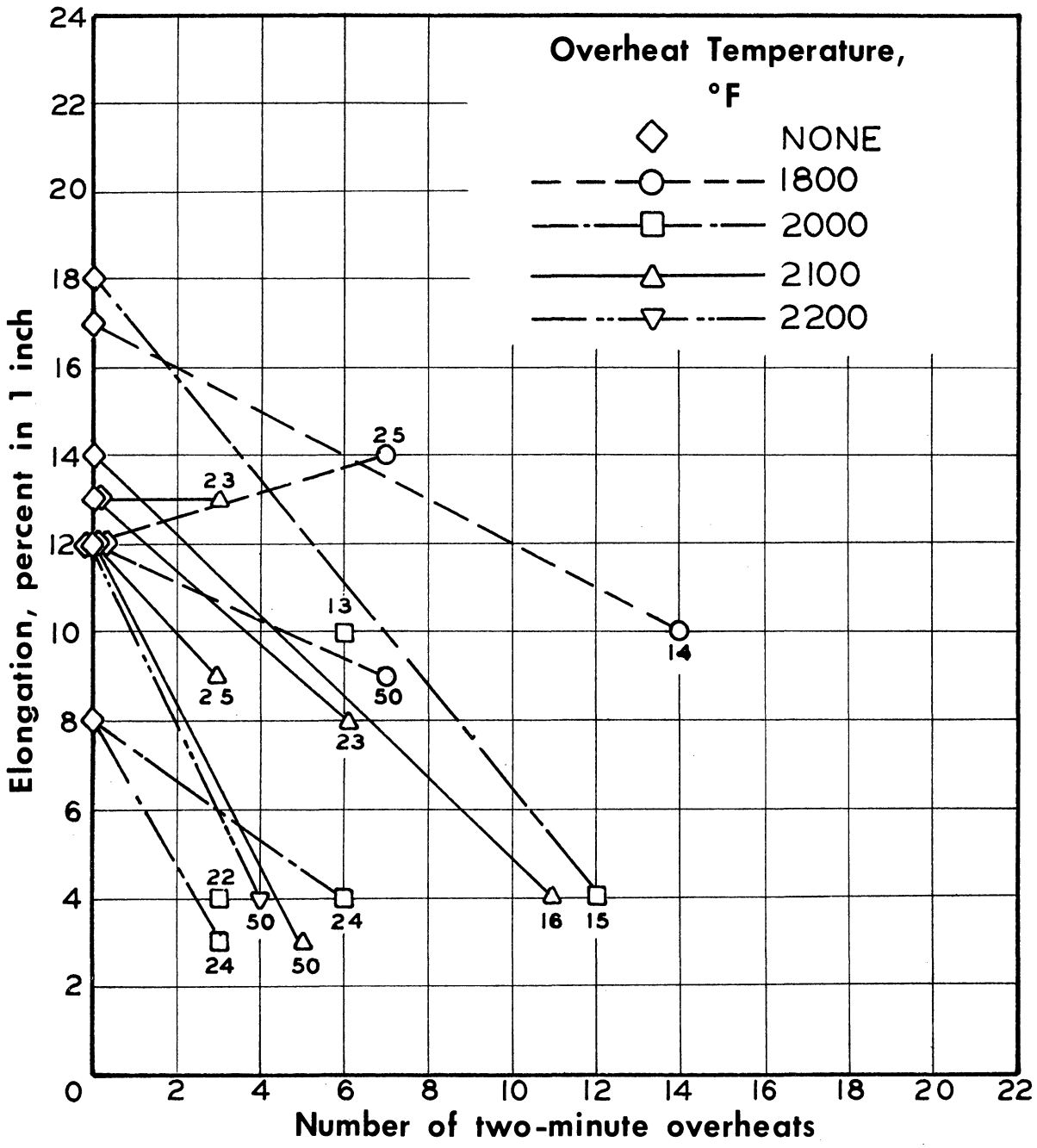

(a) Tests at 1600°F and 29,000 psi.

Figure 23. - Effect of number of overheats on the elongation at fracture of Inconel 700 alloy for the overheat temperatures and base conditions indicated. Overheats were of two minutes duration applied every five hours from the beginning of the test. Bar number indicated for each overheat test. Overheat results compared to normal test from same bar wherever possible.

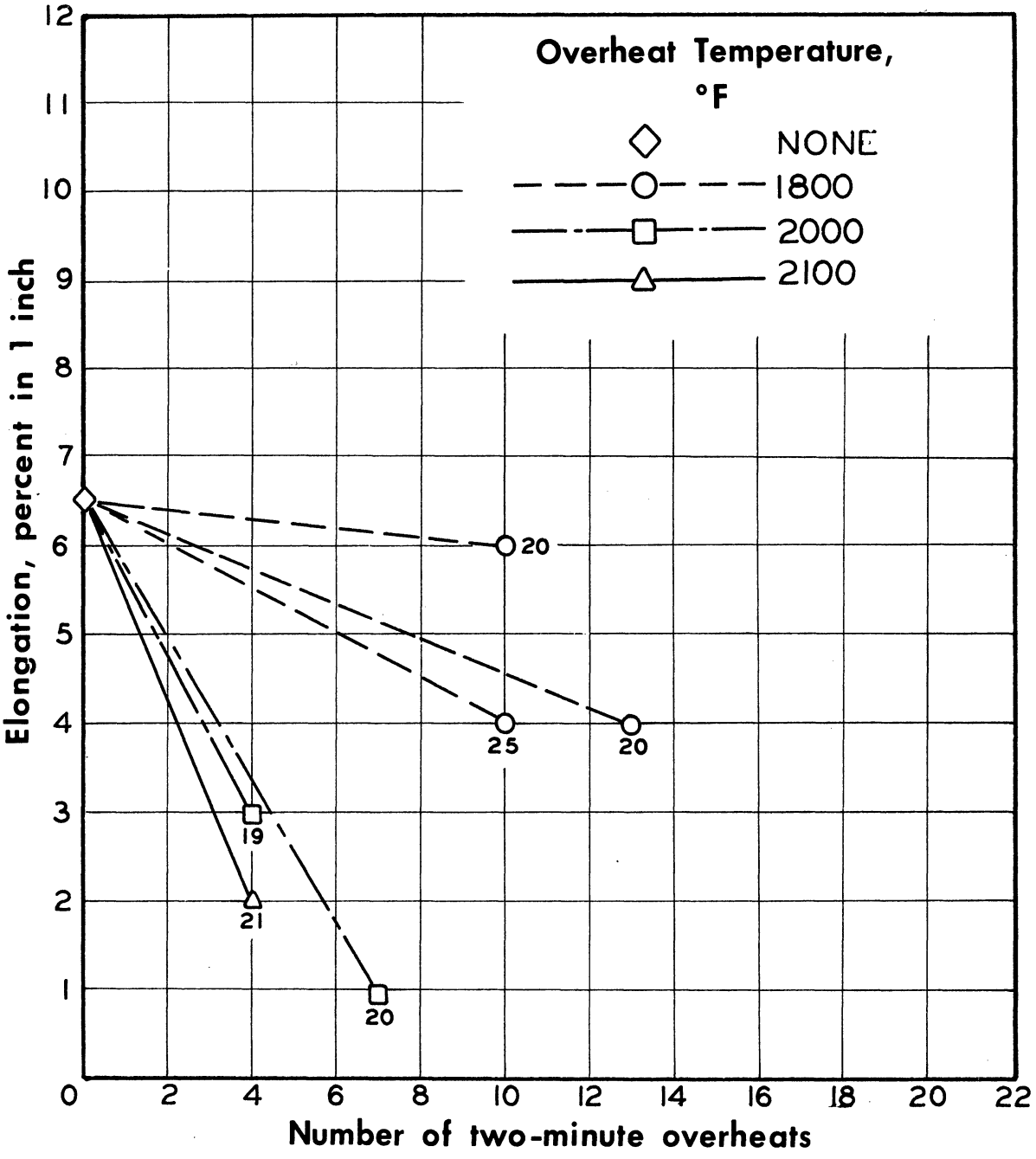

(b) Tests at 1500°F and 43,000 psi. (Values for normal tests estimated.)

Figure 23. - Concluded. Effect of number of overheats on the elongation at fracture of Inconel 700 alloy for the overheat temperatures and base conditions indicated. Overheats were of two minutes duration applied every five hours from the beginning of the test. Bar number indicated for each overheat test. Overheat results compared to normal test from same bar wherever possible.

(a) As heat treated

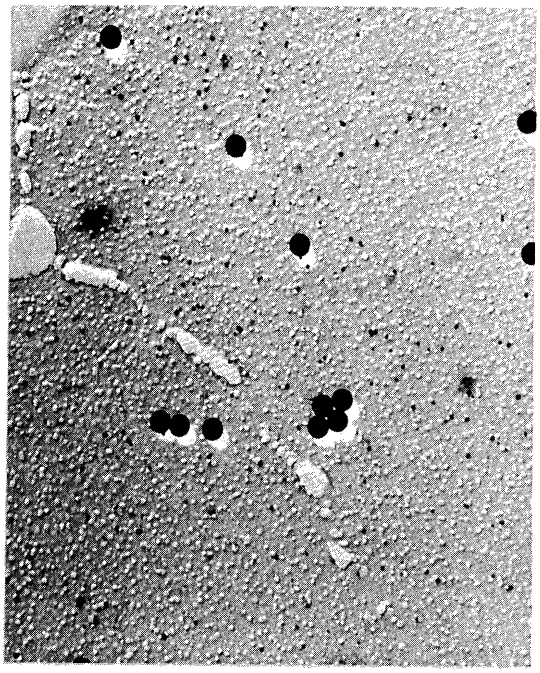

(b) 4 hours

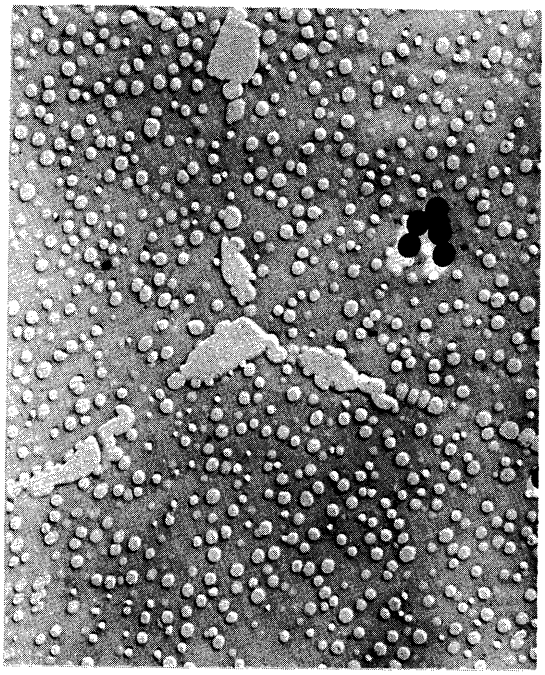

(c) 50 hours

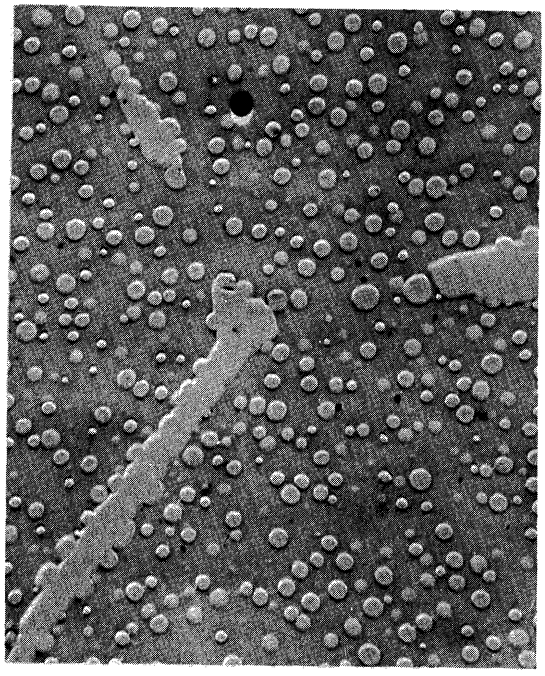

(d) 212 hours

Figure 24. - Micrographs of M252 (heat 837) samples exposed without stress at 1600°F for the indicated times. Samples received standard heat treatment prior to aging. (X11,000)

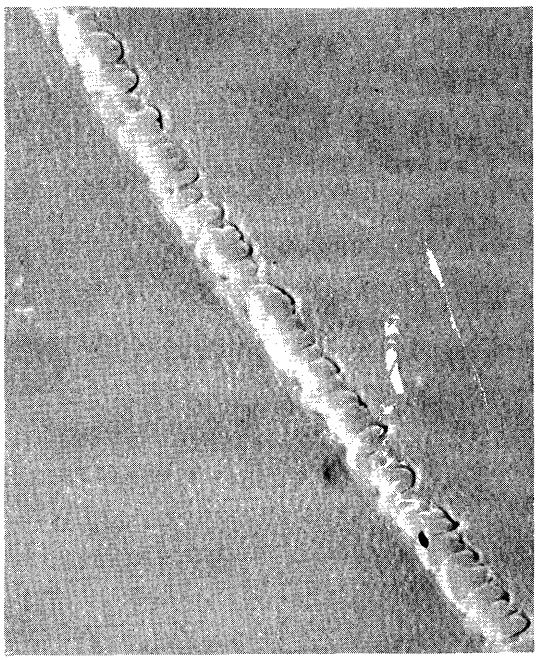

(a) As heat treated

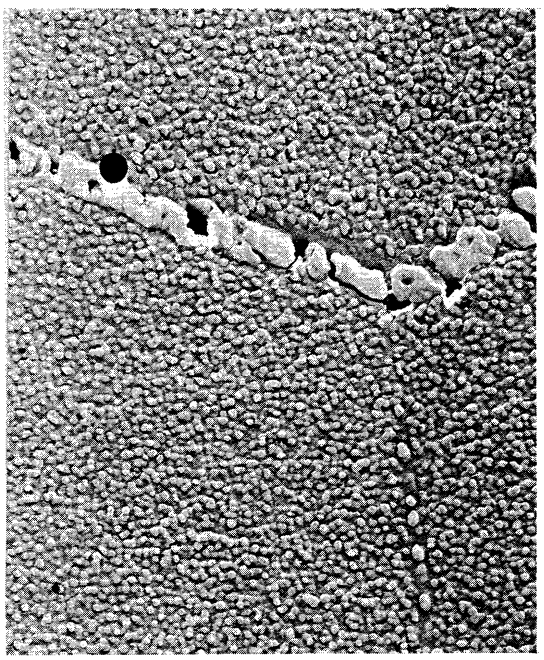

(b) 4 hours

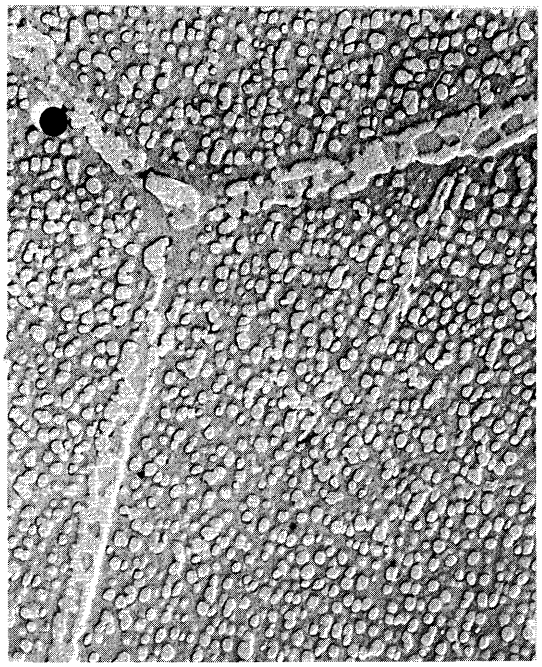

(c) 48 hours

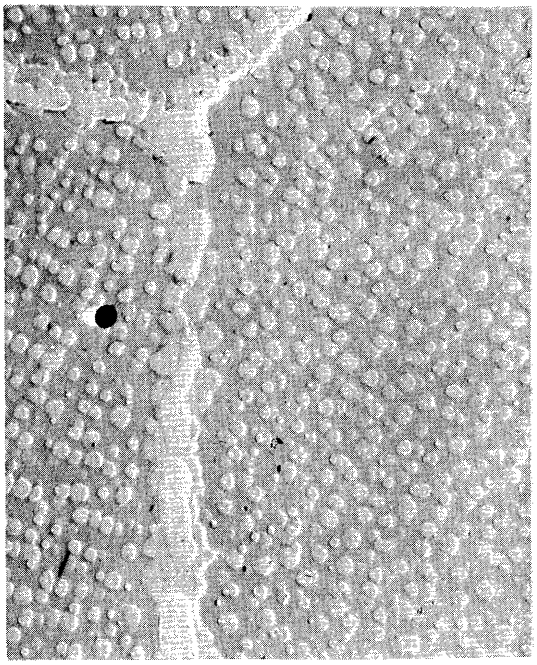

(d) 212 hours

Figure 25. - Micrographs of Inconel 700 samples exposed without stress at 1600°F for the indicated times. Samples received standard heat treatment prior to exposure. (X11,000)

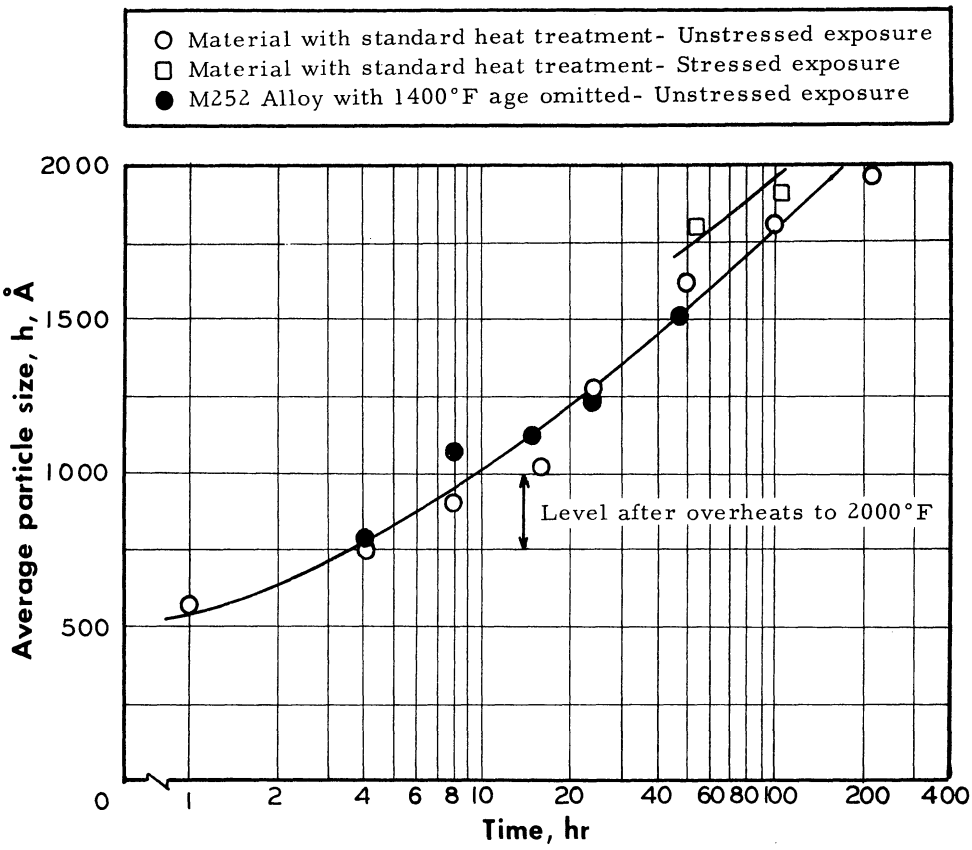

(a) M252 Alloy (heat 837)

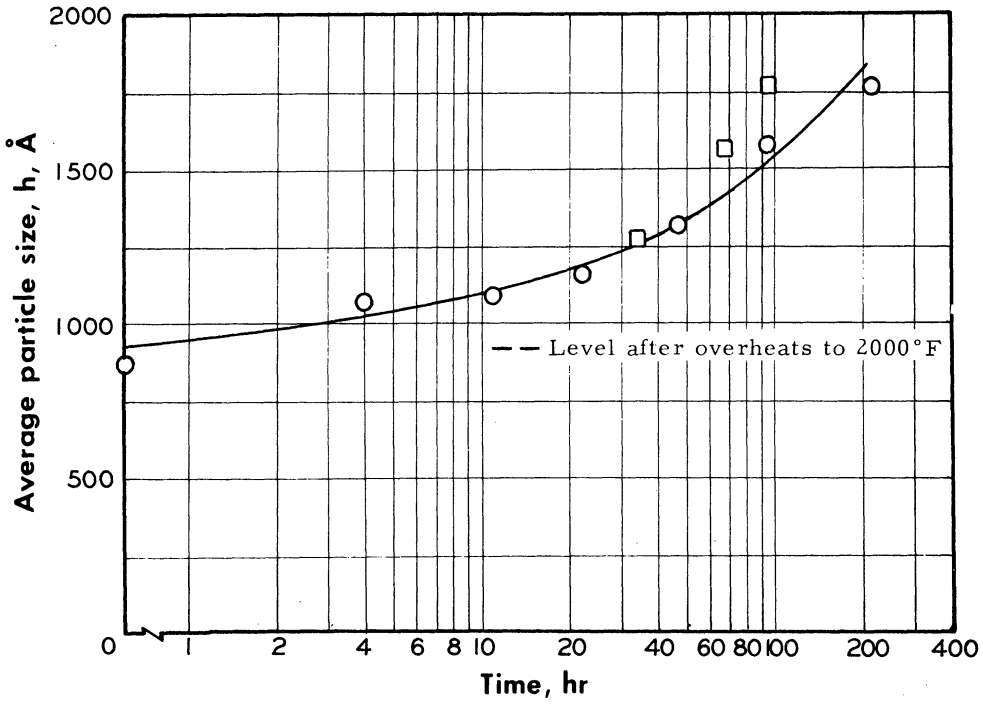

(b) Inconel 700 Alloy

Figure 26. - Effect of time at 1600°F on the average size of the γ' precipitate particles in M252 (heat 837) and Inconel 700 alloys. Materials received the standard heat treatments prior to exposure to 1600°F except as noted.

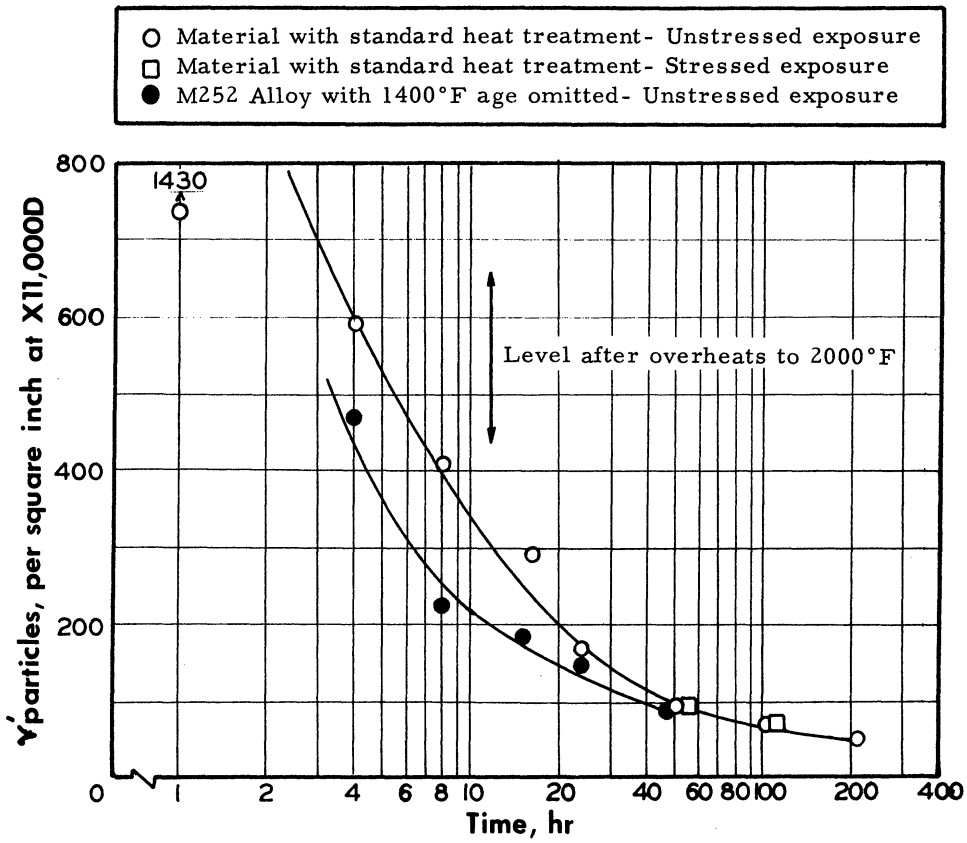

(a) M252 Alloy (heat 837)

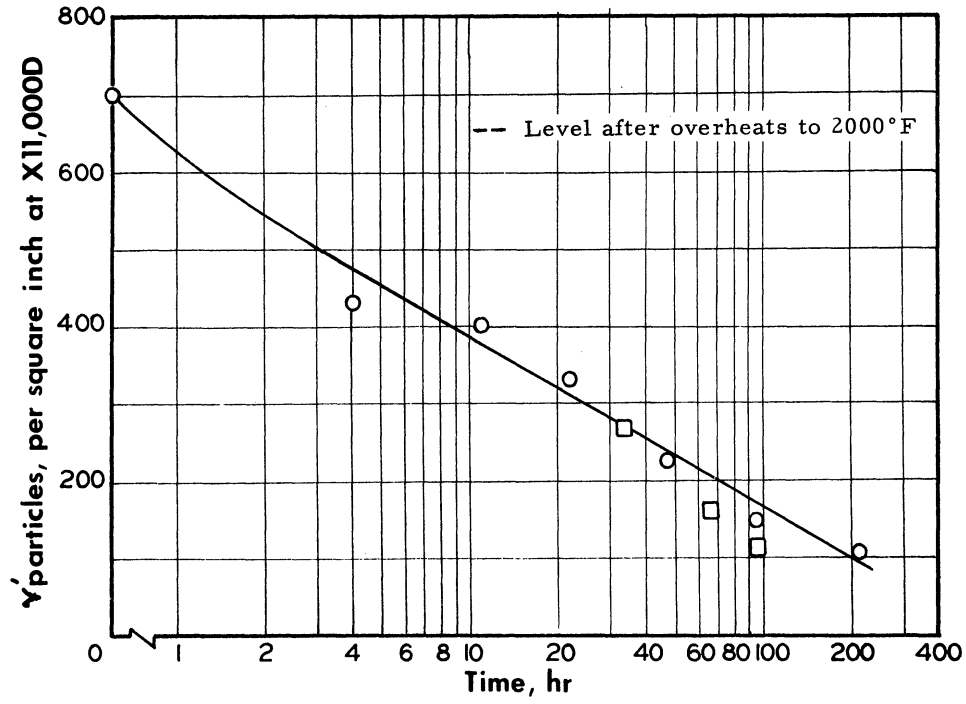

(b) Inconel 700 Alloy

Figure 27. - Effect of time at 1600°F on the number of γ' precipitate particles in M252 (heat 837) and Inconel 700 alloys. Materials received the standard heat treatments prior to exposure at 1600°F except as noted.

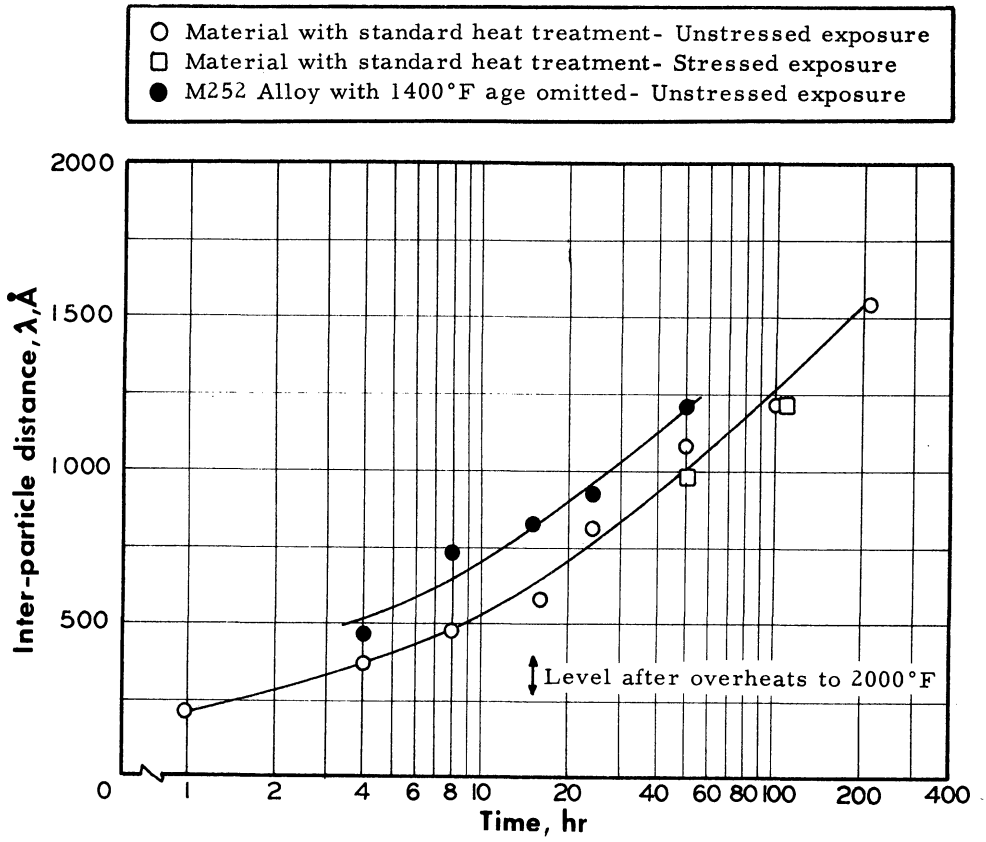

(a) M252 Alloy (heat 837)

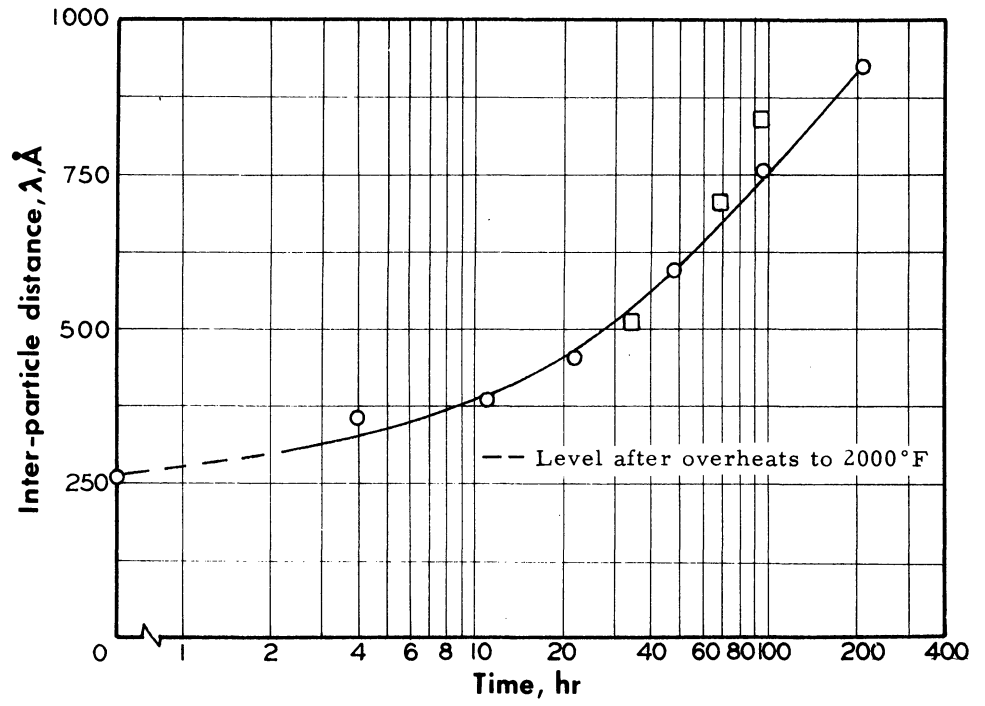

(b) Inconel 700 Alloy

Figure 28. - Effect of time at 1600°F on the average distance between the γ' precipitate particles in M252 (heat 837) and Inconel 700 alloys. Materials received the standard heat treatments prior to exposure to 1600°F except as noted.

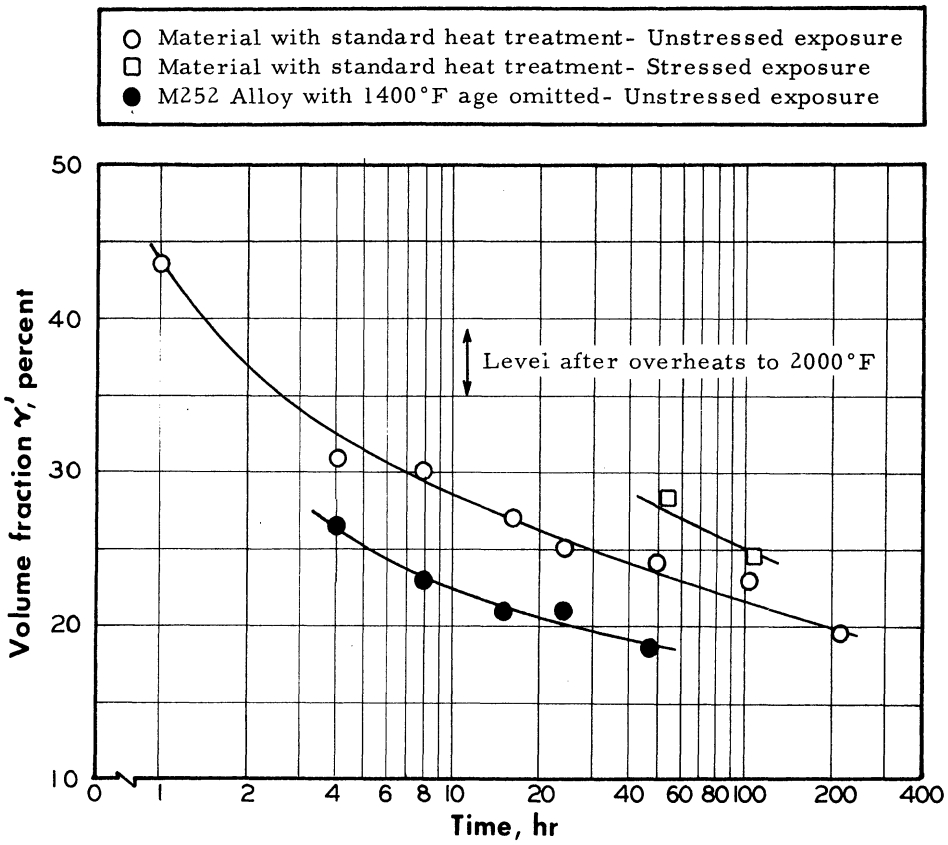

(a) M252 Alloy (heat 837)

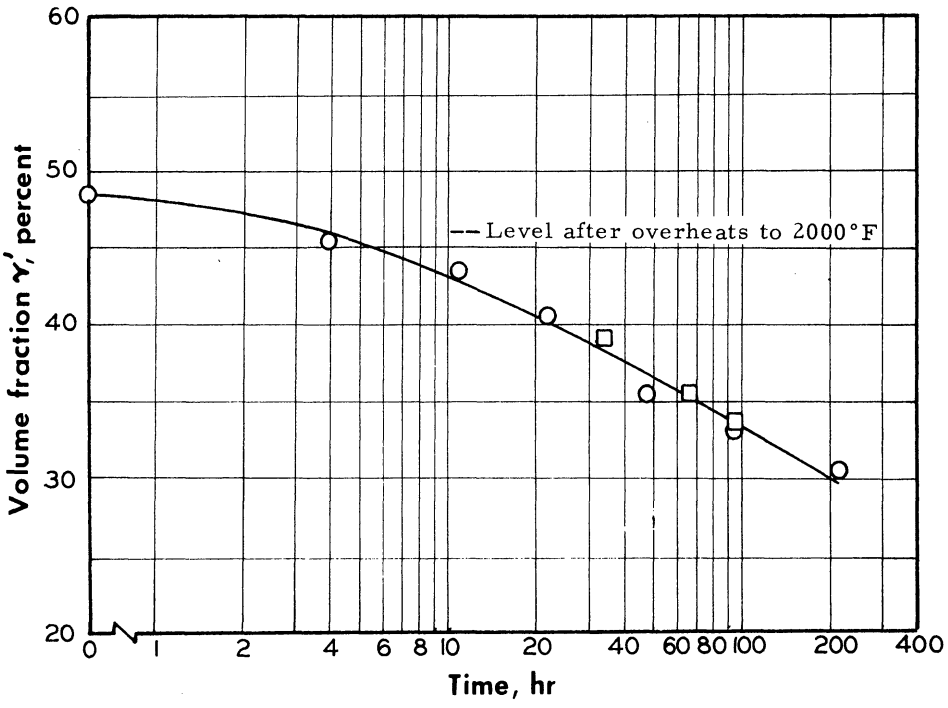

(b) Inconel 700 Alloy

Figure 29. - Effect of time at 1600°F on the amount of γ' precipitate in M252 (heat 837) and Inconel 700 alloys. Materials received the standard heat treatments prior to exposure at 1600°F except as noted.

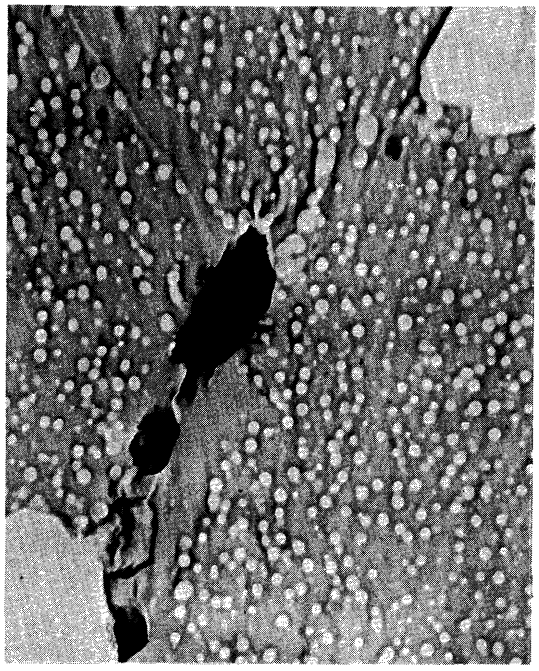

(a) Normal rupture test

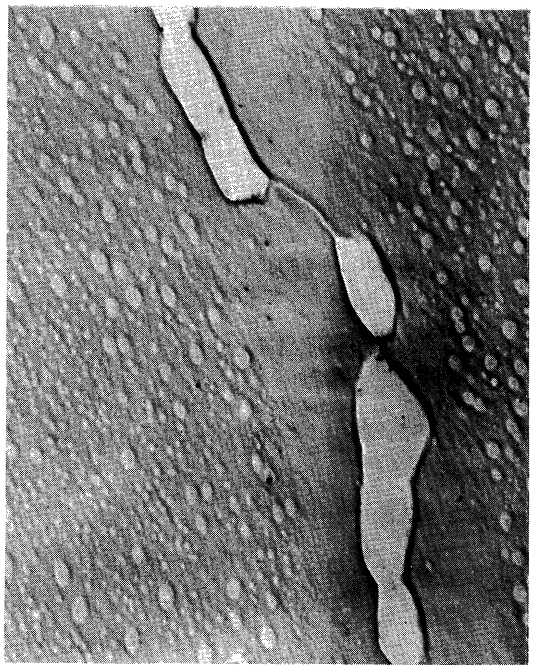

(b) 10 overheats to 1800°F

(c) 10 overheats to 2000°F

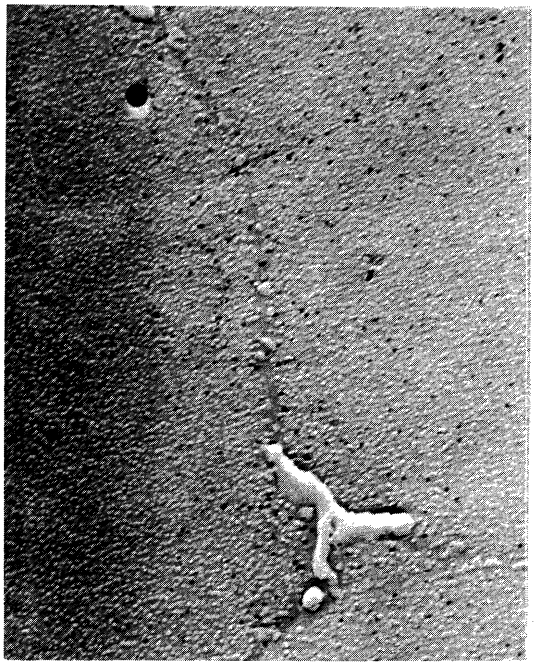

(d) 10 overheats to 2100°F

Figure 30. - Microstructures of M252 alloy (heat 837) after 50 hours at 1600°F under 18,000 psi. Tests interrupted after 50 hours under the indicated conditions. (X11,000)

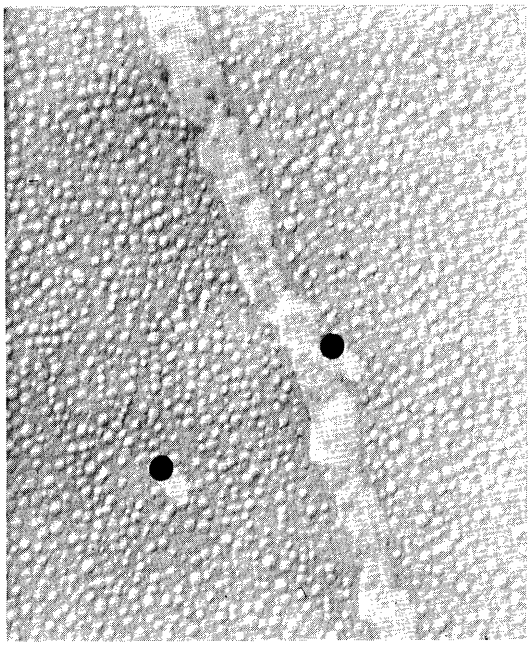

(a) Normal rupture test

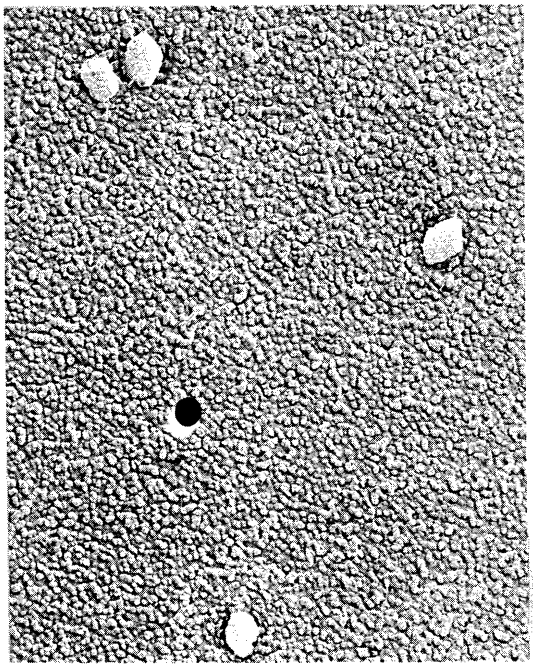

(b) 6 overheats to 2000°F

Figure 31 - Microstructures of Inconel 700 alloy after 30 hours at 1600°F under 29,000 psi. Tests interrupted after 30 hours under the indicated conditions. (X11,000)

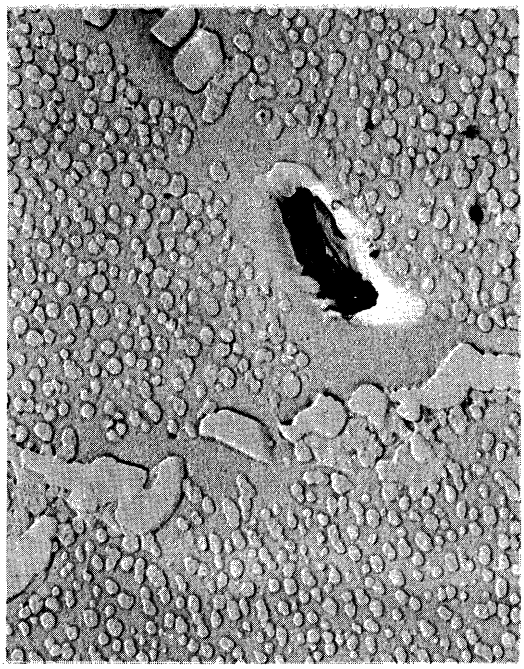

(a) Normal rupture test - 62.7 hours

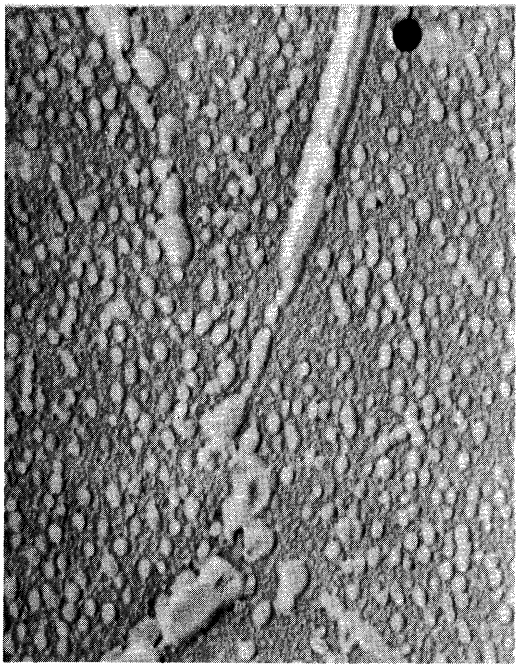

(b) Test overheated 14 times to 1800°F - 69.5 hours

(c) Test overheated 12 times to 2000°F - 55.7 hours

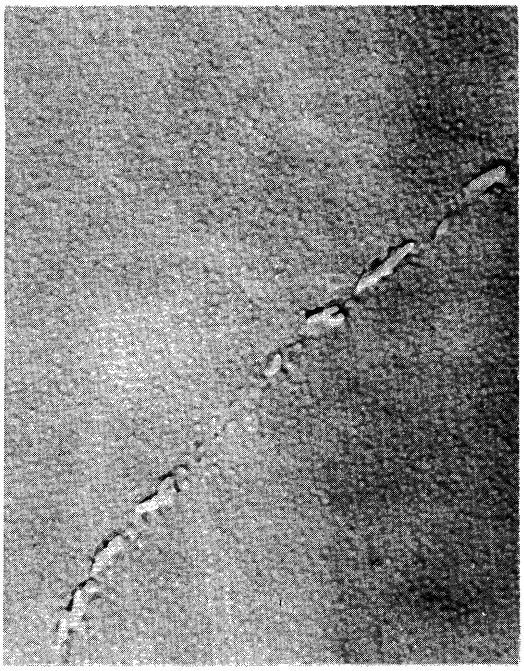

(d) Test overheated 11 times to 2100°F - 53.1 hours

Figure 32. - Micrographs from completed tests on Inconel 700 alloy samples under 1600°F and 29,000 psi. (X11,000)

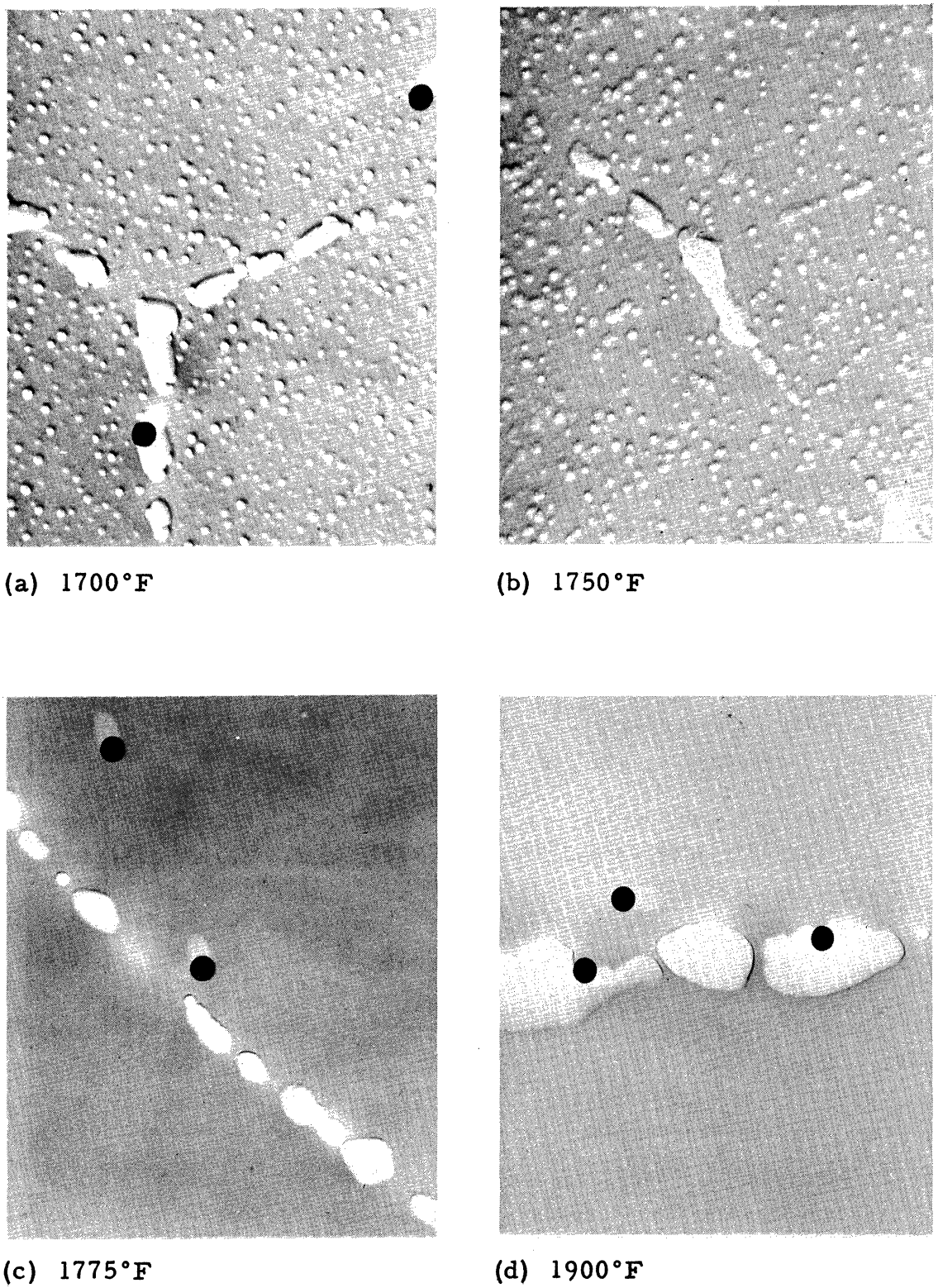

(a) 1700°F (b) 1750°F

(c) 1775°F (d) 1900°F

Figure 33. - Microstructures of M252 (heat 837) after 4 hours at the indicated temperature followed by ice brine quenching. (X11,000)

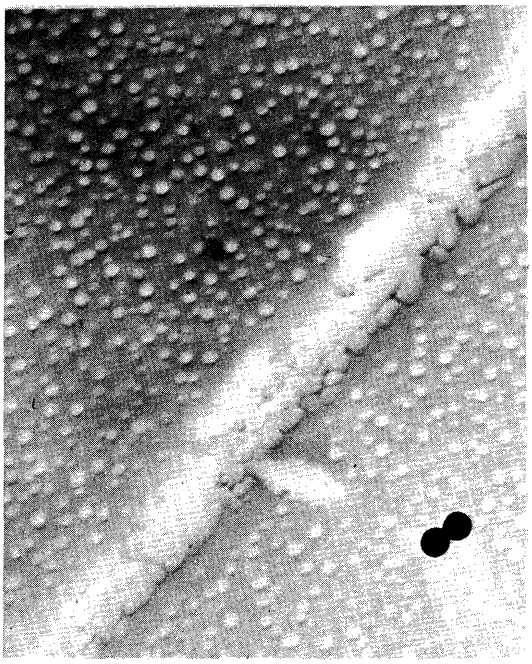

(a) 1800°F

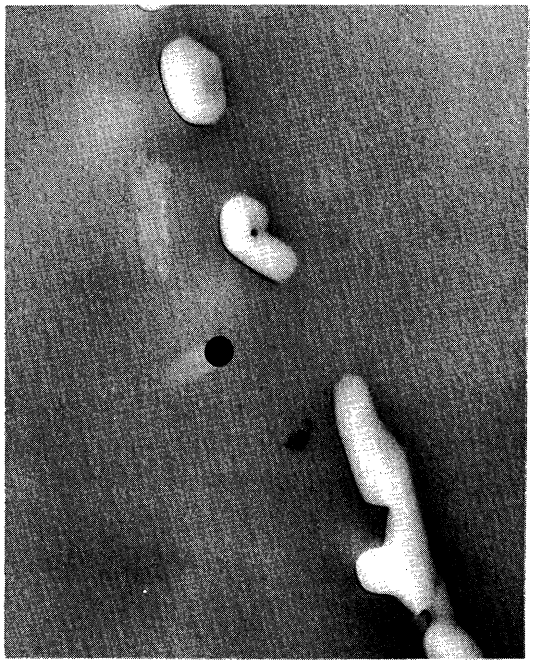

(b) 1900°F

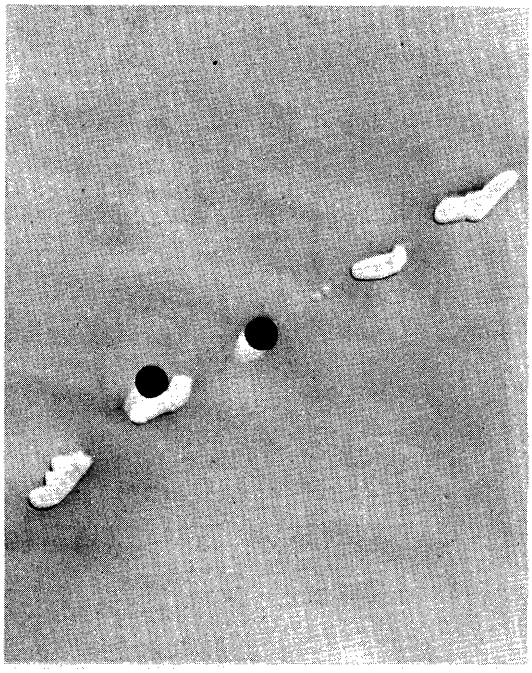

(c) 1925°F

Figure 34. - Microstructures of Inconel 700 after 4 hours at the indicated temperature followed by ice brine quenching. (X11,000)

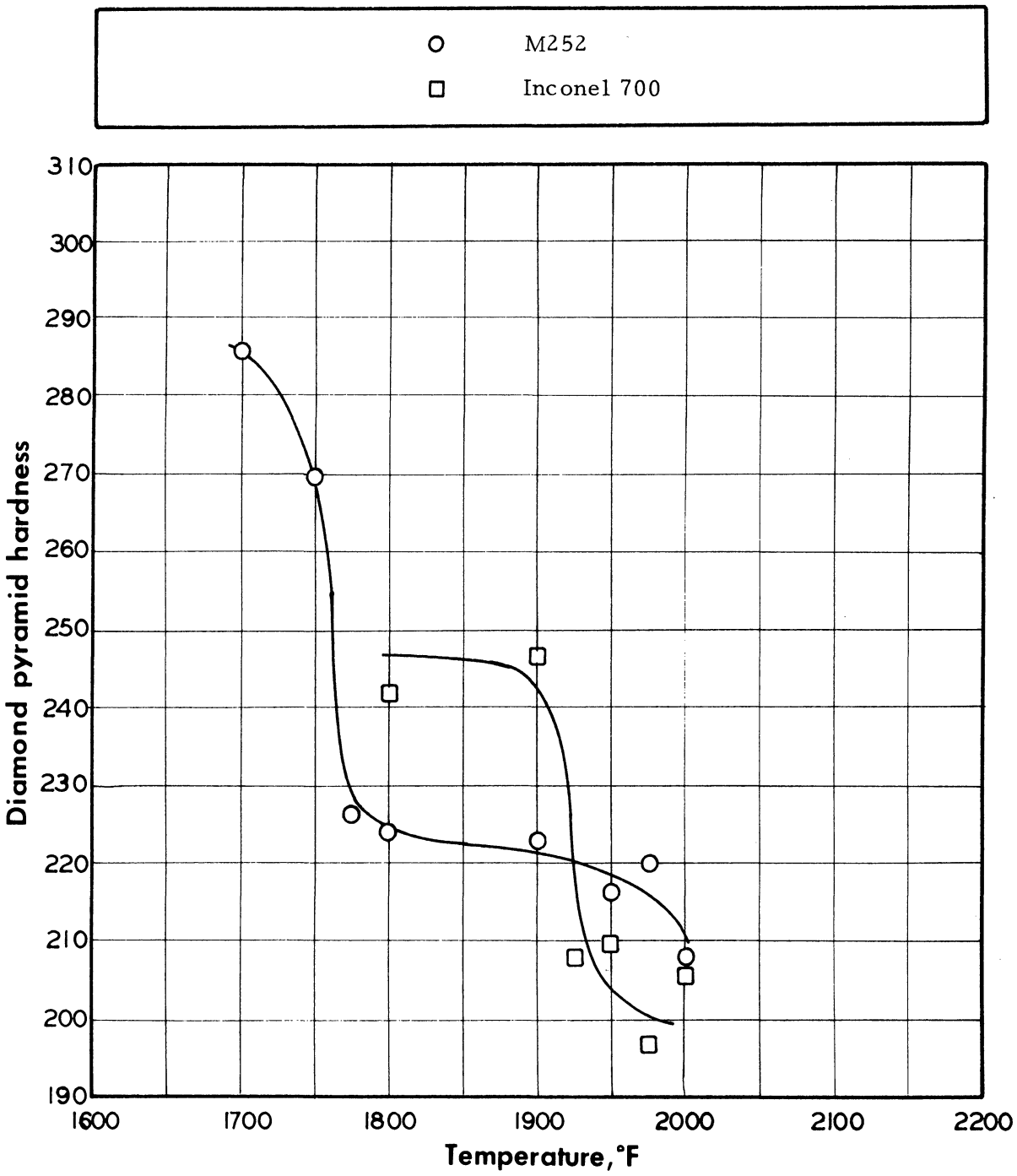

Figure 35. Effect of temperature of four-hour solution treatment on hardness of M252 (837) and Inconel 700 alloys. All samples iced-brine quenched after treatment.

Alloy	Temperature for γ' Solution (°F)	Temperature of Cooling Curve Halt (°F)
M252 (heat 837)	○	●
Inconel 700	□	■
M252 (heat HT-28)	◇	◆
Heat 1171	◁	◀
Heat 1172	△	▲
Heat 1173	▷	None

Curve shown after Betteridge and Franklin (Ref. 24)

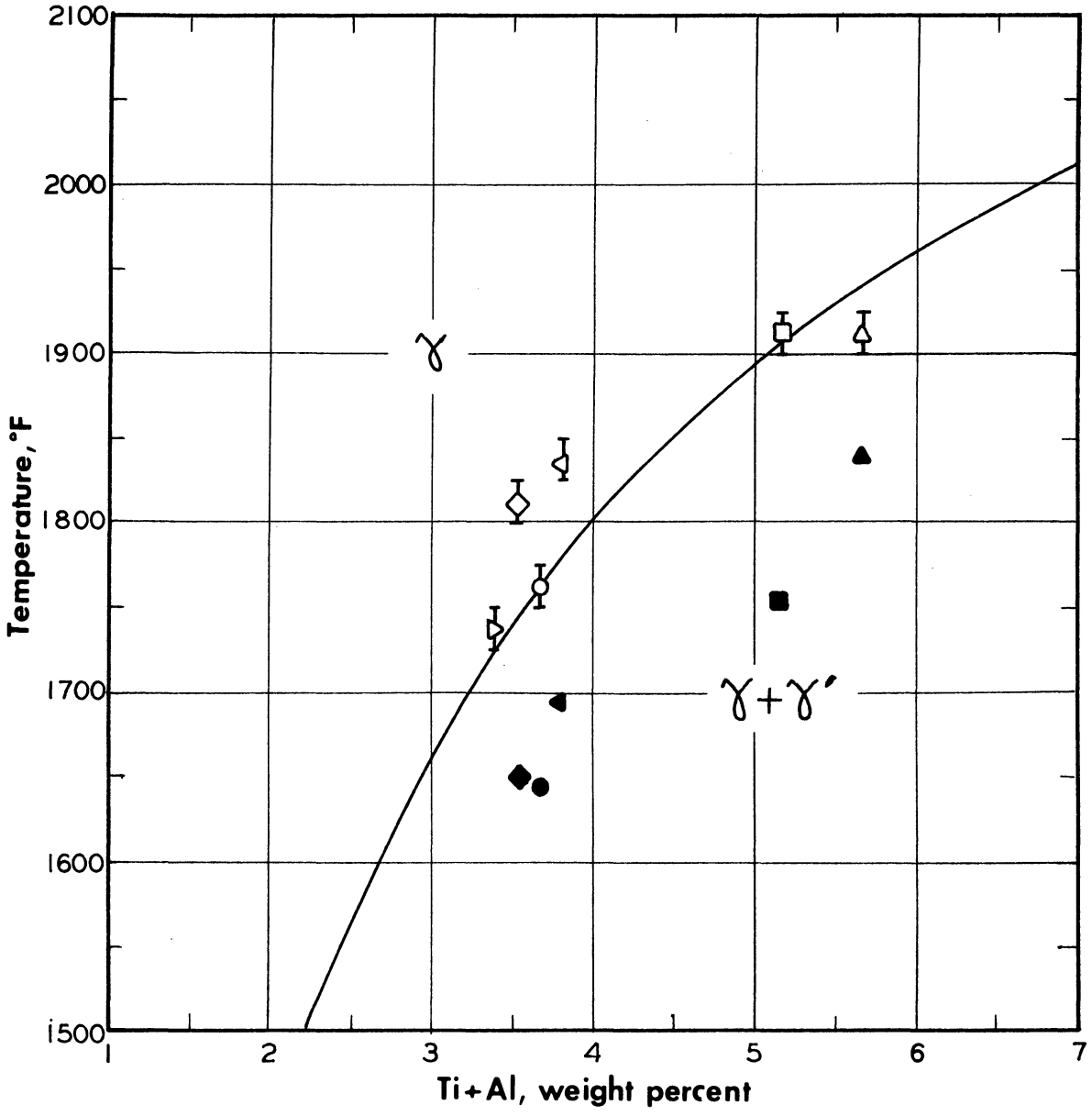

Figure 36. - Effect of Ti+Al content on the temperature for solution of γ' in four hours in the experimental materials and on the temperature at which halts appeared in the cooling curve from an overheat.

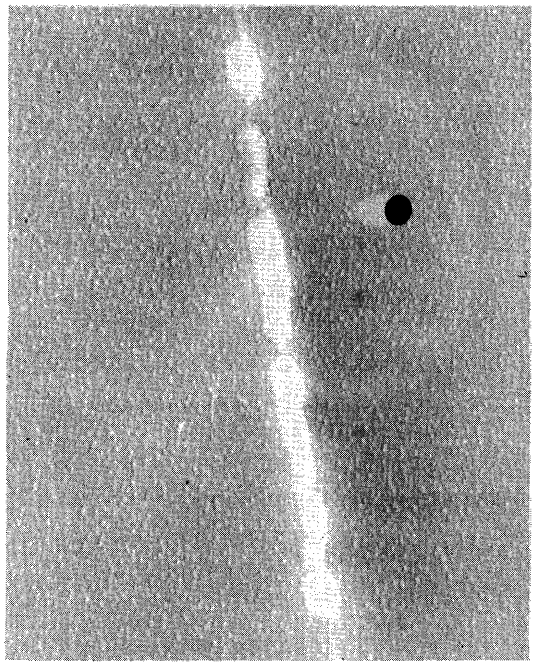

(a) 4 hours at 1600°F

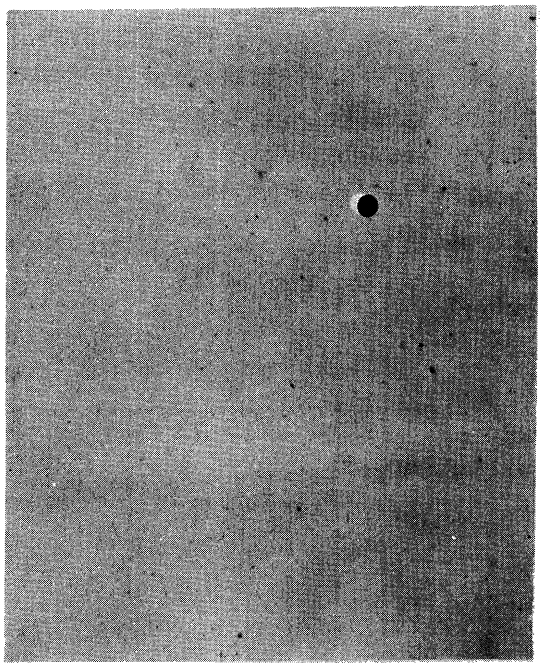

(b) (a) plus 2 minutes 2000°F

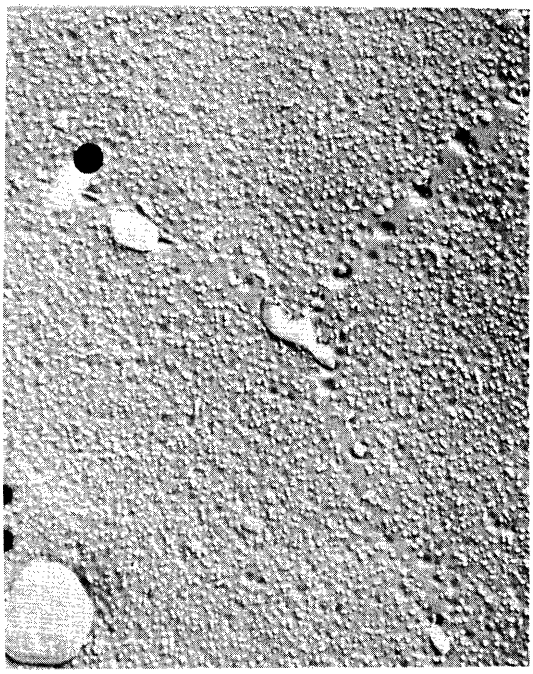

(c) (b) plus 10 minutes 1600°F

Figure 37. - Micrographs showing the effect on M252 (heat 837) of a two-minute exposure to 2000°F and the subsequent reprecipitation of the γ' at 1600°F following such an exposure. Samples quenched in iced brine following indicated exposure. (X11,000)

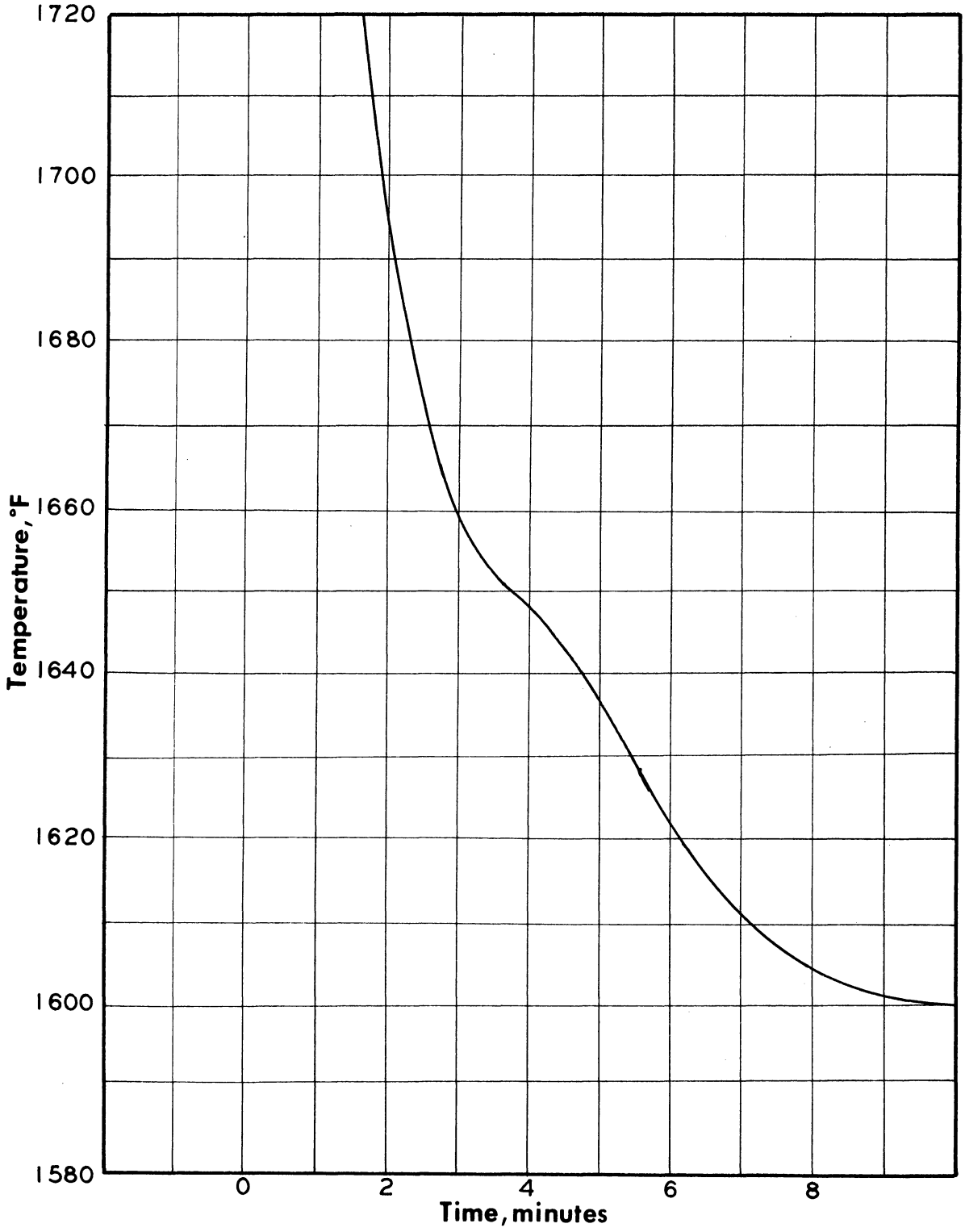

Figure 38. - Portion of cooling curve for M252 (heat 837) from an overheat to 2000°F, showing halt in curve.

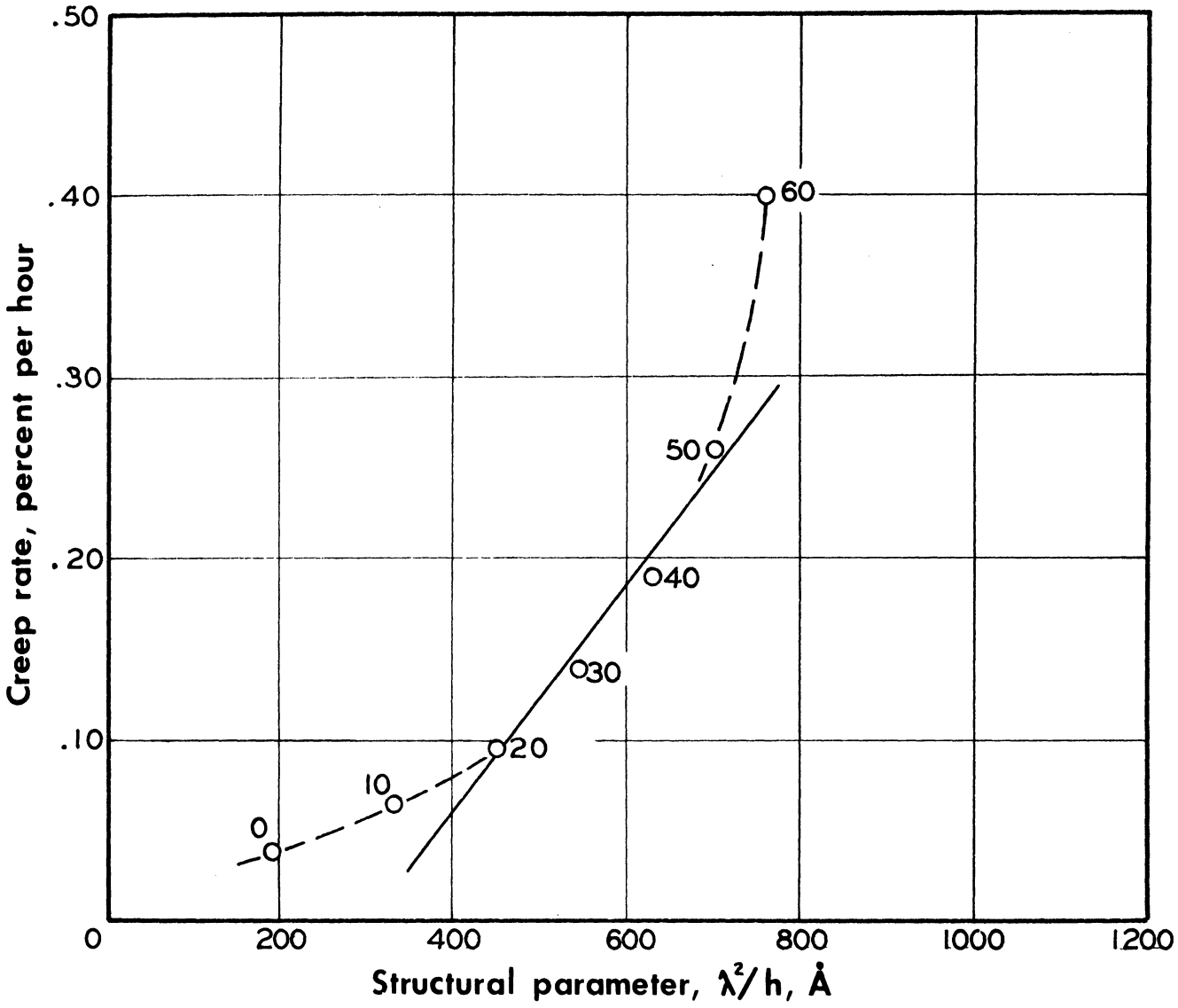

Figure 39. - Relation between creep rate at 1600°F and 18,000 psi for M252 alloy, and the structural parameter, λ^2/h. Numbers on curve indicate time at which measurements were made.

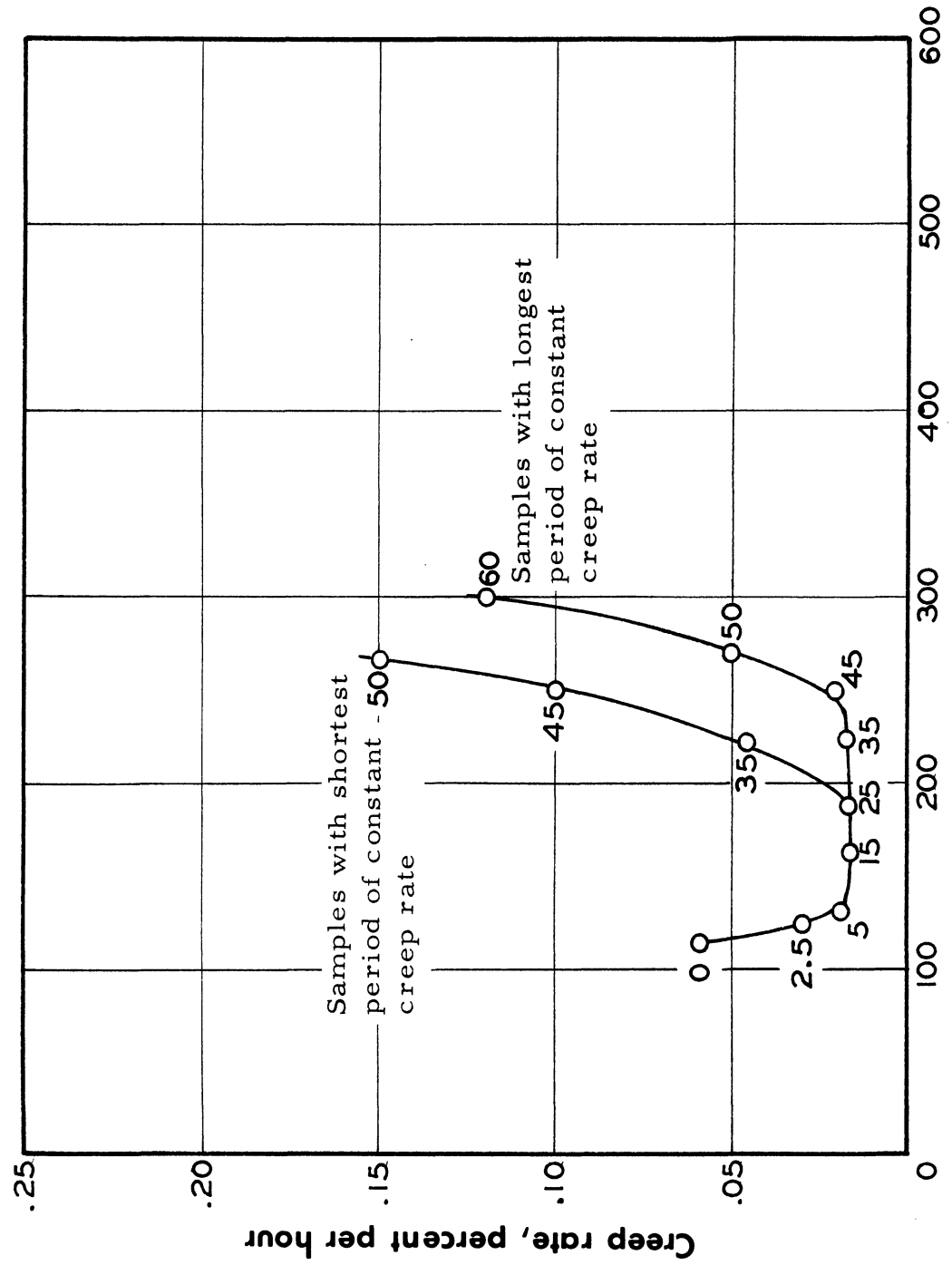

Figure 40. - Relation between creep rate at 1600°F and 29,000 psi for Inconel 700 alloy, and the structural parameter, λ^2/h. Numbers on curves indicate time at which measurements were made.

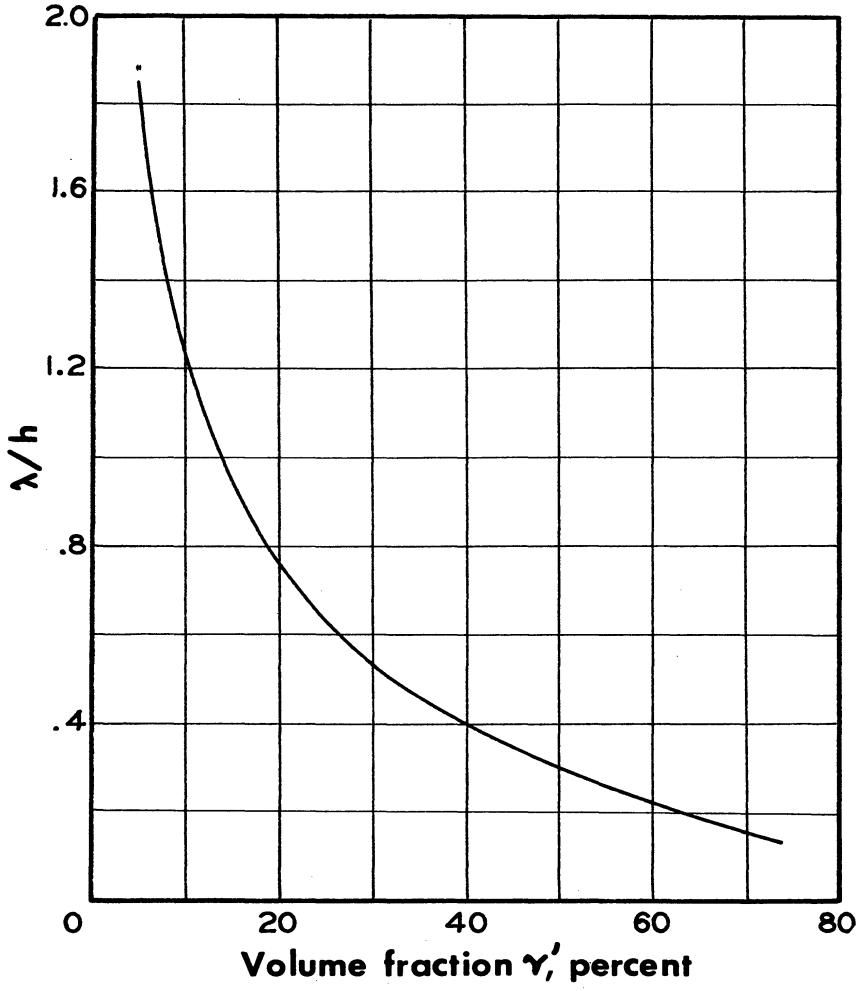

(a) λ/h as a function of volume fraction.

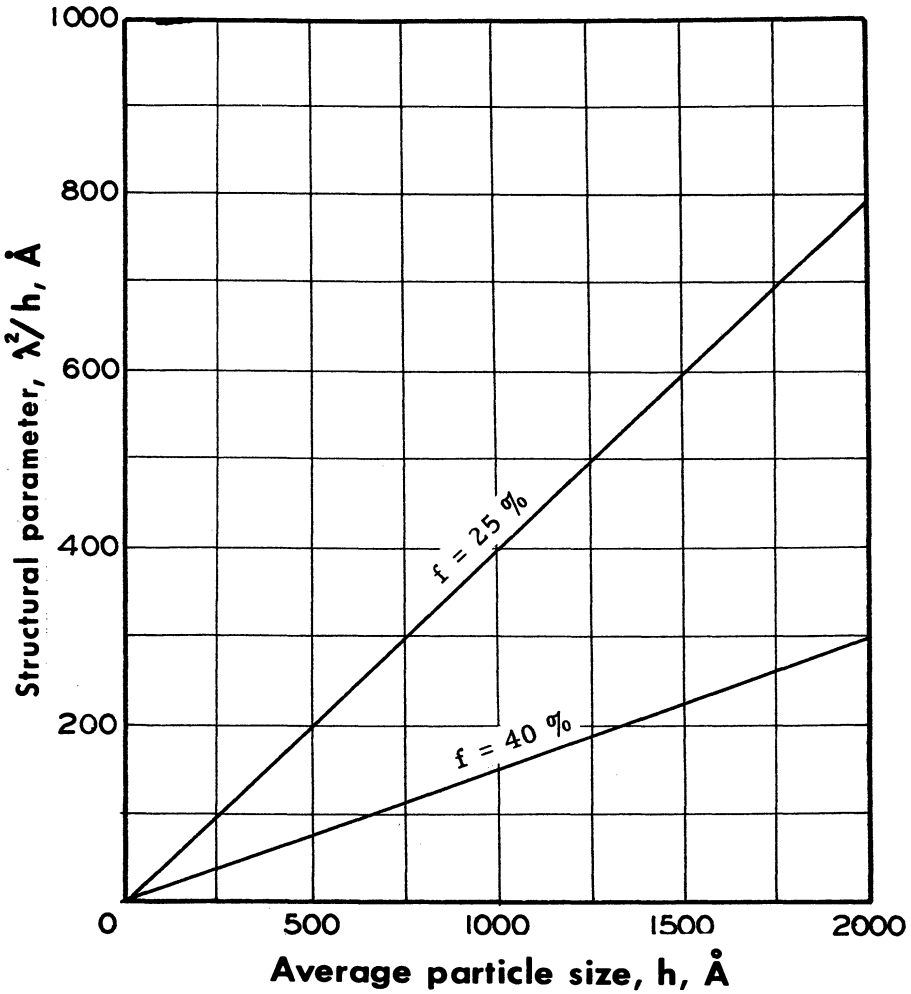

(b) λ^2/h as a function of h for two levels of f.

Figure 41. - Geometric relationships among volume fraction (f), average particle size (h), and average inter-particle distance (λ), assuming spheres uniformly arranged in a face-centered cubic array; and the resultant values of Weertman's dispersion parameter, λ^2/h.

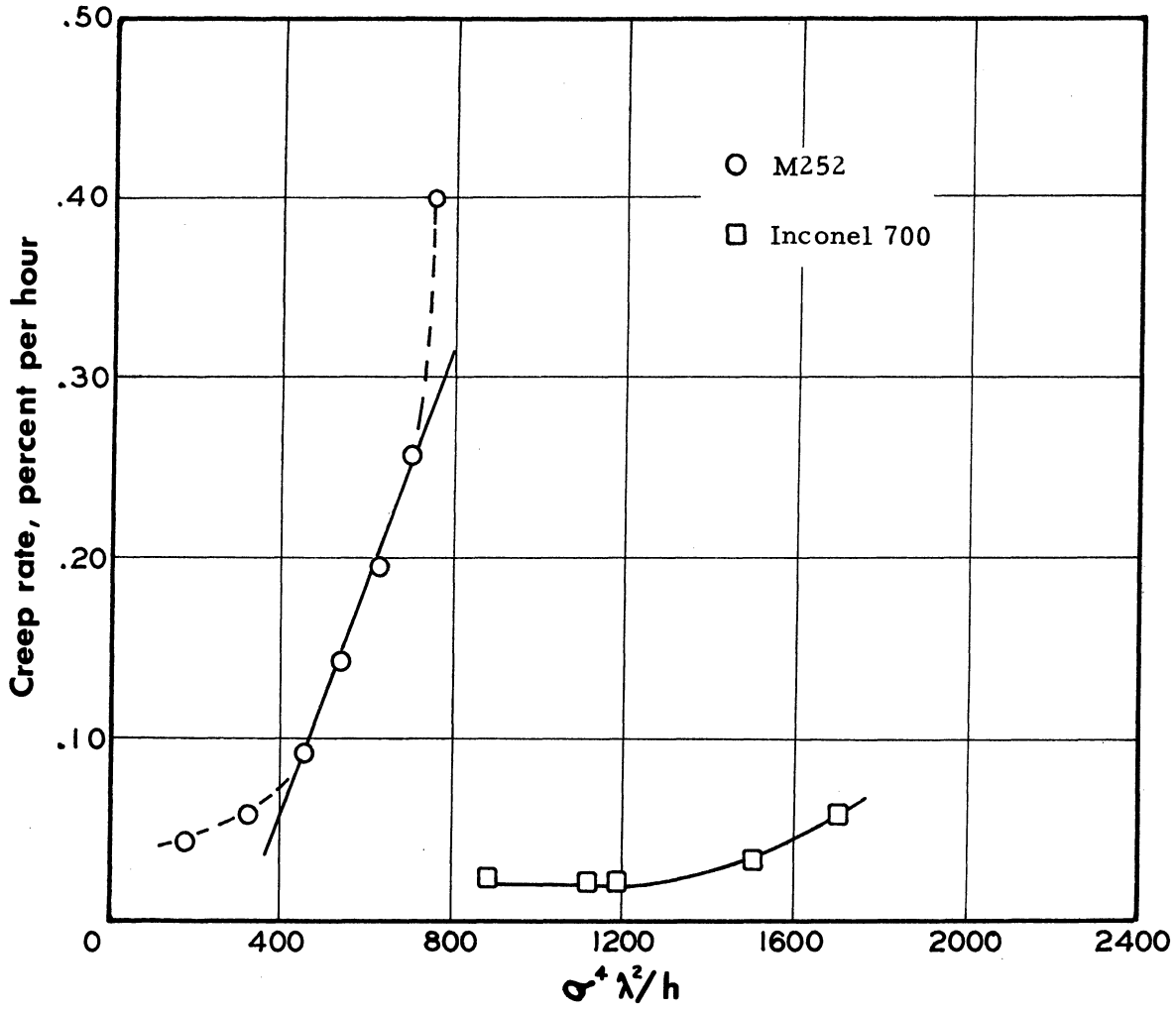

Figure 42. - Relation between creep rate and Weertman's dispersion parameter, $\sigma^4\lambda^2/h$, for M252 and Inconel 700 including the theoretical influence of stress. (Values based on data of Table IV using 18,000 psi for unit stress.)

σ = stress
λ = inter-particle spacing
h = particle size

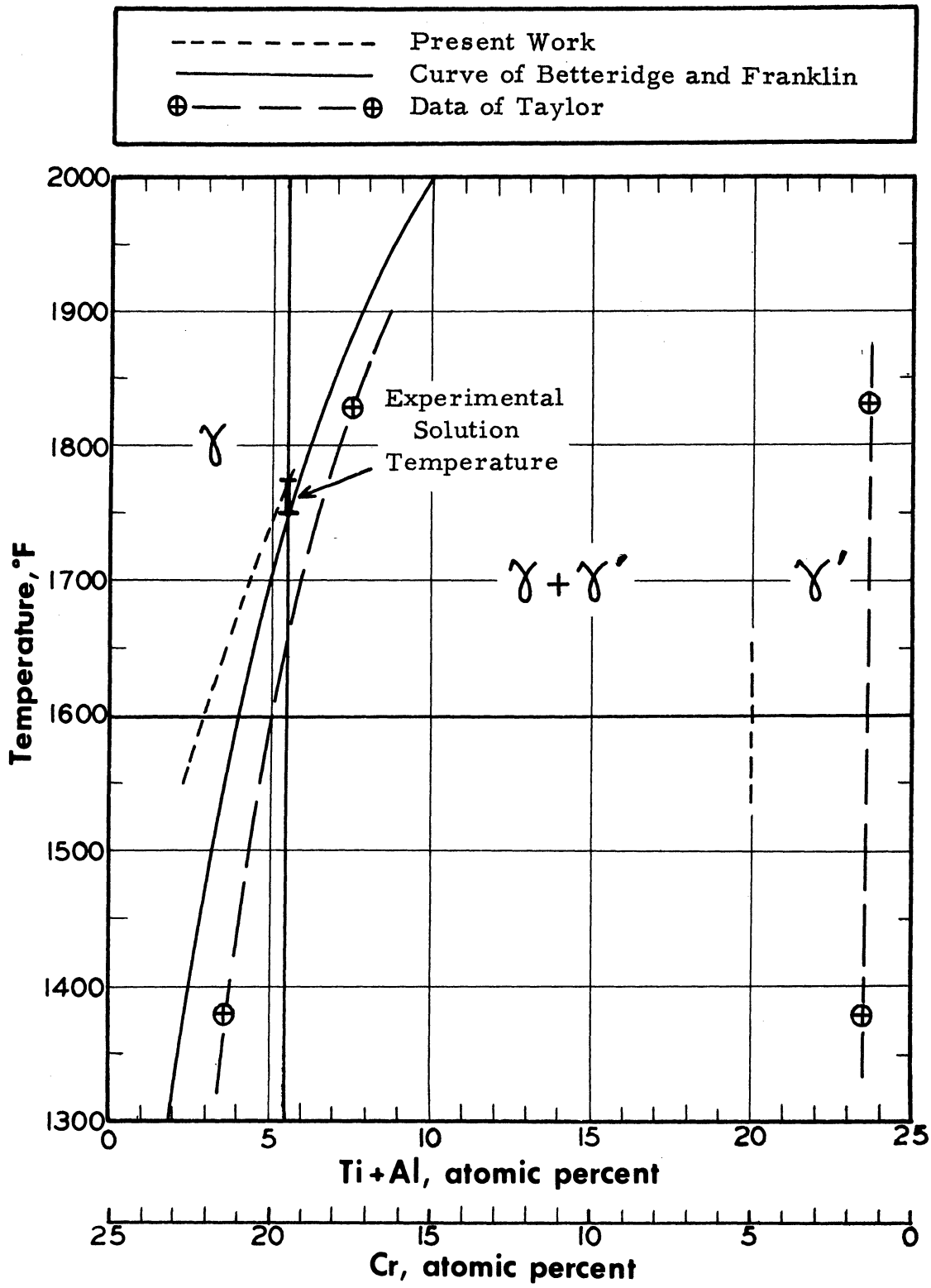

Figure 43. - Diagram of the phase boundaries for the γ-γ' reaction in M252 (heat 837) suggested by the present work compared with those of Betteridge and Franklin (ref. 8) and of Taylor (ref. 10).

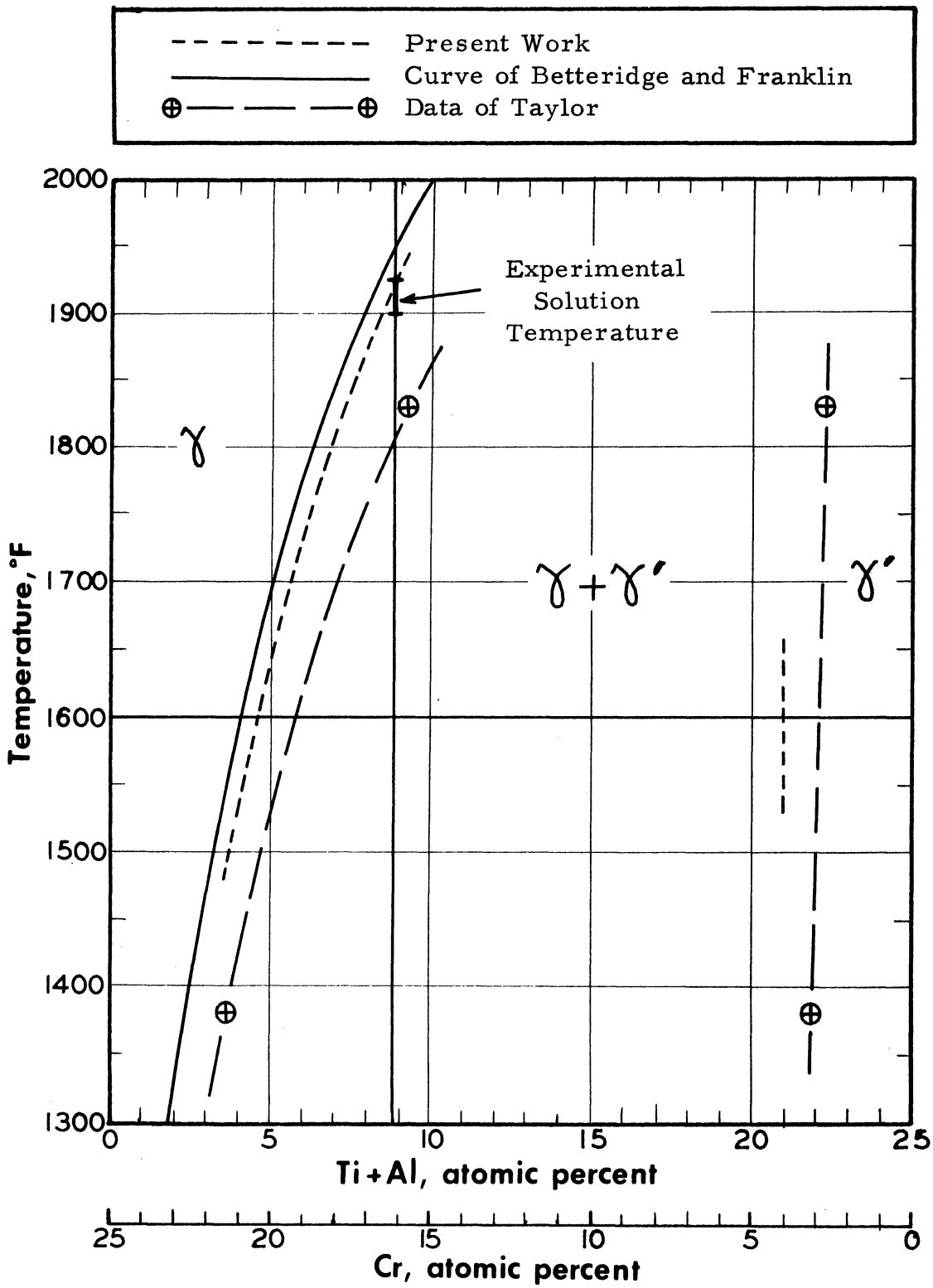

Figure 44. - Diagram of the phase boundaries for the γ-γ' reaction in Inconel 700 alloy suggested by the present work compared with those of Betteridge and Franklin (ref. 8) and of Taylor (ref. 10).

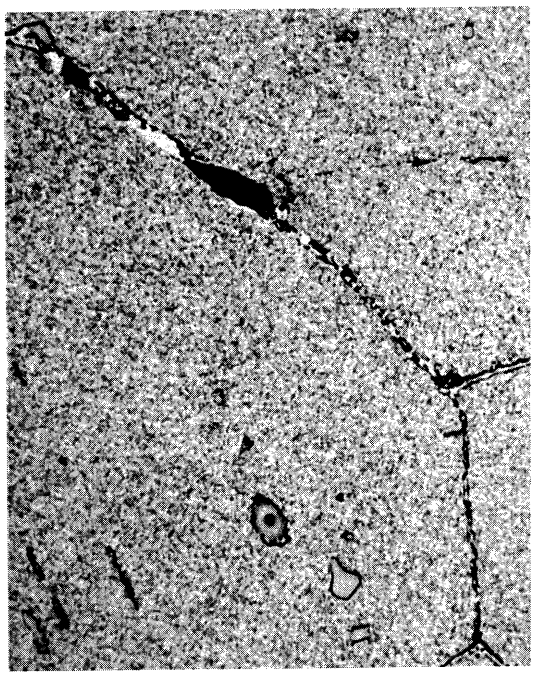

(a) X1000

(b) X11,000

Figure 45. - Micrographs of Inconel 700 alloy sample after rupture test at 1600°F (rupture time 62.7 hours) showing γ' depletion and an associated microcrack.

(a) Optical micrograph showing nearly complete absence of grain boundary precipitates (X1000)

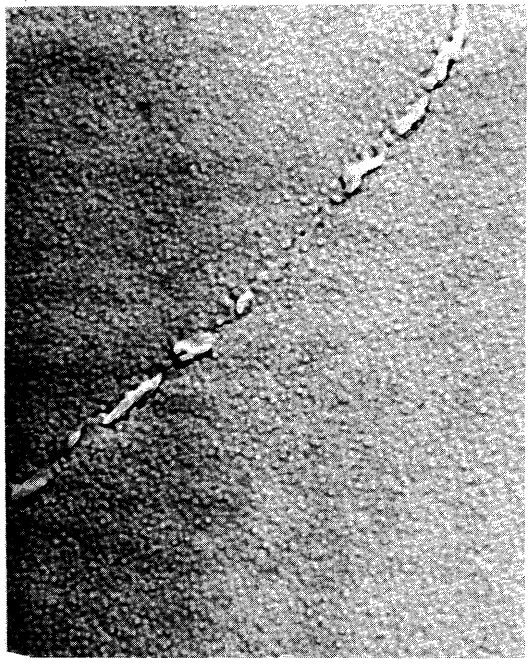

(b) Electron micrograph of grain boundary area from (a) in which some carbide precipitate remained (X11,000)

Figure 46. - Micrographs of Inconel 700 alloy sample after 12 overheats to 2000°F showing the virtual absence of grain boundary precipitates.

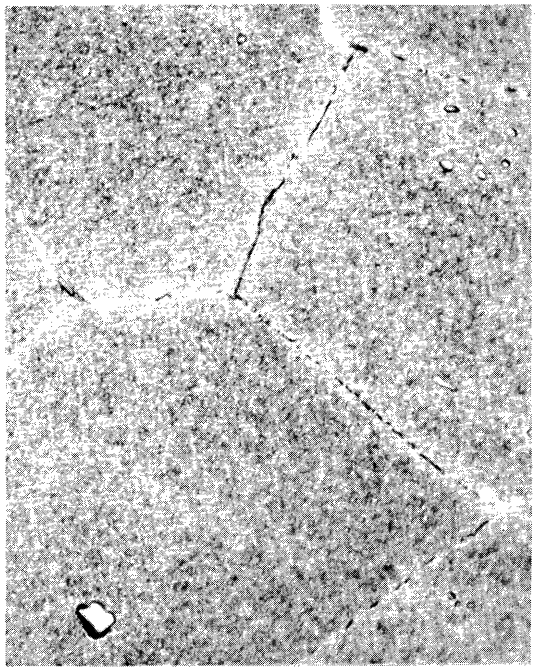

(a) X1000

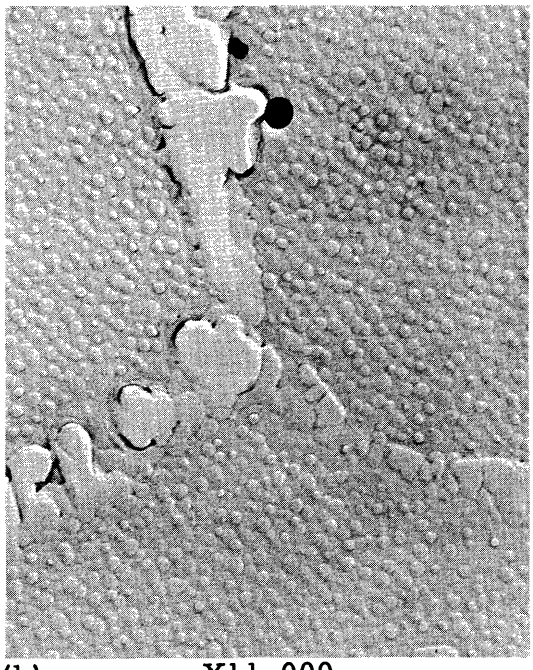

(b) X11,000

Figure 47. - Micrographs from Inconel 700 sample which continued for 24 hours to rupture after completion of six overheats to 2000°F showing the reprecipitation of grain boundary phases.

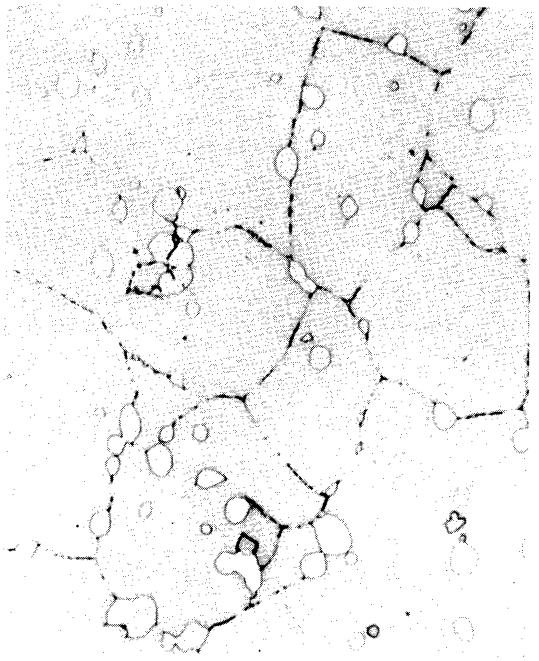

(a) Standard heat treatment

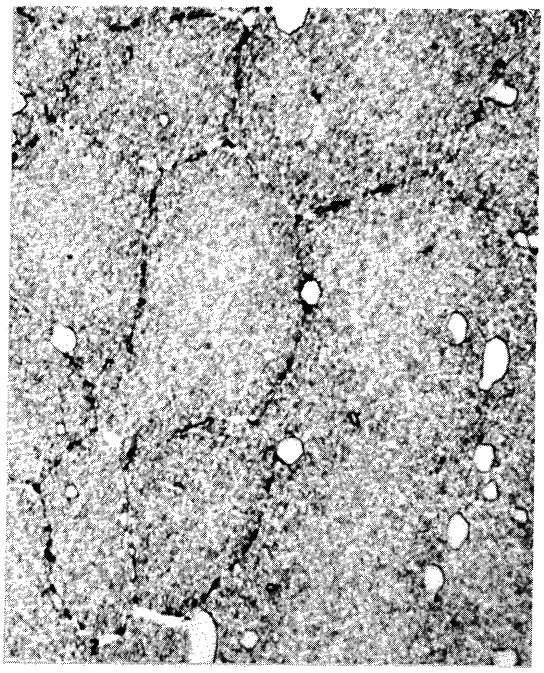

(b) Normal rupture test. Interrupted after 50 hours

(c) Test overheated 10 times to 1800°F. Interrupted after 50 hours.

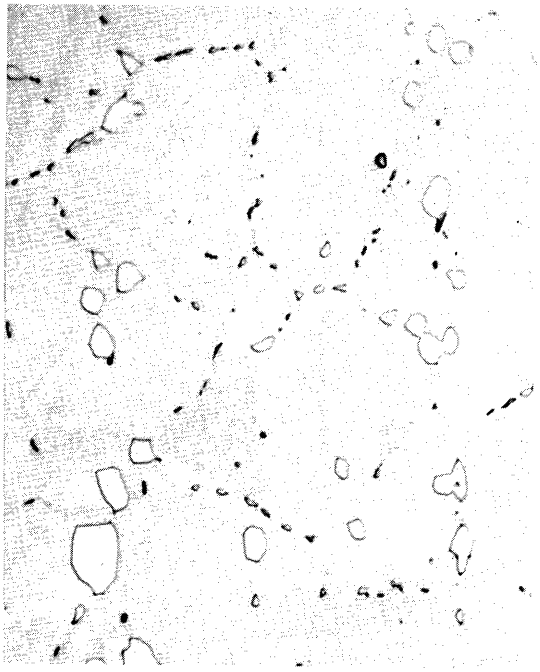

(d) Test overheated 10 times to 2000°F. Interrupted after 50 hours.

Figure 48. - Micrographs of M252 samples showing that carbide distribution was unaffected by either normal or overheat testing. Darkened matrix areas in (b) and (c) indicate presence of large particles of γ' precipitate. (X1000)

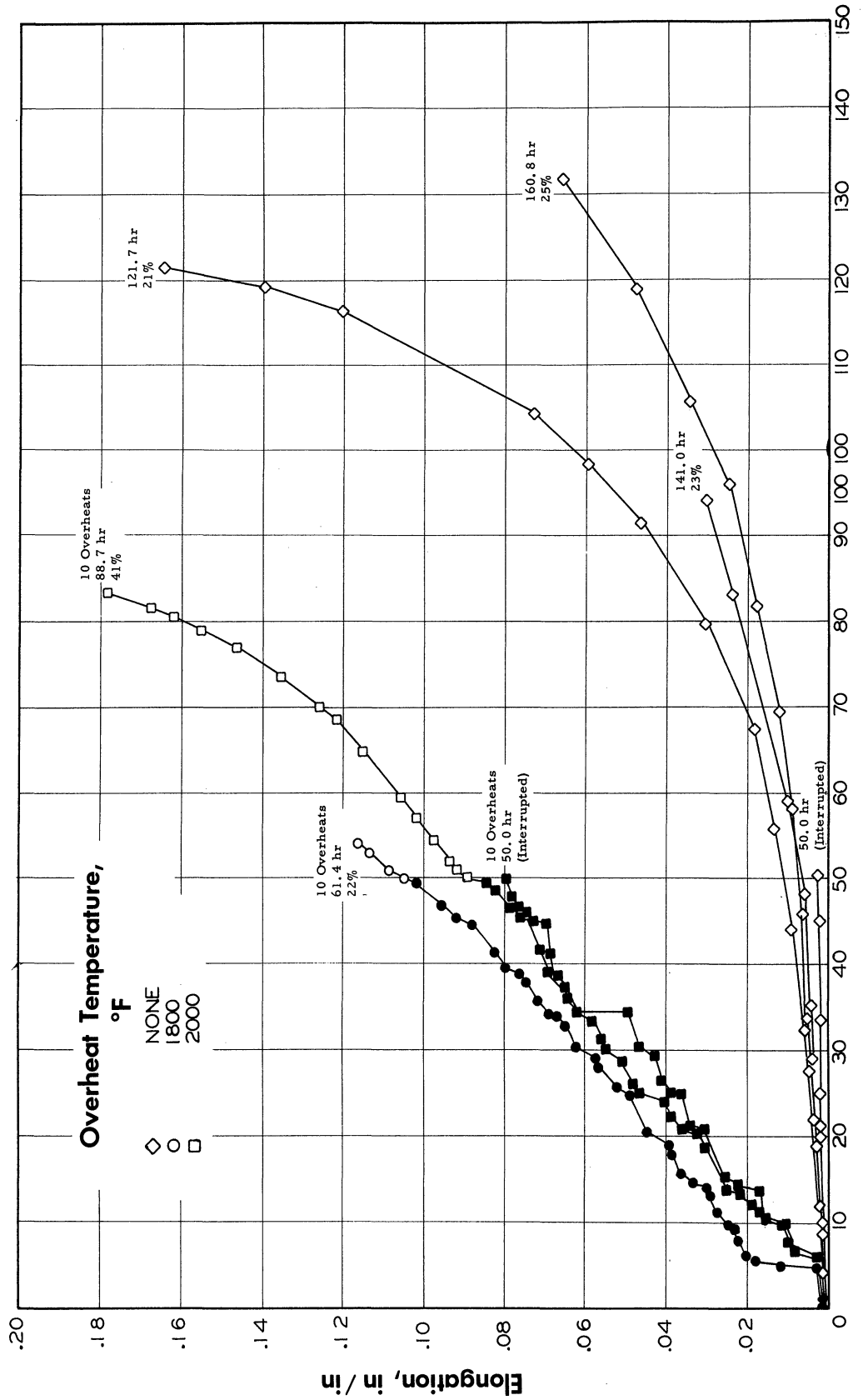

Figure 49. - Comparative creep curves at 1600°F and 16,000 psi for heat 1173 for the indicated test conditions. Solid points indicate period of application of overheats. Number of overheats, time for rupture, and elongation at rupture indicated for each curve.

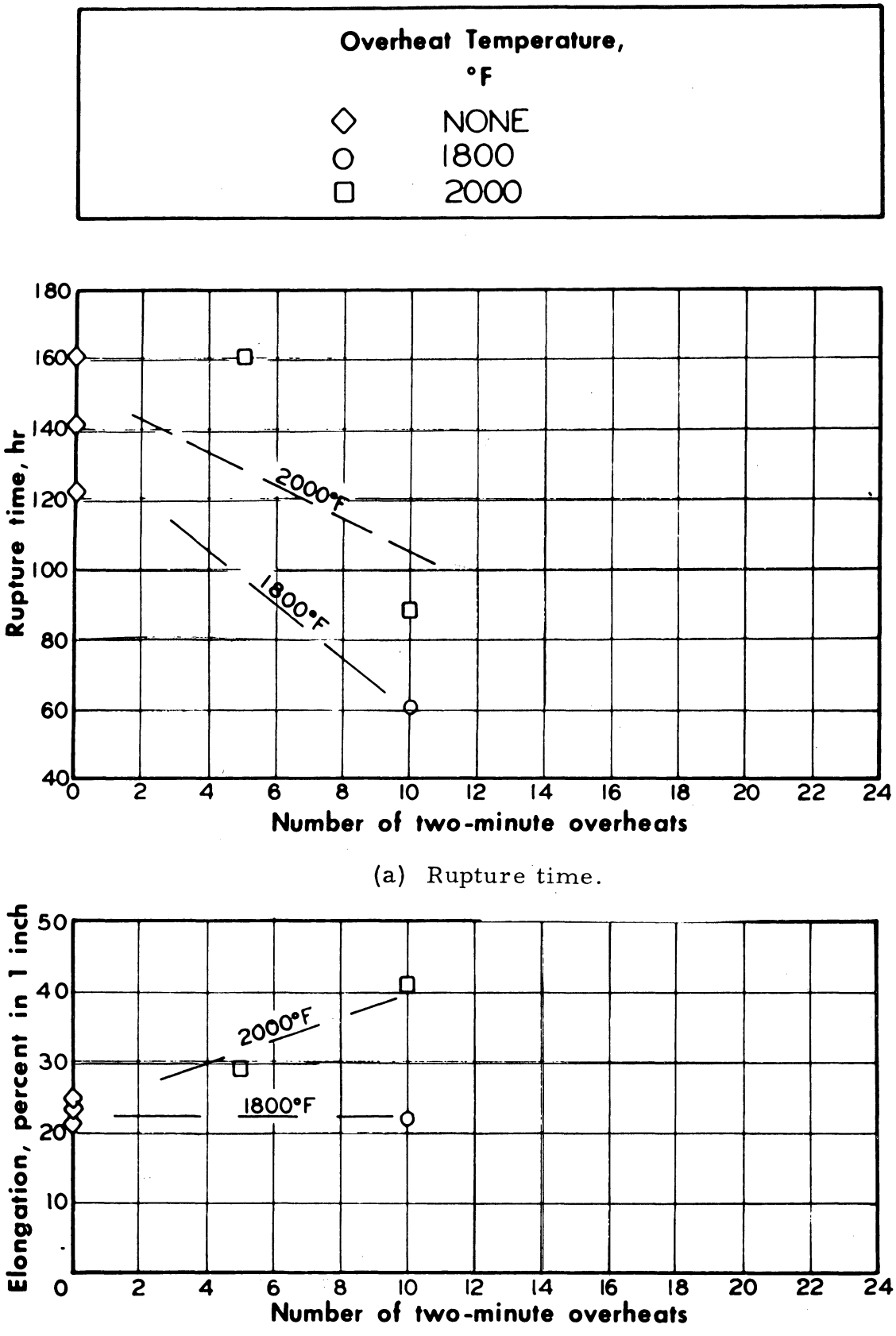

(a) Rupture time.

(b) Elongation.

Figure 50.1 - Rupture time and elongation at 1600°F and 16,000 psi as a function of number of two-minute overheats for laboratory heat 1173.

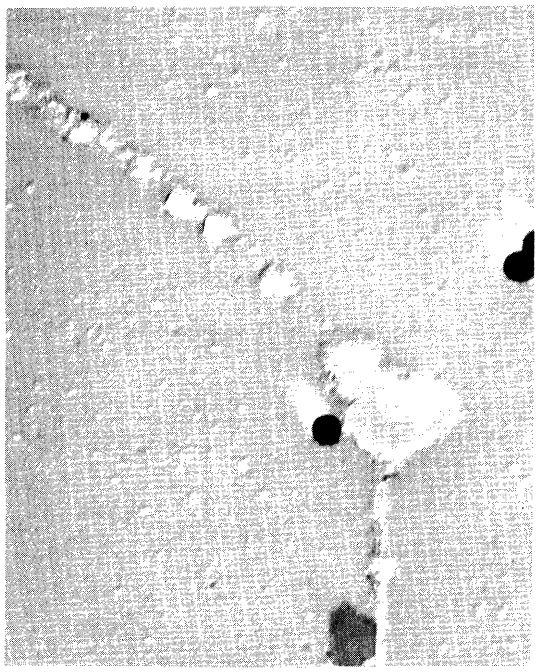

(a) Heat 1173 - 5 minutes

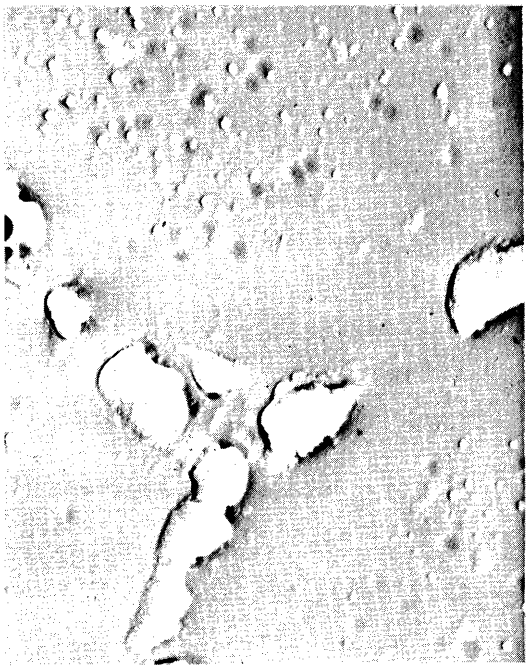

(b) Heat 1173 - 10 minutes

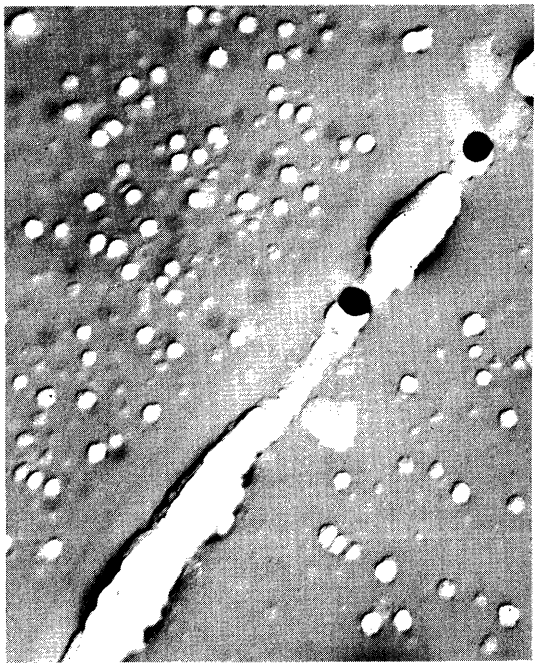

(c) Heat 1173 - 40 minutes

Figure 51. - Representative electron micrographs for heat 1173, M252 (heat 837), and a heat of commercial Waspaloy after exposure to 2000°F for 2 minutes and rapid cooling to 1600°F. Samples ice brine quenched after the indicated time at 1600°F. (X11,000)

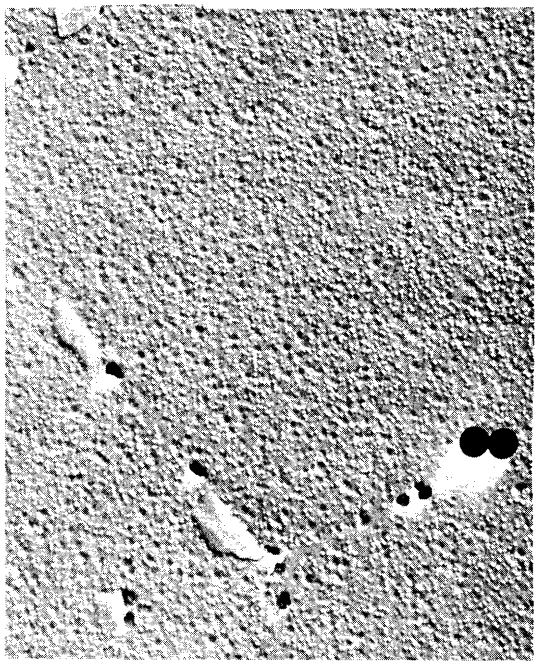

(d) M252 (heat 837) - 5 minutes

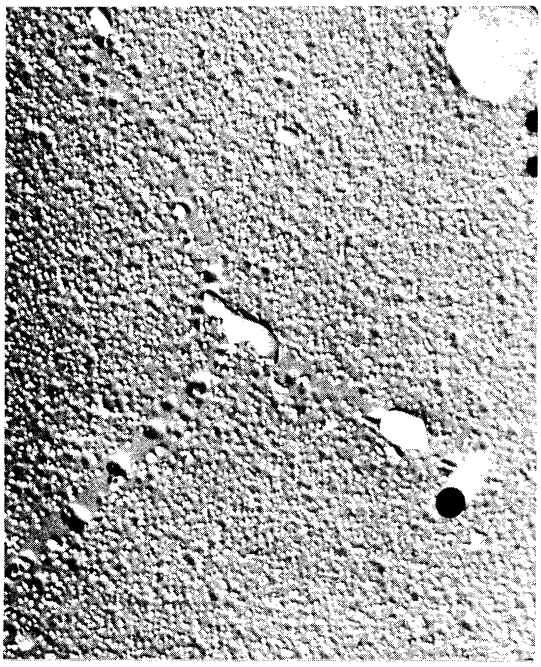

(e) M252 (heat 837) - 10 minutes

(f) Waspaloy - 5 minutes

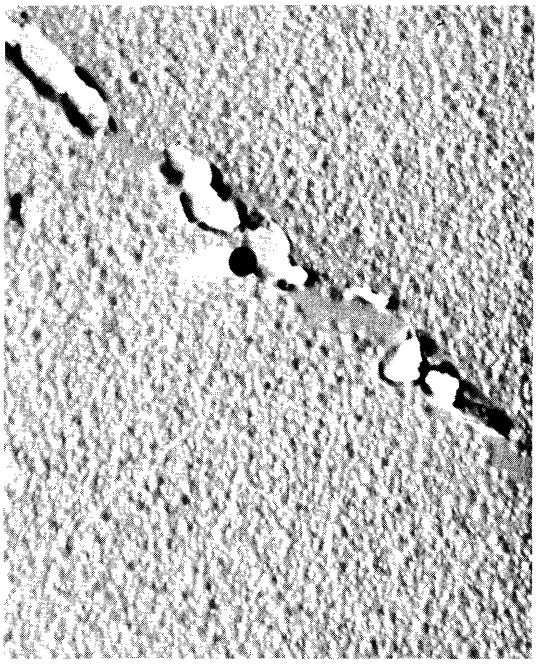

(g) Waspaloy - 10 minutes

Figure 51. - Concluded. Representative electron micrographs for heat 1173, M252 (heat 837), and a heat of commercial Waspaloy after exposure to 2000°F for 2 minutes and rapid cooling to 1600°F. Samples ice brine quenched after the indicated time at 1600°F. (X11,000)

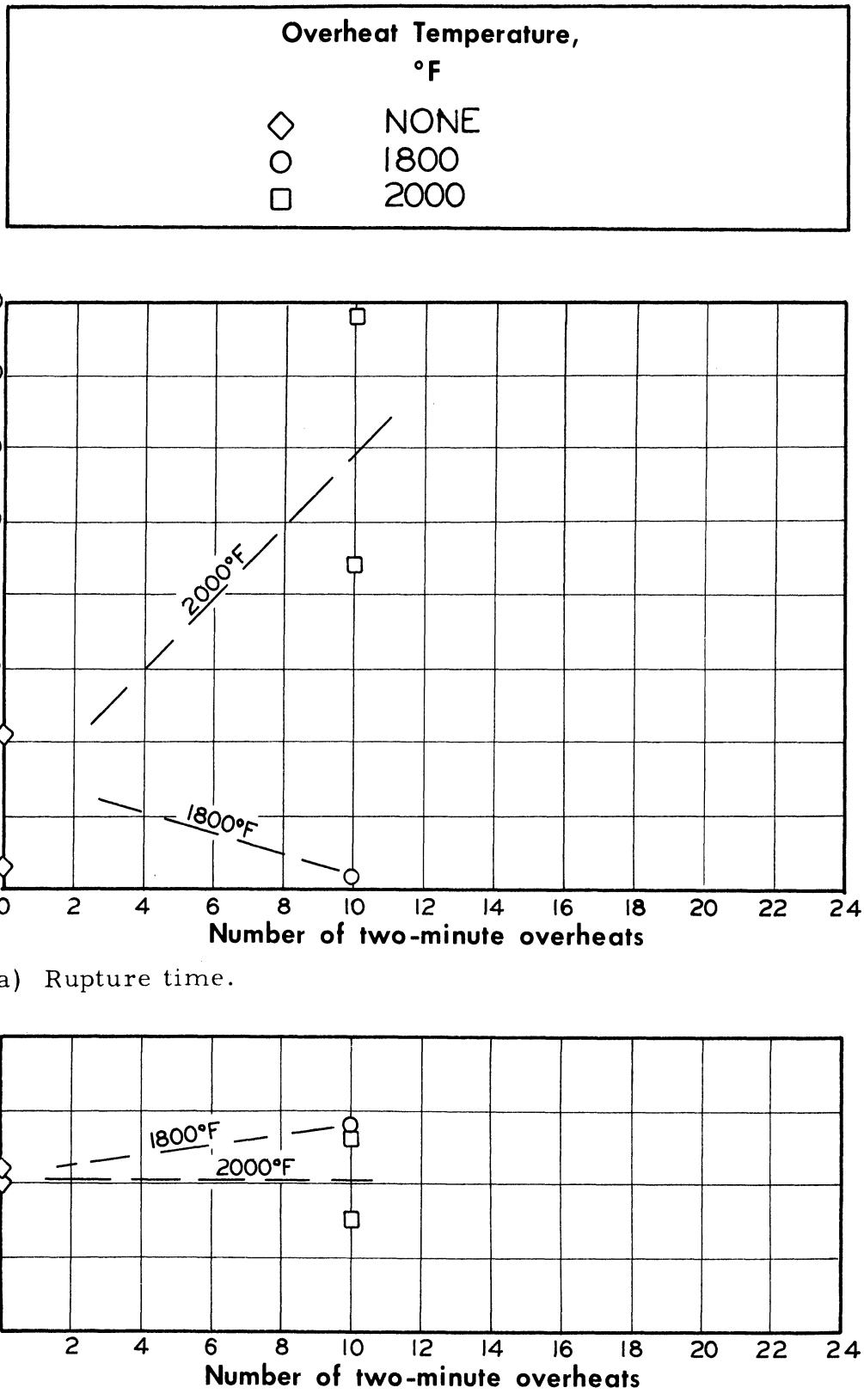

(a) Rupture time.

(b) Elongation.

Figure 52. - Rupture time and elongation at 1600°F and 20,000 psi as a function of number of two-minute overheats for laboratory heat 1172.

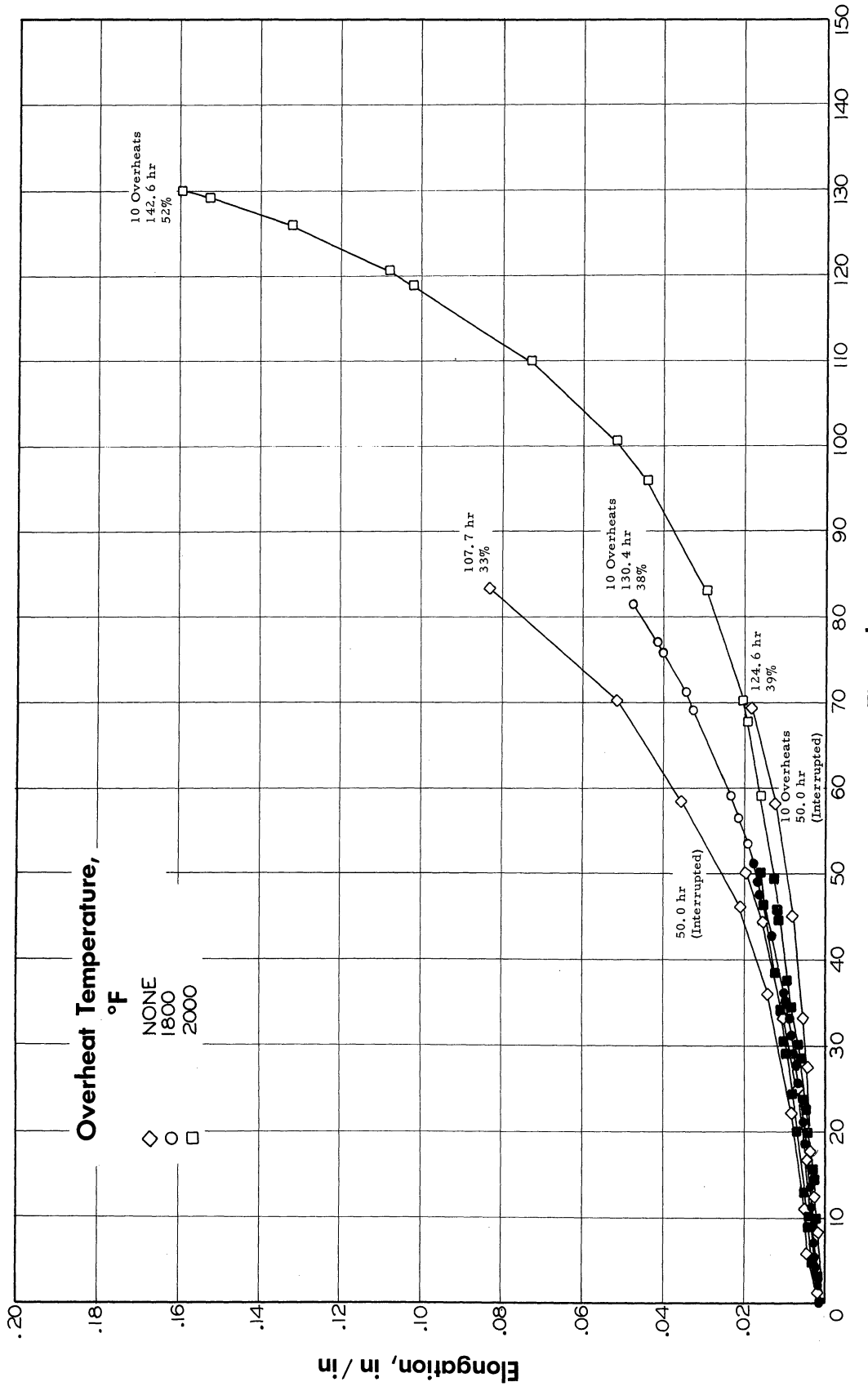

Figure 53. - Comparative creep curves at 1600°F and 20,000 psi for heat 1172 for the indicated test conditions. Solid points indicate period of application of overheats. Number of overheats, time for rupture, and elongation at rupture indicated for each curve.

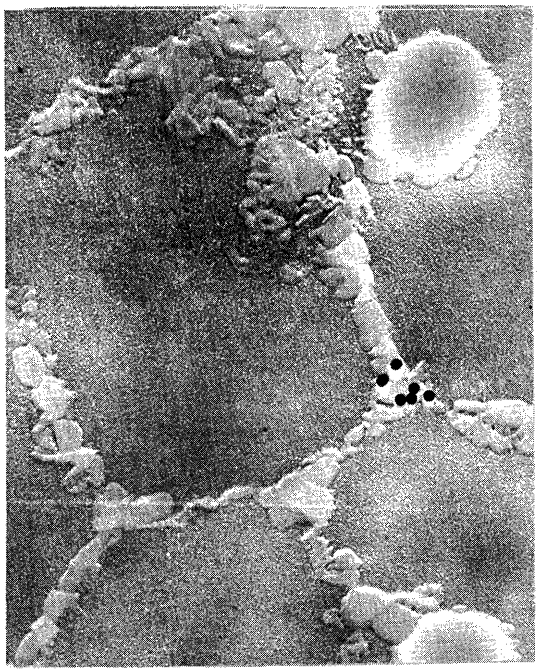

(a) After heat treatment

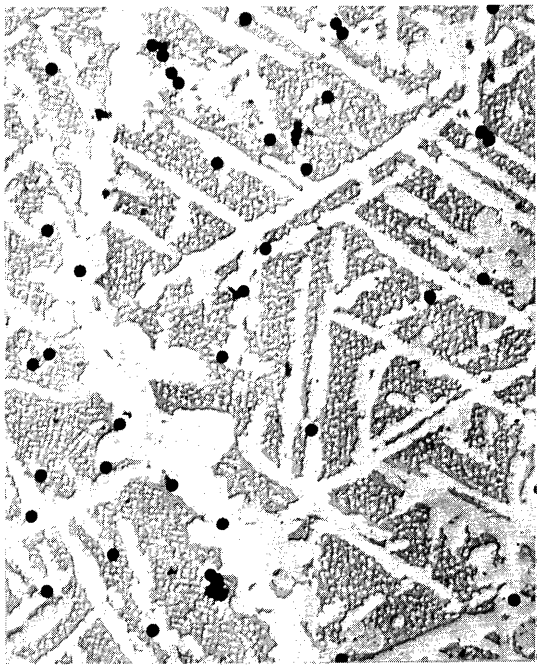

(b) Rupture test interrupted at 50 hours

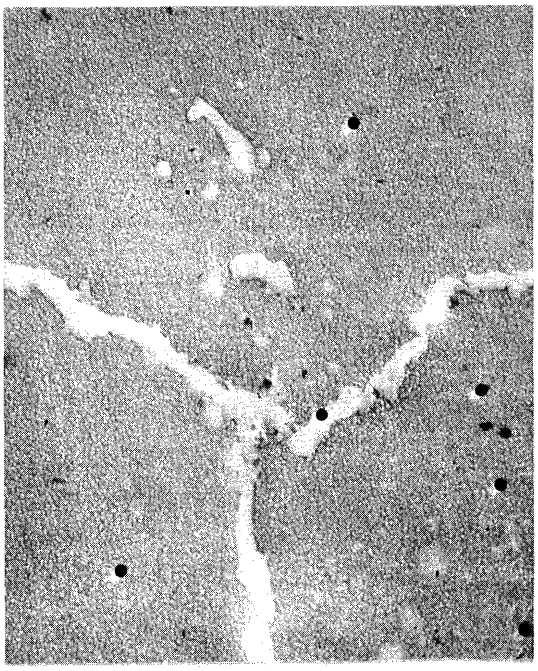

(c) Interrrupted at 50 hours after 10 overheats to 2000°F

(d) Sample run to rupture (94.3 hours) after receiving 10 overheats to 2000°F.

Figure 54. - Microstructures of heat 1172 showing effect of overheating to 2000°F on formation of sigma phase. Tests at 1600°F and 20,000 psi. (X4500)

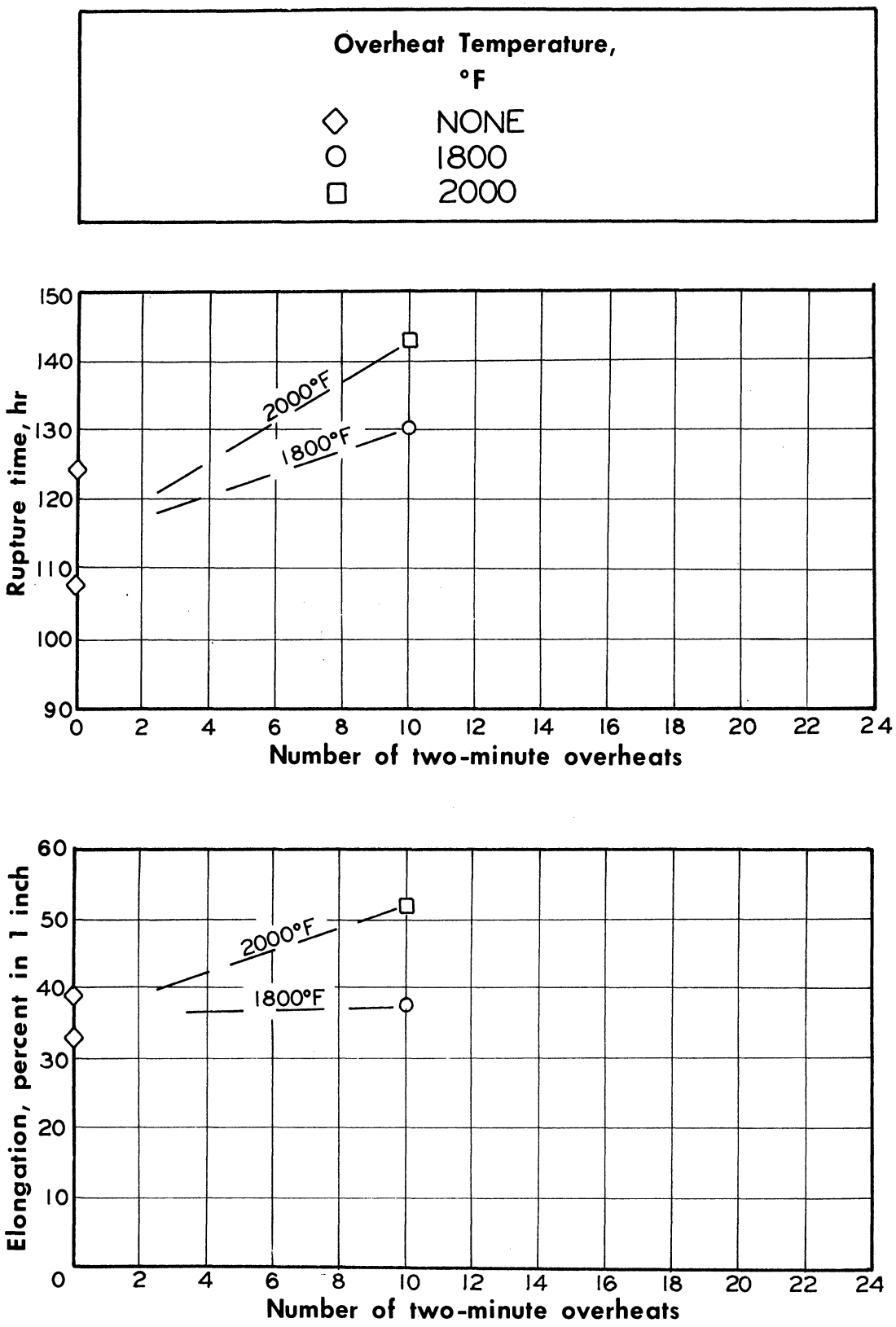

Figure 55. - Rupture time and elongation at 1600°F and 20,000 psi as a function of number of two-minute overheats for laboratory heat 1171.

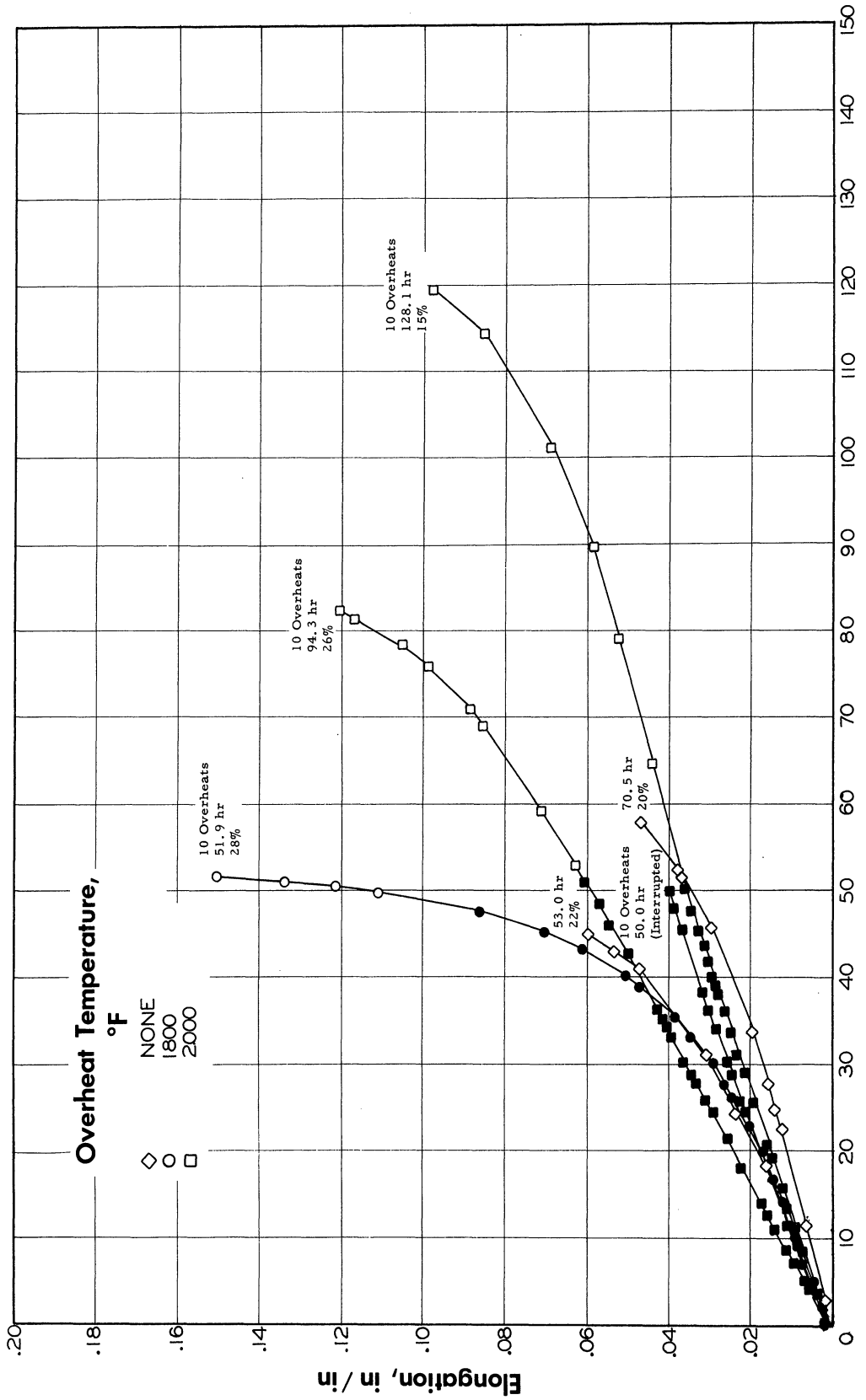

Figure 56. - Comparative creep curves at 1600°F and 20,000 psi for heat 1171 for the indicated test conditions. Solid points indicate period of application of overheats. Number of overheats, time for rupture, and elongation at rupture indicated for each curve.

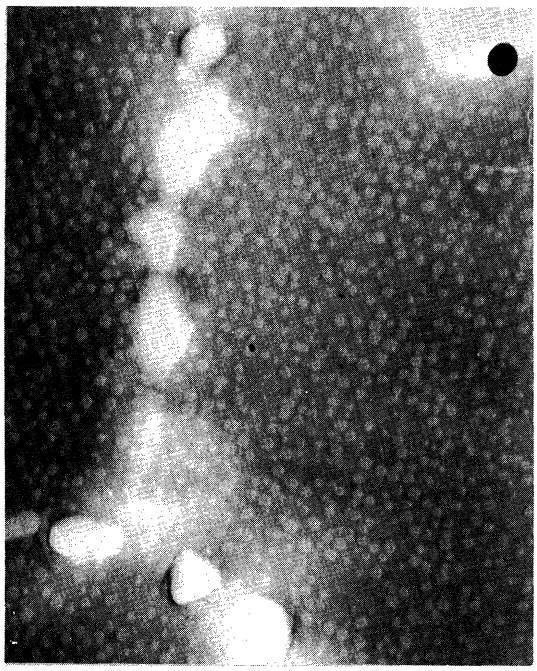

(a) Normal test

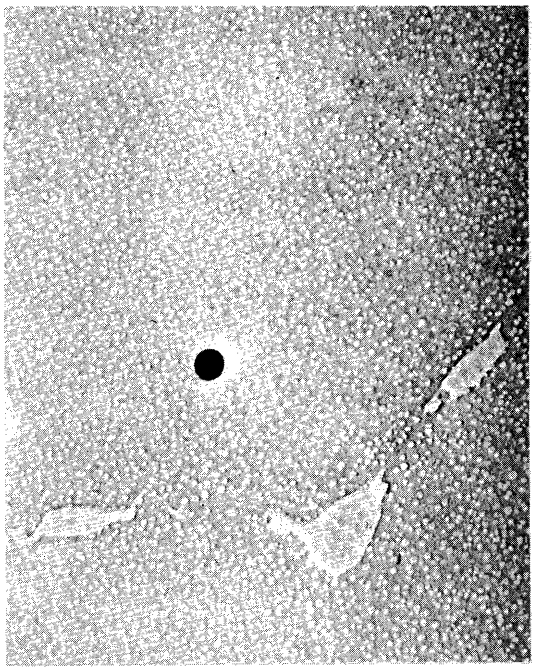

(b) 10 overheats to 2000°F

Figure 57. - Micrographs of heat 1171 after 50 hours under 20,000 psi at 1600°F and the indicated test conditions. (X11,000)